Materials Reliability Program Reactor Vessel Closure Head Penetration Safety Assessment for U.S. PWR Plants (MRP-110NP)

Evaluations Supporting the MRP Inspection Plan

1009807-NP

Final Report, April 2004

NON-PROPRIETARY INFORMATION

EPRI Project Manager
C. King

EPRI • 3412 Hillview Avenue, Palo Alto, California 94304 • PO Box 10412, Palo Alto, California 94303 • USA
800.313.3774 • 650.855.2121 • askepri@epri.com • www.epri.com

DISCLAIMER OF WARRANTIES AND LIMITATION OF LIABILITIES

ORGANIZATION(S) THAT PREPARED THIS DOCUMENT

Dominion Engineering, Inc.

ORDERING INFORMATION

Requests for copies of this report should be directed to EPRI Orders and Conferences, 1355 Willow Way, Suite 278, Concord, CA 94520. Toll-free number: 800.313.3774, press 2, or internally x5379; voice: 925.609.9169; fax: 925.609.1310.

CITATIONS

This report was prepared by

Dominion Engineering, Inc.
11730 Plaza America Drive
Suite 310
Reston, VA 20190

Principal Investigator
G. A. White

Contributors
M. R. Fleming
J. A. Gorman
E. S. Hunt
P. T. Jones
M. A. Kreider
N. S. Nordmann

This report describes research sponsored by EPRI.

The report is a corporate document that should be cited in the literature in the following manner:

Materials Reliability Program Reactor Vessel Closure Head Penetration Safety Assessment for U.S. PWR Plants (MRP-110NP): Evaluations Supporting the MRP Inspection Plan, EPRI, Palo Alto, CA: 2004. 1009807-NP.

REPORT SUMMARY

Background

Inspections of penetration nozzles in PWR vessel closure heads have shown that these Alloy 600 components may be susceptible to active aging degradation due to primary water stress corrosion cracking (PWSCC). The stresses that make the nickel-chromium-iron Alloy 600 nozzles and their Alloy 182 J-groove attachment welds susceptible to cracking are induced by the welding of the nozzle to the inside surface of the reactor vessel closure head (RVCH) during vessel fabrication. Since late 2000, inspections in the U.S. have shown that although most of the observed nozzle cracking is axial in orientation, several circumferentially oriented cracks have been detected above the top of the J-groove weld. Such circumferential cracks could potentially lead to nozzle ejection and a small- or medium-break loss of coolant accident (LOCA) if the circumferential crack were to grow most of the way around the nozzle, typically to a size of at least 330°. A second potential safety concern is boric acid corrosion of the low-alloy steel material of the reactor vessel closure head. The large wastage cavity observed at the Davis-Besse plant in 2002 resulted from what is believed to be at least six years of leakage and concentration of the borated reactor coolant. In response to these concerns, the U.S. NRC issued several generic communications, including NRC Order EA-03-009. This order, which was issued on February 11, 2003, specifies interim inspection requirements for all domestic RVCH penetrations.

Objectives

The objective of this report is to provide a final safety assessment for PWSCC of Alloy 600 RVCH nozzles and related Alloy 182 J-groove welds in PWR plants. This report and the referenced documents form the technical basis for the MRP inspection plan for RVCH penetrations, which is currently being drafted by the MRP. The MRP safety assessment and inspection plan documents are intended to form the basis for requirements that are intended to replace NRC Order EA-03-009.

Approach

This safety assessment addresses the principal potential safety concerns of nozzle ejection due to circumferential nozzle cracking and head rupture due to boric acid wastage. A detailed failure mode and effect analysis (FMEA) is used to verify that these are the main concerns and documents the material, fabrication, and operations factors that affect the likelihood and type of aging degradation mechanisms that potentially affect the RVCH penetrations and surrounding low-alloy steel head material. Deterministic and probabilistic nozzle ejection and head wastage evaluations form the core of the safety assessment, which also includes a compilation of design

data, flaw tolerance calculations, a review of inspection experience, stress and fracture mechanics calculations, a consequential damage assessment, a summary of available information on the resistance of replacement head materials to cracking, and a review of inspection capabilities.

Results

The safety assessment demonstrates that the typical case of axial nozzle cracking is not a credible mechanism leading to nozzle rupture because the critical axial crack length is much greater than the height of the nozzle region subject to welding residual stresses. The referenced nozzle ejection safety assessment reports (MRP-103, MRP-104, and MRP-105) demonstrate that there is significant margin against nozzle ejection due to circumferential cracking because of the time required for a circumferential crack to grow to the critical size, typically at least 330°. This safety assessment also demonstrates that periodic bare metal visual examination of the head top surface performed at appropriate intervals provides assurance against significant wastage of the low-alloy steel head material, even given the assumption of a leaking nozzle. Finally, MRP-105 also demonstrates a low probability of future pressure boundary leakage given an appropriate program of periodic inspections.

EPRI Perspective

This report completely replaces the interim safety assessment report (MRP-44, Part 2), which was issued in May 2001. This report is the top level safety assessment document for RVCH penetrations, and as such it references other closely related documents, including the nozzle ejection assessments (MRP-103, MRP-104, and MRP-105), crack growth rate evaluation (MRP-55, MRP-21), and inspection guidance and demonstration reports (EPRI 1007842 and MRP-89). Also referenced is MRP-111, which evaluates the expected performance of the replacement head materials—Alloy 690 nozzles and Alloy 52 welds—given the currently available data.

Keywords

Primary water stress corrosion cracking
PWSCC
Stress corrosion
Boric acid corrosion
Failure mode and effect analysis
FMEA
Alloy 600
Alloy 82/182
Alloy 690
Alloy 52/152
CRDM nozzle
CEDM nozzle
J-groove weld
Reactor vessel head
Reactor vessel closure head
Reactor vessel upper head

ABSTRACT

This safety assessment addresses the potential safety issues associated with aging degradation of reactor vessel closure head (RVCH) penetrations. A detailed failure mode and effect analysis (FMEA) is used to verify that these are the main concerns and documents the material, fabrication, and operations factors that affect the likelihood and type of aging degradation mechanisms that potentially affect the RVCH penetrations and surrounding low-alloy steel head material. Deterministic and probabilistic nozzle ejection and head wastage evaluations form the core of the safety assessment. This document is a top level safety assessment document. As such, it includes generic evaluations applicable to the entire U.S. PWR fleet, but it also references lower level documents in some areas, particularly in the areas of nozzle ejection, crack growth rate evaluations, inspection guidelines and capabilities, and the resistance to cracking of replacement head materials. Specifically:

- Section 1 provides a brief background discussion, describes the locations of Alloy 600 penetrations on reactor vessel top heads and other key design data, defines the scope of the safety assessment, and outlines the approach used.
- Section 2 describes the failure mode and effect analysis (FMEA) that was applied to potential degradation of RVCH penetrations.
- Section 3 summarizes the results of flaw and wastage tolerance calculations to determine (1) the critical crack sizes for the various crack locations and orientations of potential concern and (2) the volume of low-alloy steel that can be lost from the top surface of a reactor vessel head by boric acid corrosion without the stresses in the remaining material exceeding the ASME Code allowable values.
- Section 4 presents the RVCH penetration inspection experience through December 2003, including a chronological summary of key events and summary statistics investigating the effects of operating time, head temperature, vessel fabricator, and nozzle material supplier.
- Section 5 describes the welding residual stress and fracture mechanics calculations that have been performed as an input to the nozzle ejection and head wastage evaluations.
- Section 6 summarizes the methodologies and results of the MRP's nozzle ejection safety assessments (MRP-103, MRP-104, and MRP-105).
- Section 7 describes the evaluations used to show that adequate protection against boric acid wastage is provided by periodic bare metal visual examinations performed at appropriate intervals for evidence of leakage.
- Section 8 presents an assessment of consequential damage given nozzle ejection or rupture of the head due to boric acid wastage. This assessment shows that the conditional core damage

probability (CCDP) for standard LOCA events can be used to bound the potential effects of consequential damage.

- Section 9 summarizes the inspection tools that are available to detect nozzle leakage or cracking.
- Section 10 summarizes the findings of an MRP study (MRP-111) of the currently available laboratory test data and plant experience regarding the resistance to PWSCC of the standard replacement head materials—Alloy 690 wrought nozzle material and Alloy 52/152 weld metal.

ACKNOWLEDGMENTS

This report is a product of the Alloy 600 Issues Task Group (ITG) of the Materials Reliability Program (MRP). Larry Mathews of Southern Nuclear Operating Company is the chairman of the Alloy 600 ITG, and Craig Harrington of TXU Energy is the chairman of the Reactor Vessel Head Working Group within the Alloy 600 ITG. Christine King is the EPRI project manager for the Alloy 600 ITG.

AREVA authored major portions of Section 8, "Consequential Damage Assessment," and Section 10, "Replacement Head Materials."

ACRONYMS

The following acronyms are used in this report:

AHA	auxiliary head adapter
B&W	Babcock & Wilcox
B&WOG	Babcock & Wilcox Owners Group
BMI	(reactor vessel) bottom mounted instrumentation
BMV	bare metal visual
BWST	borated water storage tank
CCDP	conditional core damage probability
CDF	core damage frequency
CE	Combustion Engineering
CEDM	control element drive mechanism
CEOG	Combustion Engineering Owners Group
CFD	computational fluid dynamics
CGR	crack growth rate
CLT	constant load test
COA	crack opening area
COD	crack opening displacement
CRDM	control rod drive mechanism
CVCS	chemical and volume control system
DGL	de-gas line
EAC	environmentally assisted cracking
ECCS	emergency core cooling system
ECP	electrochemical potential
EDY	effective degradation year
ET	eddy current testing
FEA	finite element analysis
FMEA	failure mode and effect analysis
HPI	high-pressure injection
ICI	in-core instrumentation
IGA	intergranular attack
LERF	large early release frequency
LF-ET	low-frequency eddy current testing
LOCA	loss of coolant accident
LOF	(weld) lack of fusion
LPI	low pressure injection
LTCP	low-temperature crack propagation
MRP	EPRI Materials Reliability Program

MRPC	motorized rotating pancake coil
NDE	non-destructive examination
NSSS	nuclear steam supply system
OTSG	once through steam generator
PDF	probability density function
PFM	probabilistic fracture mechanics
POD	probability of detection
PRA	probabilistic risk assessment
PT	liquid penetrant testing
PWSCC	primary water stress corrosion cracking
RBS	reactor building sump
RCS	reactor coolant system
RPS	reactor protection system
RPV	reactor pressure vessel
RUB	reverse U-bend
RWST	refueling water storage tank
RV	reactor vessel
RVCH	reactor vessel closure head
RVH	reactor vessel head
RVLIS	reactor vessel level indication system
SCC	stress corrosion cracking
TASCS	thermal stratification, cycling, and striping
TTS	top of tubesheet
UT	ultrasonic testing

CONTENTS

1 **INTRODUCTION AND SUMMARY 1-1**

1.1 Background 1-1

1.2 Purpose 1-2

1.3 RVCH Penetration Design Data 1-2

1.4 Scope 1-2

1.5 Approach 1-3

1.6 Main Conclusions 1-4

1.7 Report Structure 1-4

1.8 References 1-7

2 **FAILURE MODE AND EFFECT ANALYSIS (FMEA) 2-1**

2.1 Purpose 2-1

2.2 Basic Structure 2-2

2.3 Input Sources 2-3

2.4 Alloy 600 Reactor Vessel Closure Head Degradation 2-3

2.4.1 Sub-Components 2-3

2.4.2 Failure / Degradation Mechanisms 2-3

2.5 Failure-Path Flow Chart 2-6

2.6 Conclusions 2-7

2.7 References 2-7

3 **SUMMARY OF FLAW AND WASTAGE TOLERANCE CALCULATIONS 3-1**

3.1 Flaw Tolerance Calculations 3-1

3.1.1 Axial Flaw in Nozzle Above J-Groove Weld 3-1

3.1.2 Circumferential Flaw in Nozzle Above J-Groove Weld 3-1

3.1.3 Lack of Fusion or Circumferential Weld Crack at J-Groove Weld Interface 3-2

3.2 Allowable Wastage Volume at Reactor Vessel Head CRDM Nozzles 3-2

3.3 References 3-3

4 INSPECTION EXPERIENCE 4-1
4.1 Introduction 4-1
4.2 Background Information 4-2
4.2.1 Alloy 600 in PWR Plants 4-2
4.2.2 Summary of Key Events 4-3
4.3 Inspection Results 4-5
4.3.1 Summary 4-5
4.3.2 Subgroup Statistics 4-7
4.4 Planned Head Replacements and Inspections 4-8
4.5 Conclusions 4-8
4.6 References 4-8

5 WELDING RESIDUAL STRESS AND STRESS INTENSITY FACTOR CALCULATIONS 5-1
5.1 Introduction 5-1
5.2 Residual Stress Analyses 5-1
5.2.1 Overview 5-1
5.2.2 DEI FEA Model 5-3
5.2.3 AREVA FEA Model (MRP-103) 5-4
5.3 Stress Intensity Factor Calculations 5-5
5.3.1 Superposition Technique (MRP-105) 5-5
5.3.2 Fracture Mechanics Finite Element Model (MRP-104) 5-6
5.3.3 AREVA Stress Intensity Factor Curve (MRP-103) 5-7
5.3.4 Other Approaches 5-7
5.4 Stress Analysis to Support Wastage Assessment 5-8
5.5 Summary 5-8
5.6 References 5-8

6 NOZZLE EJECTION EVALUATIONS 6-1
6.1 Introduction 6-1
6.2 Deterministic Inputs and Analyses 6-2
6.2.1 MRP-105 6-2
6.2.2 MRP-104 (Westinghouse and CE Design Plants) 6-3
6.2.3 MRP-103 (B&W Design Plants) 6-3
6.3 Probabilistic Analyses 6-4
6.3.1 MRP-105 6-4

6.3.2 MRP-104 (Westinghouse and CE Design Plants) 6-5
6.3.3 MRP-103 (B&W Design Plants) 6-5
6.4 Conclusion 6-6
6.5 References 6-7

7 HEAD WASTAGE EVALUATIONS 7-1
7.1 Davis-Besse Operating Experience 7-1
7.2 Relevant Industry Experience 7-2
7.2.1 U.S. Experience with Leaking CRDM Nozzles 7-2
7.2.2 U.S. Experience with Other Alloy 600 Penetrations and Alloy 182/82 Welds 7-3
7.2.3 U.S. Experience with Leakage from Mechanical Joints and Seal Welds 7-4
7.2.4 International Experience 7-5
7.3 Modeling of the Head Wastage Process 7-5
7.4 Relevant Experimental Investigations and Additional Planned Research 7-6
7.5 Conclusions 7-7
7.6 References 7-7

8 CONSEQUENTIAL DAMAGE ASSESSMENT 8-1
8.1 Introduction 8-1
8.2 Evaluation 8-2
8.3 Effect of Consequential Damage on ECCS 8-3
8.4 Effect of Consequential Damage on Reactivity Control 8-4
8.5 Generation of Loose Parts 8-6
8.6 Large Early Release Frequency (LERF) 8-7
8.7 Conclusion 8-7
8.8 Recommendations 8-8
8.9 References 8-8

9 INSPECTION CAPABILITIES 9-1
9.1 Visual Examination for Detecting Leakage 9-1
9.2 Specialized Leak Detection Sensors 9-2
9.3 Nondestructive Examination of Vessel Head Penetration Nozzles and Welds 9-2
9.3.1 Nozzle Base Metal Non-Destructive Examinations 9-3
9.3.1.1 Surface Examinations Using Eddy Current Testing 9-3
9.3.1.2 Volumetric Examination Using Ultrasonic Testing 9-3
9.3.2 Penetration Weld Metal Non-Destructive Examinations 9-4

9.3.2.1 Surface Examinations Using Eddy Current Tests 9-4
9.3.2.2 Surface Examinations Using Dye Penetrant Testing 9-5
9.4 References 9-5

***10* REPLACEMENT HEAD MATERIALS 10-1**
10.1 Introduction 10-1
10.2 Summary of Laboratory Data 10-1
10.2.1 Test Conditions 10-1
10.2.2 PWSCC Test Data for Alloy 690 Base Metal 10-2
10.2.2.1 Thin-wall (Steam Generator Tube) Materials 10-2
10.2.2.2 Thick-wall Materials 10-2
10.2.3. PWSCC Test Data for Alloy 52 and 152 Weld Metal 10-3
10.2.4. General Corrosion Rate and Metal Release Rate Tests 10-4
10.2.5. Summary of Test Results 10-4
10.2.6. Calculated Material Improvement Factors 10-4
10.3 Operating Experience for Alloy 690/52/152 Materials in PWRs 10-5
10.3.1 Steam Generator Tubing Experience 10-5
10.3.2 Other PWR Experience Including Experience with Thick-wall Materials 10-6
10.4 Conclusions 10-6
10.5 References 10-7

***A* HEAD MAPS AND PENETRATION DESIGNS A-1**
A.1 Penetration Locations on Reactor Vessel Heads A-1
A.2 Penetration Designs A-1

***B* FMEA FAILURE-PATH DISPOSITION TABLE B-1**

***C* FMEA TECHNICAL DISCUSSIONS C-1**
C.1 Materials and Effects on Cracking C-1
C.1.1 Material Properties due to Thermal Processing C-1
C.1.2 Defects due to Initial Material Processing C-2
C.1.3 Nozzle Roll Straightening During Material Processing C-2
C.2 Fabrication and Effects on Cracking C-3
C.2.1 Stress Impact of Machining, Reaming, or Grinding of Nozzle ID or OD Surfaces C-3
C.2.2 Defects Introduced by Nozzle ID Processing C-4

C.2.3 Weld Fabrication Flaws C-4
C.2.4 Nozzle Straightening After Installation C-6
C.2.5 Grinding of Weld During Head Fabrication C-7
C.2.6 Welding Residual Stresses C-7
C.2.7 Fabrication Residual Stresses C-8
C.2.8 Lack-of-Fusion Flaws C-8
C.2.9 Surface Contaminants C-11
C.3 Water Chemistry and Effects on Cracking C-13
C.3.1 Typical Primary-Side Chemistry During Power Operation C-13
C.3.2 Impact of Hydrogen at Low Temperature C-13
C.3.3 Water Chemistry During Hot Functional Testing C-14
C.3.4 Impact of Reduced Sulfur Species on Sensitized Alloy 600 ..... C-14
C.3.5 Lead Involvement in Causing PWSCC C-17
C.3.6 Conclusions on Water Chemistry C-17
C.4 PWSCC C-18
C.4.1 Weibull Distributions for PWSCC Initiation C-18
C.4.2 PWSCC Crack Growth C-19
C.4.3 PWSCC Location and Orientation C-21
C.5 Fatigue C-22
C.5.1 Plant Temperature and Pressure Changes C-23
C.5.2 Temperature Cycling Inside the CRDM Nozzle C-23
C.5.3 Mechanical Vibrations C-24
C.5.4 Summary on Fatigue C-24
C.6 Low-Temperature Crack Propagation C-25
C.7 Nozzle Repair Reliability C-25
C.7.1 Embedded Flaw Repairs C-26
C.7.2 Application of a New Structural Weld in the Existing Nozzle C-26
C.8 References C-26

_D_ FLAW AND WASTAGE TOLERANCE CALCULATIONS D-1
D.1 Limiting Crack Sizes in Nozzles and Welds D-1
D.1.1 Axial Flaw in Nozzle Above J-Groove Weld D-2
D.1.2 Circumferential Flaw in Nozzle Above J-Groove Weld D-2
D.1.3 Lack of Fusion or Circumferential Weld Crack at J-Groove Weld Interface D-4
D.2 Allowable Wastage Volume at Reactor Vessel Head CRDM Nozzles D-4

D.2.1 Allowable Corrosion Volume Based on Finite Element Analysis D-5
D.2.1.1 Allowable Wastage Volume—Wastage Located Between Nozzles D-5
D.2.1.2 Allowable Wastage Volume—Wastage Distributed Around Nozzle D-6
D.2.2 Allowable Corrosion Volume for Other Head Designs D-6
D.3 References D-6

***E* MODELING OF HEAD WASTAGE PROCESS E-1**
E.1 Volume of Boric Acid Deposits Detectable by BMV Inspection E-1
E.2 Volume of Boric Acid Deposits versus Leak Rate..... E-1
E.3 Leak Rate to Produce Rapid Corrosion E-2
E.4 Deterministic Evaluation Based on Crack Growth Rate..... E-3
E.5 Probabilistic Evaluation Based on Monte Carlo Wastage Model E-5
E.6 Description of the Probabilistic Wastage Model..... E-7
E.6.1 Wastage Model Basics..... E-8
E.6.2 Leak Rate to Produce Rapid Corrosion Based on Thermal Analysis..... E-9
E.6.3 Statistical Distributions Used for Inputs..... E-10
E.6.4 Monte Carlo Calculations E-13
E.7 Refinement of Modeling Assumptions and Inputs..... E-14
E.8 References..... E-14

LIST OF TABLES

Table 1-1 RV Closure Head Nozzle Design Data for Original Heads at Operating U.S. PWRs 1-9
Table 2-1 Plausible RVCH Aging Degradation Mechanisms 2-4
Table 2-2 Key Parameters for Plausible Aging Degradation Mechanisms 2-5
Table 3-1 Critical Flaw Angles for Through-Wall Circumferential Nozzle Flaws 3-4
Table 4-1 Chronology of Key Leading Events Related to PWSCC of Alloy 600 Type Materials in PWR Plant Applications Other Than Steam Generator Tubing 4-9
Table 4-2 Summary of Key Parameters Related to Reactor Vessel Closure Head Nozzle PWSCC 4-11
Table 4-3 Summary of Plants with Detected Reactor Vessel Closure Head Penetration Cracking 4-13
Table 4-4 Summary of Reactor Vessel Closure Head Penetration Leakage 4-14
Table 4-5 Orientation and Location for Reactor Vessel Closure Head Nozzle Cracks 4-15
Table 4-6 Summary of Nozzle Circumferential Cracks Located Above the Weld, in the Weld Elevation Zone, or Below the Weld 4-16
Table 4-7 Summary of Inspections of Reactor Vessel Closure Head Penetration J-Groove Welds 4-18
Table 4-8 Completed and Announced Reactor Vessel Closure Head Replacements (as of 1/2004) 4-19
Table 6-1 Nozzle Ejection Evaluation Summary Table 6-8
Table 7-1 U.S. PWR Experience with Leaking CRDM Nozzles Relevant to Head Wastage 7-9
Table 10-1 Specified Compositions of Alloy 600 and Alloy 690 and Associated Weld Materials (wt %) 10-10
Table 10-2 Summary of Alloy 690 Primary Water Stress Corrosion Test Data [10-2] 10-11
Table 10-3 Summary of Alloy 690/52/152 Hydrogenated and Doped Hydrogenated Steam Stress Corrosion Test Data [10-2] 10-12
Table 10-4 U.S. PWR Steam Generators with Alloy 690 Tubes (as of March 2004) 10-13
Table 10-5 International PWR Steam Generators with Alloy 690 Tubes (as of March 2004) 10-15
Table 10-6 Alloy 690/152/52 RCS (Excluding Steam Generators) Replacement Component Items and Welds for U.S. PWRs 10-17
Table 10-7 Alloy 690/152/52 Reactor Coolant System (Excluding Steam Generators) Original Equipment or Replacement Component Items and Welds for International PWRs 10-19

Table B-1 Failure Path Disposition Table for RVCH Penetration FMEA..... B-2
Table C-1 North Anna 2 CRDM Nozzle Lack-of-Fusion Indications, Fall 2002 UT Inspection..... C-10
Table C-2 Typical Values of Weibull Slopes for Steam Generator Tube PWSCC Based on Plant Data [C-40]..... C-19
Table C-3 Summary of Industry Experience Regarding Circumferential Nozzle Cracking and Leakage C-22
Table D-1 Critical Flaw Angles for Through-Wall Circumferential Nozzle Flaws D-8
Table E-1 Input Statistical Distributions Used in Monte Carlo Calculations of Wastage..... E-16

LIST OF FIGURES

Figure 1-1 Typical Reactor Vessel Head—Oconee 1 (Babcock & Wilcox Design) 1-11
Figure 1-2 Typical CRDM Nozzle (Babcock & Wilcox Design) 1-12
Figure 1-3 CRDM, CEDM and ICI Nozzle Designs 1-13
Figure 1-4 Overall Safety Assessment Process Including Inspection Results Feedback 1-14
Figure 1-5 Process for Developing the Safety Assessment for Reactor Vessel Closure Head Penetrations 1-15
Figure 1-6 Inspection Feedback Process 1-16
Figure 2-1 CRDM Nozzle and Weld Flaw Geometries 2-9
Figure 2-2 Flow Chart for MRP Failure Mode and Effect Analysis for Reactor Vessel Closure Head Penetrations 2-11
Figure 3-1 Limit Load Pressure versus Circumferential Flaw Angle for Limiting Nozzle Geometries 3-5
Figure 3-2 Finite Element Model—Wastage Between Adjacent Nozzles 3-6
Figure 4-1 Locations of Cracks in Bugey 3 CRDM Nozzle 54 (cross section through leaking crack) 4-20
Figure 4-2 Definition of Nozzle Regions with Respect to the Location of the J-Groove Weld 4-21
Figure 4-3 Reactor Vessel Closure Head Inspection Statistics—by EDY Group 4-22
Figure 4-4 Reactor Vessel Closure Head Inspection Statistics—by Head Fabricator (All EDYs) 4-23
Figure 4-5 Reactor Vessel Closure Head Inspection Statistics—by Head Fabricator (>12 EDYs) 4-23
Figure 4-6 Reactor Vessel Closure Head Inspection Statistics—by Head Fabricator (8–12 EDYs) 4-24
Figure 4-7 Reactor Vessel Closure Head Inspection Statistics—by Head Fabricator (<8 EDYs) 4-24
Figure 4-8 Reactor Vessel Closure Head Inspection Statistics—by Nozzle Material Supplier (All EDYs) 4-25
Figure 4-9 Reactor Vessel Closure Head Inspection Statistics—by Nozzle Material Supplier (>12 EDYs) 4-25
Figure 4-10 Reactor Vessel Closure Head Inspection Statistics—by Nozzle Material Supplier (8–12 EDYs) 4-26
Figure 4-11 Reactor Vessel Closure Head Inspection Statistics—by Nozzle Material Supplier (<8 EDYs) 4-26
Figure 5-1 Evolution of the DEI Penetration Finite Element Model 5-10

Figure 5-2 Example CRDM Penetration Finite Element Model 5-11
Figure 5-3 Example Fracture Mechanics Model 5-11
Figure 5-4 Stress Intensity Factors Assumed in the MRP Nozzle Ejection Safety Assessment (Downhill Centered Cracks) 5-12
Figure 5-5 Stress Intensity Factors Assumed in the MRP Nozzle Ejection Safety Assessment (Uphill Centered Cracks) 5-12
Figure 5-6 Comparison of Assumed Stress Intensity Factors with Other Available Results (Downhill Centered Cracks) 5-13
Figure 5-7 Comparison of Assumed Stress Intensity Factors with Other Available Results (Uphill Centered Cracks) 5-13
Figure 6-1 Example of Crack Growth Around Nozzle Circumference Above J-Groove Weld 6-9
Figure 8-1 Typical Reactor Vessel Head—Assembled Isometric 8-10
Figure 8-2 Typical Reactor Vessel Head—Cutaway Isometric 8-11
Figure 8-3 Typical Reactor Vessel Head—Close-up Cutaway Isometric 8-12
Figure 9-1 Available Inspection Options for RVCH Penetrations 9-6
Figure 10-1 Weibull Plot Illustrating First Method for Determining Material Improvement Factor 10-20
Figure 10-2 Weibull Plot Illustrating Second Method for Determining Material Improvement Factor 10-20

Figure A-1 Penetration Locations—Westinghouse 2-Loop Plants A-2
Figure A-2 Penetration Locations—Westinghouse 3-Loop Plants A-3
Figure A-3 Penetration Locations—Westinghouse 4-Loop Plants Without Adapters A-4
Figure A-4 Penetration Locations—Westinghouse 4-Loop Plants With Adapters A-5
Figure A-5 Penetration Locations—Combustion Engineering Plants A-6
Figure A-6 Penetration Locations—Combustion Engineering Plants A-7
Figure A-7 Penetration Locations—Combustion Engineering Plants A-8
Figure A-8 Penetration Locations—B&W Plants A-9
Figure A-9 Penetration Designs—Control Rod Drive Mechanism (CRDM) Nozzles A-10
Figure A-10 Penetration Designs—Control Element Drive Mechanism (CEDM) Nozzles A-11
Figure A-11 Penetration Designs—Incore Instrument (ICI) Nozzles A-12
Figure A-12 Penetration Designs—Head Vent Nozzles A-13
Figure A-13 Penetration Designs—Thermocouple Nozzles (Small Diameter ~1 inch) A-14
Figure A-14 Penetration Designs—Internals Support Housing Nozzles A-15
Figure A-15 Penetration Designs—Auxiliary Head Adapter Nozzles A-16
Figure A-16 Penetration Designs—De-Gas Line Nozzles A-17
Figure D-1 Basic Flaw Orientations on a Typical CRDM Nozzle D-9
Figure D-2 Finite Element Model of Typical PWR Head Used for Allowable Wastage Volume Calculation D-10

Figure D-3 Finite Element Model—Wastage Between Adjacent Nozzles D-11
Figure D-4 Finite Element Analysis Results—Wastage Between Adjacent Nozzles D-12
Figure D-5 Finite Element Model—Wastage Distributed Around Single Nozzle D-13
Figure D-6 Finite Element Analysis Results—Wastage Distributed Around Single Nozzle ... D-14
Figure E-1 Leakage Detectability E-17
Figure E-2 Through-Wall Axial Crack Profiles: a) Crack geometry based on available plant data; b) Uniform crack profile assumed in leak rate and crack growth modeling ... E-18
Figure E-3 Leak Rate versus Crack Length According to Analytical Models E-19
Figure E-4 Assumed Nominal Leak Rate versus Crack Length Relationship Based on Available Plant Data E-19
Figure E-5 Time for Leak Rate to Increase from Level Detectable by Bare Metal Visual (BMV) Inspections (2×10^{-5} gpm) to the Critical Leak Rate that May Lead to Rapid Corrosion (0.1 gpm) Using the Deterministic Crack Growth Rate Curve Recommended by Report MRP-55 [E-6] for Alloy 600 ..... E-20
Figure E-6 Simplified Flow Chart for the Probabilistic Wastage Model E-21
Figure E-7 Cavity Progression for a Top-Down Corrosion Mode E-22
Figure E-8 Photographs of Davis-Besse Wastage Cavity Adjacent to Nozzle #3 [E-7] E-23
Figure E-9 Assumed Dependence of Linear Wastage Rate on Leak Rate Based on Available Data: a) Log scale for leak rate; b) Linear scale for leak rate E-24
Figure E-10 Development of Wastage Cavity: a) Apparent actual cavity development adjacent to Davis-Besse nozzle #3; b) Cavity growth geometry assumed for the probabilistic wastage model E-25
Figure E-11 Results of the Probabilistic Wastage Calculations E-26
Figure E-12 Expansion Cooling Heat Sink Rate Versus Leak Rate E-27
Figure E-13 Example Thermal Analysis Results: Temperature Contours (°F) for a Uniform 1860 Btu/h Heat Sink on 45° Total Arc Surface Corresponding to Complete Vaporization of a 0.007 gpm Leak (Heat Transfer Coefficient on Inside Head Surface of 110 Btu/h-ft^2-°F) E-28
Figure E-14 Average Metal Temperature Along Small Cavity Leak Path Versus Heat Sink Magnitude E-29

1
INTRODUCTION AND SUMMARY

1.1 Background

Inspections of penetration nozzles in PWR reactor vessel closure heads (RVCHs) have shown that these Alloy 600 components are susceptible to aging degradation due to primary water stress corrosion cracking (PWSCC). Several PWR plants in the U.S. have experienced cracks in control rod drive mechanism (CRDM) nozzles and J-groove welds, and some of these plants have experienced primary coolant leaks from through-thickness cracks in the nozzles or welds. The stresses that make the nickel-chromium-iron Alloy 600 nozzles and their Alloy 182 J-groove attachment welds susceptible to cracking are induced by the welding of the nozzle to the inside surface of the RVCH during vessel fabrication.

Since late 2000, inspections in the U.S. have shown that although most of the observed nozzle cracking is axial in orientation, several circumferentially oriented cracks have been detected above the top of the J-groove weld. Such circumferential cracks could potentially lead to nozzle ejection and a small- or medium-break loss of coolant accident (LOCA) if the circumferential crack were to grow most of the way around the nozzle, typically to a size of at least 330°. A second potential safety concern is boric acid corrosion of the low-alloy steel material of the RVCH. The large wastage cavity observed at the Davis-Besse plant in 2002 resulted from what is believed to be at least six years of leakage and concentration of the borated reactor coolant. As of December 2003, the heads at 10 U.S. plants have been replaced due to concerns regarding PWSCC, and at least 23 additional heads have been scheduled for replacement.

In response to these concerns, the U.S. NRC has issued three bulletins and one order:

- NRC Bulletin 2001-01, "Circumferential Cracking of Reactor Pressure Vessel Head Penetration Nozzles" [1-1]
- NRC Bulletin 2002-01, "Reactor Pressure Vessel Head Degradation and Reactor Coolant Pressure Boundary Integrity" [1-2]
- NRC Bulletin 2002-02, "Reactor Pressure Vessel Head and Vessel Head Penetration Nozzle Inspection Programs" [1-3]
- NRC Order EA-03-009, "Order Establishing Interim Inspection Requirements for Reactor Pressure Vessel Heads at Pressurized Water Reactors" [1-4]

The order, which was issued on February 11, 2003 and revised on February 20, 2004 [1-5], specifies interim inspection requirements for all domestic RVCH penetrations.

1.2 Purpose

The objective of this report is to provide a final safety assessment for PWSCC of Alloy 600 RVCH nozzles and related Alloy 182 J-groove welds in PWR plants. This report and the referenced documents form the technical basis for the MRP inspection plan for RVCH penetrations, which is currently being drafted by the MRP. The MRP safety assessment and inspection plan documents are intended to form the basis for requirements that are intended to replace NRC Order EA-03-009.

1.3 RVCH Penetration Design Data

RVCHs in PWR plants have a number of penetrations that are used for various purposes including CRDM nozzles (known as control element drive mechanism—CEDM—nozzles in Combustion Engineering plants), instrument nozzles, head vent nozzles, and thermocouple nozzles. Figure 1-1 shows a typical RVCH arrangement for a plant designed by Babcock & Wilcox (B&W). The plants designed by Westinghouse and Combustion Engineering have closure head configurations similar to the B&W configuration. Figure 1-2 shows a typical CRDM nozzle that is installed into a hole in the vessel head, typically with a small interference fit, and then welded to the inside surface of the head by a partial penetration Alloy 182 J-groove attachment weld. Figure 1-3 labels the head components in the region of the J-groove weld for a typical CRDM nozzle geometry. Also shown is the similar in-core instrumentation (ICI) nozzle geometry.

Table 1-1 lists the basic design data for the 69 original heads corresponding to the set of currently operating PWR units. As noted, 10 of these heads have already been replaced, with nine using more PWSCC resistant Alloy 690 material. The table lists the designer, nozzle material supplier, head fabricator, specified nozzle interference fit, and number of RVCH penetrations of each type. The table also identifies which of the head map figures in Appendix A corresponds to each plant. Appendix A also presents sketches of each type of RVCH penetration.

1.4 Scope

This safety assessment addresses RVCH penetrations that are joined to the inside surface of the head with a J-groove attachment weld. The calculations presented in this and the referenced nozzle ejection assessment reports are based on the CRDM, CEDM, and ICI penetration geometries. These nozzles comprise 5,055 of the total 5,139 RVCH penetrations in the set of original heads for the 69 currently operating units. As shown in Table 1-1, in addition to the CRDM, CEDM, and ICI penetrations, there are also the following types of RVCH penetrations attached with J-groove welds:

- Fifty-eight J-groove head vent nozzles in 58 heads
  Each Westinghouse and CE design plant has a single head vent nozzle. Fifty-eight of these 62 nozzles are attached with a J-groove weld to the inside of the head. These nozzles are not specifically addressed in the nozzle ejection assessments because the consequences of an ejection of such a nozzle are less severe than those associated with the larger diameter

CRDM, CEDM, and ICI nozzles. The typical OD of these nozzles is 1.050 inches with a 0.742 inch ID (3/4 NPS schedule 80). In addition, 17 of these penetrations have been inspected using nonvisual NDE techniques with no reported indications despite 14 of the 17 being in heads having greater than 12 effective degradation years (EDYs) (see Table 4-2).

Because of the larger size and greater potential safety significance of CRDM, CEDM, and ICI nozzles and because of the good PWSCC experience with the small-diameter head vent nozzles to date, the RVCH penetration calculations discussed in this document are focused on the geometries of the CRDM, CEDM, and ICI penetrations.

- Sixteen small-diameter thermocouple nozzles in two B&W design plants
  All 16 of these nominal 1-inch OD nozzles were found to be cracked after leakage was detected from 13 of them based on the presence of boric acid deposits. All 16 were repaired using Alloy 690 plugs, and subsequently the two heads having these 16 nozzles have been replaced with heads using Alloy 690 nozzles.
- Eight auxiliary head adapter nozzles in two heads
  Two sister units at one Westinghouse design station have four each of this type of penetration, which is shown on the left side of Figure A-15. Note that for these nozzles the weld preparation is ground into the OD of the tube wall. Calculations specific to this particular geometry are not presented or referenced in this report. However, the results of the nozzle ejection and head wastage evaluations are not overly sensitive to nozzle and weld geometry, so the safety assessment is expected to bound these nozzles, particularly given that these nozzles are installed in heads operating near the reactor cold leg temperature. Nozzles operating near the cold leg temperature have a significantly reduced likelihood of cracking compared to nozzles operating near the hot leg temperature because PWSCC is a thermally activated process.
- Two de-gas line nozzles in two heads
  Two sister units at another Westinghouse design station have one each of this type of penetration, which is shown in Figure A-16. The design and dimensions of this nozzle are very similar to those for some of the ICI nozzles. Therefore, it is considered to be covered by this safety assessment. In addition, these nozzles are installed in heads currently operating near the reactor cold leg temperature.

The types of RVCH penetrations that do not include J-groove welds are addressed by the existing inspection requirements of Section XI of the ASME Boiler & Pressure Vessel Code. As reported in Table 1-1, there are a total of only 30 such penetrations in the entire fleet. Of these, only the four "butt weld" design head vent nozzles (Figure A-12) are installed in heads not operating near the reactor cold leg temperature.

1.5 Approach

This safety assessment addresses the principal potential safety concerns of nozzle ejection due to circumferential nozzle cracking and head rupture due to boric acid wastage. The flow chart in Figure 1-4 illustrates the overall approach, while Figures 1-5 and 1-6 show additional detail regarding the nozzle ejection evaluations, wastage evaluations, and inspection feedback process.

The detailed failure mode and effect analysis (FMEA) in Section 2 and Appendices B and C is used to verify that these are the main concerns and documents the material, fabrication, and operations factors that affect the likelihood and type of aging degradation mechanisms that potentially affect the RVCH penetrations and surrounding low-alloy steel head material. Deterministic and probabilistic nozzle ejection and head wastage evaluations form the core of the safety assessment, which also includes a compilation of design data, flaw tolerance calculations, inspection experience reviews, stress and fracture mechanics calculations, consequential damage assessment, available information on the resistance of replacement head materials to cracking, and inspection capabilities information.

1.6 Main Conclusions

The safety assessment demonstrates that the typical case of axial nozzle cracking is not a credible mechanism leading to nozzle rupture because the critical axial crack length is much greater than the height of the nozzle region subject to welding residual stresses. The referenced nozzle ejection safety assessment reports (MRP-103 [1-6], MRP-104 [1-7], and MRP-105 [1-8]) demonstrate that there is significant margin against nozzle ejection due to circumferential cracking because of the time required for a circumferential crack to grow to the critical size, typically at least 330°. This safety assessment also demonstrates that periodic bare metal visual examination of the head top surface performed at appropriate intervals provides assurance against significant wastage of the low-alloy steel head material, even given the assumption of a leaking nozzle.

The complete set of safety assessment documents supports the basic conclusion of MRP-105 that a program of periodic nonvisual NDE inspections at appropriate intervals supplemented by periodic bare metal visual examinations provides adequate protection against potential safety-significant failures resulting from aging degradation mechanisms. Furthermore, MRP-105 also shows a low probability of pressure boundary leakage resulting from the appropriate program of periodic inspections. The MRP inspection plan document for reactor vessel closure head penetrations, which is currently under development, will define the appropriate inspection intervals, coverage, and characteristics.

1.7 Report Structure

The organization of this safety assessment report is described below:

1. FAILURE MODE AND EFFECT ANALYSIS (FMEA) (SECTION 2)

   This section describes the failure mode and effect analysis (FMEA) that was applied to potential degradation of RVCH penetrations. The FMEA is a systematic methodology for determining the modes of degradation that could potentially lead to failure, here in the context of nuclear safety. The focus of the FMEA discussion is the FMEA flow chart (Figure 2-2), which shows the interrelationships among the various degradation conditions, beginning with fabrication and operating factors, moving through the potential types of aging degradation including PWSCC, and ending with the LOCA events and core damage. The FMEA results confirm that nozzle ejection and head wastage are the two major

potential safety concerns and help define the inspection capabilities that are needed to detect degradation before defense in depth is compromised.

2. SUMMARY OF FLAW AND WASTAGE TOLERANCE CALCULATIONS (SECTION 3)

   This section summarizes the results of flaw and wastage tolerance calculations to determine (1) the critical crack sizes for the various crack locations and orientations of potential concern and (2) the volume of low-alloy steel that can be lost from the top surface of a reactor vessel head by boric acid corrosion without the stresses in the remaining material exceeding the ASME Code allowable values. The results show that axial flaws long enough to cause rupture of the nozzle are not credible given the extent of the region of welding residual stresses. The results also show that relatively large nozzle or "lack of fusion" type circumferential flaws are required to produce a nozzle ejection. The wastage cavity results show that about 150 in^3 of material can be lost from the upper surface of the head without the stresses in the remaining low-alloy steel ligament exceeding the ASME Code allowable values. In summary, the RVCH and its penetrations are quite flaw tolerant.

3. INSPECTION EXPERIENCE (SECTION 4)

   This section presents the RVCH penetration inspection experience through December 2003, including a chronological summary of key events and summary statistics investigating the effects of operating time, head temperature, vessel fabricator, and nozzle material supplier. As of December 2003, all the original heads have been inspected by bare metal visual examination and/or nonvisual NDE techniques. In addition, only one of the plants having greater than 12 EDYs of operating time normalized to a head temperature of 600°F has yet to perform a nonvisual NDE inspection of all its RVCH nozzles or replace its head. The inspection experience confirms that time at temperature (EDYs) is a key factor governing PWSCC susceptibility, and the experience also shows clearly that some material and fabrication categories are experiencing significantly lower rates of degradation compared to others.

4. WELDING RESIDUAL STRESS AND FRACTURE MECHANICS CALCULATIONS (SECTION 5)

   This section describes the welding residual stress and fracture mechanics calculations that have been performed as an input to the nozzle ejection and head wastage evaluations. The stress calculations are based on a welding residual stress finite element model that includes a thermal simulation of the welding process, elastic-plastic nozzle material properties, and additional load steps simulating hydrostatic testing and operating pressure and temperature conditions. Fracture mechanics calculations to determine the crack tip stress intensity factor input to crack growth calculations for circumferential nozzle flaws have been performed by five organizations, and the reported curves are compared.

5. NOZZLE EJECTION EVALUATIONS (SECTION 6)

   This section summarizes the methodologies and results of the MRP's nozzle ejection safety assessments (MRP-103, MRP-104, and MRP-105). MRP-105 is the principal nozzle ejection safety assessment report and covers all the domestic operating units on the basis of four representative sample plants. This report includes both deterministic calculations of circumferential crack growth and a full probabilistic Monte Carlo simulation of the nozzle ejection process that reflects the uncertainties in the various process parameters. MRP-104 presents deterministic nozzle ejection calculations specifically for the 48 Westinghouse

design and 14 Combustion Engineering design plants, including an assessment of the effect of normal operating pressure and temperature on the initial interference fit between the nozzle and head. MRP-103 is specific to the seven B&W design plants and includes a deterministic calculation and an event-tree probabilistic safety assessment. As described in Section 6, these assessments are similar in form but are based on different input assumptions for a few parameters. The complementary design-specific evaluations support the basic conclusion of MRP-105 that a program of periodic nonvisual NDE inspections at appropriate intervals supplemented by periodic bare metal visual examinations provides adequate protection against nozzle ejection. Furthermore, MRP-105 also shows a low probability of pressure boundary leakage resulting from the appropriate program of periodic inspections.

6. HEAD WASTAGE EVALUATIONS (SECTION 7)

   This section describes the evaluations used to show that adequate protection against boric acid wastage is provided by bare metal visual examinations performed at appropriate intervals for evidence of leakage. The wastage evaluation is supported by the experience with over 50 leaking CRDM nozzles, including the observation that the Davis-Besse wastage cavity would have been detected relatively early in the wastage progression had bare metal visual examinations been performed at each refueling outage—and likely even if performed less frequently—with appropriate corrective action. Section 7 also references the wastage modeling work in Appendix E that supports the conclusions of the wastage evaluation.

7. CONSEQUENTIAL DAMAGE ASSESSMENT (SECTION 8)

   This section presents an assessment of consequential damage given nozzle ejection or rupture of the head due to boric acid wastage. This assessment shows that the conditional core damage probability (CCDP) for standard LOCA events can be used to bound the potential effects of consequential damage. Section 8 also includes a discussion of the potential concern for loose parts generation.

8. INSPECTION CAPABILITIES (SECTION 9)

   This section summarizes the inspection tools that are available to detect nozzle leakage or cracking. Section 8 references EPRI 1007842 [1-9], which provides guidance for bare metal visual examination, and MRP-89 [1-10], which summarized the EPRI MRP Alloy 600 ITG's demonstration program for eddy current and ultrasonic examination of RVCH nozzles and associated J-groove welds.

9. REPLACEMENT HEAD MATERIALS (SECTION 10)

   This section summarizes the findings of an MRP study (MRP-111 [1-11]) of the currently available laboratory test data and plant experience regarding the resistance to PWSCC of the standard replacement head materials—Alloy 690 wrought nozzle material and Alloy 52/152 weld metal. Based on the available data, a substantial improvement factor (e.g., at least 25) in resistance to crack initiation is expected. This result supports less frequent nonvisual NDE inspections for replacement heads using Alloy 690 materials compared to the original heads fabricated using Alloy 600 materials, given equivalent time at temperature (EDYs).

10. APPENDIX A: HEAD MAPS AND PENETRATION DESIGNS

    This appendix presents the head map layouts and penetration designs for the 69 currently operating domestic PWR units. Note that these designs reflect the original heads for these units but that 10 of the 69 heads have now been replaced. Table 1-1 in Section 1 identifies the head maps and penetration types for each plant.

11. APPENDIX B: FMEA FAILURE-PATH DISPOSITION TABLE

    This appendix is the detailed failure-path disposition table that corresponds to the FMEA flow chart (Figure 2-2). The failure-path table summarizes the various technical concerns corresponding to each potential failure path, beginning with the materials, fabrication, and operating conditions and ending with the LOCA events and core damage.

12. APPENDIX C: FMEA TECHNICAL DISCUSSIONS

    This appendix discusses various technical issues related to stress corrosion cracking and other forms of environmentally assisted cracking of the Alloy 600 nozzle material and Alloy 182 weld metal material. The discussions are organized according to the structure of the FMEA flow chart (Figure 2-2) and include fabrication and operating conditions (materials, fabrication, and water chemistry), potential types of environmentally assisted cracking (PWSCC, fatigue, and low-temperature crack propagation), and nozzle repair reliability.

13. APPENDIX D: FLAW AND WASTAGE TOLERANCE CALCULATIONS

    This appendix provides details regarding the flaw and wastage cavity tolerance calculations summarized in Section 3. In particular, results of critical size calculations for circumferential nozzle flaws located above the top of the J-groove weld are presented for all CRDM, CEDM, and ICI nozzle dimensions.

14. APPENDIX E: MODELING OF HEAD WASTAGE PROCESS

    This appendix describes deterministic and probabilistic models of the head wastage process, such as that observed at the Davis-Besse plant. These models support the conclusion that bare metal visual examinations performed at appropriate intervals provide adequate protection against wastage. The MRP is currently sponsoring an extensive experimental program to verify and refine the modeling assumptions of Appendix E. The experimental work is expected to include full-scale mockups of leaking CRDM nozzles with a wide range of leak rates and other conditions. The first results from the mockup testing are expected in 2005.

1.8 References

1-1. U.S. Nuclear Regulatory Commission, "Circumferential Cracking of Reactor Pressure Vessel Head Penetration Nozzles," NRC Bulletin 2001-01, August 3, 2001.

1-2. U.S. Nuclear Regulatory Commission, "Reactor Pressure Vessel Head Degradation and Reactor Coolant Pressure Boundary Integrity," NRC Bulletin 2002-01, March 18, 2002.

1-3. U.S. Nuclear Regulatory Commission, "Reactor Pressure Vessel Head and Vessel Head Penetration Nozzle Inspection Programs," NRC Bulletin 2002-02, August 9, 2002.

1-4. U.S. Nuclear Regulatory Commission, "Issuance of Order Establishing Interim Inspection Requirements for Reactor Pressure Vessel Heads at Pressurized Water Reactors," EA-03-009, February 11, 2003.

1-5. U.S. Nuclear Regulatory Commission, "Issuance of First Revised NRC Order (EA-03-009) Establishing Interim Inspection Requirements for Reactor Pressure Vessel Heads at Pressurized Water Reactors," EA-03-009, February 20, 2004.

1-6. *Materials Reliability Program: RV Head Nozzle and Weld Safety Assessment for B&W Plants (MRP-103)*, EPRI, Palo Alto, CA: 2004. 1009402.

1-7. *Materials Reliability Program: RV Head Nozzle and Weld Safety Assessment for Westinghouse and Combustion Engineering Plants (MRP-104)*, EPRI, Palo Alto, CA: 2004. 1009403.

1-8. *Materials Reliability Program: Probabilistic Fracture Mechanics Analysis of PWR Reactor Pressure Vessel Top Head Nozzle Cracking (MRP-105)*, EPRI, Palo Alto, CA: 2004. 1007834.

1-9. *Visual Examination for leakage of PWR Reactor Head penetrations: Revision 2 of 1006296, Includes 2002 Inspection Results and MRP Inspection Guidance*, EPRI, Palo Alto, CA: 2003. 1007842.

1-10. *Materials Reliability Program: Demonstrations of Vendor Equipment and Procedures for the Inspection of Control Rod Drive Mechanism Head Penetrations (MRP-89)*. EPRI, Palo Alto, CA: 2003. 1007831.

1-11. *Materials Reliability Program (MRP): Resistance to Primary Water Stress Corrosion Cracking and Current Operating Experience with Alloys 690, 52, and 152 in Pressurized Water Reactors (MRP-111)*, EPRI, Palo Alto, CA: 2004. 1009801.

Table 1-1
RV Closure Head Nozzle Design Data for Original Heads at Operating U.S. PWRs

Alpabetical Order	Unit Name	NSSS Design	Nozzle Material Supplier[1]	Head Fabricator[2]	Design Diametral Nozzle Interference Fit (mils)	Head Map Figure in Appendix A	*Number of J-Groove Type VHP Nozzles*[3]							*Number of Other VHP Nozzles*[4]		
							CRDM[5]	CEDM[5]	In-Core Instrument (ICI)	J-Groove Head Vent	B&W Thermocouple	Auxiliary Head Adapters	De-Gas Line	Head Vent	Internals Support Housings	Auxiliary Head Adapters
1	ANO 1	B&W	B/H	BW	0.5 – 1.5	A-8a	69									
2	ANO 2	CE	SS/H	CE	0.0 – 3.0	A-6b		81	8	1						
3	Beaver Valley 1	W	H/B	BW/CE	0.0 – 3.0	A-2b	65			1						
4	Beaver Valley 2	W	H	CE	0.0 – 3.0	A-2b	65			1						
5	Braidwood 1	W	B	BW	0.5 – 1.5	A-3a	78			1						
6	Braidwood 2	W	B	BW	0.5 – 1.5	A-3a	78			1						
7	Byron 1	W	B	BW	0.5 – 1.5	A-3a	78			1						
8	Byron 2	W	B	BW	0.5 – 1.5	A-3a	78			1						
9	Callaway	W	H	CE	0.0 – 3.0	A-3a	78			1						
10	Calvert Cliffs 1	CE	H	CE	0.0 – 3.0	A-5c		65	8	1						
11	Calvert Cliffs 2	CE	H	CE	0.0 – 3.0	A-5c		65	8	1						
12	Catawba 1	W	S	RDM	0.4 – 1.2	A-4a	78			1						4
13	Catawba 2	W	H	CE	0.0 – 3.0	A-4a	78			1						4
14	Comanche Peak 1	W	H	CE	0.0 – 3.0	A-3a	78			1						
15	Comanche Peak 2	W	H	CE	0.0 – 3.0	A-3a	78			1						
16	Cook 1	W	H	CE	0.0 – 3.0	A-3b	79			1						
17	Cook 2	W	W	CBI	0.0 – 4.0	A-3a	78			1						
18	Crystal River 3	B&W	B	BW	0.5 – 1.5	A-8a	69									
19	Davis-Besse	B&W	B/H	BW	0.5 – 1.5	A-8a	69									
20	Diablo Canyon 1	W	H	CE	0.0 – 3.0	A-3b	79			1						
21	Diablo Canyon 2	W	H	CE	0.0 – 3.0	A-3a	78			1						
22	Farley 1	W	H/B	BW/CE	0.0 – 3.0	A-2c	69			1						
23	Farley 2	W	B/H	BW/CE	0.0 – 3.0	A-2c	69			1						
24	Fort Calhoun	CE	H	CE	0.0 – 3.0	A-5a		41	6	1						
25	Ginna	W	H	BW	0.5 – 1.5	A-1a	37			1						
26	Indian Point 2	W	H	CE	0.0 – 3.0	A-3c	97							1		
27	Indian Point 3	W	H	CE	0.0 – 3.0	A-3b	78							1		
28	Kewaunee	W	H/B	BW/CE	0.0 – 3.0	A-1b	40			1						
29	McGuire 1	W	H	CE	0.0 – 3.0	A-4a	78			1						4
30	McGuire 2	W	S	RDM	0.4 – 1.2	A-4a	78			1						4
31	Millstone 2	CE	H	CE	0.0 – 3.0	A-6a		69	8	1						
32	Millstone 3	W	H	CE	0.0 – 3.0	A-3a	78			1						
33	North Anna 1	W	S	RDM	0.4 – 1.2	A-2b	65			1						
34	North Anna 2	W	S	RDM	0.4 – 1.2	A-2b	65			1						
35	Oconee 1	B&W	B	BW	0.5 – 1.5	A-8b	69				8					
36	Oconee 2	B&W	B	BW	0.5 – 1.5	A-8a	69									
37	Oconee 3	B&W	B	BW	0.5 – 1.5	A-8a	69									
38	Palisades	CE	H	CE	0.0 – 3.0	A-5b		45	8	1						
39	Palo Verde 1	CE	SS	CE	0.0 – 3.0	A-7b		97		1						
40	Palo Verde 2	CE	SS	CE	0.0 – 3.0	A-7b		97		1						
41	Palo Verde 3	CE	SS	CE	0.0 – 3.0	A-7b		97		1						
42	Point Beach 1	W	H	BW	0.5 – 1.5	A-1c	49			1						
43	Point Beach 2	W	H/B	BW/CE	0.0 – 3.0	A-1c	49			1						
44	Prairie Island 1	W	CL	CL	2.8 – 3.5	A-1b	40			1						
45	Prairie Island 2	W	A	CL	2.8 – 3.5	A-1b	40			1						
46	Robinson 2	W	H	CE	0.0 – 3.0	A-2c	69							1		
47	Salem 1	W	H	CE	0.0 – 3.0	A-3b	79							1		
48	Salem 2	W	H	CE	0.0 – 3.0	A-3a	78			1						

Table 1-1
RV Closure Head Nozzle Design Data for Original Heads at Operating U.S. PWRs (continued)

Alpabetical Order	Unit Name	NSSS Design	Nozzle Material Supplier[1]	Head Fabricator[2]	Design Diametral Nozzle Interference Fit (mils)	Head Map Figure in Appendix A	*Number of J-Groove Type VHP Nozzles*[3]							*Number of Other VHP Nozzles*[4]		
							CRDM[5]	CEDM[5]	In-Core Instrument (ICI)	J-Groove Head Vent	B&W Thermocouple	Auxiliary Head Adapters	De-Gas Line	Head Vent	Internals Support Housings	Auxiliary Head Adapters
49	San Onofre 2	CE	SS/H	CE	0.0 – 3.0	A-7a		91	10	1						
50	San Onofre 3	CE	SS/H	CE	0.0 – 3.0	A-7a		91	10	1						
51	Seabrook	W	H	CE	0.0 – 3.0	A-3a	78			1						
52	Sequoyah 1	W	S	RDM	1.0 – 1.4	A-4a	78			1		4				
53	Sequoyah 2	W	S	RDM	1.0 – 1.4	A-4a	78			1		4				
54	Shearon Harris	W	B	CBI	0.0 – 4.0	A-2b	65			1						
55	South Texas 1	W	H	CE	0.0 – 3.0	A-4b	74			1			1		3	
56	South Texas 2	W	H/B	CE	0.0 – 3.0	A-4b	74			1			1		3	
57	St. Lucie 1	CE	H	CE	0.0 – 3.0	A-6a		69	8	1						
58	St. Lucie 2	CE	SS/H	CE	0.0 – 3.0	A-7a		91	10	1						
59	Summer	W	B	CBI	0.0 – 4.0	A-2b	65			1						
60	Surry 1	W	H	BW/RDM	0.4 – 1.2	A-2a	65			1						
61	Surry 2	W	B/S	BW/RDM	0.4 – 1.2	A-2a	65			1						
62	TMI 1	B&W	B	BW	0.5 – 1.5	A-8b	69				8					
63	Turkey Point 3	W	H	BW	0.5 – 1.5	A-2a	65			1						
64	Turkey Point 4	W	H	BW	0.5 – 1.5	A-2a	65			1						
65	Vogtle 1	W	H	CE	0.0 – 3.0	A-3a	78			1						
66	Vogtle 2	W	H	CE	0.0 – 3.0	A-3a	78			1						
67	Waterford 3	CE	SS/H	CE	0.0 – 3.0	A-7a		91	10	1						
68	Watts Bar 1	W	S	RDM	0.4 – 1.2	A-4a	78			1						4
69	Wolf Creek	W	H	CE	0.0 – 3.0	A-3a	78			1						
						Totals	3871	1090	94							
							4961		94	58	16	8	2	4	6	20
							5055									
							5139							30		
							5169									

NOTES:

[1]Key for Material Suppliers:
B = B&W Tubular Products
H = Huntington
S = Sandvik
SS = Standard Steel
W = Westinghouse (Huntington)
CL = C.L. Imphy
A = Aubert et Duval

[2]Key for Head Fabricators:
BW = B&W
CBI = Chicago Bridge & Iron
CE = Combustion Engineering
RDM = Rotterdam Dockyard
CL = C.L. Imphy

[3]The basic designs of the VHP nozzles are shown in Figures A-9 through A-16 of Appendix A. The nozzle material is Alloy 600 for all J-groove type VHP nozzles.

[4]The basic designs of the VHP nozzles are shown in Figures A-9 through A-16 of Appendix A. The "Butt Weld" head vent, internals support housing, and "Butt Weld" auxiliary head adapter nozzles comprise an Alloy 600 pipe joined to the head as shown in Figures A-12, A-14, and A-15.

[5]Not all CRDM and CEDM nozzles are used for control rod (element) drive shafts. Some CRDM nozzles are empty (spares) or are used for part-length shafts, thermocouple instrumentation or the reactor vessel level instrumentation system, and some CEDM nozzles house heated junction thermocouple instrumentation.

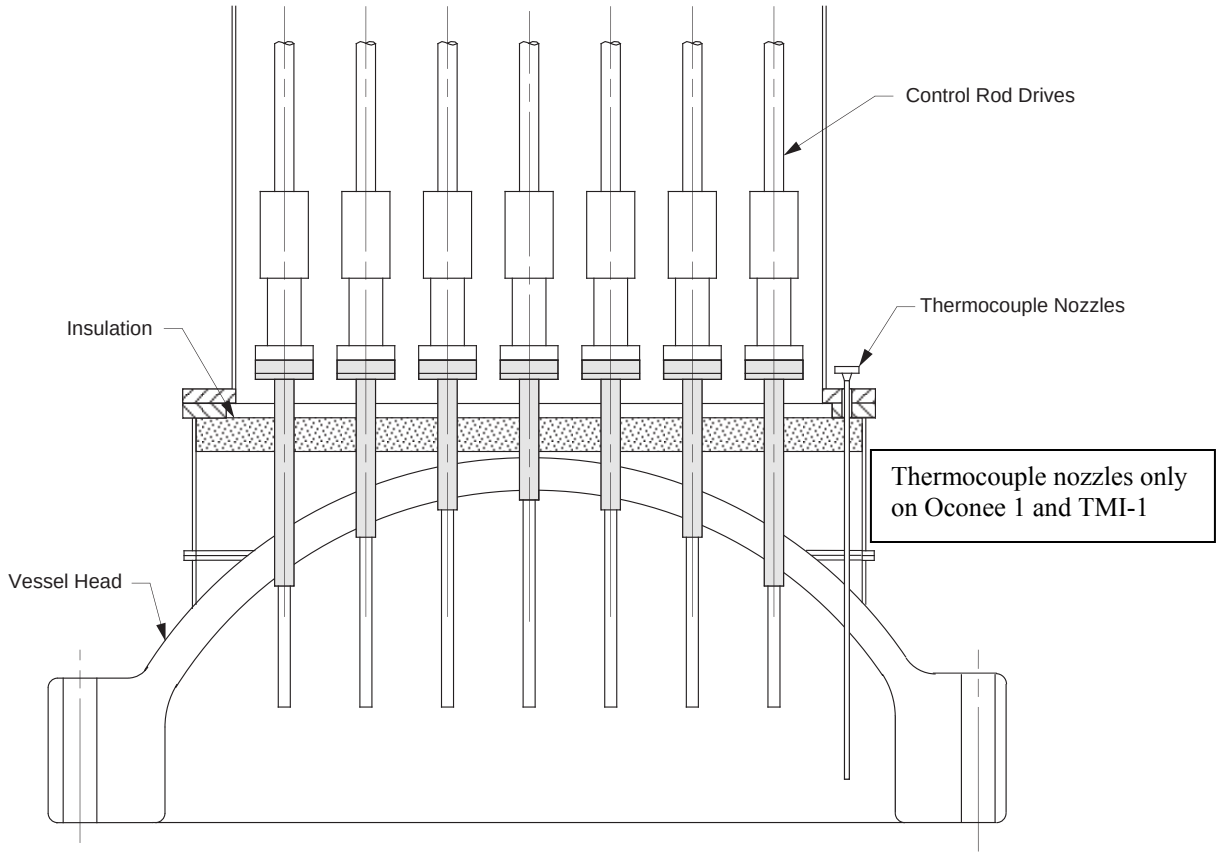

Figure 1-1
Typical Reactor Vessel Head—Oconee 1 (Babcock & Wilcox Design)

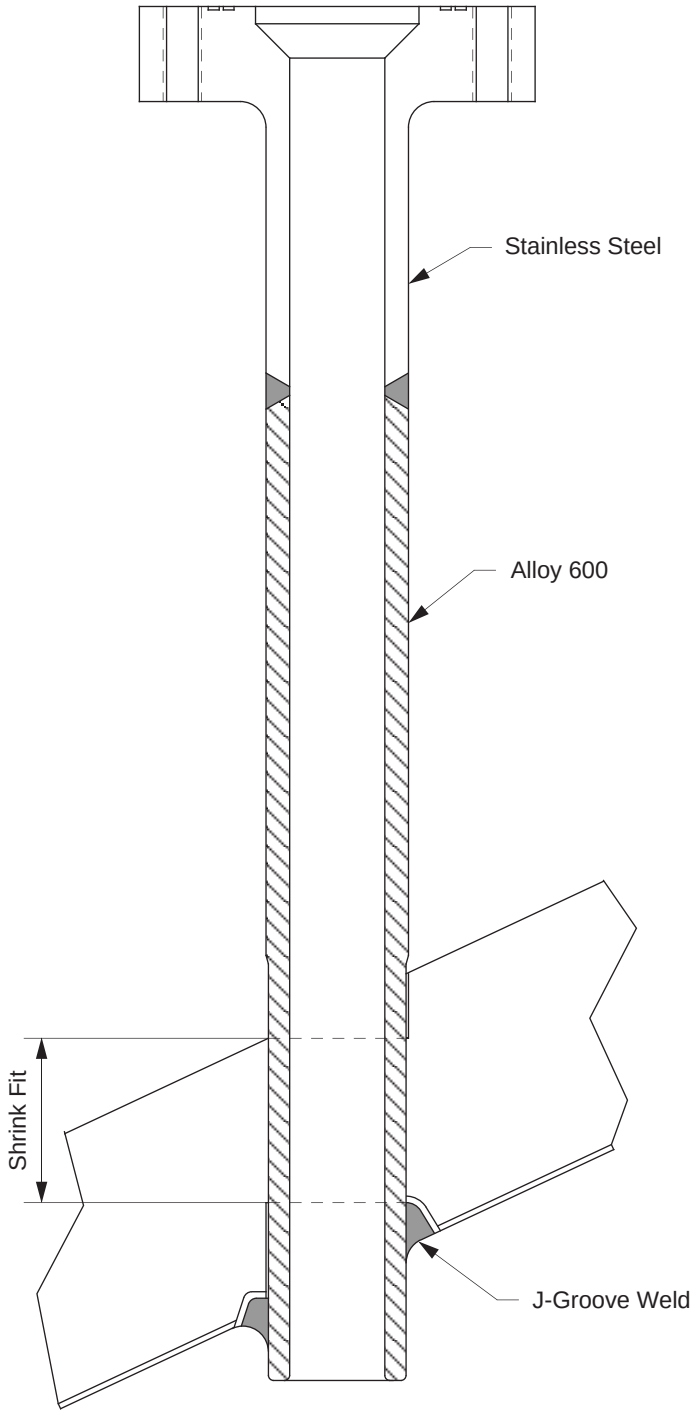

Figure 1-2
Typical CRDM Nozzle (Babcock & Wilcox Design)

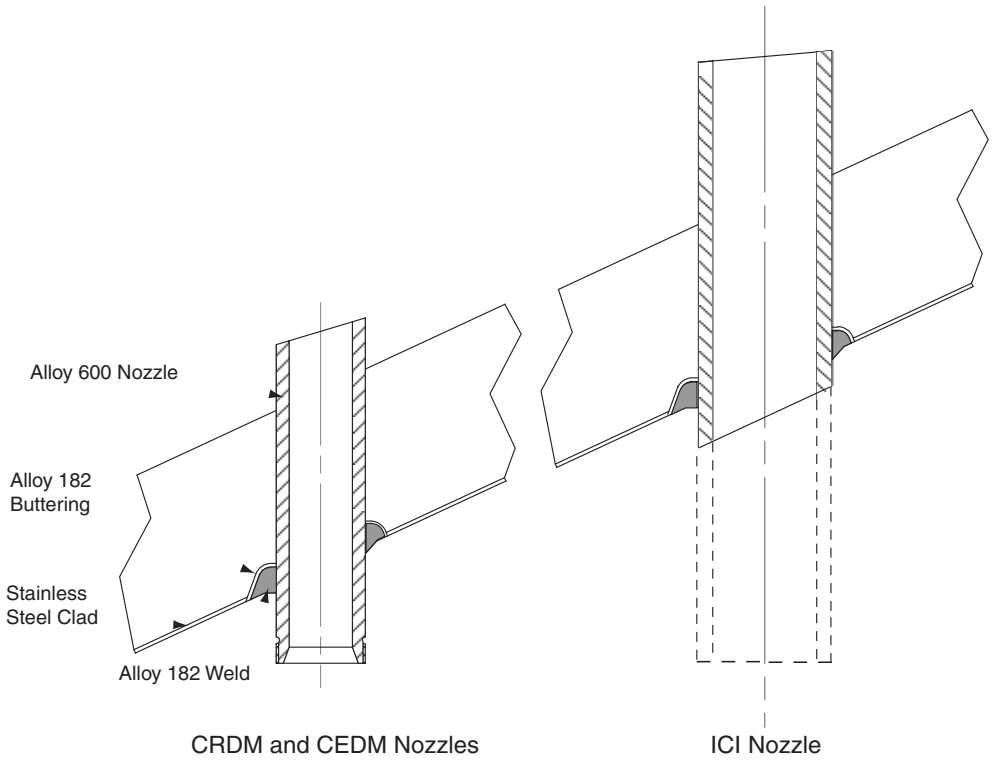

Figure 1-3
CRDM, CEDM and ICI Nozzle Designs

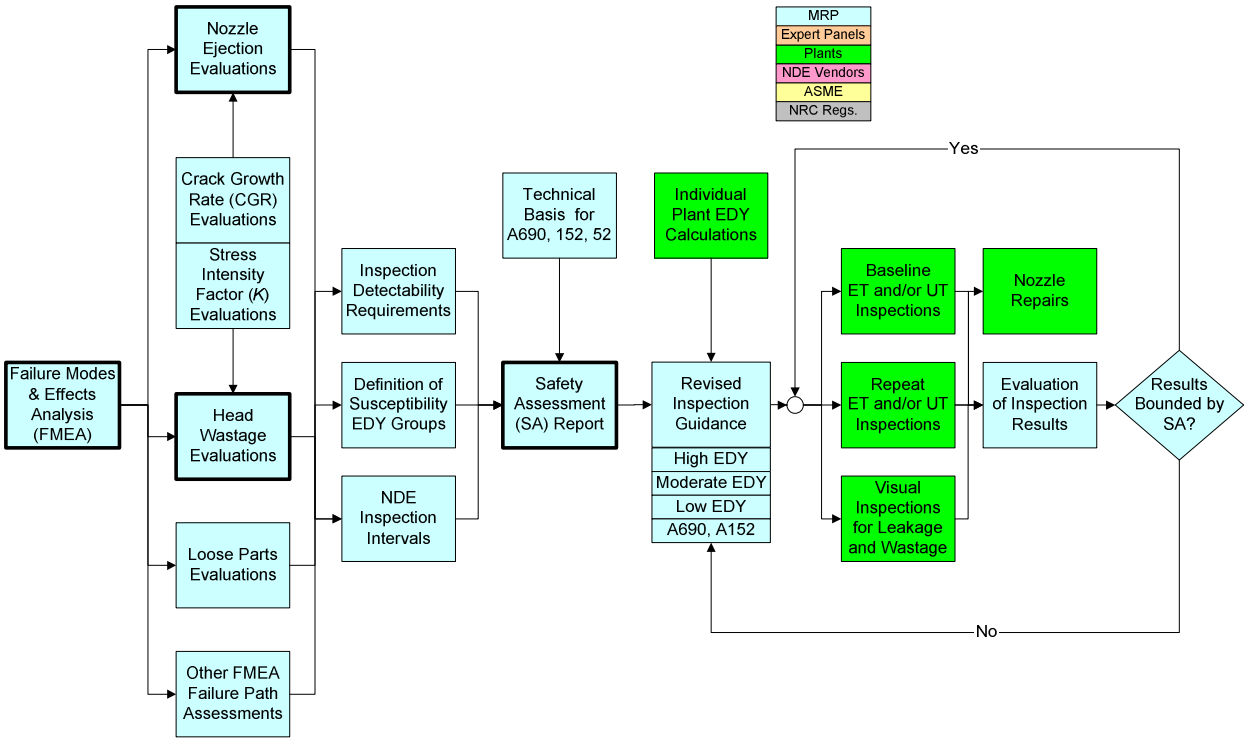

Figure 1-4
Overall Safety Assessment Process Including Inspection Results Feedback

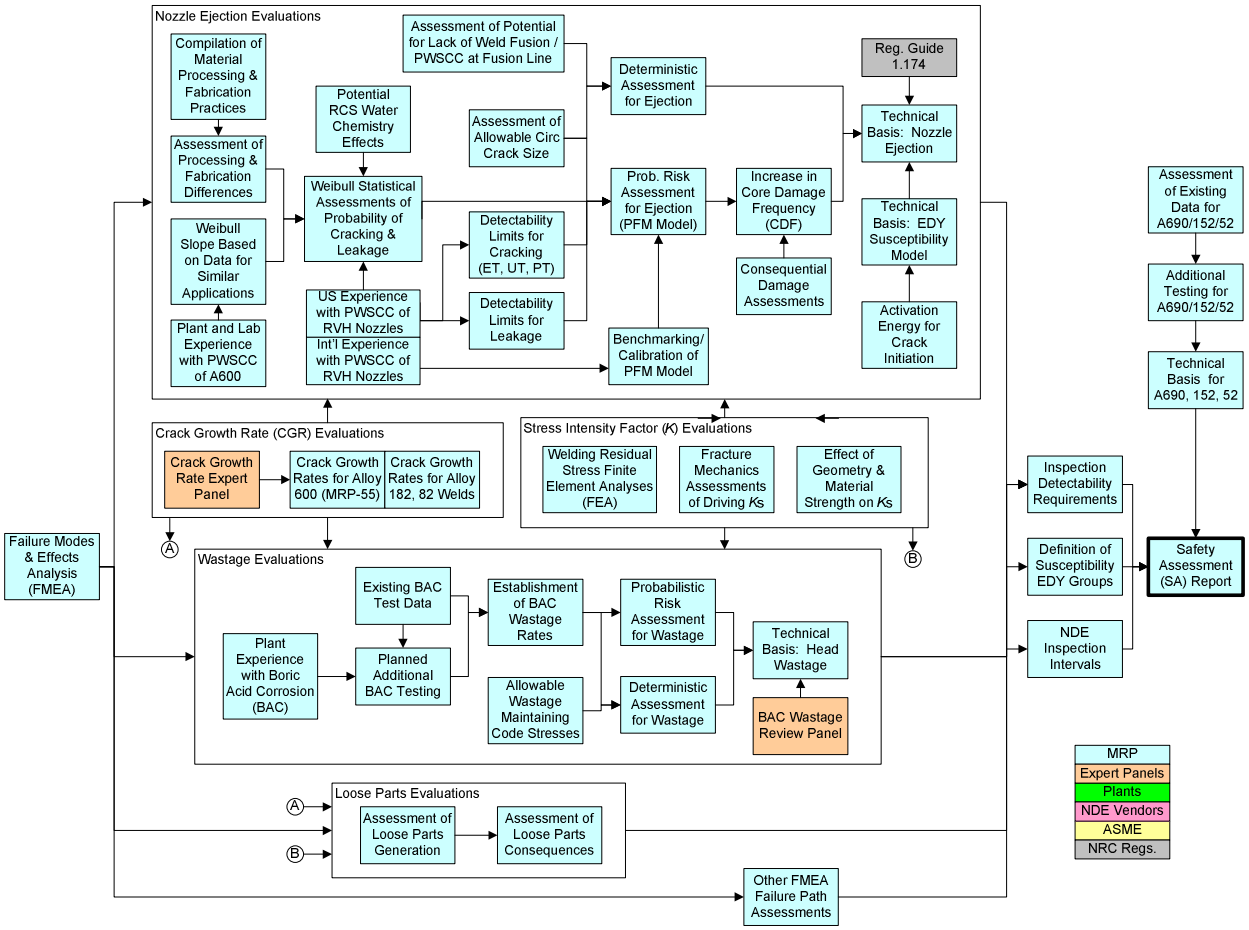

Figure 1-5
Process for Developing the Safety Assessment for Reactor Vessel Closure Head Penetrations

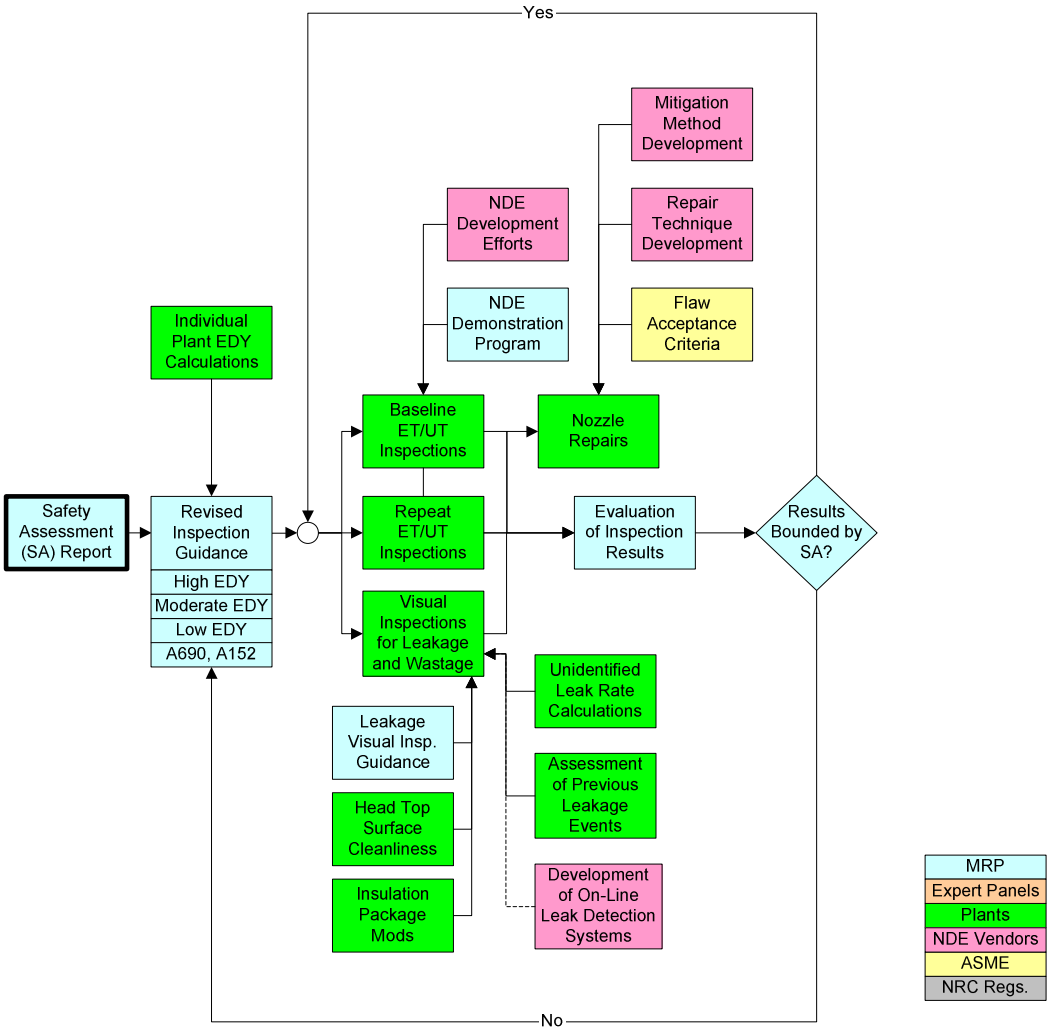

Figure 1-6
Inspection Feedback Process

2
FAILURE MODE AND EFFECT ANALYSIS (FMEA)

This section describes the failure mode and effect analysis (FMEA) that was applied to potential degradation of RVCH penetrations. The FMEA is a systematic methodology for determining the modes of degradation that could potentially lead to failure, here in the context of nuclear safety. The focus of the FMEA discussion is the FMEA flow chart (Figure 2-2), which shows the interrelationships among the various degradation conditions, beginning with fabrication and operating factors, moving through the potential types of aging degradation including PWSCC, and ending with the LOCA events and core damage.

2.1 Purpose

The purpose of the FMEA is to identify the credible failure modes that could impact nuclear safety, making the FMEA a starting point for a safety assessment for RVCH penetrations. Through identification of the credible failure modes and the interrelationships among the various steps in the credible failure modes, the FMEA identifies the detailed technical evaluations that the safety assessment must include. Ultimately, the FMEA and the technical evaluations will shape the requirements for the industry inspection plan for RVCH penetrations including:

- the definition of susceptibility groups,
- the performance of bare metal visual (BMV) inspections,
- the acceptable options for baseline nonvisual nondestructive inspections such as those performed using ultrasonic testing (UT) or eddy current testing (ET), and
- the frequency of nonvisual inspections.

The FMEA for RVCH penetrations is designed to proactively evaluate all potential modes of degradation that could potentially impact nuclear safety—not just degradation modes and geometries that have already been observed at plants. In this manner, the potential effect on nuclear safety of new degradation modes that could appear in the future will be addressed by the industry inspection plan being designed by the Materials Reliability Program (MRP). Although the possibility of circumferential nozzle cracking and significant boric acid wastage were recognized as a potential safety concern in the early to mid-1990s, the discovery of these types of RVCH penetration degradation beginning in late 2000 was a general surprise based on prior evaluations. In addition, the discovery of stress corrosion cracks initiating on the RVCH nozzle OD below the J-groove attachment weld beginning in late 2000 and widespread cracking in the J-groove welds of the RVCH penetrations at one plant in 2002 showed that past experience, including international experience, is not always a reliable predictor of the location, geometry, and morphology of cracking degradation at all units. The FMEA represented by this document is

designed to present in a comprehensive manner the types of degradation and failure modes that could possibly impact nuclear safety, including new modes as well as the types of degradation that have been observed in the field.

2.2 Basic Structure

According to Stamatis [2-1], an FMEA "is an engineering technique used to define, identify, and eliminate known and/or potential failures, problems, errors, and so on from the system, design, process, and/or service…" The scope and structure of the FMEA process may vary greatly depending on the criticality of the component, system, or process being studied and the particular industry. However, in general an FMEA is a systematic framework for identifying the potential failure modes and the causes, consequences, detectability, and frequency of occurrence of each mode. Often the relationships among the potential failure modes are illustrated using a block diagram. Typically, an FMEA either is based on historical data for similar applications or uses "inferential statistics, mathematical modeling, simulations, concurrent engineering, and reliability engineering…to identify and define the failures" [2-1].

Stamatis [2-1] states that a good FMEA:

- Identifies known and potential failure modes
- Identifies the causes and effects of each failure mode
- Prioritizes the identified failure modes according to risk based on the frequency of occurrence, severity, and detectability
- Provides for problem follow-up and corrective action

Stamatis [2-1] recommends the following eight-step process for an effective FMEA:

1. Select the team and brainstorm
2. Produce a functional block diagram and/or process flow chart
3. Prioritize
4. Collect data
5. Perform analysis
6. Produce results
7. Confirm/evaluate/measure
8. Repeat the complete process in the philosophy of continual improvement

The FMEA presented in this document is used to identify the potential RVCH penetration failure modes that may impact nuclear safety along with the technical evaluations that are required to define the in-service inspections that are necessary to ensure continued nuclear safety. Although this document contains technical discussions of many of the relevant issues, the detailed technical evaluations themselves, which include simulations and reliability assessments, are provided by the related safety assessment report. Therefore, the FMEA presented in this document represents the product of steps 1 through 3 in the process recommended by Stamatis, while the balance of the safety assessment report addresses the remaining steps.

2.3 Input Sources

The heart of the FMEA for RVCH penetrations is the flow chart presented in Figure 2-2. This chart shows the various "failure paths" that could potentially impact safety beginning with materials, fabrication, and operating factors and ending with the impact on the frequencies of core damage and large early release given the possible modes of material aging degradation and boric acid corrosion. This flow chart, which shows the various relationships among the potential degradation modes, was produced through an industry process that began with small brainstorming sessions among engineers familiar with the relevant issues and then was refined through industry review. The discussions that are presented in Appendix C present the technical background and rationale for identification of the failure modes in the flow chart and their interrelationships. These discussions are, to a large extent, based on work that the nuclear power industry has performed over the last 20–30 years to improve understanding of stress corrosion cracking and environmental fatigue of nickel-based alloys, including the effects of materials, fabrication, water chemistry, and plant operating factors. Much of this work has been managed by the Electric Power Research Institute under the sponsorship of nuclear power utilities.

2.4 Alloy 600 Reactor Vessel Closure Head Degradation

2.4.1 Sub-Components

The FMEA addresses the potential for failure modes affecting the RVCH penetrations and the surrounding head material near the intersection of the penetration nozzle and the head shell in the region of the J-groove attachment weld. Specifically, the head sub-components in this area are the nickel-based Alloy 600 penetration nozzle (tube), the nickel-based Alloy 182 buttering and J-groove attachment weld, the low-alloy steel head shell (ASTM SA302 Grade B or SA533 Grade B Class 1), and the Type 308/309 stainless steel cladding. The FMEA presented in this document considers potential failure modes for all these sub-components. As will be discussed in later sections, the high residual stresses induced by the J-groove welding process are a main driver in the principal failure modes identified by the FMEA.

In addition to the sub-components cited above, many CRDM penetration designs include a thermal sleeve or guide tube with an OD slightly smaller than the ID of the penetration nozzle. Also, most CRDM nozzles have a drive shaft that is centered inside the nozzle. However, the FMEA process did not identify any potential failure modes that involve degradation of the thermal sleeve, guide tube, or drive shaft. Finally, it is noted that a guide funnel is connected to the bottom of many CRDM nozzles.

2.4.2 Failure / Degradation Mechanisms

From past experience, the main material degradation mode for the nickel-alloy RVCH penetration sub-components—nozzle, weld, and buttering—is primary water stress corrosion cracking (PWSCC). This type of cracking has been observed in plants at this location and is the result of high tensile residual stresses in combination with the high-temperature aqueous environment and susceptible nickel-alloy material. In addition, the nozzle, weld, buttering, and

low-alloy steel head material are potentially susceptible to fatigue including environmental fatigue depending on the magnitude and frequency of transient loads on the material. Both the PWSCC and fatigue degradation modes are treated assuming separate initiation and growth regimes. The initiation regimes cover the part of the degradation process that produces flaws that are sufficiently large for the generally faster growth regimes to become active. The growth regimes are generally modeled to be driven by the crack tip stress intensity factor. Statistical reliability models are usually used to deal with PWSCC initiation, while the fatigue design rules of the ASME Boiler & Pressure Vessel Code may be applied to evaluate crack initiation due to environmental fatigue. Finally, low-temperature crack propagation associated with elevated levels of hydrogen concentration has recently been identified as a potential mode of material degradation for nickel-based alloys. Based on the detailed discussion in Appendix C, Table 2-1 identifies the plausible aging degradation mechanisms that apply to the materials within the FMEA scope, and Table 2-2 identifies the key parameters influencing these mechanisms.

Table 2-1
Plausible RVCH Aging Degradation Mechanisms

RVCH Penetration Component / Material	Plausible Aging Degradation Mechanisms
Alloy 600 Nozzle (Tube) (in J-groove region)	• PWSCC • Environmental Fatigue
OD of Alloy 600 Nozzle Above J-Groove Weld	• PWSCC • SCC in a Non-Primary Water Environment • Environmental Fatigue
Alloy 182/82 J-groove Weld	• PWSCC • Environmental Fatigue • Low-Temperature Crack Propagation (LTCP)
Alloy 182/82 Weld Buttering	• PWSCC • Environmental Fatigue • Low-Temperature Crack Propagation (LTCP)
Reactor Vessel Head Low-Alloy Steel	• Boric Acid Corrosion Wastage • Environmental Fatigue

The degradation modes in Table 2-1 may potentially lead to flaws of sufficient size to cause small leaks of primary coolant, larger breaks of the pressure boundary, or the generation of loose parts inside the reactor vessel. The potential safety concern for leakage is boric acid corrosion and/or erosion of the low-alloy steel head material. On the other hand, the nickel-alloy sub-components and the stainless steel cladding are sufficiently corrosion resistant to not be susceptible to significant boric acid wastage or erosion [2-2,2-3,2-4].[1]

[1] The Davis-Besse experience [2-3,2-4] demonstrated the potential for stress corrosion cracks to form on the top surface of unsupported stainless steel cladding given a concentrated boric acid environment. This type of

Table 2-2
Key Parameters for Plausible Aging Degradation Mechanisms

Plausible Aging Degradation Mechanisms	Key Parameters
PWSCC (Nickel-Base Alloy)	• Material alloy composition • Material structure (microstructure and defects) • Stress • Temperature
SCC in a Non-Primary Water Environment (Nickel-Base Alloy)	• Material alloy composition • Material structure (microstructure and defects) • Stress • Temperature • pH • Electrochemical potential (ECP) • Aqueous species (impurities)
Environmental Fatigue (Nickel-Base Alloy / Low-Alloy Steel)	• Material alloy composition • Material structure (microstructure and defects) • Cyclic stress range • Cyclic stress rise time • Mean stress (including residual stress) • Temperature • pH • Electrochemical potential (ECP) • Aqueous species (impurities)
Low-Temperature Crack Propagation (LTCP) (Subset of Nickel-Base Alloys)	• Dissolved hydrogen concentration • Material alloy composition • Material structure (microstructure and defects) • Stress • Temperature
Boric Acid Corrosion Wastage (Carbon and Low-Alloy Steel)	• Lithium-boron ratio in primary water • Boric acid concentration in crevice / cavity • Dissolved oxygen concentration in crevice / cavity • pH in crevice / cavity • Electrical conductivity in crevice / cavity • Leak rate • Velocity field • Wall shear stress • Temperature • Pressure • Galvanic coupling to nickel-alloy nozzle / weld and stainless steel cladding

degradation could influence the amount of boric acid wastage of the low-alloy steel material required to produce cladding blowout.

Because the safety function of the reactor vessel pressure boundary is to contain the primary pressure and keep the core cooled and covered with liquid water, rupture of the pressure boundary in the region of the RVCH penetration is a potential safety concern. Flaw tolerance calculations show that nozzle ejection due to growth of a very large circumferential flaw through most of the nozzle cross section or due to propagation of a very large circumferential flaw around the interface between the nozzle and J-groove weld are potential ways that a rupture of the pressure boundary could occur. On the other hand, flaw tolerance calculations also show that rupture of the nozzle due to long axial, through-wall cracks is not credible because such cracks would have to extend many inches beyond the high stress zone before rupture would occur. Rupture of the pressure boundary could also potentially occur due to boric acid corrosion of the low-alloy steel material that produces a large wastage cavity. Such rupture could occur in an unsupported section of the stainless steel cladding or possibly in the low-alloy steel material adjacent to the cavity.

Circumferential cracking around the complete nozzle circumference, or possibly intersecting axial and circumferential cracks, located below the elevation of the J-groove weld have the potential of producing loose parts. The generation of loose parts is a potential safety concern for several reasons. Examples of the possible impact of the release of loose nozzle parts include the prevention of a control rod drop and damage to fuel pins, the steam generator tubes or tubesheet, or the reactor vessel bottom area.

Therefore, based on the above discussion, the three principal failure modes that could impact nuclear safety are:

- nozzle ejection caused by net section collapse given large circumferential flaws,
- cladding blowout or head rupture due to boric acid corrosion of the low-alloy steel head material following penetration leakage, and
- damage to the reactor coolant system due to the release of loose parts.

The detailed technical discussions presented in Appendix C of this report confirm that these are in fact the failure modes that are a potential safety concern. The detailed FMEA also shows the plausible ways that flaws in a RVCH penetration could lead to such failures. Figure 2-1 shows the basic potential flaw geometries that can exist in the nozzle and weld as well as the location of the interference fit zone (often termed the annulus) on the nozzle OD above the J-groove weld. Any cracking through the nozzle, weld, or buttering that leads to the interference fit zone constitutes a leak path.

Note that the low alloy steel reactor vessel material is potentially susceptible to environmental fatigue. This possibility is discussed in Section 4 of MRP-103 [1-6]. Such fatigue is expected to be insignificant over several cycles.

2.5 Failure-Path Flow Chart

The FMEA flow chart provided in Figure 2-2 shows the interrelationships among the various failure modes for RVCH penetrations. As mentioned, this flow chart was produced through an

industry process that began with small brainstorming sessions among engineers familiar with the relevant issues and then was refined through industry review.

The flow chart generally flows upward to higher failure levels, culminating in accident scenarios that could impact nuclear safety. Each box in the chart represents a condition of one of several types as indicated by the color key in the upper right hand corner. Each arrow represents a "failure path" from one condition to a higher level condition. Each failure path begins with a fabrication/material condition or a plant operating/water chemistry condition and continues through the nickel-alloy aging degradation modes of PWSCC, environmental fatigue, or low temperature crack propagation. Because cracking can lead to leakage, some failure paths lead to boric acid corrosion and head wastage. Other failure paths lead to nozzle ejection or the release of loose parts.

The color coding of the failure paths indicates the credibility of that failure path possibility and, if credible, whether that failure path is actionable or not. The failure path color scheme is defined as follows:

- A *not credible* [Red] classification reflects a determination that the identified condition or mechanism cannot occur to a high degree of certainty and is supported by a strong technical argument and thorough documentation with a high threshold.
- A *not actionable* [Blue] classification reflects a determination that the condition can occur but cannot be reliably detected or quantified and therefore requires that adequate protection be provided at a higher level in the failure process.
- An *actionable* [Green] classification reflects a determination that the condition can occur and can be reliably detected or quantified. These conditions are inputs to the probabilistic and deterministic evaluations and ultimately shape the detectability requirements for inspections.

2.6 Conclusions

The FMEA results confirm that nozzle ejection and head wastage are the two major potential safety concerns and help define the inspection capabilities that are needed to detect degradation before defense in depth is compromised. The generation of loose parts is a potential third concern that helps to set the required inspection area for periodic nonvisual inspections. In addition, the FMEA investigations have shown that environmentally assisted fatigue due to natural circulation and thermal cycling cannot be dismissed as a potential source of crack growth. However, the plant experience, which is documented in Section 4, has not identified this as an active degradation mode.

2.7 References

2-1. D. H. Stamatis, *Failure Mode and Effect Analysis: FMEA from Theory to Execution*, ASQ Quality Press, Milwaukee, 1995.

2-2. *Boric Acid Corrosion Guidebook, Revision 1: Managing Boric Acid Corrosion Issues at PWR Power Stations*, EPRI, Palo Alto, CA: 2001. 1000975.

2-3. *Root Cause Analysis Report: Significant Degradation of the Reactor Pressure Vessel Head*, Davis-Besse Nuclear Power Station report CR 2002-0891, April 2002.

2-4. *Examination of the Reactor Vessel (RV) Head Degradation at Davis-Besse*, Final Report, BWXT Services, Inc., Lynchburg, VA: 2003. 1140-025-02-24.

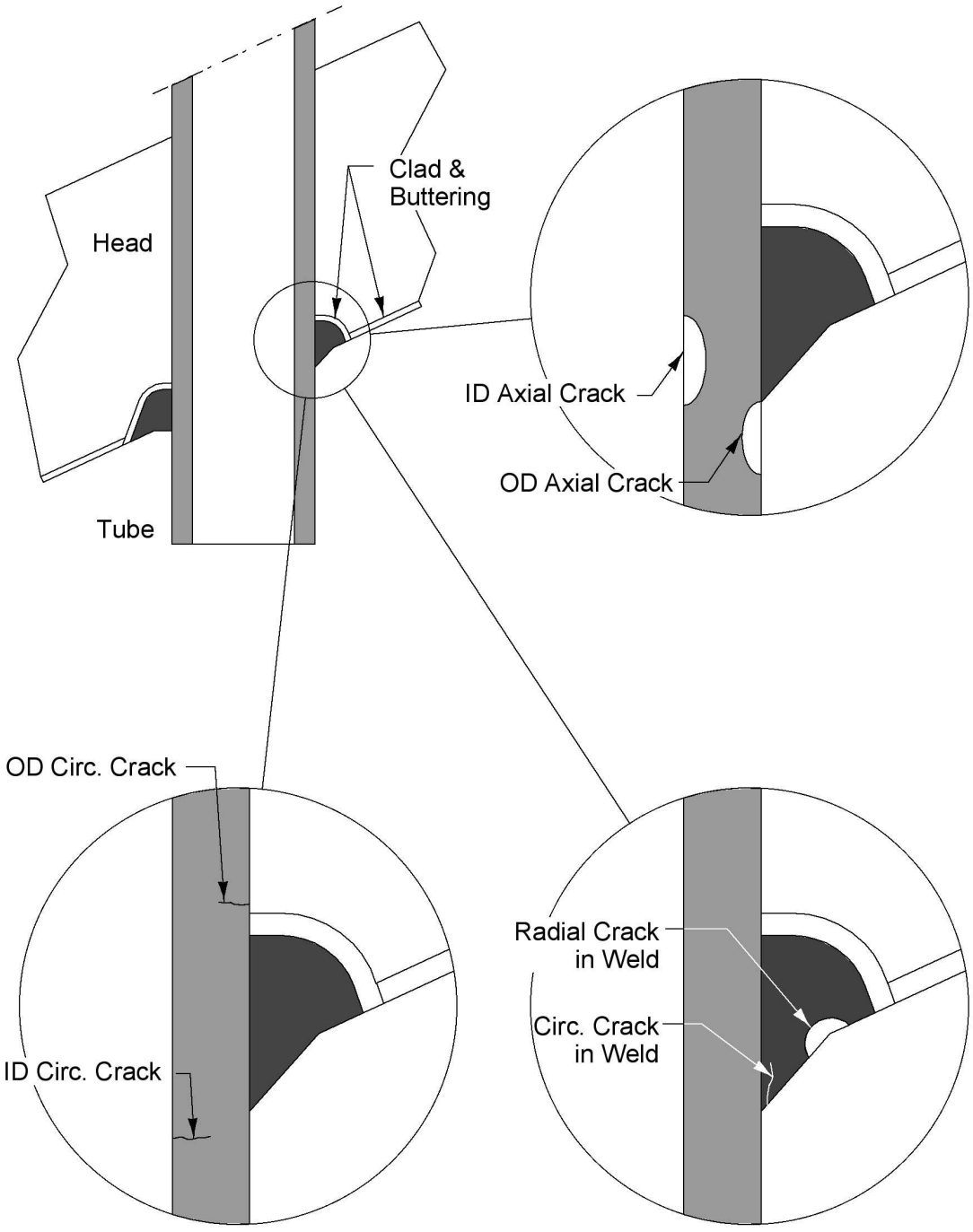

Figure 2-1
CRDM Nozzle and Weld Flaw Geometries

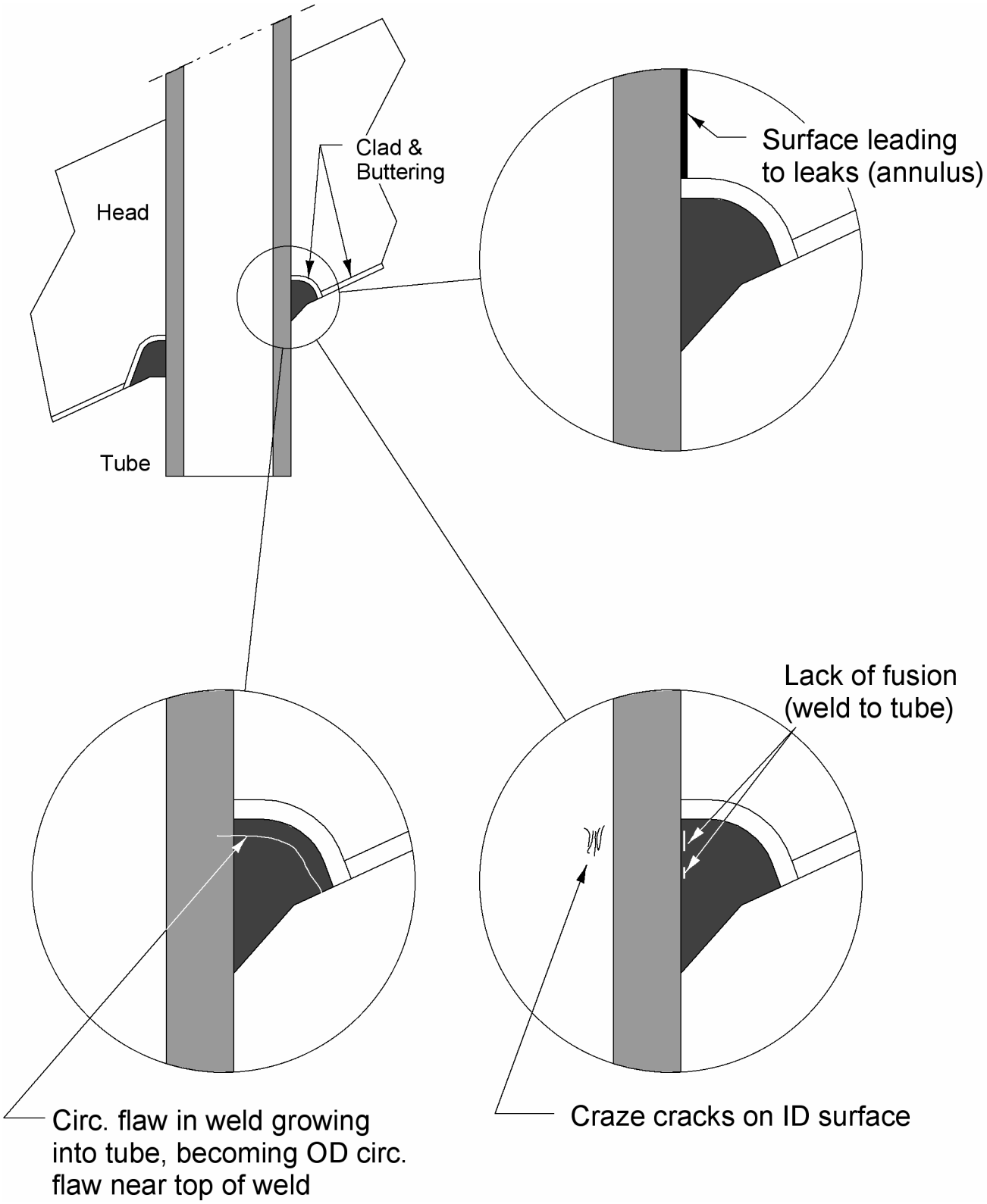

Figure 2-1
CRDM Nozzle and Weld Flaw Geometries (continued)

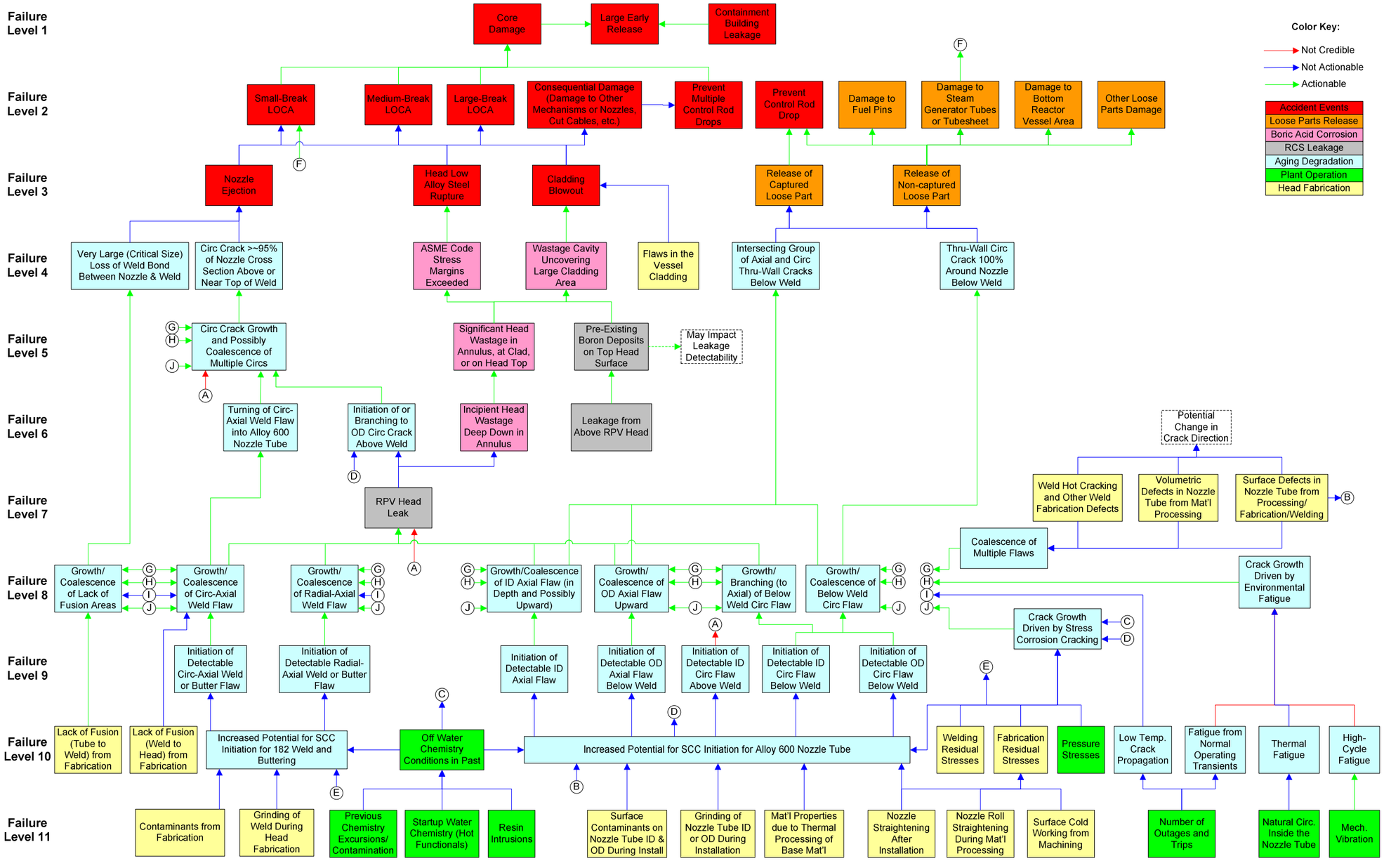

Figure 2-2
Flow Chart for MRP Failure Mode and Effect Analysis for Reactor Vessel Closure Head Penetrations

3
SUMMARY OF FLAW AND WASTAGE TOLERANCE CALCULATIONS

This chapter summarizes the results of the flaw and wastage tolerance calculations presented in Appendix D. Axial and circumferential nozzle flaws, circumferential "lack-of-fusion" type flaws at the interface between the nozzle and the J-groove weld, and head wastage cavities are evaluated. The results show that relatively large nozzle or "lack of fusion" type circumferential flaws are required to produce a nozzle ejection, while axial flaws long enough to cause rupture of the nozzle are not credible given the extent of the region of welding residual stresses. The wastage cavity results show that about 150 in^3 of material can be lost from the upper surface of the head without the stresses in the remaining low-alloy steel ligament exceeding the relevant ASME Code allowable values. In summary, the reactor vessel closure head and its penetrations are quite flaw tolerant.

3.1 Flaw Tolerance Calculations

There are three types of RVCH penetration crack geometries of potential concern for producing a pressure boundary break:

1. an axial through-wall flaw in the nozzle above the J-groove weld,
2. a through-wall circumferential flaw above the J-groove weld, and
3. a circumferential flaw at the fusion line between the nozzle and the J-groove weld.

3.1.1 Axial Flaw in Nozzle Above J-Groove Weld

The calculations in Appendix D.1.1 show that for a typical CRDM nozzle geometry the axial flaw length resulting in rupture at the standard design pressure of 2500 psi is about 14 inches. With a factor of safety of 2.7 on the pressure loading (6750 psi), the corresponding critical flaw length is 5.1 inches, a significantly greater length than the height of the region of the nozzle subject to significant welding residual stresses. Therefore, axial nozzle cracking resulting in nozzle rupture is not a credible concern.

3.1.2 Circumferential Flaw in Nozzle Above J-Groove Weld

The calculations in Appendix D.1.2 have been performed covering the design parameters for the original heads in all 69 domestic PWR units for CRDM, CEDM, and ICI nozzles. The results show that, for most CRDM and CEDM nozzles, a circumferential crack above the J-groove weld of approximately 330° in circumferential size will support the standard design pressure of 2500 psi. Larger flaws are calculated to produce net section collapse of the remaining nozzle

wall ligament at a pressure of 2500 psi. Assuming a pressure loading of 2500 psi, the critical sizes for specific CRDM and CEDM nozzle configurations range from 318° to 334° and are presented in Table 3-1, which also includes results for the ICI nozzles in CE design plants and for a pressure loading including a factor of safety of 2.7.

These values are in close agreement with other published results:

- MRP-104 [3-2] reports a typical critical flaw length of 330° for CRDM and CEDM nozzles. Eight types of CRDM nozzles in Westinghouse design plants were considered, including various vessel head manufacturers and different geometries. Five different geometries were considered for CE design plants in this report.
- Calculations documented in MRP-103 [3-3] show a critical flaw size of 330° for B&W design units.
- Work reported by Engineering Mechanics Corporation of Columbus (EMC^2) [3-4] showed an allowable through-wall crack size of 262° to 269°, with a safety factor of 3 applied to the pressure loading. Note that the results presented by EMC^2 assume a slightly different flow stress definition than was applied in Appendix D.

Figure 3-1 shows how the limit load pressure varies as a function of the circumferential flaw angle for the limiting CRDM, CEDM, and ICI nozzle types as identified in Table 3-1.

3.1.3 Lack of Fusion or Circumferential Weld Crack at J-Groove Weld Interface

Appendix D.1.3 calculates that a typical CRDM penetration geometry will support the standard design pressure of 2500 psi given a circumferential area of lack of fusion between the weld and nozzle wall extending roughly 325° around the nozzle. Applying a factor of safety of 2.7 on the pressure loading, the typical CRDM penetration geometry will support a pressure of 6750 psi given a circumferential area of lack of fusion between the weld and nozzle wall extending roughly 265° around the nozzle.

Therefore, similar flaw angles can be tolerated for circumferential nozzle cracks located above the J-groove weld and for lack-of-fusion type defects between the nozzle and weld.

Other analyses have been reported for the Swedish plant Ringhals Unit 2 [3-5]. These results showed that a fusion area between the nozzle and weld of only 1.45 in^2 was required to avoid failure, corresponding to a circumferential extent of lack of fusion of about 330° for the outermost CRDM penetration.

3.2 Allowable Wastage Volume at Reactor Vessel Head CRDM Nozzles

The finite-element calculations in Appendix D.2 for an example reactor vessel closure head show that about 150 in^3 of material can be lost from the upper surface of the example head without the stresses in the remaining low-alloy steel ligament exceeding the ASME Code allowables for primary membrane and membrane-plus-bending stresses. Figure 3-2 shows the pattern of material loss between two adjacent nozzles assumed in the finite-element analysis. The results in

Appendix D.2 also demonstrate that a greater volume of material can be lost symmetrically distributed around a CRDM nozzle in comparison to the pattern shown in Figure 3-2 without the Code allowable stresses being exceeded.

The results presented in Appendix D.2 are considered representative for other PWR vessels since the design analyzed had a relatively high diameter-to-thickness ratio and, therefore, a relatively low margin of excess thickness over that required to meet the Code minimum wall thickness.

3.3 References

3-1. *Materials Reliability Program: Probabilistic Fracture Mechanics Analysis of PWR Reactor Pressure Vessel Top Head Nozzle Cracking (MRP-105)*, EPRI, Palo Alto, CA: 2004. 1007834.

3-2. *Materials Reliability Program: RV Head Nozzle and Weld Safety Assessment for Westinghouse and Combustion Engineering Plants (MRP-104)*, EPRI, Palo Alto, CA: 2004. 1009403.

3-3. *Materials Reliability Program: RV Head Nozzle and Weld Safety Assessment for B&W Plants (MRP-103)*, EPRI, Palo Alto, CA: 2004. 1009402.

3-4. G. Wilkowski, et al., "NRC-Funded CRDM Critical Crack Size Analyses by Engineering Mechanics Corporation of Columbus," NRC/Industry Meeting, Rockville, Maryland, November 8, 2001.

3-5. J. Lagerström, B. Wilson, B. Persson, W. H. Bamford, and B. Bevilacqua, "Experiences with Detection and Disposition of Indications in Head Penetrations of Swedish Plants," PVP-Vol. 288, *Service Experience and Reliability Improvement: Nuclear, Fossil, and Petrochemical Plants*, ASME, 1994.

Table 3-1
Critical Flaw Angles for Through-Wall Circumferential Nozzle Flaws

Nozzle Type	Nozzle Geometry	*OD* (in)	Flaw Angle θ for P_{flow} = 2500 psi (deg)	Flaw Angle θ for P_{flow} = 6750 psi (deg)	Limiting Nozzle of Type
CRDM	Westinghouse CRDM	4.000	330	285	
			329	281	
	B&W CRDM	4.002	328	281	✓
CEDM	CE CEDM Type 1a	4.050	331	288	
	CE CEDM Type 1b	4.050	331	288	
	CE CEDM Type 2	3.850	323	268	
	CE CEDM Type 3/4	3.495	318	254	✓
	CE CEDM Type 5	4.275	334	293	
ICI	CE ICI Type 1	5.563	293	195	✓
	CE ICI Type 2	4.500	309	232	
	CE ICI Type 3	6.625	313	244	

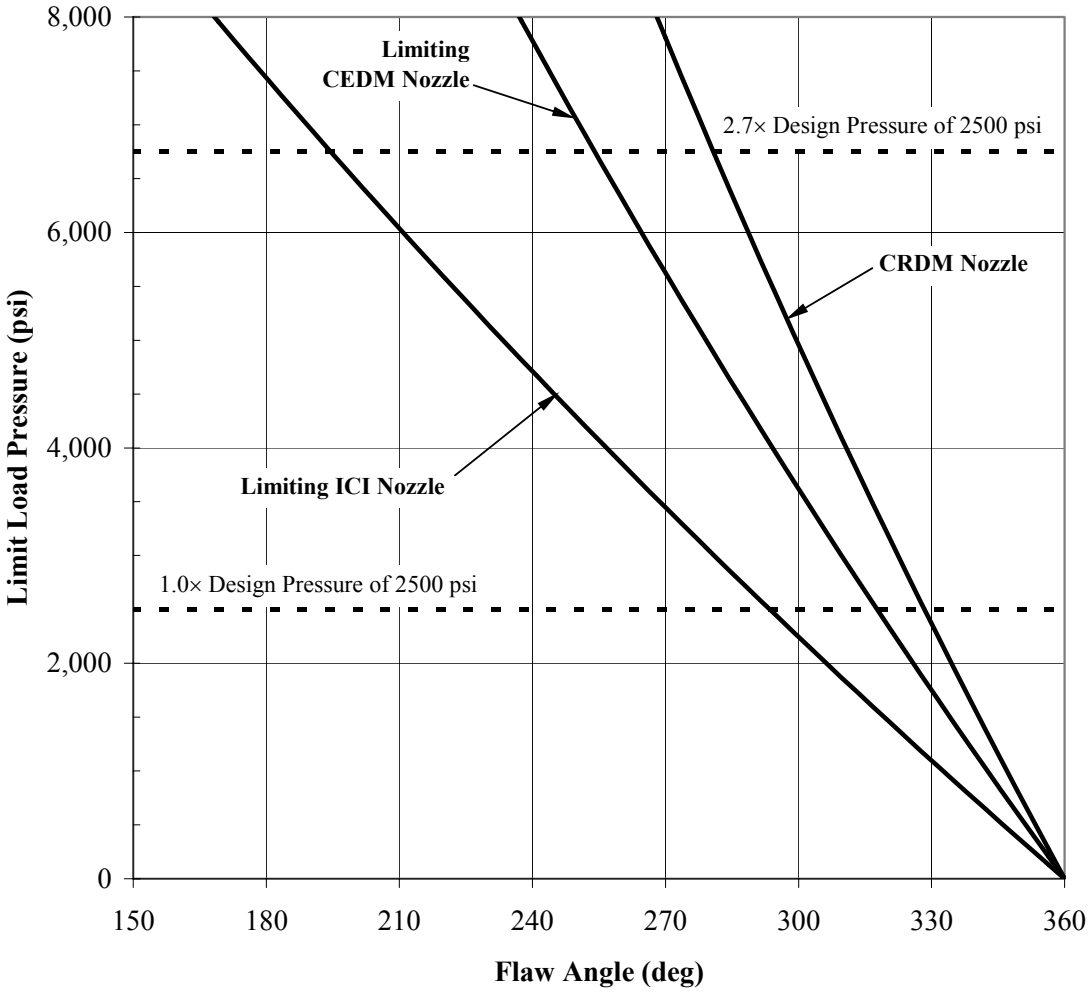

Figure 3-1
Limit Load Pressure versus Circumferential Flaw Angle for Limiting Nozzle Geometries

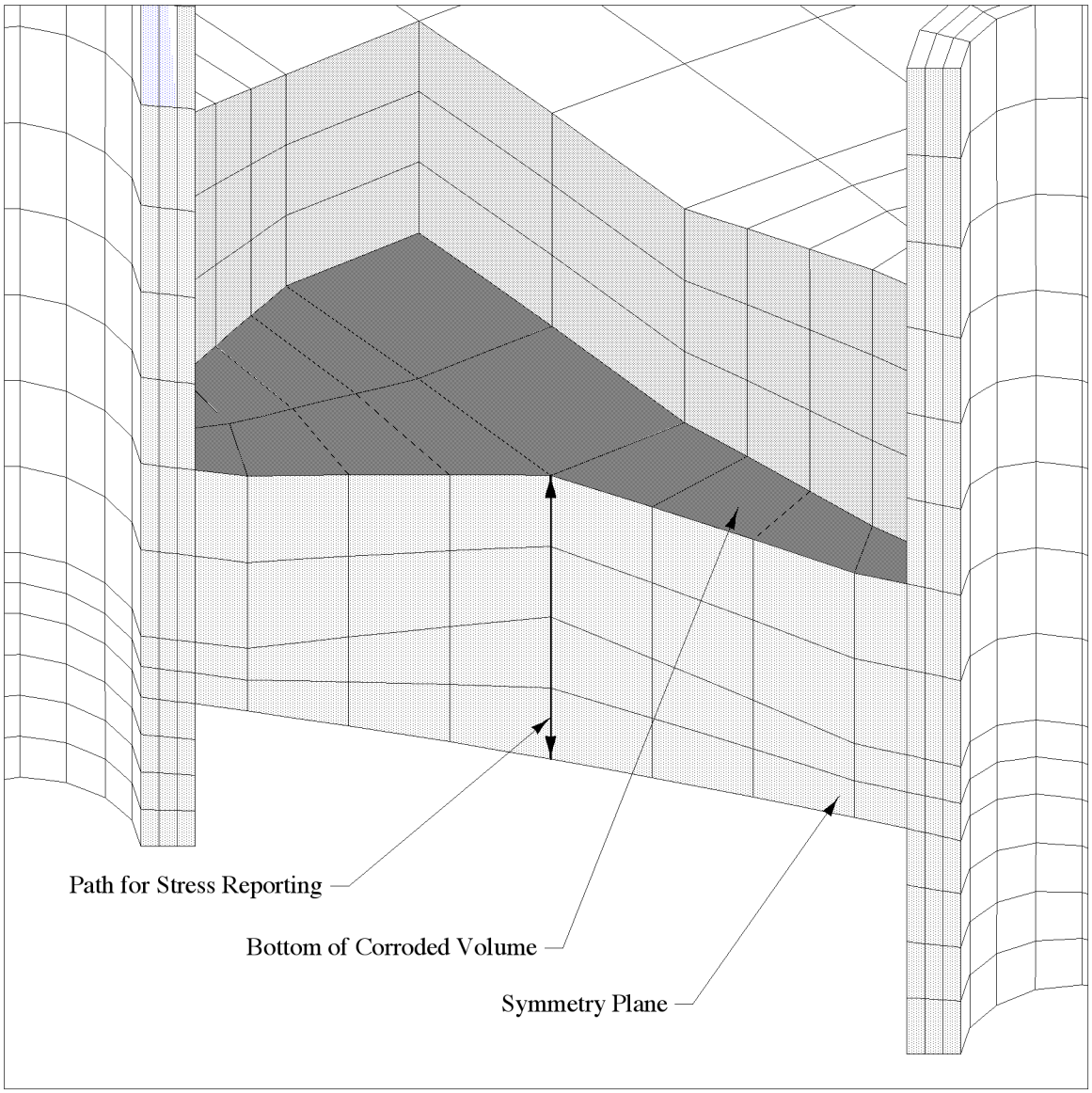

Figure 3-2
Finite Element Model—Wastage Between Adjacent Nozzles

4
INSPECTION EXPERIENCE

This section presents the RVCH penetration inspection experience through December 2003, including a chronological summary of key events and summary statistics investigating the effects of operating time, head temperature, vessel fabricator, and nozzle material supplier. As of December 2003, all the original heads have been inspected by bare metal visual examination and/or nonvisual NDE techniques. The inspection experience confirms that time at temperature (EDYs) is a key factor governing PWSCC susceptibility, and the experience also shows clearly that some material and fabrication categories are experiencing significantly lower rates of degradation compared to others.

Experience with detected PWSCC in Alloy 600 nozzles and Alloy 82/182 welds located in the reactor coolant systems of domestic PWRs but at locations other than the reactor vessel closure head is documented in MRP-87 [4-1]. Most of this experience is related to pressurizer heater sleeves, pressurizer instrumentation nozzles, and hot leg piping instrumentation nozzles. These nozzles are typically about 1 inch in diameter, significantly smaller than typical RVCH nozzles.

4.1 Introduction

The results of reactor vessel head (RVH) nozzle inspections in the U.S. have tended to support the time-at-temperature model that has been used to prioritize inspections in the U.S. since the first evidence of RVH nozzle leakage was detected in late 2000. The time-at-temperature model, which ranks each plant on the basis of operating time scaled for differences in the RVH operating temperature, is based on voluminous laboratory and plant data showing that primary water stress corrosion cracking (PWSCC) of nickel-based alloys is a thermally-activated aging mechanism. As of December 2003, 100% of the more than 5,000 RVH penetrations at the 69 U.S. PWR units have been inspected either by bare metal visual (BMV) examination, eddy current testing (ET) surface examination, ultrasonic testing (UT) volumetric examination or liquid penetrant testing (PT)—or have been removed (head replacement). The 55 leaking CRDM nozzles and all but 23 of the approximately 137 cracked nozzles detected have been from the 15 highest ranked units on the basis of time at temperature. However, the RVH nozzle inspection results also show that nozzle material processing and head fabrication differences are major factors affecting the cracking susceptibility of Alloy 600 RVH nozzles and their Alloy 182 attachment welds. Little or no cracking has been detected to date at plants having several combinations of Alloy 600 material supplier and RVH fabricator even though several of these plants are highly ranked in terms of time at temperature.

Inspection summary statistics are used for a number of purposes including:

- Verifying time-at-temperature (Effective Degradation Years, EDY) as a predictor of PWSCC susceptibility,
- Revealing cracking trends for subgroups of reactor vessel heads including the head fabricator and the nozzle material supplier,
- Providing safety assessment inputs such as Weibull models of time to crack initiation or leakage, confirming laboratory crack growth test data, confirming the location and orientation of cracks, and supporting low-alloy steel wastage models,
- Facilitating periodic evaluations of industry inspection plans.

4.2 Background Information

PWSCC of Alloy 600 type materials in non-steam generator tubing PWR applications has been discovered at various locations since 1986. The following section gives a brief overview of the key events associated with PWSCC at those locations.

4.2.1 Alloy 600 in PWR Plants

Primary water stress corrosion cracking (PWSCC) has resulted in leaks from penetrations and thick-section Alloy 600 materials in PWR plants at various operating temperatures, for example: pressurizers (≈650°F), hot legs (≈600°F), and cold legs (≈550°F).

The following summarizes the number of reactor vessel closure head (RVCH) penetrations in the 69 operating PWR plants in the U.S. that have Alloy 600 nozzles attached to the head by J-groove welds:

- 3,871 CRDM nozzles (55 units)
- 1,090 CEDM nozzles (14 units)
- 94 in-core instrument (ICI) nozzles (11 units)
- 58 vent line nozzles (58 units)
- 16 small-bore thermocouple nozzles (2 units – have been replaced)
- 8 auxiliary head adapter nozzles (2 units)
- 2 de-gas line nozzles (2 units)

Several of the 69 PWR plants have Alloy 600 nozzles that are not attached to the head by J-groove welds. These are:

- 4 full-penetration weld vent nozzles (4 units)
- 6 internals support housing nozzles (2 units)
- 20 auxiliary head adapter nozzles (5 units)

Figure 2-1 in Section 2 shows the locations of PWSCC that have been discovered in RVCH control rod drive mechanism (CRDM) nozzles in B&W and Westinghouse design plants and control element drive mechanism (CEDM) nozzles in Combustion Engineering design plants. The cracks have been located in the Alloy 600 nozzle tubes and in the Alloy 82/182 welds near the J-groove weld where high tensile residual stresses from welding combine with operating pressure and temperature stresses. Figures A-9 through A-16 show a typical CRDM/CEDM nozzle, an ICI nozzle (CE design plant), a thermocouple nozzle, a head vent nozzle, an internal support housing nozzle, an auxiliary head adapter (AHA) nozzle, and a de-gas line (DGL) nozzle.

4.2.2 Summary of Key Events

Table 4-1 gives a brief overview of the chronology of key events relating to PWSCC of Alloy 600 material in non-steam generator tubing PWR plant applications.

- The first leak on a CRDM penetration was discovered at Bugey 3 in France in 1991. A small leak [<1 liter/hr (0.004 gpm)] was discovered, and it was traced to an axial crack in the nozzle that had initiated on the inside surface at the elevation of the J-groove weld and then propagated through the nozzle wall thickness. Water was discovered leaking from the annulus between the nozzle and hole in the vessel head during a hydrostatic test. Laboratory examination showed a small [3 mm (0.12 inch) long and 2.25 mm (0.09 inch) deep] circumferentially oriented indication above the weld on the outside surface of the nozzle near the through-wall axial crack. There was also a small [15 mm (0.59 inch) long and 2 mm (0.08 inch) deep] extension of the main through-wall crack into the J-groove weld, and a relatively long [3.5 mm (0.14 inch) deep and 110° circumferential arc length] crack penetrating into the weld from the annulus between the nozzle and the vessel shell. This crack was reported as primarily a weld defect, but with some evidence of PWSCC.

  Eddy current inspections of the other 65 CRDM nozzles in Bugey 3 showed part-depth axial cracks in one other outer row nozzle. Failure analysis confirmed that the crack which caused the leak was PWSCC and that susceptible material microstructure, stress concentration at a counterbore on the nozzle inside surface, high hardness of the cold worked machined surface, and high residual stresses induced in the nozzle during welding were significant contributing factors. Laboratory examinations associated with the Bugey 3 leak showed several features in addition to the axial cracks as shown in Figure 4-1.

There was no evidence that any of the above conditions represented an immediate safety problem. However, the presence of cracks in the nozzles on many heads (these cracks have been predominantly axial) led to a program to replace all of the reactor vessel heads in EDF plants with new heads fabricated using Alloy 690 nozzle materials and Alloy 52/152 J-groove welds.

As a result of the Bugey 3 experience, many plants worldwide have inspected the inside surfaces of their CRDM nozzles for PWSCC. Axial cracks have been discovered on the inside surfaces of CRDM nozzles in reactor vessel heads in Sweden, Japan, Switzerland, and Belgium. Cracks discovered in the CRDM nozzles, and fabrication related defects in J-groove welds, led to the replacement of reactor vessel heads at Ringhals 2 and 4. In the U.S., inspections have been performed since the Bugey 3 event, and many axial cracks have been found since late 2000. As

of December 2003, it has been estimated that approximately 91% of the indications with a detectable depth by NDE techniques on CRDM/CEDM nozzles are axial, as expected based on the welding residual stress analyses. Of the axial indications, about 29% are ID axial flaws while 62% are OD-initiated.

- Between 1991 and 2000, inspections were performed at several plants in the United States, and cracks were discovered at four units. The most significant crack was 6.8 mm (0.27 inch) deep (43% through-wall) at D.C. Cook 2. This crack was partially ground out from the inside of the nozzle and weld repaired, leaving a portion of the crack in place. Millstone 2, Oconee 2, and Ginna detected shallow "craze type cracks", which are groups of shallow, predominantly axial cracks less than the 2 mm (0.08 inch) ultrasonic depth sizing limit. Selected nozzles at Oconee 2 with shallow axial indications on the inside surface found in 1994 were reinspected in 1996 and again in 1999. No crack growth was detected. Inspections of Oconee 1 and 3 nozzles from under the head were deferred based on the findings from the Oconee 2 inspections. Palisades performed eddy current inspections of the ICI nozzles at the periphery of the vessel head with no indications reported.
- In November 2000, leaks due to PWSCC were discovered for the first time in the U.S. on RVH penetrations, at Oconee 1, both on CRDM and T/C nozzles. The CRDM leak was traced to a crack primarily in the J-groove weld that was subsequently weld repaired. The leaks at Oconee 1 were evidenced by small quantities (less than one cubic inch total volume) of boric acid crystal deposits at the locations where the nozzles penetrated the holes in the vessel head. Eddy current and ultrasonic inspections of the insides of the nozzles showed through-wall axial cracks in all eight thermocouple nozzles. Metallurgical examinations of samples showed the cracks to be PWSCC. The thermocouple nozzles were removed and the holes in the head plugged. Inspections and tests of the leaking Oconee 1 CRDM nozzle showed an axial/radial PWSCC crack that appeared to initiate in the J-groove weld that attached the nozzle to the inside of the vessel head. This crack grew in a predominantly axial/radial direction through the J-groove weld and part-depth into the Alloy 600 CRDM nozzle base material from the outside surface.

  The Oconee 1 experience was different from previous industry experience, which showed that almost all flaws initiated on the inside surface of the nozzles. The crack in the nozzle and weld was removed, and the nozzle was weld repaired using a temper bead process. The crack in the weld arrested when it reached the low-alloy steel vessel head material. In February 2001, a visual inspection of the top surface of the Oconee 3 reactor vessel head indicated that nine CRDM nozzles had developed small leaks. Eddy current, ultrasonic, and liquid penetrant inspections of the leaking nozzles confirmed the presence of through-wall and partial depth axial cracks, predominantly originating on the outside surface of the nozzles below the J-groove weld. These inspections also showed several partial-depth circumferential cracks located on the outside surface of the nozzles below the welds. During the repair effort, deep circumferential cracks were discovered on the outside surface of two of the leaking nozzles above the J-groove welds. These deep circumferential cracks followed the weld contour, extending up to about 165° around the nozzle and continuing through-wall in some locations.
- In March 2001, a visual inspection of the top surface of the Arkansas Nuclear One Unit 1 (ANO-1) reactor vessel head showed the presence of boric acid deposits that were traced to

an axially oriented, part-depth (0.2 inch deep) crack that initiated on the outside surface of an Alloy 600 CRDM nozzle below the J-groove weld. The crack extended vertically upward to a point 1.3 inches above the J-groove weld. A short distance below the J-groove weld, the crack developed a "Y" branch with two short circumferentially oriented legs.

- Over the next 15 months, leaks were discovered from CRDM nozzles at all seven B&W design plants and between 2000 and 2003, 55 CRDM nozzles were discovered to be leaking in 10 of the 69 U.S. pressurized water reactors and were subsequently repaired. These plants are among the top 15 of the highest susceptibility ranked units based on EDY calculations. The "high susceptibility" group defined by the NRC currently contains 28 units.

To conclude, and more recently:

- Most of the PWSCC cracks have been detected in the tube (predominantly axial cracks, on the ID or OD of the nozzle), but six units have experienced leaks due to weld cracking. At North Anna 2, six nozzles were found to be leaking in 2002, and the NDE results showed that most of the 65 CRDM J-groove welds had cracks requiring repair; the head was then replaced during the outage.
- Leaks were discovered on small-bore thermocouple nozzles at Oconee 1 and TMI 1 in 2000 and 2001 respectively, as previously noted (all 16 T/C nozzles were cracked at both units). However, to date, no leaks have been found on ICI, vent line, AHA or DGL nozzles.
- Through-wall circumferential cracks above the J-groove weld were discovered first at Oconee 3 in 2001, and then at Oconee 2 (2001), Crystal River 3 (2001), North Anna 2 (close to the top of the weld, 2002) and Davis-Besse (2002). The leaks from two CRDM nozzles at Davis-Besse led to significant boric acid wastage of the low-alloy steel top head material requiring replacement of the head in 2003. As of December 2003, 33 PWR units have plans to replace, are considering replacing, or have replaced the reactor vessel head.

Table 4-2 provides a summary of the cumulative inspection results for the CRDM, CEDM, J-groove vent and other J-groove nozzles in the U.S. recorded since November 2000.

4.3 Inspection Results

Inspection results and cumulative summary statistics are available since the first significant cracks were discovered at Oconee 1 in late 2000 as discussed below.

4.3.1 Summary

Significant data regarding RVCH inspection results and summary statistics have been collected and updated between 2000 and 2003, including cumulative results for each outage season, on an individual flaw and nozzle basis. These data are processed to provide the desired summary statistics and permit the assessment of the influence of various parameters. Therefore, information is available for all domestic PWR RVH nozzles in the context of the key design, fabrication (tube material supplier, vessel head fabricator, material properties), and operating parameters (operating temperature, outage schedule, EDYs).

The inspection techniques that have been applied to detect cracks and leaks are described in Section 9 and illustrated in Figure 9-1; these techniques include visual inspections for evidence of leakage, surface examination using eddy current and liquid penetrant techniques, and volumetric examination using ultrasonic testing.

Table 4-2 summarizes the status of RVCH inspections in the U.S. through the fall 2003 refueling outages. This table was compiled from documents prepared for utility responses to requests for information in the relevant NRC bulletins and from other information compiled by the EPRI Materials Reliability Program (MRP). The data show the inspection status of every RVCH nozzle in each of the 69 original PWR heads in the U.S. The plants are listed in the order of decreasing effective degradation years (EDYs) and are separated into three groups based on the number of EDYs tabulated by the MRP as of February 2001.

Since 2000, about 55 CRDM nozzles have been found to be leaking. All of the leaks occurred in plants with more than 16 EDY[2] of operation at the time of the inspection. As of January 2004, about 20% of the 69 PWR units had accumulated more than 16 EDYs (not including the plants that have already replaced their reactor vessel heads). Also, 42 of the leaks occurred in CRDM penetrations in the seven operating B&W design plants. This represents almost 9% of the nozzles in B&W design plants. The remaining leaking nozzles are in the three Westinghouse plants with heads fabricated by the Rotterdam Dockyard Company (RDY). These leaks were all associated with cracks in welds.

A summary of domestic cracking experience with RVCH penetrations and their J-groove attachment welds is presented in Tables 4-3 through 4-7:

- Table 4-3 focuses on the 14 plants with detected RVCH nozzle PWSCC. More than 80% of the cracked nozzles have been observed at seven B&W plants with B&W Tubular Products material (60 CRDM penetrations exhibiting mostly tube cracking) and at three Westinghouse plants with Rotterdam-fabricated heads (54 CRDM nozzles, mostly weld cracking).

- Table 4-4 provides a summary of plants with detected leakage due to tube- or weld-initiated flaws, including the type of repair or replacement performed. Approximately 40% of the leaks are due to cracking that has initiated in the weld material. More than half of the nozzles were repaired with a method that would likely have detected significant wastage of the low-alloy steel head material if it had occurred. Little or no wastage has been detected in these units except for Davis-Besse.

- Table 4-5 provides a summary of the orientation and location of PWSCC cracks in nozzles. As discussed in Section 4.2.2, nozzle cracking has been predominantly axial. Only 35 of the 386 detected nozzle cracks requiring repair have been circumferential and only two circumferential cracks above, or near, the top of the J-groove weld have been through-wall. Definitions of nozzle locations relative to the weld are shown in Figure 4-2.

[2] Based on a reference temperature of 600°F and a thermal activation energy of 50 kcal/mole.

- Table 4-6 gives a summary of the circumferential cracks that have been detected that are located above the weld in the nozzle tube, in the weld zone elevation, or below the weld. Less than 25% of the detected circumferential cracks are above or near the top of the weld, and five out of these seven indications have a circumferential angle not exceeding 100° and a through-wall depth of less than 50%. Definitions of nozzle locations relative to the weld are shown in Figure 4-2.

- Table 4-7 provides information on weld inspection and cracked welds requiring repair. Leaks and cracks in the welds have been detected only in plants with greater than 12 EDYs, but 86% of the welds inspected have been in the high susceptibility plants.

4.3.2 Subgroup Statistics

In addition to the overall summary, evaluations for several subgroups have been performed to assess the influence of various parameters. These subgroups were developed on the basis of time at temperature (EDY), head fabricators and nozzle material suppliers. One objective is to determine if factors other than time at temperature have a significant effect on PWSCC susceptibility.

Data in Figure 4-3 through Figure 4-11 reflect inspections performed between December 2000 and December 2003. Earlier inspections are not included given the limited awareness of the potential for PWSCC on the nozzle OD surfaces and welds prior to December 2000.

Figure 4-3 shows that 100% of the 4,961 CRDM and CEDM nozzles have been examined by BMV, UT and/or ET; or the head has been replaced. Note that all penetrations on the 10 reactor vessel heads that have been replaced so far have been inspected by typical NDE techniques, except for the 37 nozzles at Ginna where other methods have been used. About 80% of the penetrations on units that have accumulated more than 12 EDYs have been inspected by nonvisual non-destructive examinations; as a comparison, only 5% have been inspected by UT/ET for units with less than 8 EDYs. Also, all the detected leaks and cracks requiring repair have been discovered in units in the high susceptibility group. Approximately 6.6% of the penetrations in this group have been leaking or had cracks requiring repair. However, cracking was detected at 14 nozzles at Millstone 2 and one nozzle at Cook 2 when these plants had between 8 and 12 EDYs (moderate susceptibility).

Data in Figure 4-4 through Figure 4-7 provide information on inspection results by head fabricator. The incidence of PWSCC in heads fabricated by Combustion Engineering is relatively low, and comparisons by EDY group show that these differences reflect more than just differences in temperature: less than 2% of the penetrations in CE fabricated heads inspected nonvisually have shown cracks, but the result is close to 12% for B&W fabricated heads and 46% for RDY heads.

Figure 4-8 through Figure 4-11 show the inspection results by nozzle material supplier. The incidence of cracking in nozzles fabricated of materials supplied by Huntington Alloys or Standard Steel has been relatively low. Again, comparisons by EDY group show that these differences reflect more than just differences in temperature: 1.1% of the nozzles fabricated from

Huntington Alloys or Standard Steel material inspected nonvisually have shown cracks, whereas cracks have been detected on 11% of the nozzles fabricated from B&W Tubular Products material and inspected by UT/ET.[3]

Finally, Table 4-7 shows that cracks in welds have been limited to vessels fabricated by Rotterdam Dockyard and B&W designed units, although most of the nozzles inspected have been in CE vessels. There are 3,106 CRDM, CEDM, and ICI penetrations in CE fabricated vessels out of a total of 5,055 of these types of penetrations in all 69 PWR units, and 377 of the 529 inspected welds have been in vessels fabricated by CE.

4.4 Planned Head Replacements and Inspections

Table 4-8 is a list of the 33 plants that have replaced or have announced plans to replace their reactor vessel heads. As of January 2004, 10 plants have replaced their reactor vessel heads. At least another two units have set replacement plans. Also, 28 of the 29 plants in the NRC's high susceptibility category have plans to replace or are considering replacing the RVH. Finally, eight of the 17 plants with 8 to 12 EDYs have plans for head replacement in the next 2–3 years.

4.5 Conclusions

The conclusions are as follows:

- Time at temperature is an important susceptibility factor for nozzle/weld PWSCC.
- The head fabricator and nozzle material supplier are also important factors.
- Relatively little cracking has been detected in heads fabricated by Combustion Engineering using nozzle material supplied by Huntington Alloys or Standard Steel.
- No weld cracking has been detected in heads fabricated by Combustion Engineering.
- The reasons for the better performance of Combustion Engineering fabricated heads with Huntington Alloys or Standard Steel nozzle material are not known, but are likely related to processing parameters such as annealing temperature, cooling rate, straightening practices, machining practices and welding procedure details.

4.6 References

4-1. Materials Reliability Program PWSCC of Alloy 600 Type Materials in Non-Steam Generator Tubing Applications—Survey Report Through June 2002: Part 1: PWSCC in Components Other Than CRDM/CEDM Penetrations (MRP-87), EPRI, Palo Alto, CA: 2003. 1007832.

[3] Note that the 16 small-diameter thermocouple nozzles in two B&W design units were all found to have PWSCC indications. These nozzles were fabricated from nozzle material supplied by Huntington Alloys. However, because of the large geometry differences, including the relatively large size of the thermocouple nozzle welds in comparison to the nozzle size, the PWSCC performance of the small-diameter thermocouple nozzles is not indicative of the performance expected for CRDM and other large-diameter RVCH penetrations.

Table 4-1
Chronology of Key Leading Events Related to PWSCC of Alloy 600 Type Materials in PWR Plant Applications Other Than Steam Generator Tubing*

1959	-	Coriou reported on the cracking of high nickel alloys in "high purity" water at 662°F.
1986	-	A leak occurred from a pressurizer instrument nozzle at San Onofre Unit 3. This instrument nozzle was welded into the pressure vessel by a J-groove weld.
1987	-	A leak was discovered from a pressurizer heater sleeve at Arkansas Nuclear One Unit 2. Swelling of a failed electric heater element inside the sleeve was identified as a contributing cause of the PWSCC.
1988	-	A leak was discovered from two steam generator drain nozzles at Shearon Harris. The drain nozzles had been roll expanded into the steam generator head and then seal welded on the inside surface of the head.
1989	-	Leaks were discovered from 20 pressurizer heater sleeves at Calvert Cliffs Unit 2. Cold working of the inside surface of these sleeves produced by reaming the inside surface before welding into the pressure vessel head was identified as a contributing cause of the PWSCC. The repair was completed about a year after the course of action was established.
1989	-	A steam generator tube plug failed at North Anna 1 leading to the top of the plug being propelled upward through the tube and rupturing the tube at the U-bend region.
1989	-	Leaks were discovered in pressurizer instrument nozzles in two EDF plants (Nogent 1 and Cattenom 2). These instrument nozzles were roll expanded into the pressure vessel shell and then welded to the inside of the vessel shell by a J-groove weld. Subsequent examinations at other plants showed shallow circumferential cracks in pressurizer instrument nozzles in two other plants (Belleville 1 and Flamanville 2).
1991	-	A leak was discovered from a control rod drive mechanism nozzle in Bugey 3.
1992	-	Cracks were discovered in CRDM nozzles at an EDF plant with a "cold head" reported to operate at about 290°C (554°F).
1992	-	A leak was discovered from a pressurizer instrument nozzle that had been replaced at San Onofre 3 in 1986 as a result of PWSCC of the original nozzle.
1992	-	Cracks were discovered in two of eight hot leg piping instrument nozzles which were preventively removed from Palo Verde 2.
1992		Several indications were found on the outside surface of the leaking Bugey 3 nozzle which had been removed for destructive examination. These indications were located near the top of the J-groove weld and included a circumferentially oriented crack on the outside of the nozzle and cracks in the J-groove weld.
1993	-	A leak occurred from a circumferential crack in an Alloy 600 pressurizer relief valve nozzle safe end at Palisades.
1993	-	A crack from a leaking pressurizer instrument nozzle at St. Lucie 2 was chased for a considerable depth into the J-groove weld. A temper bead repair was required before installing a new nozzle.
1994	-	A 7 mm (0.276 inch) deep crack was discovered in a CRDM nozzle at D.C. Cook 2.
2000	-	Shallow ID cracks were found in hot leg nozzle butt welds at Ringhals 3 & 4.
2000	-	A leak was discovered at a reactor vessel hot leg nozzle pipe butt weld at V. C. Summer.
2000	-	Leaks were discovered from a CRDM nozzle and five thermocouple nozzles located on the Oconee 1 reactor vessel head.
2001	-	A through-wall circumferential crack was discovered above the J-groove weld in an Oconee 3 CRDM nozzle.
2002	-	Leaks from two CRDM nozzles at Davis-Besse led to significant boric acid wastage of the reactor vessel top head surface.
2002	-	Inspections following several nozzle leaks at North Anna 2 showed than most of the J-groove welds had cracks with many requiring repair. The vessel head was replaced.
2003	-	Two bottom mounted instrument (BMI) nozzles at South Texas Project Unit 1 were found to be leaking during a bare metal visual inspection of the bottom reactor head. A root cause investigation determined that the leakage was due to PWSCC. Pre-existing weld fabrications defects appeared to be an aggravating factor.
2003	-	Circumferential through-wall cracks were detected in five of 36 Alloy 600 pressurizer heater sleeves at Palo Verde Unit 2. All the cracks were located above the J-groove weld, inside the pressure boundary.

*Only the initial occurrence of each type is reported.

Table 4-2
Summary of Key Parameters Related to Reactor Vessel Closure Head Nozzle PWSCC

EDYs MRP-48 (2/2001)	Current Head Temp. (°F)	Unit Name	Material Supplier[1]	Vessel Fabricator[2]	Max Nozzle Fit[3]	Insulation Type	Refueling Outage Schedule				EDYs Reported in Responses to Bulletin 2002-02		Replacing Head[5]	No. of CRDM/CEDM Nozzles	CRDM/CEDM Inspection Methods Since 11/2000 and Through 12/2003			
							Spr 03	Fall 03	Spr 04	Fall 04	EDYs	Date			Note	Visual	Nozzle NDE	Weld NDE
22.1	602.0	Oconee 1	B	BW	1.5	Reflective Horizontal		X			23.2	Fall 2003	Fall 2003	69		BMV	UT(23), ET(8), PT(2)	PT(3)
22.0	602.0	Oconee 2	B	BW	1.5	Reflective Horizontal			X		23.7	Oct-2002	Spring 2004	69		BMV	UT, PT(9), ET(4)	PT(9)
21.7	602.0	Oconee 3	B	BW	1.5	Reflective Horizontal	Apr-03			X	22.5	Spring 2003	Spring 2003	69		BMV	UT, ET(18), PT(12)	PT(12)
19.5	602.0	ANO 1	B/H	BW	1.5	Reflective Horizontal			X		19.5	Oct-2002	Fall 2005	69		BMV	UT, PT(3)	PT(3)
19.4	600.1	North Anna 1	S	RDM	1.2	Reflective Stepped	Mar-03			X	21.4	Mar-2003	Spring 2003	65		BMV	ET(30), UT(8), PT(4)	ET(25), PT(4)
19.0	599.7	Robinson 2	H	CE	3.0	Blanket Contoured			Apr-04		>19	*Since MRP-48*	Fall 2005	69		BMV	ET, UT(17)	ET
18.6	597.8	Surry 1	H	BW/RDM	1.2	Reflective Stepped	Apr-03			X	20.5	Apr-2003	Spring 2003	65		BMV	UT(16)	PT(10)
18.6	597.8	Surry 2	B/S	BW/RDM	1.2	Reflective Stepped		Sep-03			20.9	Sep-2003	Fall 2003	65		BMV		
18.3	600.1	North Anna 2	S	RDM	1.2	Reflective Stepped			X		19.8	Sep-2002	Fall 2002	65		BMV	ET(63), UT(35)	ET(59), PT(6)
17.9	605.0	Davis-Besse	B/H	BW	1.5	Reflective Horizontal					0.0	Fall 2002	Fall 2002	69		BMV	UT	
17.5	601.0	TMI 1	B	BW	1.5	Reflective Horizontal		X			*Note 4*	*Note 4*	Fall 2003	69		BMV	UT(12), PT(12)	PT(12)
16.7	594.4	Turkey Point 3	H	BW	1.5	Blanket Contoured	Mar-03			X	18.3	Mar-2003	Fall 2004	65		BMV	UT	
16.6	594.4	Turkey Point 4	H	BW	1.5	Blanket Contoured		Oct-03			18.6	Oct-2003	Spring 2005	65		BMV	UT	
15.8	596.5	Farley 1	H/B	BW/CE	3.0	Reflective Stepped	Mar-03			X	17.5	Mar-2003	Fall 2004	69		BMV	ET, UT	
15.6	601.0	Crystal River 3	B	BW	1.5	Reflective Horizontal		X			*Note 4*	*Note 4*	Fall 2003	69		BMV	UT(9)	
15.1	580.2	Ginna	H	BW	1.5	Block Contoured Cemented		X			*Note 4*	*Note 4*	Fall 2003	37	6			
14.9	591.6	Point Beach 2	H/B	BW/CE	3.0	Modified for BMV		Sep-03			16.6	Sep-2003	Spring 2005	49		BMV	UT	
14.7	590.6	St. Lucie 1	H	CE	3.0	Modified for BMV			X		15.8	Sep-2002	Fall 2005	69		BMV	UT	
14.5	596.9	Farley 2	B/H	BW/CE	3.0	Reflective Stepped			X		15.6	Sep-2002	Fall 2005	69		BMV	UT	
14.5	590.5	San Onofre 2	SS/H	CE	3.0	Modified for BMV			Feb-04		15.5	Aug-2002	Assessing	91		BMV	ET, UT	ET(46), PT(1)
14.4	590.6	San Onofre 3	SS/H	CE	3.0	Modified for BMV	Jan-03		X		15.2	Aug-2002	Assessing	91		BMV	ET, UT	ET
14.2	593.7	Calvert Cliffs 1	H	CE	3.0	Removable Collars			Mar-04		16.3	Mar-2004	Spring 2006	65		BMV		
14.1	599.7	Waterford 3	SS/H	CE	3.0	Modified for BMV		X			*Note 4*	*Note 4*		91		BMV	UT	
13.8	593.7	Calvert Cliffs 2	H	CE	3.0	Blanket Contoured	Feb-03				15.2	Feb-2003	Spring 2007	65		BMV	UT	
13.5	591.6	Point Beach 1	H	BW	1.5	Modified for BMV			X		14.5	Sep-2002	Fall 2005	49		BMV	UT	PT(1)
13.0	600.7	Cook 2	W	CBI	4.0	Reflective Stepped	Apr-03			X	14.6	Apr-03	Fall 2007	78	7	BMV	UT(69), ET, PT(3)	ET(10), PT(2)
12.4	595.0	Beaver Valley 1	H/B	BW/CE	3.0	Reflective Stepped	Mar-03			X	14.0	Mar-2003	Spring 2006	65		BMV	ET, UT(27)	ET
12.3	595.6	St. Lucie 2	SS/H	CE	3.0	Modified for BMV	Apr-03			X	14.0	Apr-2003	Fall 2007	91		BMV	UT	
10.8	588.0	Fort Calhoun	H	CE	3.0	Reflective Stepped		Sep-03			11.8	Sep-2003	Fall 2006	41		BMV		
10.8	583.1	Kewaunee	H/B	BW/CE	3.0	Reflective Panels	Apr-03			X	< 12	Spring 2003	Fall 2004	40		BMV		
10.6	593.5	Indian Point 3	H	CE	3.0	Reflective Stepped	Mar-03				11.2	Mar-2003		78		BMV	ET(41), UT(41)	
10.6	594.7	Salem 1	H	CE	3.0	Reflective Horizontal			X		11.9	Oct-2002	Fall 2005	79		BMV		
10.5	594.8	ANO 2	SS/H	CE	3.0	Collars Around Nozzles		X			*Note 4*	*Note 4*		81	8	LFET	UT, ET(1)	PT(2)
10.5	593.9	Millstone 2	H	CE	3.0	Modified for BMV		Oct-03			12.7	Oct-2003	Spring 2005	69		BMV	UT, PT(9)	PT(3)
9.9	580.2	Prairie Island 1	CL	CL	3.5	Reflective Horizontal			X		< 11	Winter 2002	Spring 2006	40		BMV		
9.9	580.2	Prairie Island 2	A	CL	3.5	Reflective Horizontal		X			< 11	Fall 2003	Spring 2005	40		BMV		
9.6	593.0	Diablo Canyon 2	H	CE	3.0	Reflective Stepped	Feb-03			X	10.9	Feb-2003		78		BMV		
9.5	578.0	Cook 1	H	CE	3.0	Reflective Stepped		Oct-03			*10.3*	Oct-2003	Fall 2006	79		BMV	UT(64), ET(22), PT(2)	ET(23), PT(2)
9.4	592.0	Palo Verde 1	SS	CE	3.0	Will Be Modified for BMV			X		11.2	Fall 2002		97		BMV(25)	ET, UT	ET(13)
9.1	591.7	Palo Verde 2	SS	CE	3.0	Modified for BMV		X			10.5	Spring 2002		97		BMV	ET, UT	ET(22)
9.1	592.2	Palo Verde 3	SS	CE	3.0	Will Be Modified for BMV	Apr-03			X	11.1	Spring 2003		97			ET, UT	ET(14)
8.9	586.4	Palisades	H	CE	3.0	Blanket Contoured	Mar-03			X	< 10	Spring 2003		45	9	BMV		
8.4	589.1	Diablo Canyon 1	H	CE	3.0	Reflective Stepped			Feb-04		10.2	Feb-2004		79		BMV		
8.3	595.0	Beaver Valley 2	H	CE	3.0	Reflective Stepped		Sep-03			10.1	Sep-2003		65		BMV	UT	
8.3	594.1	Salem 2	H	CE	3.0	Reflective Horizontal		Oct-03			10.3	Oct-2003	Spring 2005	78		BMV		
7.1	585.5	Indian Point 2	H	CE	3.0	Reflective Stepped				X	8.0	Oct-2002		97		BMV	UT(92), ET(56)	PT(1)
11.1	561.0	South Texas 2	H/B	CE	3.0	Reflective Stepped			X		5.3	Oct-2002		74	10	BMV		
10.7	561.0	South Texas 1	H	CE	3.0	Reflective Stepped	Mar-03			X	4.5	Mar-2003		74	10	BMV		
2.3	556.8	Callaway	H	CE	3.0	Reflective Stepped			X		2.5	Oct-2002		78		BMV		
2.3	557.3	Summer	B	CBI	4.0	Reflective Stepped		X			2.5	Apr-2002		65		BMV		
2.2	557.0	McGuire 1	H	CE	3.0	Reflective Horizontal			X		2 to 3	Fall 2003		78		BMV		
2.2	557.0	McGuire 2	S	RDM	1.2	Reflective Horizontal		X			2 to 3	Fall 2003		78		BMV		
2.2	560.0	Vogtle 1	H	CE	3.0	Reflective Stepped		Sep-03			2.7	Sep-2003		78		BMV		
2.2	558.0	Wolf Creek	H	CE	3.0	Reflective Stepped		X			2.4	Sep-2002		78		BMV		
2.1	557.0	Catawba 1	S	RDM	1.2	Reflective Stepped		X			2 to 3	Fall 2003		78		BMV		
2.0	558.0	Shearon Harris	B	CBI	4.0	Reflective Stepped	Apr-03			X	2.1	Sep-2002		65		BMV		
1.9	557.0	Catawba 2	H	CE	3.0	Reflective Stepped	Mar-03			X	2 to 3	Fall 2003		78		BMV		
1.9	560.0	Vogtle 2	H	CE	3.0	Reflective Stepped			X		2.2	Oct-2002		78		BMV		
1.7	561.0	Comanche Peak 1	H	CE	3.0	Reflective Stepped			X		2.1	Oct-2002		78		BMV		
1.6	551.0	Byron 1	B	BW	1.5	Reflective Horizontal		Sep-03			2.0	Sep-2003		78		BMV		
1.6	558.4	Millstone 3	H	CE	3.0	Reflective Horizontal			X		1.9	Sep-2002		78		BMV		
1.6	559.9	Seabrook	H	CE	3.0	Reflective Stepped		Oct-03			1.8	Aug-2002		78		BMV		
1.5	556.0	Braidwood 1	B	BW	1.5	Reflective Horizontal	Apr-03			X	1.7	Apr-2003		78		BMV		
1.4	552.0	Braidwood 2	B	BW	1.5	Reflective Horizontal		Oct-03			1.7	Oct-2003		78		BMV		
1.4	550.4	Byron 2	B	BW	1.5	Reflective Horizontal			X		1.8	Sep-2002		78		BMV		
1.3	561.0	Comanche Peak 2	H	CE	3.0	Reflective Stepped		X			1.8	Fall 2003		78		BMV		
1.3	547.0	Sequoyah 1	S	RDM	1.4	Reflective Horizontal	Mar-03			X	1.5	Spring 2003		78		BMV	UT(6)	PT(1)
1.3	547.0	Sequoyah 2	S	RDM	1.4	Reflective Horizontal		X			1.6	Fall 2003		78		BMV		
0.7	557.3	Watts Bar 1	S	RDM	1.2	Reflective Horizontal		X			1.1	Fall 2003		78		BMV		

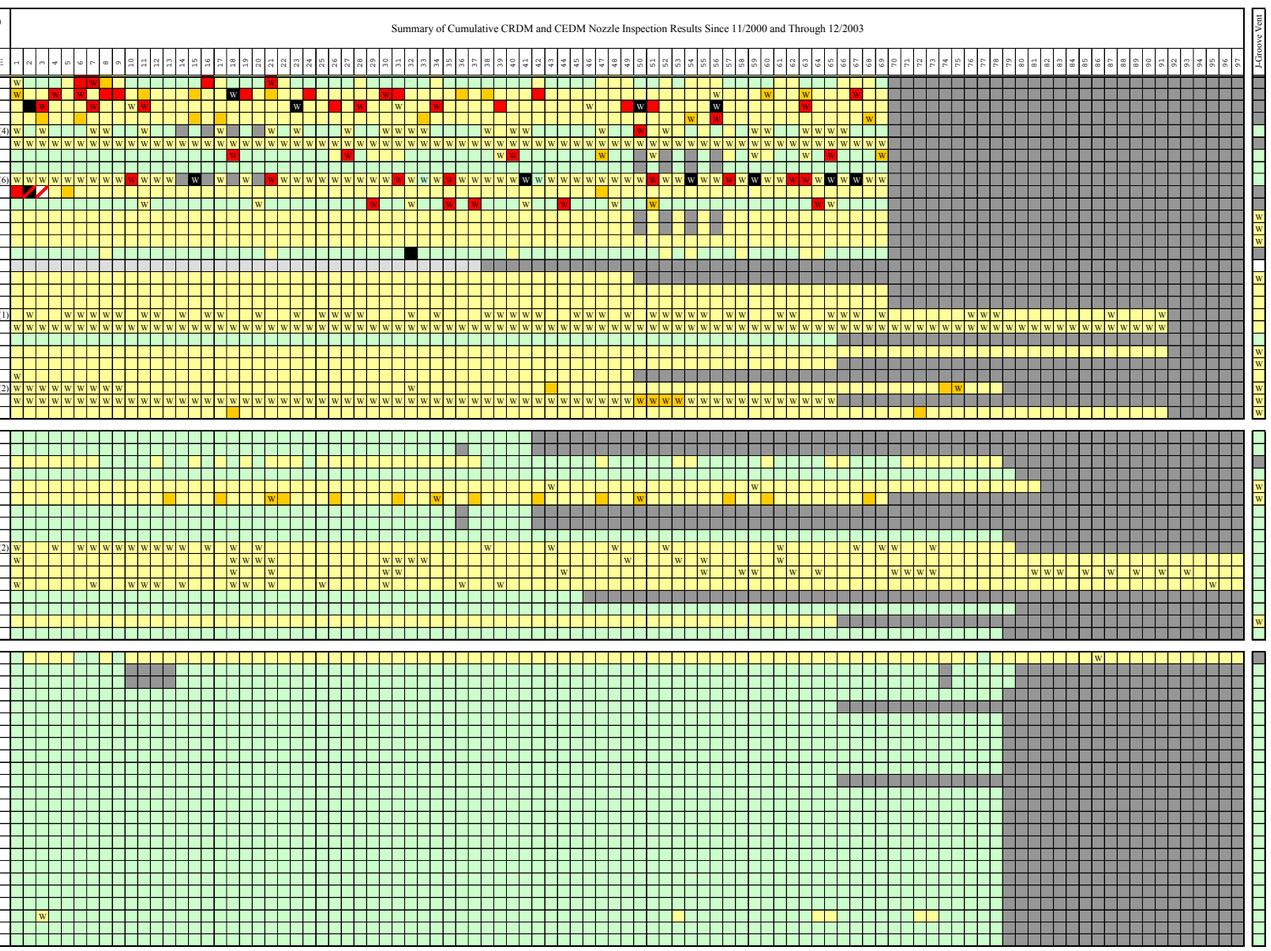

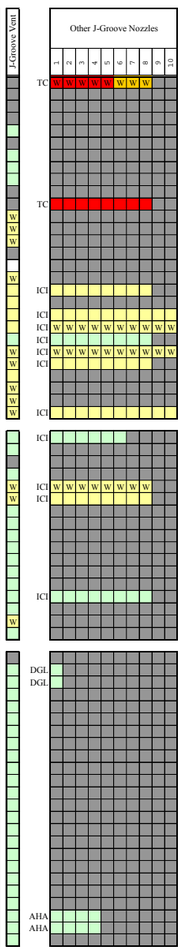

Notes

1. Key for Material Suppliers: B = B&W Tubular Products, H = Huntington, S = Sandvik, SS = Standard Steel, W = Westinghouse (Huntington), CL = C.L. Imphy, A = Aubert et Duval
2. Key for Vessel Fabricators: BW = B&W, CBI = Chicago Bridge & Iron, CE = Combustion Engineering, RDM = Rotterdam Dockyard, CL = C.L. Imphy
3. Maximum Specified Diametral Interference Fit (mils).
4. Not reported in Response to Bulletin 2002-02 (e.g., because of head replacement).
5. Green = Head Replaced.
6. Because of cemented head insulation, performed special inspections in spring 2002:
   100% visual above insulation, removed insulation in two suspect areas, no evidence of leakage;
   100% visual of seal weld joint between CRDM adaptor and CRDM, no indications; and
   UT at center of head and four instrument port penetration locations, through thickness direction of head to assure no voids similar to Davis-Besse experience.
   Also 100% inspection of ID surface of all head penetrations by ET in 1999 with no recordable indications.
7. Axial cracks detected on ID of Nozzle 75 in October 1994.
8. No BMV inspection, but Low Frequency Eddy Current Testing (LFET) of the head from the ID of the nozzles, to examine for cavity in the low alloy steel material, in addition to standard UT leak path techniques.
9. ET for all ICI nozzles in 1995.
10. Modification to EDY calculation based on re-evaluation of head temperature.

Inspection Status Code

- No nozzle associated with this location
- Not yet inspected (since first CRDM leakage was discovered in December 2000)
- Visual not meeting 100% BMV requirements (e.g., < 100% nozzle inspected by BMV, insulation not removed or lifted)
- Bare Metal Visual (BMV) inspection with no leaks
- Non-visual inspection (UT or ET) of nozzle base metal with no leaks or cracks (indications having detectable depth)
- Non-visual inspection (UT, ET or PT) of nozzle base metal with cracks requiring repair
- Leaking nozzle (according to BMV but not including masked nozzles found not to be leaking by UT/ET)
- Circumferential crack above or near top of J-groove weld
- Significant wastage of low alloy steel head material
- W = Weld inspected by PT or ET

Other J-Groove Nozzle Code

AHA = Auxiliary Head Adapter
DGL = De-Gas Line Nozzle
ICI = In-Core Instrument Nozzle
TC = B&W Thermocouple Nozzle

Table 4-3
Summary of Plants with Detected Reactor Vessel Closure Head Penetration Cracking

Number	Unit	EDYs thru Feb. 2001 (@ 600°F) (MRP-48)	Current Head Temp. (°F)	NSSS Supplier	Vessel Fabricator (Note 1)	Nozzle Material Supplier (Note 2)	No. of CRDM or CEDM Nozzles on Head	Number Cracked Penetrations Detected (Note 3)			Notes
								Total	Due to Tube Cracking	Due to Weld Cracking	
1	ANO 1	19.5	602.0	B&W	BW	B/H	69	8	7	2	
2	Beaver Valley 1	12.4	595.0	W	BW/CE	H/B	65	4	4	0	
3	Cook 2	13.0	600.7	W	CBI	W	78	3	3	0	
4	Crystal River 3	15.6	601.0	B&W	BW	B	69	1	1	1	
5	Davis-Besse	17.9	605.0	B&W	BW	B/H	69	5	5	0	
6	Millstone 2	10.5	593.9	CE	CE	H	69	14	14	0	
7	North Anna 1	19.4	600.1	W	RDM	S	65	6	6	1	
8	North Anna 2	18.3	600.1	W	RDM	S	65	42	8	42	
9	Oconee 1	22.1	602.0	B&W	BW	B	69	5	5	2	4
10	Oconee 2	22.0	602.0	B&W	BW	B	69	19	18	4	
11	Oconee 3	21.7	602.0	B&W	BW	B	69	14	14	2	
12	St. Lucie 2	12.3	595.6	CE	CE	SS/H	91	2	2	0	5
13	Surry 1	18.6	597.8	W	BW/RDM	H	65	6	0	6	
14	TMI 1	17.5	601.0	B&W	BW	B	69	8	7	4	4
							Unique Penetration Totals	137	94	64	

NOTES:

1. Key for Vessel Fabricators: BW = B&W, CBI = Chicago Bridge & Iron, CE = Combustion Engineering, RDM = Rotterdam Dockyard, CL = C.L. Imphy
2. Key for Material Suppliers: B = B&W Tubular Products, H = Huntington, S = Sandvik, SS = Standard Steel, W = Westinghouse, CL = C.L. Imphy, A = Aubert et Duval
3. The totals reflect CRDM and CEDM nozzles that were found to have cracks requiring repairs. In addition, the 8 small-diameter B&W thermocouple nozzles each at Oconee 1 and TMI 1 were found to be cracked. No other types of reactor vessel head penetrations have been reported to have PWSCC indications. Note that NDE of the welds is often not as complete as for the tubes, so some weld cracks may have not been found during inspections and thus not reflected in this table.
4. Also all 8 small-diameter B&W thermocouple nozzles were found to be cracked.
5. The CEDM nozzle material at this plant was supplied by Standard Steel, and the ICI nozzle material was supplied by Huntington Alloys.

Table 4-4
Summary of Reactor Vessel Closure Head Penetration Leakage

Inspection Number	Unit	NSSS Supplier	Approx. EDYs at Insp.	Insp. Date	No. of CRDM Nozzles on Head	Number Leaking Penetrations (Note 1)			Notes
						Total	Due to Tube Cracking	Due to Weld Cracking	
1	ANO 1	B&W	19.6	Mar-2001	69	1	1	0	
2			21.1	Oct-2002	69	1	1	0	2
3	Crystal River 3	B&W	16.2	Oct-2001	69	1	1	0	
4	Davis-Besse	B&W	19.2	Apr-2002	69	3	3	0	3
5	North Anna 1	W	21.4	Mar-2003	65	1	0	1	
6	North Anna 2	W	19.0	Nov-2001	65	3	0	3	
7			19.7	Sep-2002	65	6	0	6	4, 5
8	Oconee 1	B&W	21.8	Nov-2000	69	1	0	1	6
9			23.2	Mar-2002	69	1	0	1	
10			24.7	Sep-2003	69	2	2	0	7, 8
11	Oconee 2	B&W	22.2	Apr-2001	69	4	4	0	
12			23.7	Oct-2002	69	10	7	3	
13	Oconee 3	B&W	21.7	Feb-2001	69	9	9	0	
14			22.5	Nov-2001	69	5	5	0	
15	Surry 1	W	19.1	Oct-2001	65	4	0	4	
16	TMI 1	B&W	18.1	Oct-2001	69	5	1	4	9
				Unique Penetration Totals		55	33	22	

NOTES:

1. No CEDM, ICI, or other types of reactor vessel head nozzles have been found to be leaking (other than the B&W thermocouple nozzles at the two units that have this type of nozzle). Note that NDE of the welds is often not as complete as for the tubes, so some leak path cracks through the weld metal from the wetted weld surface to the nozzle annulus may have not been found during inspections and thus not reflected in this table.
2. The leaking nozzle that was repaired in March 2001 was found to be leaking again in October
3. Detailed destructive examinations of the original Davis-Besse head have been performed to characterize the extent of wastage. The destructive examinations showed an axial crack through most of the weld cross section at the location of the long axial tube crack in Nozzle #3, which was adjacent to the large wastage cavity.
4. One of the leaking nozzles that was repaired in late 2001 was found to be leaking again in September 2002.
5. Some cracked nozzles have been extracted from the original North Anna 2 head for destructive testing including characterization of tube and weld cracks, among other tests.
6. Also 5 of the 8 small-diameter B&W thermocouple nozzles were found to be leaking.
7. It is assumed in the table that these two penetrations were found to be leaking due to base metal cracking although no inspections were performed to investigate before head replacement.
8. Also one small-diameter thermocouple penetration that was previously repaired with an Alloy 690 plug was found to be leaking. The cause of the leakage (incomplete weld coverage, cracking, etc.) was not determined as the head was replaced.
9. Also all 8 small-diameter B&W thermocouple nozzles were found to be leaking.

Table 4-5
Orientation and Location for Reactor Vessel Closure Head Nozzle Cracks

Type / *Location*		No. of Indications on the Nozzle ID	No. of Indications on the Nozzle OD	*Total*
No. of Axial Tube Indications		112	239	*351*
No. of Circumferential Tube Indications	**Above Weld**	0	7	*7*
	Weld Elevation	0	12	*12*
	Below Weld	6	10	*16*
	Total	*118*	*268*	*386*

Note: Craze cracking and other shallow indications with no depth detectable by UT are not included.

Table 4-6
Summary of Nozzle Circumferential Cracks Located Above the Weld, in the Weld Elevation Zone, or Below the Weld

OD Circumferential Flaws above the Weld											
				Inspection Results							
Unit	*NSSS Design*	*Nozzle ID*	*Nozzle Angle (°)*	*Date*	*Approx. EDYs*	*OD/ ID*	*Axial Location*	*Circ. Angle (°)*	*UH/DH Side*	*Depth (in)*	*TW Depth (%)*
Crystal River 3	B&W	32	26.2	Oct-01	16.2	OD	above weld	91	DH	0.29	47%
Davis-Besse	B&W	2	8.0	Mar-02	19.2	OD	above weld	34	DH	0.31	50%
Oconee 2	B&W	18	18.2	Apr-01	22.2	OD	above weld	36	DH	0.07	11%
Oconee 3	B&W	23	23.2	Feb-01	21.7	OD	above weld	66	DH	0.22	35%
		50	35.1			OD	above weld	165	UH	0.62	pin holes
		56	35.1			OD	above weld	165	UH/DH	0.62	100%
		2	8.0	Nov-01	22.5	OD	above weld	48	DH	0.18	29%

OD Circumferential Flaws at the Weld Elevation											
				Inspection Results							
Unit	*NSSS Design*	*Nozzle ID*	*Nozzle Angle (°)*	*Date*	*Approx. EDYs*	*OD/ ID*	*Axial Location*	*Circ. Angle (°)*	*UH/DH Side*	*Depth (in)*	*TW Depth (%)*
North Anna 2	W	15	19.8	Sep-02	19.7	OD	≥1.12" below root	5	DH	0.23	36%
		41	33.1			OD	≥0.52" below root	46	DH	0.10	16%
		54	38.6			OD	≥0.04" below root	79	UH	0.23	36%
						OD	≥0.28" below root	32	DH	0.16	25%
		59	40.0			OD	≥0.31" below root	76	DH	0.15	24%
						OD	≥0.32" below root	50	UH	0.15	24%
		65	42.6			OD	≥0.32" below root	72	DH	0.15	24%
						OD	≥0.20" below root	30	UH	0.08	12%
		67	42.6			OD	≥0.80" below root	44	DH	0.09	15%
Oconee 3	B&W	11	16.2	Feb-01	21.7	OD	over weld	153	DH	0.36	57%
						OD	over weld	113	UH	0.25	40%
		26	24.7	Nov-01	22.5	OD	over weld	44	DH	0.07	11%

Table 4-6
Summary of Nozzle Circumferential Cracks Located Above the Weld, in the Weld Elevation Zone, or Below the Weld (continued)

OD Circumferential Flaws below the Weld											
				Inspection Results							
Unit	*NSSS Design*	*Nozzle ID*	*Nozzle Angle (°)*	*Date*	*Approx. EDYs*	*OD/ ID*	*Axial Location*	*Circ. Angle (°)*	*UH/DH Side*	*Depth (in)*	*TW Depth (%)*
ANO-1	B&W	56	35.1	Mar-01	19.6	OD	below weld	51	DH	< 0.2	< 32%
Crystal River 3	B&W	32	26.2	Oct-01	16.2	OD	below weld	31	UH	0.47	76%
							below weld	195	UH	0.62	100%
Millstone 2	CE	21	25.3	Mar-02	11.2	OD	below weld	23	DH	0.20	40%
		34	32.7			OD	below weld	26	DH	0.10	20%
Oconee 3	B&W	23	23.2	Feb-01	21.7	OD	below weld	62	DH	0.42	68%
							below weld	58	UH	0.33	53%
		50	35.1			OD	below weld	78	UH	0.57	92%
							below weld	70	DH	0.27	43%
		56	35.1			OD	below weld	24	DH	0.08	13%

ID Circumferential Flaws below the Weld											
				Inspection Results							
Unit	*NSSS Design*	*Nozzle ID*	*Nozzle Angle (°)*	*Date*	*Approx. EDYs*	*OD/ ID*	*Axial Location*	*Circ. Angle (°)*	*UH/DH Side*	*Depth (in)*	*TW Depth (%)*
Oconee 3	B&W	11	16.2	Feb-01	21.7	ID	below weld	25	UH	0.08	14%
		50	35.1			ID	below weld	48	UH	0.06	10%
							below weld	96	UH	0.08	13%
		56	35.1			ID	below weld	57	UH	0.10	16%
							below weld	48	UH	0.05	8%
							below weld	39	UH	0.03	5%

Table 4-7
Summary of Inspections of Reactor Vessel Closure Head Penetration J-Groove Welds

	Vessel Fabricator[1]	CRDM, CEDM and ICI Nozzles on Original Heads					Notes
		No. of Plants	*Total No. of Nozzles*	*No. of Welds Inspected by ET or PT*	*No. of Welds Cracked*[2]	*No. of Welds Leaking*	
All EDYs	CE	40	3106	377	0	0	
	B&W	15	1011	40	15	9	
	RDM	9	650	101	49	13	**4**
	CBI	3	208	11	0	0	
	CL	2	80	0	0	0	
		Unique Penetration Totals	**5055**	**529** *10.5%*	**64** *1.3%*	**22** *0.4%*	
> 12 EDYs[3]	CE	14	1114	304	0	0	
	B&W	11	699	40	15	9	
	RDM	4	260	100	49	13	**4**
	CBI	1	78	11	0	0	
	CL	0	0	0	0	0	
		Unique Penetration Totals	**2151**	**455** *21.2%*	**64** *3.0%*	**22** *1.0%*	
8 - 12 EDYs[3]	CE	15	1115	72	0	0	
	B&W	0	0	0	0	0	
	RDM	0	0	0	0	0	
	CBI	0	0	0	0	0	
	CL	2	80	0	0	0	
		Unique Penetration Totals	**1195**	**72** *6.0%*	**0**	**0**	
< 8 EDYs[3]	CE	11	877	1	0	0	
	B&W	4	312	0	0	0	
	RDM	5	390	1	0	0	
	CBI	2	130	0	0	0	
	CL	0	0	0	0	0	
		Unique Penetration Totals	**1709**	**2** *0.1%*	**0**	**0**	

NOTES:
1. Key for Vessel Fabricators: CE = Combustion Engineering, B&W = Babcock & Wilcox, RDM = Rotterdam Dockyard, CBI = Chicago Bridge & Iron, CL = C.L. Imphy
2. The totals reflect welds that were found to have cracks requiring repairs.
3. EDYs at the time of the most recent inspection.
4. Most of the indications for RDM vessels can be attributed to North Anna 2 (42 cracked and 8 leaking welds).

Table 4-8
Completed and Announced Reactor Vessel Closure Head Replacements (as of 1/2004)

Status	Year	Season	No.	Unit Name
Already Replaced	2002	Fall	1	Davis-Besse
			2	North Anna 2
	2003	Spring	3	North Anna 1
			4	Oconee 3
			5	Surry 1
		Fall	6	Crystal River 3
			7	Ginna
			8	Oconee 1
			9	Surry 2
			10	TMI 1
Announced Plans	2004	Spring	11	Oconee 2
		Fall	12	Farley 1
			13	Kewaunee
			14	Turkey Point 3
	2005	Spring	15	Millstone 2
			16	Point Beach 2
			17	Prairie Island 2
			18	Turkey Point 4
			19	Salem 2
		Fall	20	ANO 1
			21	Farley 2
			22	Point Beach 1
			23	Robinson 2
			24	St. Lucie 1
			25	Salem 1
	2006	Spring	26	Beaver Valley 1
			27	Calvert Cliffs 1
			28	Prairie Island 1
		Fall	29	Cook 1
			30	Fort Calhoun
	2007	Spring	31	Calvert Cliffs 2
		Fall	32	St. Lucie 2
			33	Cook 2

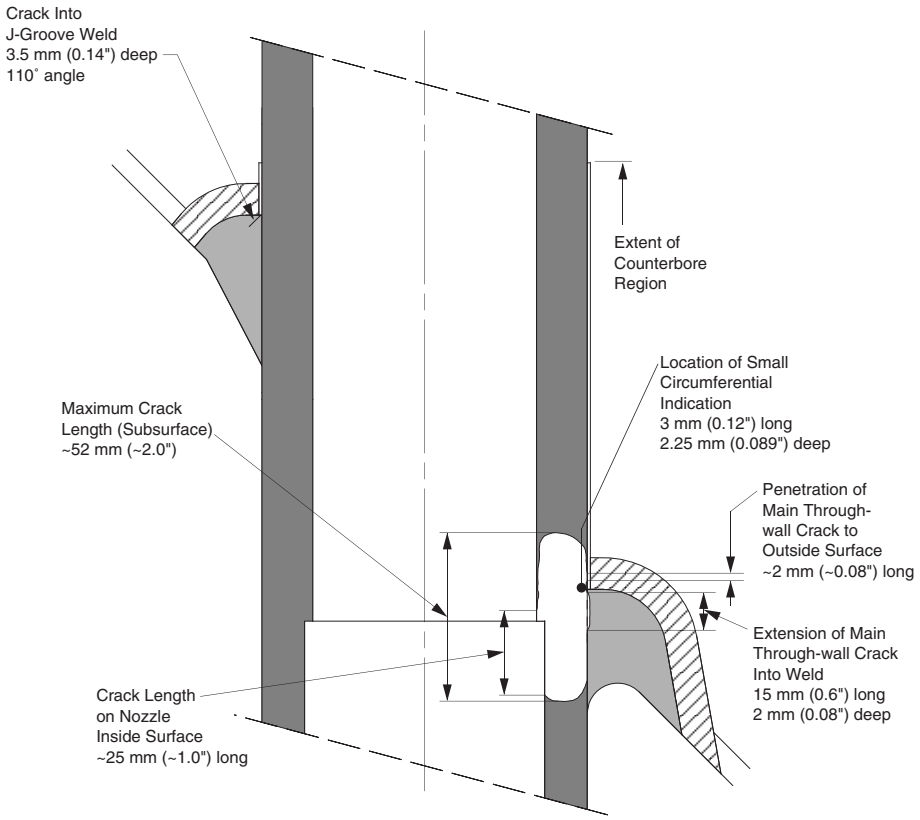

Figure 4-1
Locations of Cracks in Bugey 3 CRDM Nozzle 54 (cross section through leaking crack)

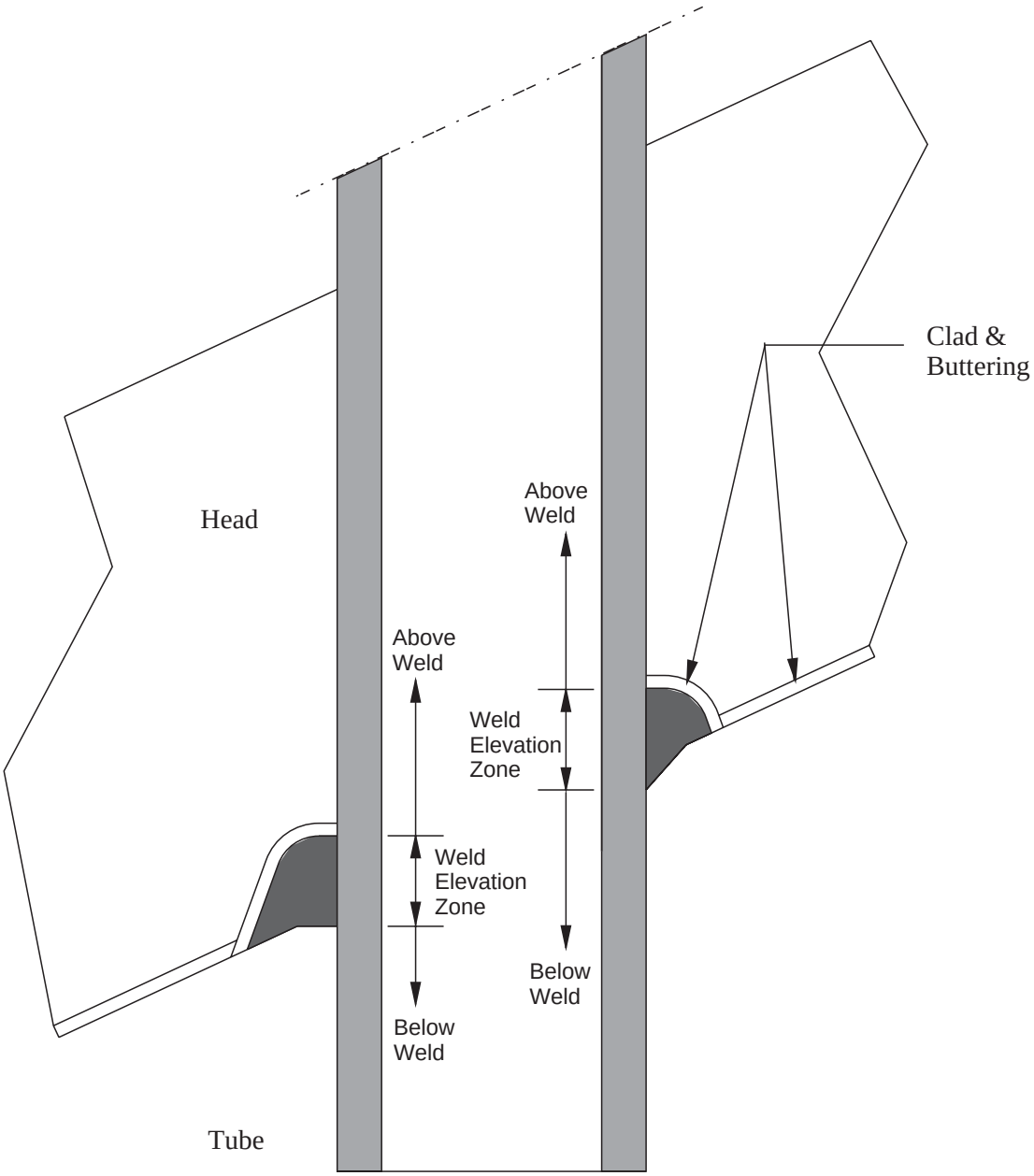

Figure 4-2
Definition of Nozzle Regions with Respect to the Location of the J-Groove Weld

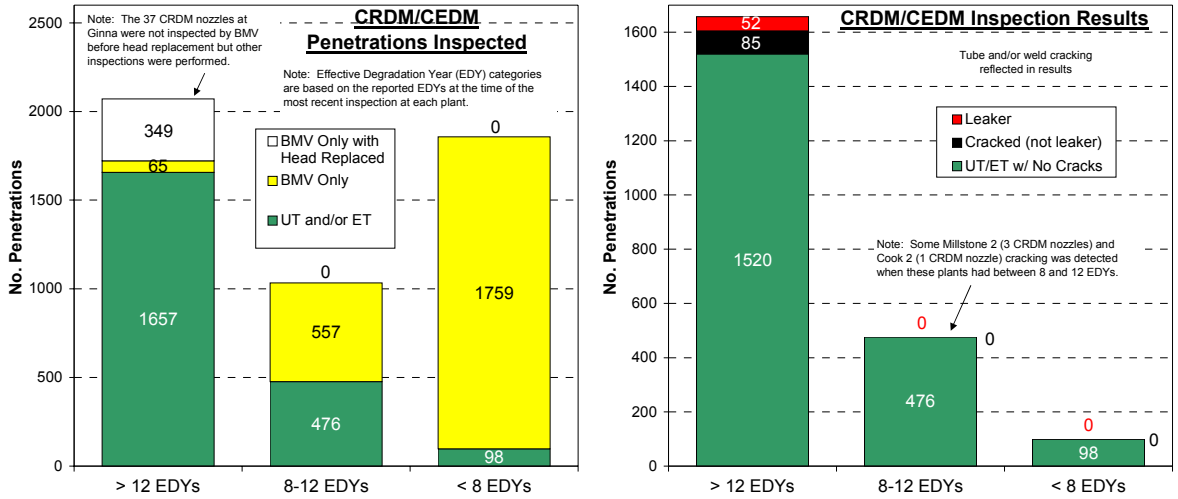

Figure 4-3
Reactor Vessel Closure Head Inspection Statistics—by EDY Group

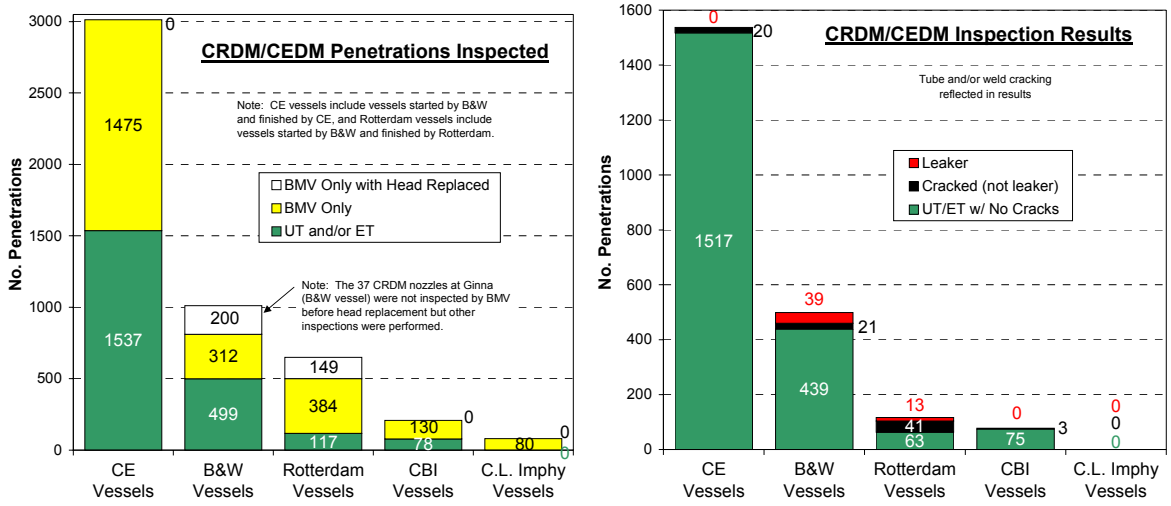

Figure 4-4
Reactor Vessel Closure Head Inspection Statistics—by Head Fabricator (All EDYs)

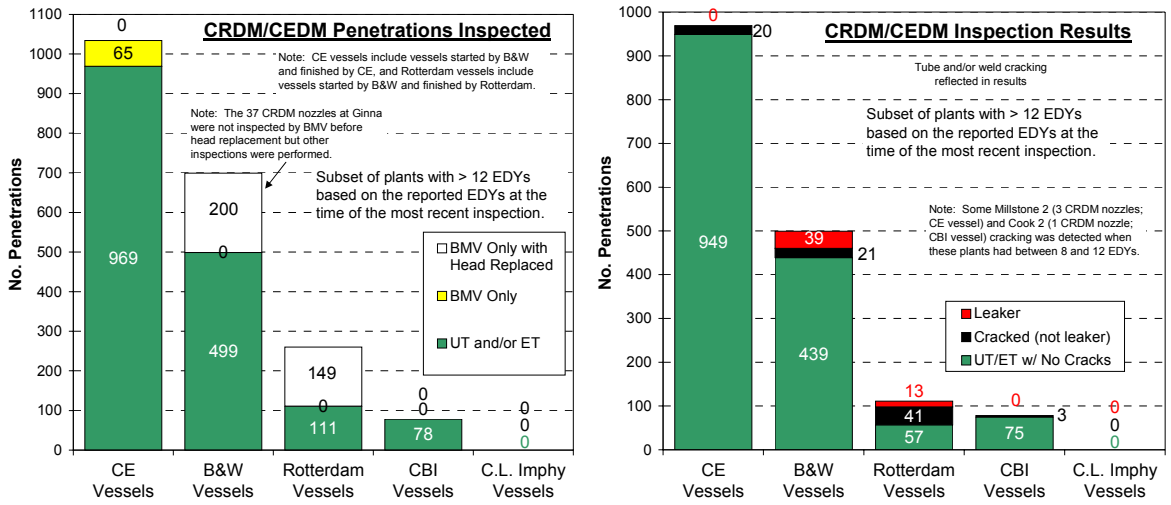

Figure 4-5
Reactor Vessel Closure Head Inspection Statistics—by Head Fabricator (>12 EDYs)

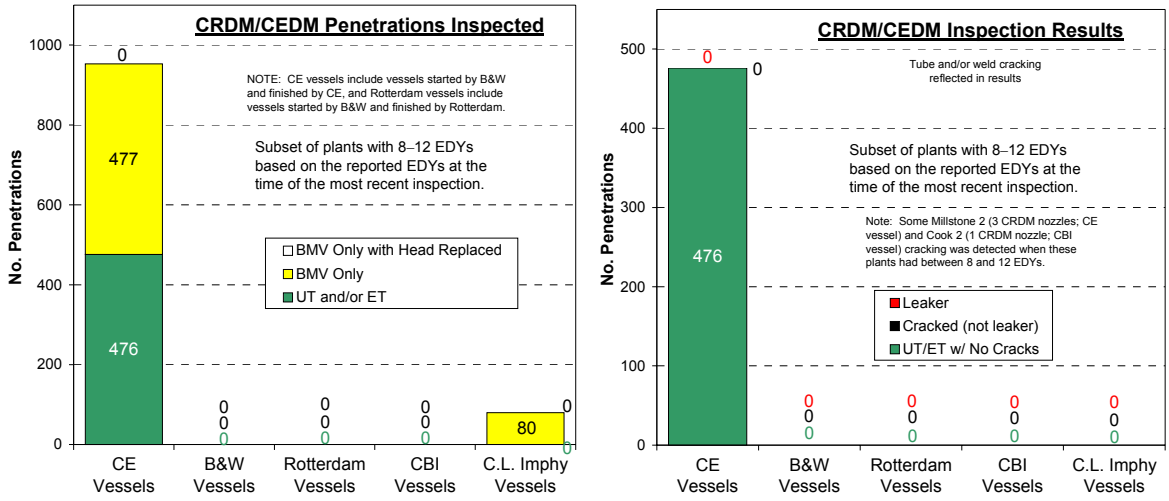

Figure 4-6
Reactor Vessel Closure Head Inspection Statistics—by Head Fabricator (8–12 EDYs)

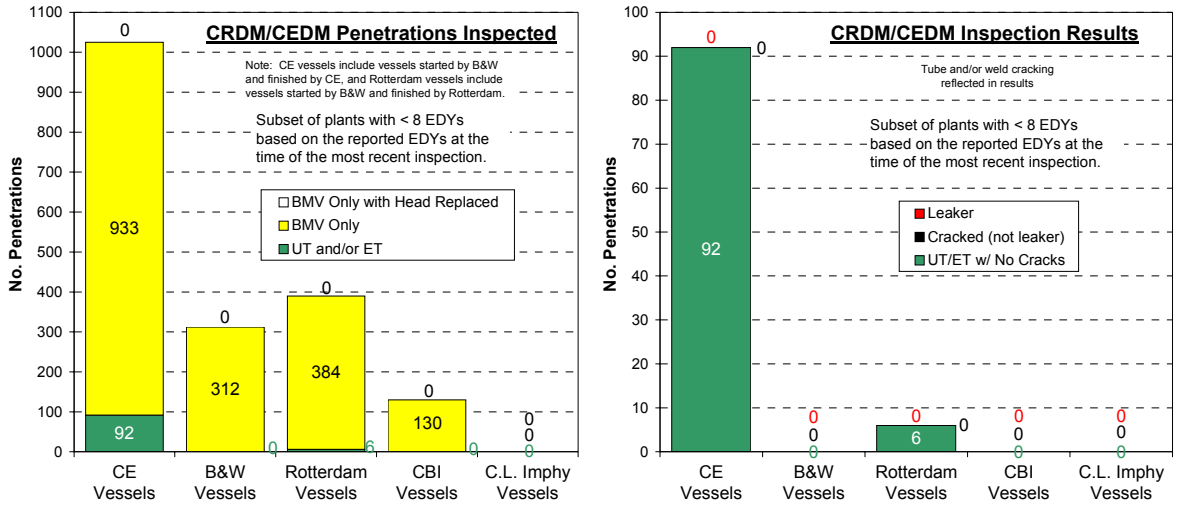

Figure 4-7
Reactor Vessel Closure Head Inspection Statistics—by Head Fabricator (<8 EDYs)

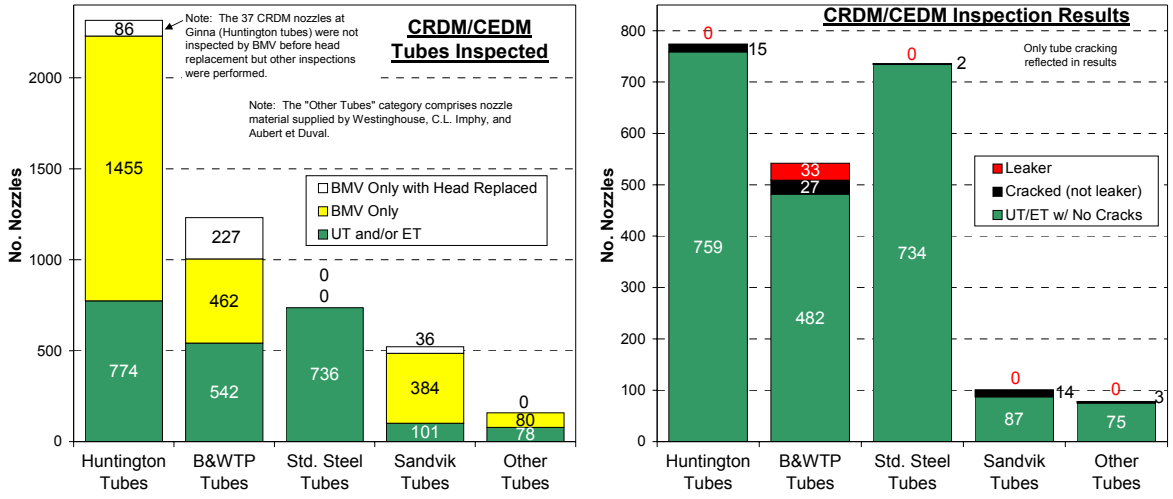

Figure 4-8
Reactor Vessel Closure Head Inspection Statistics—by Nozzle Material Supplier (All EDYs)

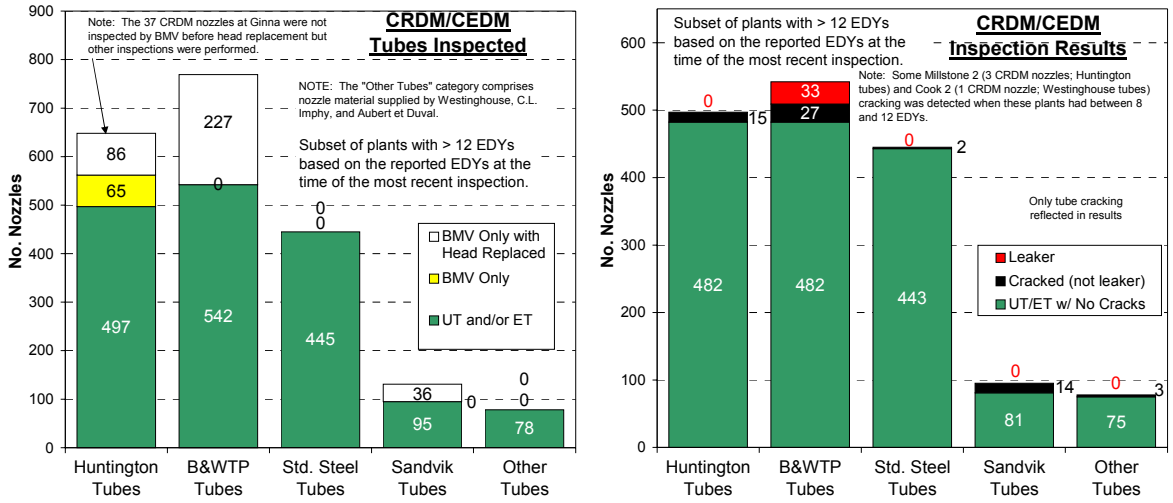

Figure 4-9
Reactor Vessel Closure Head Inspection Statistics—by Nozzle Material Supplier (>12 EDYs)

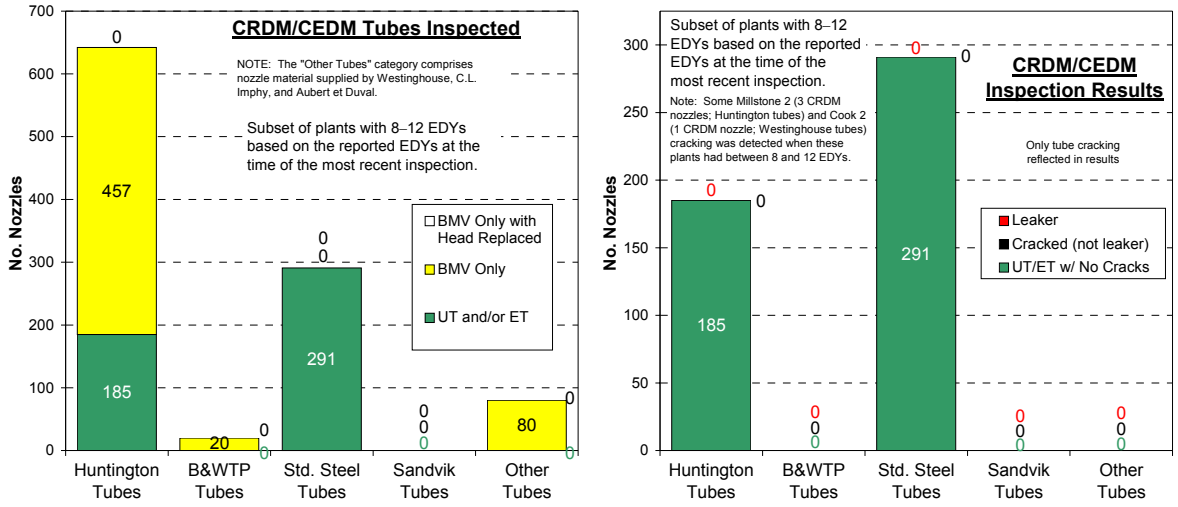

Figure 4-10
Reactor Vessel Closure Head Inspection Statistics—by Nozzle Material Supplier (8–12 EDYs)

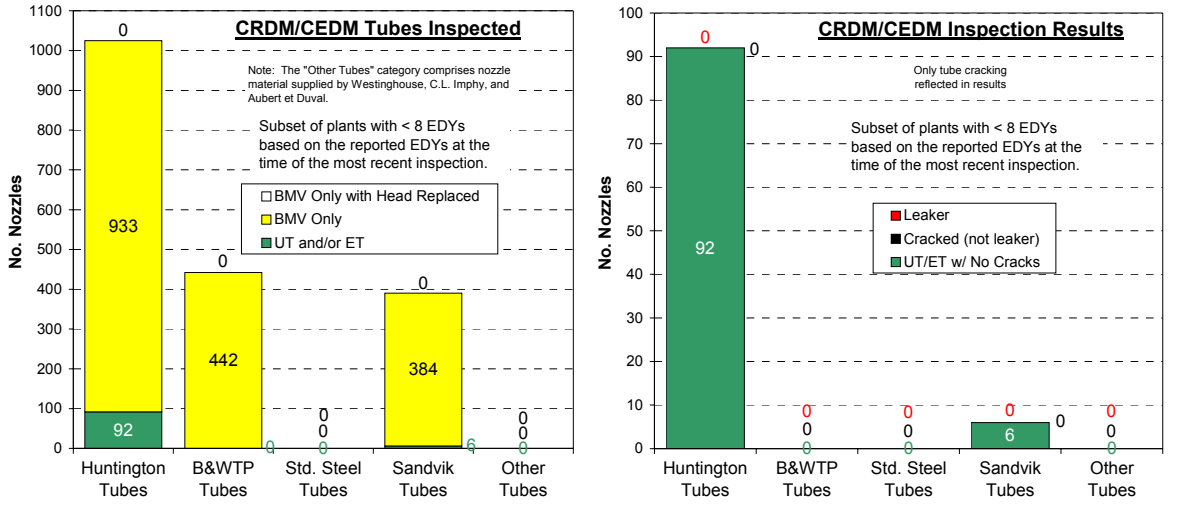

Figure 4-11
Reactor Vessel Closure Head Inspection Statistics—by Nozzle Material Supplier (<8 EDYs)

5
WELDING RESIDUAL STRESS AND STRESS INTENSITY FACTOR CALCULATIONS

5.1 Introduction

The stress fields in reactor vessel closure head (RVCH) penetrations due to both welding residual and primary stresses—and the crack tip stress intensity factor at flaws in critical locations of interest which results from these fields—are key inputs to the MRP safety assessments [5-1, 5-2,5-3]. This section provides a basic overview of the different approaches taken to compute welding residual stresses and crack tip stress intensity factors and highlights the primary industry references that document the calculation methods and results.

Welding Residual Stress Analyses. Calculation of the stress fields in reactor vessel head nozzles through finite element analysis facilitates the evaluation of crack tip stress intensity factors for hypothetical crack geometries, which then are applied to crack growth calculations of the time to leakage or nozzle ejection. In addition to facilitating stress intensity factor calculations, finite element stress modeling has been used applied to determine the size of the annulus gap on the nozzle OD under normal operating pressure and temperature conditions and to determine the crack opening displacement for through-wall cracks as an input to boric acid wastage evaluations. The approaches for evaluating residual stresses in head penetrations have been reported extensively in the literature, and are highlighted in Section 5.2 of this report.

Stress Intensity Factors. Crack tip stress intensity factors are a key input to crack growth calculations, which are used to determine the time that is required for hypothetical cracks of an assumed initial size to grow to produce leakage or nozzle ejection. As described in Section 6 primarily for the case of nozzle ejection, the crack growth results are applied to both deterministic and probabilistic safety assessments. Because the nozzle ejection case is a primary safety concern, Section 5.3 below includes brief descriptions of the complementary methods used to calculate the crack tip stress intensity factor inputs to the MRP nozzle ejection safety assessments [5-1,5-2,5-3]. In addition, comparisons are made to other published results for hypothetical circumferential nozzle cracks located above the top of the J-groove weld.

5.2 Residual Stress Analyses

5.2.1 Overview

The primary means by which the industry has evaluated residual stresses in vessel head penetrations is the three-dimensional finite element analysis (FEA) model developed by

Dominion Engineering, Inc. (DEI). The DEI model, which has been reported extensively in the literature [5-4 through 5-8], was initially developed in 1990 to evaluate pressurizer heater sleeves. In 1991, the model was extended to evaluate RV top head penetrations. At a time when nozzle PWSCC experience was limited and included only axially-oriented flaws and craze cracking, early applications focused on enhancing the industry's understanding of stresses and nozzle ovalization in these penetrations. As nozzle PWSCC experience broadened to include circumferentially oriented cracks, and cracks at both the nozzle ID and OD as well as in the J-groove weld, the regions of interest in head penetrations have also broadened. Consequently, the DEI model has been extended to the extent practical to include an increasing number of relevant effects, and to facilitate parametric analyses to support industry needs. The basic history of the DEI model is reflected in Figure 5-1.

Analysis results based on the DEI FEA stress model are applied in different ways to support current industry safety assessments:

- ***MRP-105 [5-1].*** Structural Integrity Associates (SIA) applied results derived from the DEI reactor vessel head penetration FEA stress model for four different representative penetration geometries (see also Section 5.2.2) to a PFM analysis of RVCH nozzle ejection (summarized in Section 6). The MRP-105 PFM analysis has been developed for B&W, CE and Westinghouse plants.
- ***MRP-104 [5-2].*** Westinghouse applied analysis results obtained with the DEI FEA model to its safety assessment for the Westinghouse/CE plants. The DEI FEA model was used to analyze multiple penetration geometries at each of two representative plants (one each for Westinghouse and CE designs). For these MRP-104 stress analyses, the temperature-dependent Alloy 600 nozzle material properties required by the DEI model incorporated Westinghouse-proprietary cyclic stress-strain data [5-9].
- ***MRP-103 [5-3].*** AREVA[4] applied analysis results obtained with the DEI welding residual stress model to its Monte Carlo simulation of nozzle ejection, and also for use in an alternate deterministic nozzle ejection calculation, for the B&W design plants. The DEI stress model was used to analyze the CRDM penetration geometry common to all seven B&W design plants. Specifically, an outer row CRDM nozzle having the highest yield strength in any of the B&W design plants was used in order to produce conservatively high stresses.

A nonlinear elastic-plastic finite element model of CRDM penetrations was also developed independently by AREVA [5-10,5-11]. Like the DEI model, the AREVA model was initially developed in the early 1990s. The results derived from the AREVA model were used as the stress field input to the main deterministic crack growth calculations reported in MRP-103 [5-3]. These deterministic crack growth calculations included axial and circumferential nozzle crack geometries, an axial weld crack geometry, and the circumferential "lack of fusion" flaw geometry at the interface between the nozzle and weld.

[4] Framatome ANP is a member of the AREVA group and is an AREVA and Siemens company.

5.2.2 DEI FEA Model

The DEI RVH penetration FEA model is a three-dimensional elastic-plastic finite element model which makes use of temperature-dependent material properties. The model, illustrated in Figure 5-2, includes a sector of the low-alloy steel head with stainless steel cladding on the inside surface, a single Alloy 600 nozzle (the model allows for the nozzle angle to be varied to simulate geometries for penetrations at various positions relative to head center), the weld buttering layer in the J-groove weld prep, and the Alloy 182 weld material (which is generally divided into two "passes" of approximately equal volume for CRDM/CEDM penetrations). The stainless steel cladding layer is included in the model because this material has a significantly different coefficient of thermal conductivity compared to the low-alloy steel vessel head and therefore influences the weld cooling process.

Because thermal and structural analyses are both executed by the FEA model, thermal and structural finite elements are applied by the model. The thermal analysis is performed first using eight-node three-dimensional thermal solid elements, with heat transfer between the nozzle and head limited to conduction through the J-groove region. This assumption was made because the head penetrations for most plants are counterbored at the upper and often lower portions of the penetration, and because thermal communication between the surfaces above the weld that are nominally in contact is believed to be poor.

Once the thermal analysis is completed, a three-dimensional structural analysis is performed using eight-node three-dimensional isoparametric solid elements and two-node interface (gap) elements to simulate the contact in the penetration region. Use of the interface elements in the annular region between the nozzle OD and the RVH penetration ID ensure that nozzle displacements due to weld cooling are appropriately bounded by the RVH penetration ID.

The model includes a conical sector of the vessel shell. Nodes on the conical boundary plane were permitted to move only in the spherical radial direction to simulate the vessel head stiffness and to accurately simulate pressure stresses in the shell remote from the penetrations.

The model simulates the key steps in the installation of the nozzles in the reactor vessel closure heads as follows:

- *Welding Simulation*: The modeling of the butter weld deposition and the J-groove welding make use of the same basic steps to simulate the thermal and mechanical effects of a weld. Each Alloy 182 weld "pass" is modeled as a complete ring of weld material elements that are heated simultaneously.

  The analytical simulation of the welding process consists of combined thermal and structural analyses. The thermal analysis is used first to generate nodal temperature distributions at several points in time during the welding process. These nodal temperatures are then used as loading inputs to the structural analysis, which calculates the thermally induced stresses at the same times.

- *Thermal Stress Relief*: After completion of the butter deposition, but prior to J-groove welding, the entire model is uniformly raised to 1100°F and then uniformly lowered to room temperature to simulate the effect of the thermal stress relief (post-weld heat treatment)

performed on the vessel head. In order to simulate the resulting stress relaxation, the elastic limit material properties of the head shell and butter materials at 1100°F are set at values consistent with this relaxation effect.

- *Hydrostatic Testing*: The components were hydrostatically tested to approximately 3125 psia after manufacturing and again after installation. These operations are included in the DEI model since the applied hydrostatic pressure further yielded the Alloy 600 nozzle material and resulted in a reduction in peak residual tensile stresses when the hydrostatic test pressure was released. In this manner, the hydrostatic testing represented a form of "mechanical stress improvement" in areas of high stress.
- *Operating Conditions*: Operating conditions are simulated by pressurizing the inside surfaces of the model (including the "cap loads" at the top of the nozzle) to operating pressure and heating all of the material to the uniform operating temperature. Stresses produced by differential thermal expansion arising from the small temperature gradient within the vessel head and nozzle during the heatup and cooldown transients are neglected.

Throughout its development, the DEI model has been benchmarked using a number of different approaches. To date, model validations have included:

- Correlation with measured nozzle lateral deflection and ovality for pressurizer heater sleeves, CRDM nozzles and bottom head instrument nozzles.
- Correlation of high stress areas with reported crack locations and orientations for pressurizer heater sleeves, CRDM nozzles, bottom head instrument nozzles, and pipe butt welds.
- Correlations with x-ray and strain gauge hole drilling residual stress measurements for CRDM nozzle and pressurizer heater sleeve mockups.
- Comparison of material properties and predicted stresses with models prepared by other organizations such as Engineering Mechanics Corporation of Columbus (EMC^2).

5.2.3 AREVA FEA Model (MRP-103)

MRP-103 reports that the AREVA stress analyses [5-10,5-11] made use of nonlinear elastic-plastic FEA and considered both a center nozzle and an outermost peripheral nozzle (at a nozzle set-up angle of 38.5°). Analysis of the center nozzle penetration was performed using a symmetric two-dimensional nozzle, while the peripheral nozzle was analyzed using a three-dimensional model.

The AREVA modeling incorporated the following effects:

- The shrink fit of the CRDM nozzle within the reactor vessel head during installation (nominal diametral interference was set to 0.0010 inches),
- Simulated welding of the nozzle to the reactor vessel head (the weld material is heated to 2470°F during welding, followed by cooldown),
- Cold hydrostatic testing at 3125 psig, and
- Operation under steady-state conditions of 600°F and 2250 psig.

The Alloy 600 material properties used in the model were based on material having a 64 ksi room temperature yield strength.

5.3 Stress Intensity Factor Calculations

The crack tip stress intensity factor is a necessary input to a number of different analyses which support industry safety assessments, including probabilistic analyses of flaw growth and nozzle ejection. To support these analyses, a number of different and complementary approaches for computing stress intensity factors are used:

MRP-105. To support PFM analysis of nozzle ejection, Structural Integrity Associates (SIA) employs a well-known superposition technique for the computation of stress intensity factors for hypothesized circumferential flaws. Stresses derived from the DEI RVH penetration FEA model are used as inputs. The superposition technique does not capture the effects of redistribution of secondary (residual) weld stresses as cracks grow. It thus generally produces higher stress intensity factor values than other approaches which account for the redistribution.

MRP-104. Westinghouse reports the use of two different approaches in MRP-104 for computing crack tip stress intensity factor for circumferential flaws:

- For the Westinghouse plants, a customized DEI elastic fracture mechanics FEA model (discussed in Section 5.3.2 and illustrated in Figure 5-3) was used to compute stress intensity factor values for hypothesized circumferential cracks in the nozzle. The DEI fracture mechanics FEA model takes as inputs computed stresses from the DEI elastic-plastic FEA stress model for RVH penetrations. For MRP-104, a single representative Westinghouse plant was analyzed (nozzle material properties were tailored for this analysis to include Westinghouse-proprietary cyclic stress-strain data).
- For the CE units, values were computed by applying a stress intensity factor expression developed by the NRC [5-12] using available information in late 2001. This curve is plotted in Figures 5-4 and 5-5, and compared with other results in Figures 5-6 and 5-7.

MRP-103. For the B&W units, AREVA independently developed a relationship between stress intensity factor and circumferential crack length using stress results for the outermost CRDM penetration geometry common to the set of original heads in the seven B&W design plants. In addition, MRP-103 presents an alternate case of deterministic circumferential crack growth calculations based on stress intensity factors calculated using the DEI fracture mechanics model, also for the outermost CRDM penetration geometry.

5.3.1 Superposition Technique (MRP-105)

The approach used to determine stress intensity factors in MRP-105 for the assumed top head nozzle cracks is the superposition technique for fracture mechanics analysis of complex geometries and stresses [5-13]. This required that operating and residual stresses be computed in the nozzle, head and J-groove weld region in the absence of cracks. These stresses were then superimposed on simplified elastic finite element models of just the nozzles (i.e., without the

vessel head or J-groove welds) with cracks of various lengths and depths built into the models—and with boundary conditions applied that represent the constraints imposed by the vessel head and J-groove welds. The stress intensity factors were calculated based on "enveloping stresses" perpendicular to the crack plane that correspond to a meandering crack plane through the highest stress locations above the weld (i.e., the circumferential crack was assumed to move to the elevation having the highest stress perpendicular to the crack plane as the crack progresses around the circumference).

To limit the analyses to a practical number of cases, a set of characteristic plants was considered in MRP-105 (Section 3.2 of MRP-105 demonstrates that the characteristic plants selected for analysis bound the U.S. PWR fleet with regard to parameters important to nozzle stresses in the vicinity of the reactor vessel closure head J-groove welds). The plants analyzed in MRP-105 were as follows (results were obtained from proprietary stress analyses performed with the DEI FEA stress model):

- A typical B&W type plant with nozzle angles ranging from 0° to 38° and reported nozzle yield strengths ranging from 36.8 to 50 ksi.
- A Westinghouse 2-loop plant with nozzle angles ranging from 0° to 43.5° and reported nozzle yield strength of 58 ksi.
- A Westinghouse 4-loop plant with nozzle angles ranging from 0° to 48.8° and reported nozzle yield strength of 63 ksi.
- A large CE-type plant with nozzle angles ranging from 0° to 49.7° and reported nozzle yield strengths ranging from 52.5 to 59 ksi. This plant also contained ICI nozzles with a 55.3° nozzle angle and a yield strength of 39.5 ksi.

Of the various techniques used to compute stress intensity factors for circumferential cracks for the current safety assessment, the superposition approach used in MRP-105 generally produces the most conservative results for downhill-centered cracks (see Figures 5-4 and 5-6), i.e., values computed with this technique are generally greater than those reported for other techniques.

5.3.2 Fracture Mechanics Finite Element Model (MRP-104)

Stress intensity factor values in MRP-104 for the Westinghouse plants were generated using a customized fracture mechanics FEA model which takes as inputs the nozzle stress fields computed with the DEI elastic-plastic FEA stress model (using Westinghouse-proprietary cyclic stress-strain curves). This approach is able to model the effects of relaxation of the welding residual stresses as circumferential cracks grow around the nozzle. Figure 5-3 shows a typical DEI fracture mechanics FEA model with a 180° crack above the J-groove weld.

The fracture mechanics module, which is implemented using custom software developed specifically for this purpose, calculates the J-integral using numerical volume integration. This approach captures the effects of Modes I, II & III crack opening displacements (CODs). The J-integrals are averaged across the nozzle wall and the equivalent stress intensity factor is calculated from the J-integral using the expression:

$$K_{eq} = \sqrt{\frac{J_{avg} E}{1 - \nu^2}}$$

where:

K	=	crack tip stress intensity factor
J	=	calculated J-integral value
E	=	modulus of elasticity
ν	=	Poisson's ratio

Figures 5-4 and 5-5 show predictions made with the DEI fracture mechanics FEA model ("MRP-104 (Westinghouse-Design SA)") as well as those based on the SIA and AREVA approaches. It should be noted that the results are similar to results obtained by EMC^2 and reported in NUREG/CP-0180.

Since the new module is based on custom software which calculates the J-integral (rather than using the ANSYS elements for linear elastic fracture mechanics), multiple test cases were run to validate the J-integral calculation:

- The first validation case was for a through-wall circumferential crack in an axially loaded pipe from EPRI report NP-6301-D [5-14].
- The second validation case was for a through-wall crack in a finite-width plate as treated in Rooke and Cartwright [5-15]. This model is considered to represent the case of CRDM nozzles without welding residual stresses given the constraint conditions for CRDM nozzles in the head.

The results showed good agreement for the case of large flaws where the welding residual stresses have been relaxed by crack growth.

5.3.3 AREVA Stress Intensity Factor Curve (MRP-103)

AREVA independently developed stress intensity factors for hypothetical circumferential nozzle flaws for the B&W design units. The results of this effort are shown in Figures 5-4 and 5-5 with the other MRP safety assessment results. Alternate estimates of circumferential crack growth have also been reported in MRP-103 using stress intensity factors calculated by DEI for the outermost CRDM penetration geometry common to B&W design plants and that include the effects of stress redistribution with crack growth as described in 5.3.2 above.

5.3.4 Other Approaches

It is worth noting that, in addition to the stress intensity factor results that are discussed in Sections 5.3.1 through 5.3.3 for the three safety assessments, a number of other stress intensity factor curves have been generated during recent years. A comparison to some of these curves is presented in Figures 5-6 and 5-7.

Of particular note is the stress intensity factor curve generated by Engineering Mechanics of Columbus Corporation (EMC^2) [5-16], which is based on finite element modeling performed independent of work sponsored by the MRP. As shown in Figure 5-6, the stress intensity factors computed for the three safety assessment reports are generally higher than the EMC^2 curve for downhill cracks.

5.4 Stress Analysis to Support Wastage Assessment

Stress analyses also serve as inputs to wastage-related assessments. More specifically, hoop stresses above the top of the J-groove weld were used as a basis for a stress intensity factor estimate used to calculate the time for axial crack growth. This is discussed in Appendix E of this report.

5.5 Summary

The safety assessments for RV top head nozzle penetration PWSCC rely, in part, on PFM analyses of nozzle ejection and assessments of wastage. These areas of analysis require as inputs the stress fields in the reactor vessel top head penetration, and the resulting stress intensity factors for hypothesized flaws.

The industry has employed a number of different approaches for evaluating stresses and stress intensity factors. This section has highlighted these approaches as well as many of the significant industry references for this work. As discussed, for most plants, nozzle penetration stresses have been evaluated using elastic-plastic finite element models developed by Dominion Engineering, Inc. and AREVA. For stress intensity factors, a range of complementary methods have been used, including the superposition technique and a customized elastic fracture mechanics finite element model. The results of these approaches are plotted in Figures 5-4 and 5-5.

5.6 References

5-1. *Materials Reliability Program: Probabilistic Fracture Mechanics Analysis of PWR Reactor Pressure Vessel Top Head Nozzle Cracking (MRP-105)*, EPRI, Palo Alto, CA: 2004. 1007834.

5-2. *Materials Reliability Program: RV Head Nozzle and Weld Safety Assessment for Westinghouse and Combustion Engineering Plants (MRP-104)*, EPRI, Palo Alto, CA: 2004. 1009403.

5-3. *Materials Reliability Program: RV Head Nozzle and Weld Safety Assessment for B&W Plants (MRP-103)*, EPRI, Palo Alto, CA: 2004. 1009402.

5-4. E. S. Hunt, "Stress Analysis of Nozzles Affected by PWSCC," *Proceedings: 1991 EPRI Workshop on PWSCC of Alloy 600 in PWRs* (Charlotte, NC, October 9–11, 1991), EPRI, Palo Alto, CA: 1992. TR-100852, pp. E7-1 through E7-22.

5-5. E. S. Hunt and W. S. Zemitis, "Stress Analysis of CRDM Nozzle Mockups," *Proceedings: 1992 EPRI Workshop on PWSCC of Alloy 600 in PWRs* (Orlando, FL, December 1–3, 1992), EPRI, Palo Alto, CA: 1993. TR-103345, pp. E3-1 through E3-31.

5-6. E. S. Hunt and D. J. Gross, "Parametric Stress Analysis of CRDM Nozzles," *Proceedings: 1994 EPRI Workshop on PWSCC of Alloy 600 in PWRs* (Tampa, FL, November 15–17, 1994), EPRI, Palo Alto, CA: 1995. TR-105406-P2, pp. C3-1 through C3-18.

5-7. E. S. Hunt, D. J. Gross, G. A. White, and R. Pathania, "Stress Predictive Algorithms for CRDM Nozzles," *Proceedings: 1997 EPRI Workshop on PWSCC of Alloy 600 in PWRs* (Daytona Beach, FL, February 25–27, 1997), EPRI, Palo Alto, CA: 1997. TR-109138-P2, pp. E18-1 through E18-16.

5-8. *PWSCC of Alloy 600 Materials in PWR Primary System Penetrations*, EPRI, Palo Alto, CA: 1994. TR-103696.

5-9. M. G. Ball et al., "RV Closure Head Penetration Alloy 600 PWSCC," WCAP-13525, Revision 1, Westinghouse Electric Corporation, 1992 (Westinghouse proprietary).

5-10. *Safety Evaluation for B&W-Design Reactor Vessel Head Control Rod Drive Mechanism Nozzle Cracking*, BAW-10190P (Proprietary), BAW-10190 (Non-Proprietary), B&W Nuclear Technologies, May and June 1993.

5-11. Killian, D.E., "OC-3 CRDM Nozzle Circumferential Flaw Evaluations," 32-5012403-00, (AREVA proprietary), April 2001.

5-12. U.S. Nuclear Regulatory Commission, *Preliminary Staff Technical Assessment for Pressurized Water Reactor Vessel Head Penetration Nozzles Associated with NRC Bulletin 2001-01, "Circumferential Cracking of Reactor Pressure Vessel Head Penetration Nozzles,"* November 2001, proprietary designation removed December 4, 2001.

5-13. T. L. Anderson, *Fracture Mechanics Fundamentals and Applications*, CRC Press, 1991.

5-14. *Ductile Fracture Handbook*, EPRI, Palo Alto, CA: 1989. NP-6301-D, Volume 1.

5-15. D. P. Rooke and D. J. Cartwright, *Compendium of Stress Intensity Factors*, Her Majesty's Stationary Office, London, 1976.

5-16. W. J. Shack, "Parametric Studies of the Probability of Failure of CRDM Nozzles," Argonne National Laboratory, Presented at the NRC Nuclear Safety Research Conference, Washington, DC, NUREG/CP-0180, October 28–30, 2002.

5-17. Dominion Engineering, Inc., Calculation No. C-3515-00-4, Revision 0, September 2003.

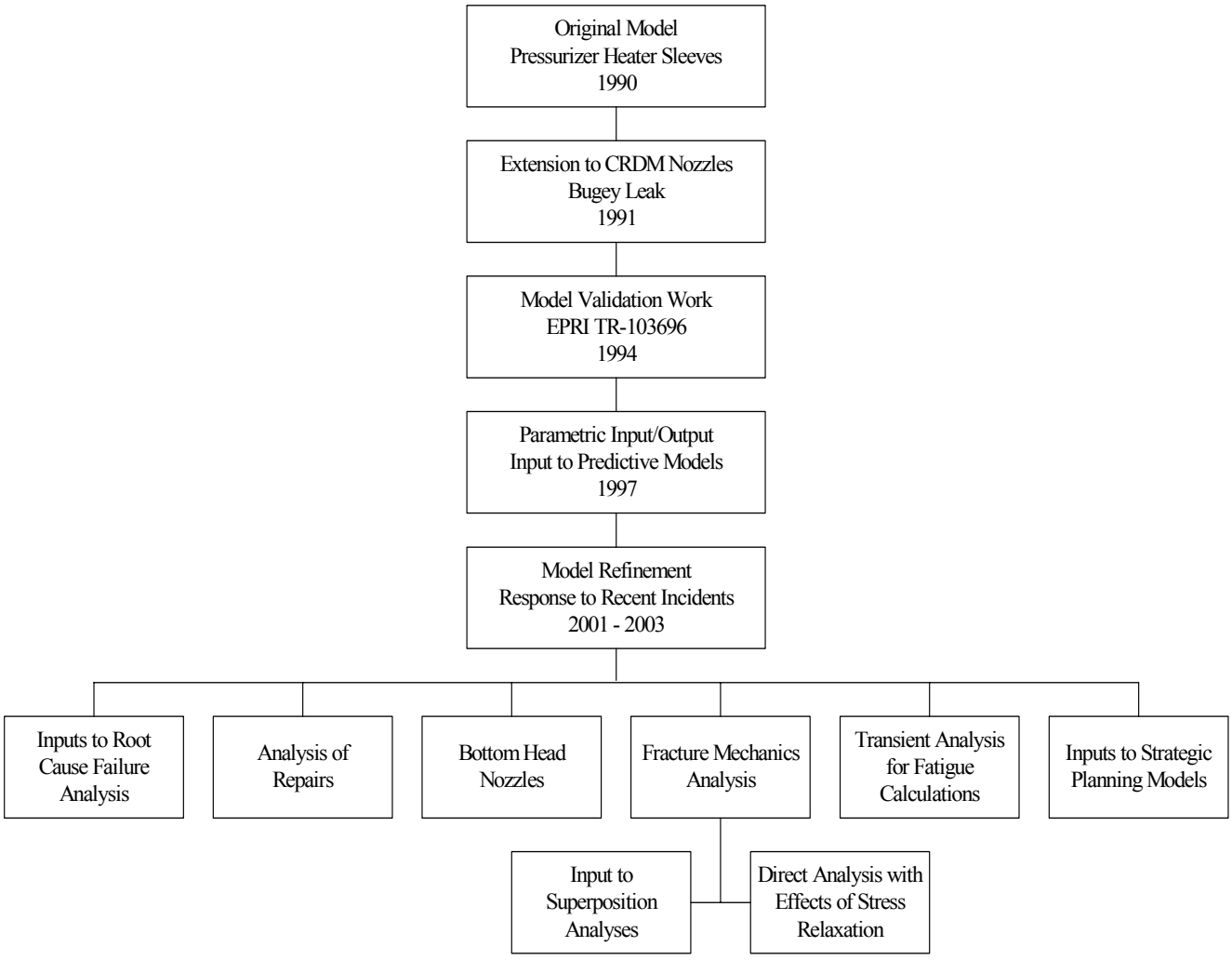

Figure 5-1
Evolution of the DEI Penetration Finite Element Model

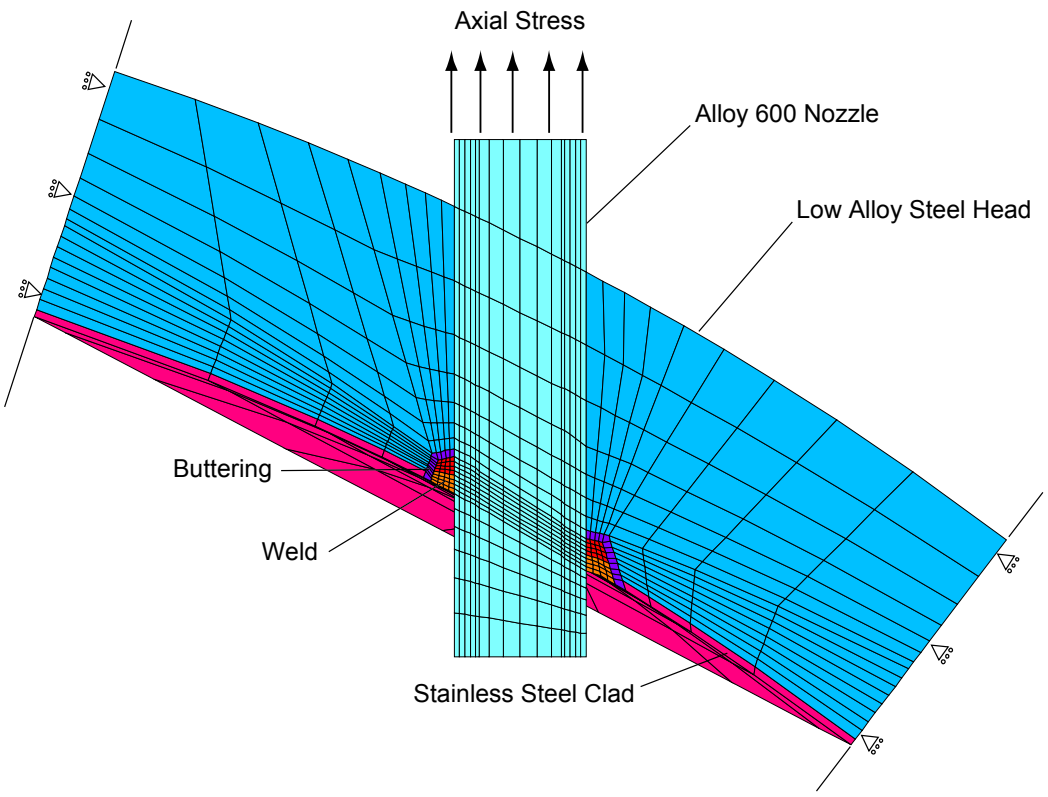

Figure 5-2
Example CRDM Penetration Finite Element Model

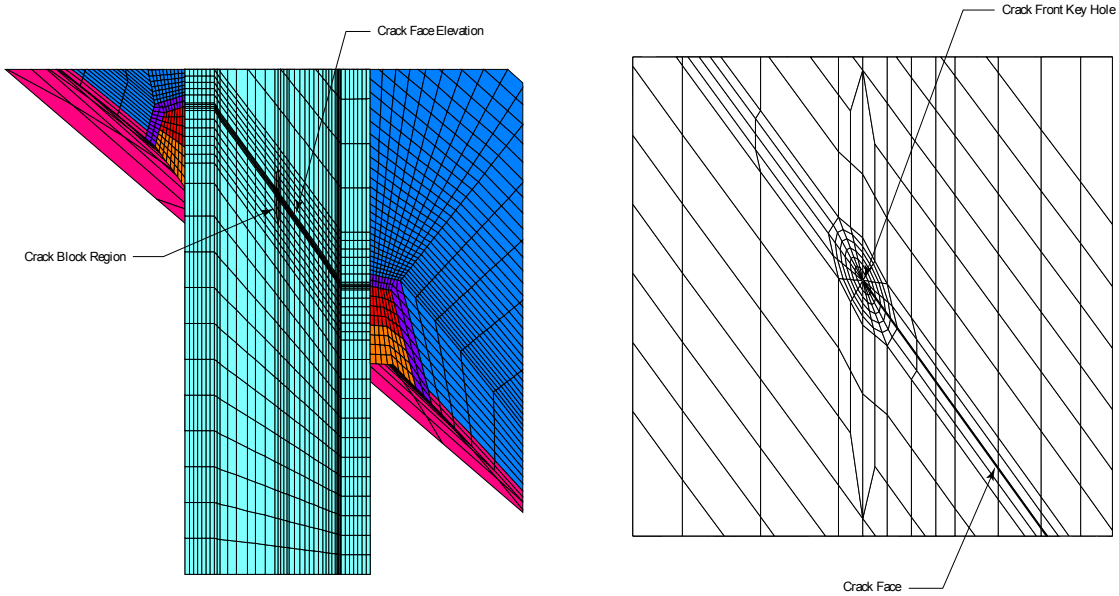

Figure 5-3
Example Fracture Mechanics Model

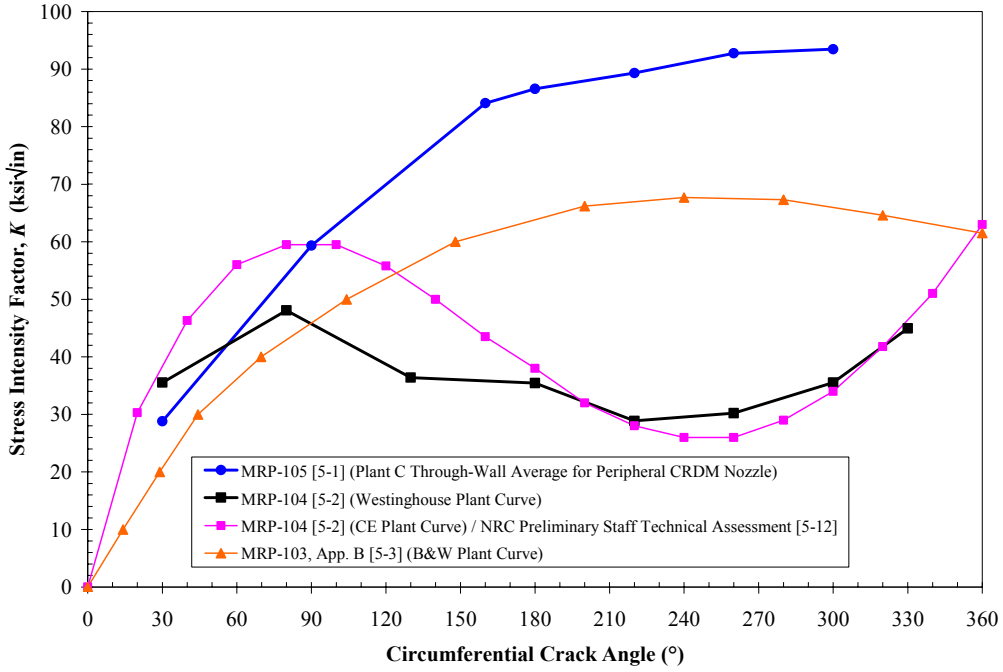

Figure 5-4
Stress Intensity Factors Assumed in the MRP Nozzle Ejection Safety Assessment (Downhill Centered Cracks)

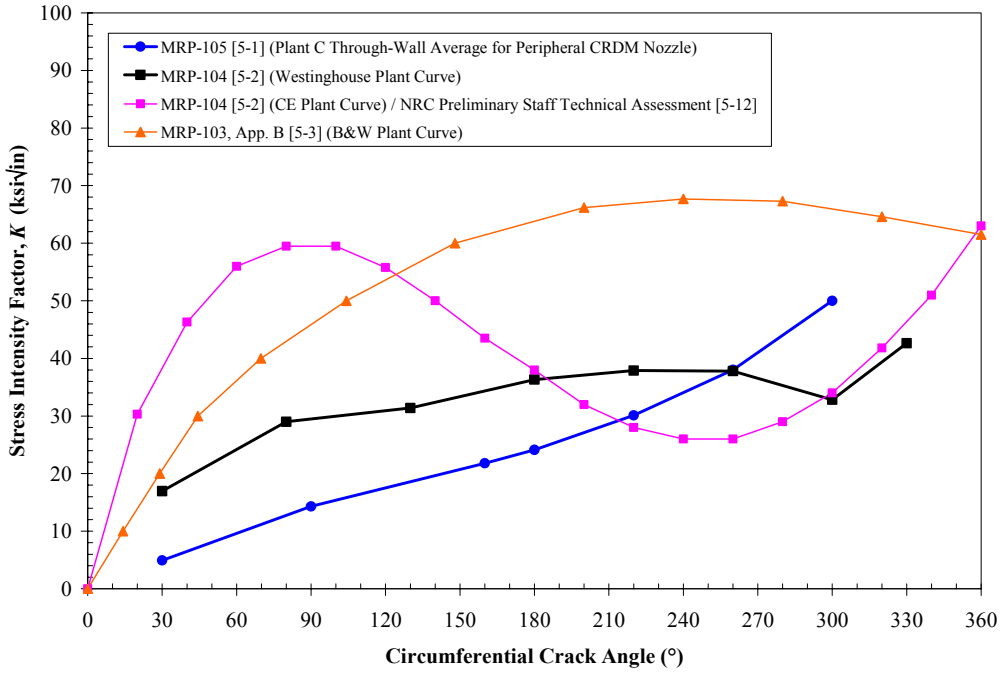

Figure 5-5
Stress Intensity Factors Assumed in the MRP Nozzle Ejection Safety Assessment (Uphill Centered Cracks)

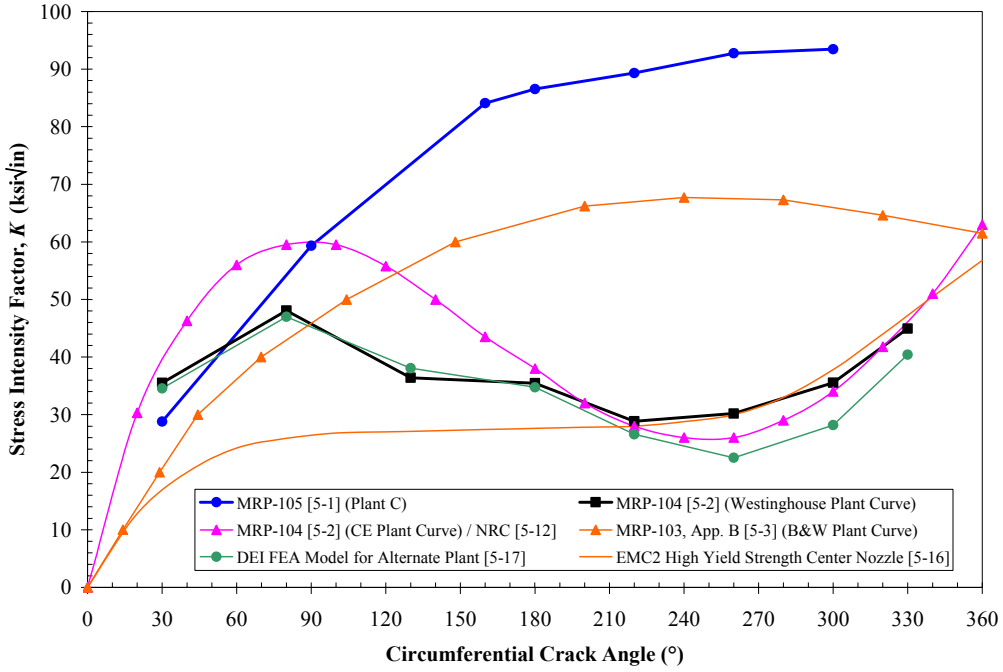

Figure 5-6
Comparison of Assumed Stress Intensity Factors with Other Available Results (Downhill Centered Cracks)

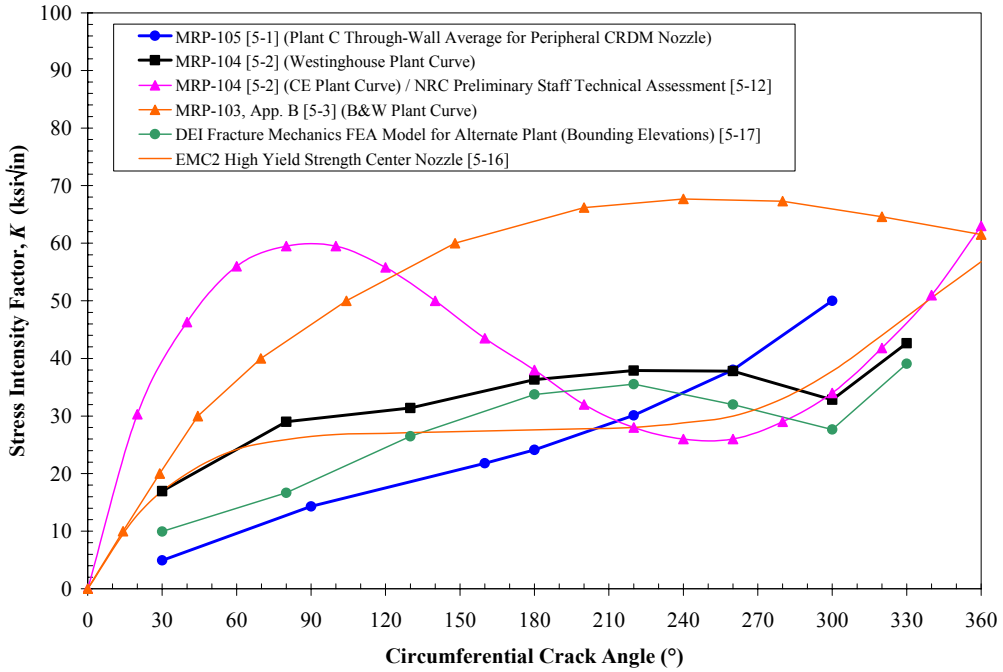

Figure 5-7
Comparison of Assumed Stress Intensity Factors with Other Available Results (Uphill Centered Cracks)

6
NOZZLE EJECTION EVALUATIONS

This section summarizes the different approaches for calculating the probability of a nozzle ejection type failure—or the time required for such a failure when treated deterministically—that are documented in MRP-105 [6-1], MRP-104 [6-2], and MRP-103 [6-3]. The nozzle ejection evaluations in MRP-105 cover the entire domestic PWR fleet and include Monte Carlo probabilistic fracture mechanics modeling. Complementary nozzle ejection evaluations specific to each of the three original NSSS designers are provided in MRP-104 and MRP-103.

The complementary design-specific evaluations support the basic conclusion of MRP-105 that a program of periodic nonvisual NDE inspections at appropriate intervals supplemented by periodic bare metal visual examinations provides adequate protection against nozzle ejection. Furthermore, MRP-105 also shows a low probability of pressure boundary leakage resulting from the appropriate program of periodic inspections.

6.1 Introduction

The main concern regarding nozzle ejection is the potential for a circumferential crack above the J-groove weld, through the nozzle wall, to grow to a critical length. There is less concern with ejection due to a "lack-of-fusion" type flaw since this flaw would have to be perfectly concentric for the nozzle to eject. Any deviation from a pure cylinder would create protrusions that would tend to "pin" the nozzle in place and prevent ejection. The evaluations reported in MRP-105, MRP-104, and MRP-103 are based on deterministic and probabilistic calculations. The main input parameters are described in Table 6-1.

The crack growth rates (CGRs) used to evaluate the time or probability for a nozzle to be ejected once a crack/leak occurs are based on stress intensity factor calculations and field and laboratory data. The three-dimensional welding residual stress model developed by Dominion Engineering, Inc. (DEI) and used by the industry for evaluating stresses in most plants is described in Section 5. This model is used in MRP-105, MRP-104, and partially in MRP-103. The stress intensity factor calculations are based on stresses obtained from this model, as described in Section 5.3.

The analyses in the three reports generally address three main factors in ensuring an extremely low risk of nozzle ejection:

- The nonvisual examinations ensure that the nozzle and welds are free of significant defects at the time of the inspection (cracks/leaks) to a certain confidence, depending on the probability of detection (POD) curves for each inspection technique considered;

- Time is required for cracks to initiate in the nozzle or the weld and grow to the point where they result in a leak;
- Once a leak has occurred, it is conservatively assumed that a part-depth or through-wall circumferential crack exists in the nozzle above the J-groove weld because of the high stress field above the weld and the exposure to the primary water environment (see Figure 6-1). The time for this crack to grow from the initial length to a limiting arc length is determined based on fracture mechanics calculations and crack growth rates reported in MRP-55 [6-4] or MRP-103 [6-3]. At this point, net section collapse could occur, leading to a pressure boundary break.

6.2 Deterministic Inputs and Analyses

Deterministic analyses were performed in all three reports: MRP-105, MRP-104 and MRP-103. These include time to crack or leak initiation, stress intensity factor calculations, and crack growth rate calculations.

Limit load analysis was used to determine critical circumferential crack lengths in the nozzles. In some cases, for the deterministic crack growth calculations, the limit load critical crack lengths are reduced through the application of a safety factor on the pressure loading based on the approach used in Section XI of the ASME Boiler and Pressure Vessel Code for acceptance of flaws for continued operation.

6.2.1 MRP-105

The characteristic plants considered in this report for analysis are described in Section 5. The head temperature, penetration type, penetration angles, and yield strengths used for the calculations are summarized in Table 6-1. Westinghouse (2 and 4 loops, CRDM nozzles), B&W (CRDM nozzles) and CE (CEDM and ICI nozzles) design plants have all been analyzed. The four units selected represent reasonable bounds for weld geometry and nozzle material yield strengths. The highest angle nozzles for each plant, as well as intermediate and low angles, were analyzed. Since the plants selected in this study bound the U.S. PWR fleet, the results are considered applicable to the 69 operating reactor vessel heads.

Parameters considered include the calculated stress field, the location of flaw origination (uphill versus downhill centered), the elevation of the flaw plane, and the extent of interference fit between the nozzle and head. In this model, a through-wall 30° circumferential flaw is used as the starting crack size when leakage is predicted to occur based on Weibull statistical modeling and plant inspection data (including findings for 30 plants since late 2000). The crack growth rate calculations are based on the work reported in MRP-55 [6-4], with a multiplicative factor of 2.0 applied to the crack growth rate to account for potential uncertainties in knowledge of the exact chemical environment on the nozzle OD. The deterministic evaluation results reported in MRP-105 predict crack propagation times—for a circumferential crack to grow from the assumed initial size (30º) to the size at which Section XI stress margins are exceeded (300º)—of greater than 8.2 EFPY for the highest stressed, highest temperature head. See Section 6.3.1 for the associated probabilistic calculations.

6.2.2 MRP-104 (Westinghouse and CE Design Plants)

Westinghouse and Combustion Engineering design plants were analyzed in this report using a deterministic approach.

The purpose of the calculations was to determine: 1) the time for an ID or OD flaw to propagate through the wall of the nozzle (or through the weld) and create a leak path to the point where that flaw or another flaw could branch or initiate above the weld, on the OD of the nozzle exposed to primary water, and 2) the time for this OD flaw to propagate around the circumference of the penetration.

The time required for a surface flaw to grow through-wall and create a leak path was conservatively ignored in the calculations. In addition, a circumferential crack is assumed to initiate on the OD of the nozzle above the top of the J-groove weld immediately upon leakage. The flaw is postulated to propagate along the maximum stress plane parallel to the weld, eventually reaching the point where a complete separation of the nozzle is possible due to net section collapse (330° based on the calculations). The OD flaw was assumed to grow through-wall first and then to propagate circumferentially, but the time period for a surface crack to become through-wall was conservatively ignored.

As discussed in Section 5, two models developed by Dominion Engineering, Inc. were used for the stress analysis in MRP-104: one for the Westinghouse design plants and one for the Combustion Engineering design plants. Five CRDM nozzle angles were considered for the Westinghouse model, four for the CE model, and one for the ICI penetrations, as indicated in Table 6-1. Calculations were performed for surface flaws using the Raju and Newman stress intensity factor expression [6-2], but, as noted above, the time for a surface flaw to grow through-wall and/or create a leak was conservatively ignored in the results. The crack growth rates were obtained from MRP-55 [6-4] at a temperature of 600°F.

Circumferential cracks initiating both on the uphill and downhill sides of the nozzle were analyzed. The results of the evaluations performed in MRP-104 show that at least 17 years would be required for a through-wall circumferential flaw to reach a critical length that could lead to nozzle ejection. Finally, MRP-104 also estimates that the interference zones on the OD of 95% of the nozzles in Westinghouse and CE design plants would open up to form gaps that would facilitate the visual detection of leaks.

6.2.3 MRP-103 (B&W Design Plants)

The evaluations reported in MRP-103 [6-3] are specific to the seven B&W design plants. Five of the seven plants have already replaced their reactor vessel heads, with the other two plants expected to install replacement heads by the end of 2005.

MRP-103 assumes that an axial flaw or a flaw in the J-groove weld that leads to leakage occurs before initiation of a circumferential flaw in the nozzle wall. For an axial flaw, crack growth calculations were performed with a length-to-depth ratio of six at the highest stress location, and the crack growth rates were obtained from a model reported by Peter Scott [6-4] with the power

law coefficient set on the basis of a heat that displayed relatively high crack growth rates in testing. The results showed that it would take 4 years for the crack to grow through-wall, and then at least 4 more years to propagate above the weld and create a leak path. However, crack growth calculations for Alloy 182 weld metal [6-5] showed that a crack could grow through the J-groove weld within only 1 or 2 years and create a leak.

After leakage through the axial flaw in the nozzle or through the weld flaw, a circumferential crack could then initiate on the OD of the nozzle. The evaluations performed in MRP-103 showed that it would take at least 10 years for a short semi-elliptical flaw (length-to-depth ratio of six) to grow through the wall of the nozzle. However, a long circumferential flaw (or several initiation sites with 180° extent) could grow through-wall in 3.5 years. It would take an additional 4 years—a total of at least 7.5 years—for the flaw to grow to 270°, and the remaining ligament in that case would still satisfy the limit load critical crack length with a safety factor of 3.0. MRP-103 also presents alternate deterministic crack growth calculations using stress intensity factors calculated by DEI using a fracture mechanics methodology described in Section 5.3.2. These results show that it would take approximately 23 years for a downhill-centered 180° circumferential through-wall crack to grow to 270°, and approximately 19 years if the crack is centered on the uphill side. Thus, nozzle ejection in B&W design plants does not present an immediate safety concern since all the original B&W heads will have been replaced by the end of 2005.

6.3 Probabilistic Analyses

6.3.1 MRP-105

The probabilistic analyses in MRP-105 are based on Monte Carlo simulations and statistical distributions of the key parameters and inputs (instead of choosing single values). Log-normal, triangular, and log-triangular distributions are used to obtain a statistical distribution of the parameters for each trial. The probability of nozzle ejection is calculated as the number of Monte Carlo trials for which at least one net section collapse is predicted to occur during a particular year divided by the total number of Monte Carlo trials.

When leakage is predicted to occur, a crack is assumed to immediately initiate on the OD of the nozzle above the top of the weld. The probability of leakage is calculated based on a Weibull statistical analysis, which is based on the operating time, the vessel top head temperature, the thermal activation energy, and the Weibull scale and slope parameters derived from U.S. plant inspection data. The Weibull distribution for a given heat of material is randomly selected from a triangular distribution of the Weibull scale parameter. A random number is also used to obtain the local variation on time-to-leakage for each individual nozzle within a heat of material.

Crack growth rates are based on MRP-55 [6-4], and, similar to the method for predicting crack initiation, heat variability and within-heat factors are included in the analysis. These random factors are assumed to be statistically correlated with the crack initiation factors. Log-normal or log-triangular distributions are used for the crack growth power-law coefficient and the local variability in crack growth rate by heat of material.

A number of other parameters are also incorporated:

- *Number of Cracks per Nozzle*. This parameter is determined randomly with a Poisson distribution when initiation is assumed to occur. At least one crack is assumed to be present.
- *Crack Characteristics*. OD cracks above the top of the weld are initiated either on the uphill side or the downhill side. The stress intensity factors are interpolated based on the crack length and depth depending on the particular nozzle and plant considered in that trial. The leaking crack is initiated at some fraction of the time-to-leakage obtained from the Weibull calculation, with a random initial size. Therefore, the crack might be detected before the leak occurs.
- *Inspection*. The evaluation considers several inspection options, including inspections in accordance with the NRC Order, and two alternative inspection schedules. The model has the capability to address the inspection interval, the time for inspection, and the inspection method along with the probability of detection (POD) curve and the percentage coverage (see Table 6-1). When cracks and leaks are detected in an inspected nozzle, it is assumed that the penetration is properly repaired (no defects are left in service), and the nozzle is not included in the calculation of the probability of leakage or failure for subsequent operation.
- *Other Factors Considered.* Nozzle angle, nominal nozzle interference fit, head temperature, nozzle material yield strength, and critical OD circumferential crack length are additional factors considered.

Based on the sensitivity and benchmark analyses performed in MRP-105, this reports shows that a program of periodic nonvisual NDE inspections at appropriate intervals supplemented by periodic bare metal visual examinations will provide adequate protection against nozzle ejection. Furthermore, MRP-105 also shows a low probability of pressure boundary leakage resulting from the appropriate program of periodic inspections.

6.3.2 MRP-104 (Westinghouse and CE Design Plants)

Only deterministic calculations have been performed in this report.

6.3.3 MRP-103 (B&W Design Plants)

The probabilistic analyses in MRP-103 are based on a combination of Monte Carlo simulations and an event tree model, covering approximately a four-year period of operation. The conclusion from these probabilistic analyses is that there is an extremely low risk to the public due to CRDM nozzle cracking.

The outer row CRDM penetration geometry common to the seven B&W plants was selected for the probabilistic calculation. Because the highest nominal yield strength for the heats of nozzle material in the set of original B&W plant heads was assumed, worst case stresses were calculated for use in the nozzle ejection evaluations. The stress profile was developed by Dominion Engineering, Inc. as described in Section 5. Crack growth rates are based on a model reported by

Peter Scott [6-4] as described in 6.2.3, with a log-normal distribution on the power law coefficient.

The model assumes that a net section collapse and nozzle ejection is caused by OD circumferential cracks that are initiated due to primary water leaking into the nozzle annulus from undetected ID or OD axial through-wall cracks or J-groove weld cracks. It is assumed that multiple circumferential cracks initiate at the downhill side since the OD stresses are greater at this location. The multiple flaws are simulated by a single semi-elliptical shallow flaw with a circumferential extent log-normally distributed between 0° and 180°.

Several factors are considered in the event tree probabilities and initiating event frequencies:

- *Frequency of weld or nozzle leak through the annulus, based on a Weibull distribution.* The distribution is based on the most limiting B&WOG plant experience corrected with an estimated human error probability.
- *Probability that the leakage is not detected.* Several POD values for visual techniques have been considered, including the effect of human error (see Table 6-1).
- *Probability that an undetected crack will propagate circumferentially on the nozzle OD and lead to a nozzle ejection.* Several POD values for nonvisual volumetric techniques (UT) have been considered, and no credit was taken for the detection of the axial cracks that are too shallow to create a leak.
- *Probability of core damage from the resulting LOCA.*

As identified in Table 6-1, a sensitivity study was performed for some key variables. For example, the critical crack size with and without a safety factor on the pressure loading was considered in the probabilistic nozzle ejection evaluation. As an alternate scenario that could lead to nozzle ejection, ID-initiated circumferential flaws were also considered in MRP-103. Another sensitivity case assumed that no UT inspection was performed.

6.4 Conclusion

The analyses reported in MRP-105, MRP-104, and MRP-103 are based on complementary approaches. MRP-105 is based on a probabilistic assessment applicable to all U.S. PWR units, while MRP-104 applies a deterministic approach to Westinghouse and Combustion Engineering design units, and MRP-103 considers the results of deterministic and probabilistic calculations for the seven B&W design units. Five of the seven B&W plants have already replaced their reactor vessel heads, with the other two plants expected to install replacement heads by the end of 2005.

The nozzle ejection evaluations show that a program of periodic nonvisual NDE inspections at appropriate intervals supplemented by periodic bare metal visual examinations provides adequate protection against the potential for nozzle ejection. MRP-105 also shows a low probability of pressure boundary leakage resulting from the appropriate program of periodic inspections. The MRP inspection plan document for reactor vessel closure head penetrations, which is currently

under development, will define the appropriate inspection intervals, coverage, and characteristics.

6.5 References

6-1. *Materials Reliability Program: Probabilistic Fracture Mechanics Analysis of PWR Reactor Pressure Vessel Top Head Nozzle Cracking (MRP-105)*, EPRI, Palo Alto, CA: 2004. 1007834.

6-2. *Materials Reliability Program: RV Head Nozzle and Weld Safety Assessment for Westinghouse and Combustion Engineering Plants (MRP-104)*, EPRI, Palo Alto, CA: 2004. 1009403.

6-3. *Materials Reliability Program: RV Head Nozzle and Weld Safety Assessment for B&W Plants (MRP-103)*, EPRI, Palo Alto, CA: 2004. 1009402.

6-4. *Materials Reliability Program (MRP) Crack Growth Rates for Evaluating Primary Water Stress Corrosion Cracking (PWSCC) of Thick-Wall Alloy 600 Materials (MRP-55) Revision 1*, EPRI, Palo Alto, CA: 2002. 1006695.

6-5. *Crack Growth of Alloy 182 Weld Metal in PWR Environments (PWRMRP-21)*, EPRI, Palo Alto, CA: 2000. 1000037.

Table 6-1
Nozzle Ejection Evaluation Summary Table

	Report / Description	MRP-105 [6-1]	MRP-104 [6-2]	MRP-103 [6-3]
Analysis	***Author***	*Structural Integrity Associates*	*Westinghouse*	*AREVA*
	Plants Analyzed	B&W, W 2-loop, W 4-loop, CE (results applicable to all U.S. PWRs)	W, CE	B&W
	Deterministic Analysis	✓	✓	✓
	Probabilistic Analysis	Monte Carlo (≥100,000 trials)	—	Monte Carlo, Event Tree
Plant Data	**Head Temperature**	From 567°F to 596°F (probabilistic), 605°F (deterministic)	600°F	602°F and 605°F
	Penetration Types	CRDM, CEDM and ICI	CRDM, CEDM and ICI	CRDM
	Penetration Angles	CRDM (B&W): 38.5°, 26.0°, 18.0°, 0° CRDM (W 2-loop): 43.5°, 30.0°, 13.6°, 0° CRDM (W 4-loop): 48.8° CEDM: 49.7°, 7.8°, 0° ICI: 55.3°	CRDM: 42.6°, 40.0°, 38.6°, 28.6°, 0° CEDM: 49.7°, 29.1°, 7.8°, 0° ICI: 55.3°	Outer row penetration geometry common to the B&W plants (38.5°)
	Yield Strength (ksi)	B&W: High: 50, Low: 37 W 2-loop: 58 W 4-loop: 63 CE: High: 59, Low: 52.5 ICI: 39.5	Proprietary	The highest yield strength of all the nozzles analyzed has been retained for the probabilistic calculations
Stresses	**Stress Analyses**	FEA (performed by DEI); envelope curve, 1400 and 1500 planes (OD cracks); the interference fit is considered	FEA (performed by DEI) for W and CE	FEA (performed by DEI, worst case stresses)
Leak Assessment	**Weibull (Crack/Leak)**	β=3, extrapolation back, time to first leak based on U.S. plant inspection data	—	β=3 for leak frequency
	Probability of Leakage	Based on Weibull calculations above, θ = 15.2 ± 6, β = 3, Q = 50 kcal/mol, triangular distribution for a given heat and distribution within heat for each nozzle	—	θ = 35.6 and β = 3 based on the most limiting B&WOG plant experience corrected with an estimated Human Error Probability
NDE Inspections	**No. of NDE Inspections**	NRC Order and two MRP inspection alternatives analyzed	—	See below
	NDE Inspections	Visual, non-visual	—	Visual each outage, one-time UT inspection or no UT inspection
	POD (Leakage)	Function of the initial shrink fit, time when leakage starts (leaking nozzle already missed or not) and % coverage	—	Human Error Probability = 0.05 (0.1 for past inspections) and 0.1 (1.0 for past inspections) (2 cases)
	POD (Crack)	Full-V UT POD curve (function of crack size) with a maximum of 95%, percentage coverage considered	—	90% or 99% for a through-wall circ. crack (2 cases); 50% or 97% for a circ. crack (not yet through-wall); 0% for the axial cracks that do not cause a leak
Crack Growth Rates	**Base Metal CGR**	MRP-55 [6-4]	MRP-55 [6-4]	Modified Peter Scott model with heat 91069 [6-3]; MRP-55 [6-4] for the alternate deterministic nozzle ejection calculation
	Base Metal CGR Distribution	Log-normal or Log-triangular distributions (constant term in the crack growth law, variability in CGR by heat of material)	—	Log-normal distribution
	Weld Material CGR	—	—	MRP-21 [6-5]
Flaw Inputs	**Crack Geometry Cases**	OD circ. flaw assumed at initiation (correlation factor between crack initiation and CGR considered)	OD circ. flaw assumed at initiation	1) Axial nozzle flaw or weld flaw 2) ID circ. flaw 3) Axial nozzle flaw (50% through-wall) that turns circumferential 4) OD circ. flaw
	Flaw Location (ID vs. OD)	OD	OD	ID and OD
	Flaw Location (UH vs. DH)	Centered at UH or DH	UH and DH	DH
	Flaw Location (Elevation)	At the top of the weld, propagating in worst stress plane	0, 0.25, 0.5 and 1.0 inch above the top of the weld	At the top of the weld
	Aspect Ratio (Part-Depth Circ. Flaws)	—	6:1	6:1
	OD Environment Effect on CGR	Factor of 2.0	Factor of 2.0	Factor of 1.0
	Initial OD Circ. Flaw	30° through-wall	1) Part-depth OD circ. flaw 2) Through-wall OD circ. flaw immediately at the beginning	Log-normally distributed between 0° and 180° (with a median extent of 66°); depth is 20 mils ± 10 mils
	Critical OD Circ. Flaw	300° (probabilistic and deterministic)	330° (deterministic)	330° and 293° (probabilistic); 270° (deterministic)

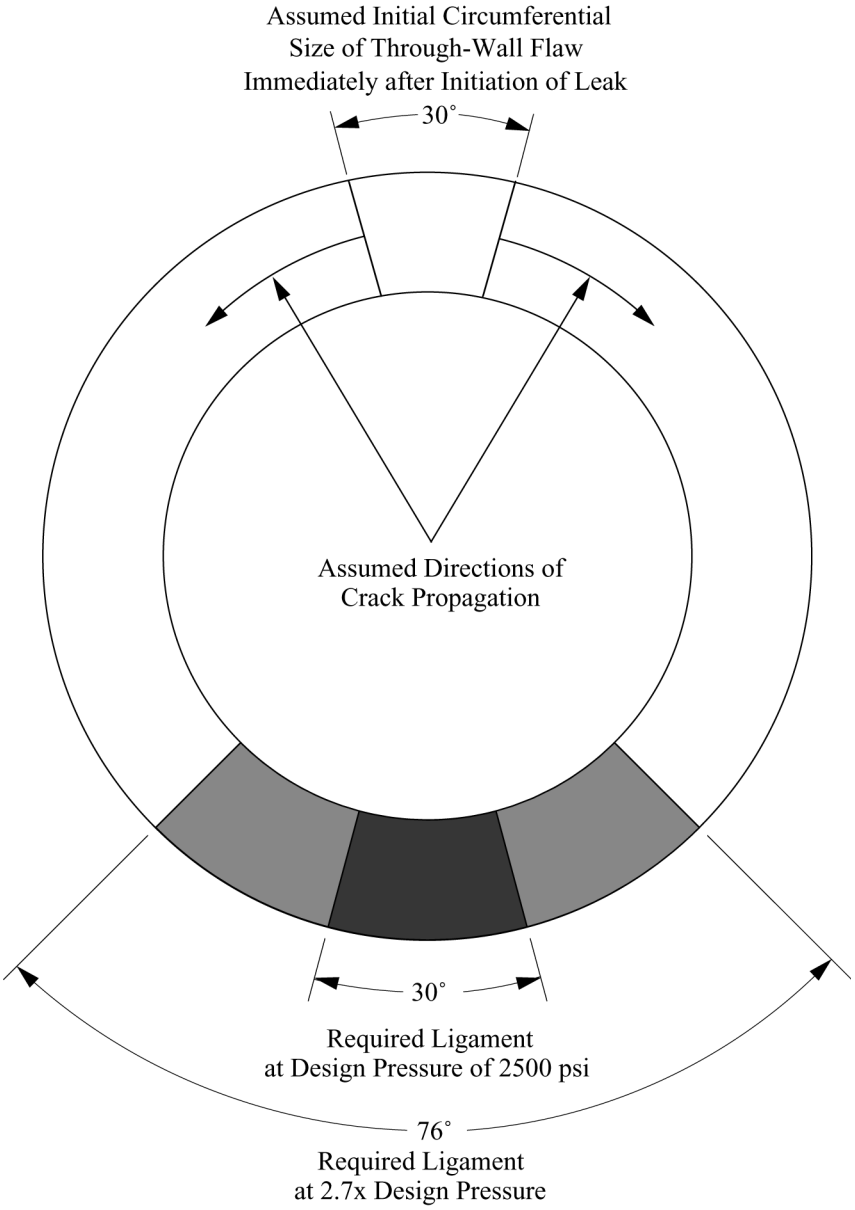

Figure 6-1
Example of Crack Growth Around Nozzle Circumference Above J-Groove Weld

7
HEAD WASTAGE EVALUATIONS

This section describes the evaluations used to show that adequate protection against boric acid wastage is provided by bare metal visual examinations performed at appropriate intervals for evidence of leakage. This conclusion is supported by the experience with over 50 leaking CRDM nozzles, including the observation that the Davis-Besse wastage cavity would have been detected relatively early in the wastage progression had bare metal visual examinations been performed at each refueling outage—and likely even if performed less frequently—with appropriate corrective action. The MRP inspection plan for reactor vessel closure heads, which is currently under development, will define appropriate bare metal visual inspection intervals.

7.1 Davis-Besse Operating Experience

Despite uncertainties in the exact progression of the Davis-Besse leak rate and wastage volume over recent operating cycles, it is instructive to examine the Davis-Besse nozzle #3 experience [7-1,7-2] in greater detail. First, it should be noted that Davis-Besse has the highest reported head temperature of any PWR plant in the United States (605°F). In addition, the original Davis-Besse head had several nozzles from an Alloy 600 heat that has demonstrated the greatest potential for cracking of any heat of CRDM nozzle material in the United States based on inspections performed through August 2003.

The evidence indicating the likely progression for the leak through Davis-Besse CRDM nozzle #3 and the associated large corrosion cavity is summarized in Figure 26 of the Davis-Besse root cause report [7-1], "Timeline of Key Events Related to Reactor Vessel Head Boric Acid Corrosion." This figure shows that after cleaning the vessel head in 1994, the first evidence of leakage from the head was reported at 10RFO in 1996. The boric acid deposits produced by the leakage were such that they blocked visual inspection of four of the 69 nozzles, including nozzle #3. Therefore, the leakage in 1996 was many times larger than that required to be detectable through BMV inspection.

The timeline figure from the root cause report [7-1] documents several indications that it took more than two years of operation after the 1996 refueling outage for the leak rate to increase to the 0.1 gpm considered necessary for rapid corrosion of relatively large areas of the head. These indications include the progression of the unidentified primary system leakage rate, video evidence of the increase in the size of the pile of boric acid deposits on the head surface, clogging of the containment air coolers, and plugging of the containment radiation monitor filters.

On this basis, a BMV inspection at 1.5–2.0 year intervals would have detected the leakage at least four years prior to the relatively large volume of wastage being discovered at 13RFO in 2002, assuming a hypothetical timing of refueling outages such that the boric acid accumulation was just missed in 1996. The presence of red-colored boric acid deposits on the vessel flange at 11RFO in 1998 was another indicator that the situation warranted evaluation because a red or orange color for boric acid deposits indicates the presence of iron corrosion products, whereas boric acid deposits that do not incorporate corrosion products are white in appearance. While the significance of these indications was missed at Davis-Besse, it is highly unlikely that their significance will be improperly interpreted in the future by any plant. Plants with lower head temperatures than Davis-Besse would tend to require more time to reach equivalent conditions due to lower crack growth rates.

7.2 Relevant Industry Experience

As described below, the industry experience—including leaking CRDM nozzles, other leaking primary system components, international experience, and the incident at Davis-Besse—supports the conclusion that bare metal visual inspections performed at appropriate intervals will prevent significant wastage of the reactor vessel head material. See Section 4 for a presentation of the CRDM nozzle inspection results through December 2003. The summaries in MRP-87 [7-3] and a recent paper by Bamford and Hall [7-4] cover experience with other Alloy 600 applications within the PWR RCS.

7.2.1 U.S. Experience with Leaking CRDM Nozzles

Based on plant submittals to the NRC and discussions with plant personnel, Table 7-1 summarizes the U.S. experience with leaking CRDM nozzles as of December 2003. Of the 55 leaking CRDM nozzles detected in U.S. PWR reactor vessel closure heads, 34 were repaired in a manner such that if significant wastage had occurred, it would likely have been detected. Of the remaining 21 nozzles that leaked, several are planned to be investigated for the presence of wastage through destructive examinations. Of the 34 repaired in such a manner as to reveal wastage, only Davis-Besse nozzle nos. 2 and 3 showed significant wastage in the surrounding head material. The wastage at these nozzles was accompanied by evidence of leakage that was readily detectable several years prior to the large cavity adjacent to nozzle #3 being discovered. In general, the remaining nozzles tended to show small amounts of wastage in the surrounding head material, typically evident through ultrasonic "leak path technology" inspections that showed small gaps between the Alloy 600 nozzle material and the low-alloy steel head material for areas expected to have an interference fit. However, in two cases, visible but small wastage volumes have been observed [7-5]. In one case, a small cavity was visible in the low-alloy steel material at the bottom of the annulus that was approximately 3/16" deep. In another case, some minor material loss was visible at the top head surface adjacent to the nozzle. The wastage volumes for these two cases are estimated to have been less than 1 in^3, and these two cases were clearly insignificant in terms of the structural integrity of the head.

Because of the detailed characterization work that was performed, the best characterized wastage volumes were those resulting from leaks at Davis-Besse. The large wastage cavity adjacent to

nozzle #3 was accompanied by evidence of leakage years before its discovery as discussed above in paragraph 3.6. Wastage around nozzle #2 had maximum dimensions of 4 inches by 3/8 inch by 2 inches [7-1]. The wastage around nozzle #1 was less than 1/16 inch deep [7-1]. These dimensions, as well as those from other plants, are well below the maximum allowable wastage volume calculated in Section 3.

Note that Davis-Besse is the only plant known to have significant amounts of boric acid wastage due to CRDM nozzle PWSCC even though BMV examinations were not performed regularly in the industry until late 2000. Furthermore, based on the number of leaking nozzles and the size of the observed cracking, it is likely that many of the 34 CRDM nozzles that were repaired in a manner that would likely have revealed significant wastage had it been present were leaking for at least two operating cycles.

7.2.2 U.S. Experience with Other Alloy 600 Penetrations and Alloy 182/82 Welds

Other Alloy 600 penetrations and Alloy 182/82 welds in the primary system have developed leaks, including the following:

- Pressurizer instrument nozzles
- Pressurizer safe end nozzles
- Pressurizer heater sleeves
- RCS hot leg instrument nozzles
- RCS reactor hot-leg piping nozzle butt welds
- Reactor vessel closure head thermocouple nozzles

A database was recently compiled to document experience with cracks and leaks in these locations [7-3]. The typical method for detection of leakage due to PWSCC at these locations has been by visual inspection for the accumulation of boric acid deposits and/or corrosion products at the location of the leak. Despite over 100 of these components reported to have leaked due to PWSCC, significant wastage of the surrounding low-alloy steel material has rarely been reported. The repair activities that were performed subsequent to such leakage being detected would generally have been expected to reveal significant wastage given the guidance developed by plants regarding boric acid corrosion following NRC Generic Letter 88-05 [7-6].

The following specific incidents are reported in the EPRI *Boric Acid Corrosion Guidebook* [7-7]:

- Leakage from a heater sleeve (~0.002 gpm) at ANO Unit 2 in 1987 resulted in corrosion of the low-alloy steel bottom pressurizer head approximately 1.5 inches in diameter and 0.75 inch deep over an operating period of approximately six months.
- A crack in an Alloy 182 nozzle safe end weld at VC Summer in 2000 lead to leakage and the accumulation of more than 200 pounds of boric acid crystals. There was visible corrosion of the carbon steel nozzle material, but not enough to be measured.

7.2.3 U.S. Experience with Leakage from Mechanical Joints and Seal Welds

Following are some of the most significant domestic reported occurrences of boric acid wastage of the reactor vessel closure head due to leakage from mechanical joints and seal welds:

- In 1986, a leak was discovered from a Conoseal joint above the reactor vessel head at Turkey Point 4 [7-7]. Primary water had leaked onto the reactor vessel head causing the accumulation of a reported minimum of 500 pounds of boric acid deposits. The leakage resulted in corrosion of the reactor vessel head steel to a depth of approximately 1/4 inch. The average leak rate for the Turkey Point 4 incident was reported to be less than 0.45 gpm. For the reported six months of leakage and assuming a boron concentration of 750 ppm, the required leak rate to produce the reported minimum of 500 pounds of boric acid deposits is 0.053 gpm.
- Another instance of boric acid solution dripping onto the reactor pressure vessel head and causing wastage occurred at Salem 2 [7-7]. In 1987, a pin hole leak in an instrument seal weld led to the accumulation of approximately 15 ft^3 of boric acid deposits on the head. Beneath the deposit pile, nine corrosion pits were discovered. The pits were on the order of 1–3 inches in diameter with a maximum depth of about 0.4 inch.
- In late 2002, a relatively minor amount of wastage was discovered on the Sequoyah 2 reactor vessel closure head due to reactor coolant leakage from above the head [7-8,7-9]. During inspections to locate and correct a suspected RCS leak, Sequoyah personnel identified an accumulation of boric acid deposits on the reactor vessel head insulation which had resulted from a leaking reactor vessel level indication system (RVLIS) compression fitting. The RVLIS compression fitting had been disconnected and reconnected approximately eight months earlier during a refueling outage. The leakage had seeped through a seam in the insulation onto the reactor vessel head and resulted in minor boric acid corrosion of the head. The amount of material loss from the head was small, in the shape of a groove, about 1/8" deep.

Two of the other most significant instances of boric acid corrosion in domestic PWRs due to leakage from mechanical joints and seal welds are as follows:

- In 1986, high-pressure safety injection (HPI) nozzles at Arkansas Nuclear One (ANO) Unit 1 were being nondestructively inspected during a normal refueling outage [7-7]. When the insulation was removed from a nozzle, severe corrosion was discovered on the nozzle outside surface. At its deepest point, the corrosion extended two-thirds through the nozzle wall thickness. The corrosion was traced to leakage from the body-to-bonnet joint of the HPI isolation valve that is located about eight feet above the corroded area. This valve had operated with a known leak of less than 0.1 gpm for at least five months prior to discovering the corrosion.
- A visual inspection of the Ft. Calhoun reactor coolant system during a 1980 refueling outage showed that water was dripping from the reactor coolant pump insulation [7-7]. Further investigation showed that the leakage was coming from the spiral-wound gaskets and that three studs on one pump and four studs on another pump were severely corroded. The corrosion took on an hourglass shape over a region extending about 3.75 inches above the top of the pump casing flange. The diameters of the worst case studs were reduced from the

original 3.5 inches to 1.0–1.5 inches. This represented a significant reduction to less than 20% of the original cross sectional area on worst case studs.

7.2.4 International Experience

A review of the worldwide experience with cracking of CRDM nozzles conducted in 2000 [7-10] indicated that hundreds of PWSCC indications had been observed abroad, primarily in France, but also in Sweden, Switzerland, Belgium, South Africa, and South Korea.

However, the only CRDM nozzle indication reported to have resulted in a through-wall leak was Nozzle 54 at Bugey 3 (EDF). During a hydraulic pressure test of the reactor vessel, primary water was visually observed leaking from the reactor vessel head [7-11]. Subsequently, moisture and boric acid deposits were observed at Nozzle 54, located at the periphery of the reactor vessel head. Corrosion of the head opened a narrow gap between the nozzle and the borehole approximately 65 μm (2 to 3 mils) wide. The corrosion was centered on a "trail" leading from the point in the borehole adjacent to the crack upward to the vessel head surface. It was estimated that the crack had been leaking for approximately 20,000 hours (2.3 years).

Three additional reported incidents have occurred at European plants that are relevant. In the first, a head vent leak at Bugey 3 resulted in the accumulation of approximately 33 pounds of boric acid deposits on the reactor vessel head and wastage of the head top surface extending to approximately a depth of 3/4 inch [7-12]. In the second incident, a canopy seal or CRDM flange leak at one EDF plant apparently led to wastage about 3/8 inch deep on the reactor vessel head [7-12]. Finally, at Beznau in 1970, leakage above the reactor vessel head led to the accumulation of 1–2 m^3 (60,000–120,000 in^3) of boric acid deposits and a maximum wastage depth into the top head surface of 1.6 inches [7-12]. The volume of boric acid deposits reported for the Beznau incident indicates a leak rate during the corrosion progression likely greater than 0.1 gpm.

7.3 Modeling of the Head Wastage Process

Based on the plant experience, bare metal visual (BMV) inspections performed at appropriate intervals are expected to be highly effective at preventing significant boric acid wastage. The purpose of the modeling work presented in Appendix E is to support the plant experience in the determination of the appropriate BMV interval for plants of different PWSCC susceptibilities. Specifically, the modeling work shows high confidence that periodic BMV inspections will detect CRDM nozzle leakage before that leakage could lead to low-alloy steel wastage having a volume such that the reactor vessel head stresses exceed the Code allowable values. The calculated stresses that are compared to the allowable Code values are the primary membrane and primary membrane plus bending stresses in the remaining ligament of the low-alloy steel material of the reactor vessel head.

Both deterministic and probabilistic approaches are taken in Appendix E to evaluate the BMV inspection interval. The stress calculation used to determine the allowable wastage volume to maintain stresses below the Code allowables is presented in Section 3 and Appendix D.2. The probabilistic evaluation shows that the probability of the Code allowables for primary membrane

and membrane plus bending stresses being exceeded in the head material is less than 1×10^{-4} given a leaking CRDM nozzle and BMV inspections performed during each refueling outage. Note that credit for the performance of periodic nonvisual examinations is not taken in the modeling. Rather, the modeling is conservatively predicated on the existence of a leaking CRDM nozzle

7.4 Relevant Experimental Investigations and Additional Planned Research

The following three experimental investigations are particularly relevant:

ABB-CE Tests: High-temperature (316°C–600°F) boric acid solution (1000 ppm B) was leaked through a PWSCC crack in an Alloy 600 steam generator tube into the annular gap between the tube and a clearance hole in a SA 533 Grade B Class 1 steel block (Test M in [7-7]). The annular gap opened downwards. Leak rates tested ranged from 0.02 to 0.12 gpm. The test showed the highest corrosion rate at the edge of the annulus (i.e., at the exit). The highest measured corrosion rate was 2.15 in/year, which led to a metal loss rate of approximately 1.07 in^3/year.

EPRI Tests: High temperature (316°C–600°F) boric acid solution (2000 ppm B) was leaked through an A302 Grade B steel block into the annulus between the block and a stainless steel cylindrical insert (Test EPRI-6 in [7-7]). The annulus was sealed at the bottom. Leak rates tested ranged from 0.01 to 0.1 gpm. The surface of the carbon steel block at the annulus exit was either horizontal or angled (i.e., to simulate either a central CRDM nozzle or a peripheral CRDM nozzle). The test showed the highest corrosion rate near the injection point (deep in the annulus). The highest corrosion rate measured was 2.37 in/year.

CE Impingement Test: High-temperature (316°C–600°F) boric acid solution (1000 ppm B) was pumped through a hole in a heated SA 533B steel block at rates ranging from 0.05 to 0.1 gpm (Test L in [7-7]). The hole was oriented horizontally, and the exit stream was sprayed onto a SA 533B steel target plate. Corrosion rates of up to 1.2 in/year and 11.1 in/year were measured in the hole and on the target, respectively. At locations where there was no direct impingement on the target block, the corrosion rate was measured to be 0.4 to 0.6 in/yr. This test showed that under some conditions corrosion rates of up to 10 in/yr or higher can occur. However, the impingement of a two-phase jet on a plate in an open, aerated environment is not representative of the conditions expected to occur during the early stages of wastage deep down in an annulus on the OD of a CRDM nozzle.

The MRP is currently sponsoring an extensive experimental program to verify and refine the modeling assumptions of Appendix E. The experimental work is expected to include full-scale mockups of leaking CRDM nozzles with a wide range of leak rates and other conditions. The first results from the mockup testing are expected in 2005.

7.5 Conclusions

The Davis-Besse experience indicates that BMV inspections performed every refueling outage—and likely even if performed less frequently—with proper follow-up action would have caught the head degradation early in the material loss process. Moreover, an analysis of the other U.S. and foreign industry experience supports the reliability of BMV inspections to prevent significant boric acid wastage of reactor vessel closure heads due to PWSCC. The results of modeling work of the wastage process based on current understanding support the conclusion that bare metal visual inspections performed at appropriate intervals provide high confidence that Code allowable stresses in the low-alloy steel head material will not be exceeded due to wastage.

7.6 References

7-1. *Root Cause Analysis Report: Significant Degradation of the Reactor Pressure Vessel Head*, Davis-Besse Nuclear Power Station report CR 2002-0891, April 2002.

7-2. *Examination of the Reactor Vessel (RV) Head Degradation at Davis-Besse*, Final Report, BWXT Services, Inc., Lynchburg, VA: 2003. 1140-025-02-24.

7-3. *Materials Reliability Program PWSCC of Alloy 600 Type Materials in Non-Steam Generator Tubing Applications—Survey Report Through June 2002: Part 1: PWSCC in Components Other Than CRDM/CEDM Penetrations (MRP-87),* EPRI, Palo Alto, CA: 2003. 1007832.

7-4. W. Bamford and J. Hall, "A Review of Alloy 600 Cracking in Operating Nuclear Plants: Historical Experience and Future Trends," *11th International Symposium on Environmental Degradation of Materials in Nuclear Power Systems—Water Reactors* (Stevenson, WA, August 11–14, 2003), American Nuclear Society.

7-5. *Materials Reliability Program: EPRI Boric Acid Corrosion Workshop, July 25-26, 2002 (MRP-77)*, EPRI, Palo Alto, CA: 2002. 1007336.

7-6. U.S. Nuclear Regulatory Commission, "Boric Acid Corrosion of Carbon Steel Reactor Pressure Boundary Components in PWR Plants," NRC Generic Letter 88-05, March 17, 1988.

7-7. *Boric Acid Corrosion Guidebook, Revision 1: Managing Boric Acid Corrosion Issues at PWR Power Stations*, EPRI, Palo Alto, CA: 2001. 1000975.

7-8. U.S. Nuclear Regulatory Commission, "Recent Experience with Reactor Coolant System Leakage and Boric Acid Corrosion," NRC Information Notice 2003-02, January 16, 2003.

7-9. Letter from TVA (P. Salas) to NRC, "Sequoyah Nuclear Plant (SQN) – Unit 2 – Response to NRC Request for Additional Information Regarding Licensee Identified Material Wastage (TAC No. MB4579)," dated February 3, 2003. ADAMS Accession No. ML030030863.

7-10. W. Bamford, D. Boyle, and J. Duran, "An Update on World Inspection Experience for RV Head Penetrations," *Proceedings: 2000 EPRI Workshop on PWSCC of Alloy 600 in PWRs* (PWRMRP-27), EPRI, Palo Alto, CA: 2000. 1000873.

7-11. "RPV Head Wastage—Review of French Experience," EPRI Memo from A. Machiels to MRP Distribution List, April 3, 2002.

7-12. R. Kilian, P. Scott, A. Roth, and U. Wesseling, "Boric Acid Corrosion - European Experience," *Materials Reliability Program: EPRI Boric Acid Corrosion Workshop, July 25-26, 2002 (MRP-77)*, EPRI, Palo Alto, CA: 2002. 1007336.

Table 7-1
U.S. PWR Experience with Leaking CRDM Nozzles Relevant to Head Wastage

Inspection Number	Unit	NSSS Supplier	Approx. EDYs at Insp.	Insp. Date	No. of CRDM Nozzles on Head	Number Leaking Penetrations (Note 1)			Repair Technique (Note 2)	Repair Method Would Likely Have Detected Significant Wastage?	Notes
						Total	Due to Tube Cracking	Due to Weld Cracking			
1	ANO 1	B&W	19.6	Mar-2001	69	1	1	0	Embedded flaw	No	3
2			21.1	Oct-2002	69	1	1	0	ID temper-bead	Yes	4
3	Crystal River 3	B&W	16.2	Oct-2001	69	1	1	0	ID temper-bead	Yes	
4	Davis-Besse	B&W	19.2	Apr-2002	69	3	3	0	Replaced head	Yes	5
5	North Anna 1	W	21.4	Mar-2003	65	1	0	1	Replaced head	No	
6	North Anna 2	W	19.0	Nov-2001	65	3	0	3	Weld overlay	No	
7			19.7	Sep-2002	65	6	0	6	Replaced head	See Note 7	6
8	Oconee 1	B&W	21.8	Nov-2000	69	1	0	1	Weld repair	No	8
9			23.2	Mar-2002	69	1	0	1	ID temper-bead	Yes	
10			24.7	Sep-2003	69	2	2	0	Replaced head	No	9, 10
11	Oconee 2	B&W	22.2	Apr-2001	69	4	4	0	ID temper-bead	Yes	
12			23.7	Oct-2002	69	10	7	3	ID temper-bead	Yes	
13	Oconee 3	B&W	21.7	Feb-2001	69	9	9	0	Weld repair	No	
14			22.5	Nov-2001	69	5	5	0	ID temper-bead	Yes	
15	Surry 1	W	19.1	Oct-2001	65	4	0	4	ID temper-bead	Yes	
16	TMI 1	B&W	18.1	Oct-2001	69	5	1	4	ID temper-bead	Yes	11
				Unique Penetration Totals		55	33	22			

NOTES:

1. No CEDM, ICI, or other types of reactor vessel head nozzles have been found to be leaking (other than the B&W thermocouple nozzles at the two units that have this type of nozzle). Note that NDE of the welds is often not as complete as for the tubes, so some leak path cracks through the weld metal from the wetted weld surface to the nozzle annulus may have not been found during inspections and thus not reflected in this table.
2. The "ID temper-bead" repair method for leaking nozzles involves cutting out the lower section of the nozzle, which makes the surface of the penetration hole in the head shell visible.
3. Although the 2001 repair of this nozzle would not have revealed the presence of low-alloy steel wastage, the subsequent repair in 2002 likely would have.
4. The leaking nozzle that was repaired in March 2001 was found to be leaking again in October 2002.
5. Detailed destructive examinations of the original Davis-Besse head have been performed to characterize the extent of wastage. The destructive examinations showed an axial crack through most of the weld cross section at the location of the long axial tube crack in Nozzle #3, which was adjacent to the large wastage cavity.
6. One of the leaking nozzles that was repaired in late 2001 was found to be leaking again in September 2002.
7. Some leaking nozzles have been extracted from the original North Anna 2 head and may be examined for signs of wastage of the low-alloy steel shell material, among other tests.
8. Also 5 of the 8 small-diameter B&W thermocouple nozzles were found to be leaking.
9. It is assumed in the table that these two penetrations were found to be leaking due to base metal cracking although no inspections were performed to investigate before head replacement.
10. Also one small-diameter thermocouple penetration that was previously repaired with an Alloy 690 plug was found to be leaking. The cause of the leakage (incomplete weld coverage, cracking, etc.) was not determined as the head was replaced.
11. Also all 8 small-diameter B&W thermocouple nozzles were found to be leaking.

8
CONSEQUENTIAL DAMAGE ASSESSMENT

This section presents an assessment of consequential damage given nozzle ejection. This assessment shows that the conditional core damage probability (CCDP) for standard LOCA events can be used to bound the potential effects of consequential damage.

Although the discussion presented below is specific to LOCAs initiated by a nozzle ejection event, the assessment presented largely applies to the case of a LOCA due to rupture of the head or cladding caused by extensive boric acid wastage. The potential consequences of head rupture due to wastage are similar to the description below for nozzle ejection, although a larger LOCA could occur.

8.1 Introduction

"Consequential damage" refers to the secondary damage that might occur in the unlikely event that a control rod drive mechanism (CRDM) nozzle detaches from the reactor vessel (RV) head. Figure 8-1 through Figure 8-3 show a typical design of a reactor vessel head and a missile shield. The issue evaluated by this section is whether the consequential damage from the detached CRDM may challenge successful mitigation of the event, such that it leads to an increase in the conditional core damage probability (CCDP) beyond what would be expected given a loss of coolant accident (LOCA) of similar size (i.e., single detached CRDM).

As shown in the MRP nozzle ejection safety assessments (MRP-105 [8-1], MRP-104 [8-2], and MRP-103 [8-3]), periodic visual and nonvisual examinations ensure that the likelihood of CRDM nozzle detachment is small.[5] Hence the likelihood of the associated consequential damage is reduced as well. However, the purpose of this section is to assess, given that CRDM nozzle detachment occurs, whether the CCDP for a similar-sized LOCA is representative.

If a complete and sudden severance of the CRDM nozzle occurs, the break size will be within the range that most probabilistic risk assessments (PRAs) identify as a small to medium break LOCA. The CCDP given a conventional small or medium LOCA can be determined from plant-specific PRAs. From the perspective of LOCA mitigation, the top of the vessel is a favorable break location and use of the CCDP for a small or medium break LOCA of the kind typically considered in PRAs should be conservative. However, if a CRDM nozzle detaches, it is possible that the resulting forces and/or debris may cause consequential damage to adjacent CRDMs or other components. The objective of this section is to assess whether there is a potential increase

[5] These evaluations are conservative in that no credit is taken for the likely detection of large circumferential cracks before detachment could occur through an observed increase in the unidentified RCS leak rate.

in the CCDP over that of the representative LOCA because of consequential damage that might result from the failure of a CRDM nozzle.

The EPRI Materials Reliability Program (MRP), with contributions from member utilities and the vendors, has evaluated the significance of this potential consequential damage. This section summarizes the consensus reached as a result of the evaluation.

8.2 Evaluation

This section evaluates the consequential damage that may occur upon accidental detachment of a CRDM nozzle, and whether this consequential damage provides a challenge to accident mitigation that is different or worse than what was assumed for the "standard" LOCA in the various plant PRAs. This will determine whether the CCDP for a LOCA is representative of the risk from CRDM nozzle failure. Possible consequential damage that has been postulated as a result of CRDM ejection includes:

- Damage caused by the CRDM missile to components in its trajectory, including adjacent CRDMs and support systems,
- Water jet impingement from the broken head penetration,
- Loose parts generated inside or outside of the vessel due to nozzle detachment, and
- Damage to the RV head and/or adjacent CRDM nozzle penetrations that have been previously weakened by boric acid wastage from the leaking nozzle.

The investigations by MRP and the NRC [8-4] are in agreement that detailed mechanical analysis of potential damage is not useful because there appears to be abundant shutdown margin and emergency core cooling system (ECCS) capability for mitigation of this accident. Rather than address mechanistically whether these secondary failure modes could actually occur, the approach taken was to first ascertain whether any of these failure modes, if they did occur, would have any impact upon the consequences of the accident, that is, the CCDP.

For an equivalent-sized LOCA in the reactor coolant system (RCS) loop, the mission success definition associated with the CCDP is typically based upon standard LOCA analysis assumptions, which credit only a portion of the total available rod worth. To evaluate the case of a LOCA involving a broken CRDM penetration, any impact upon the CCDP from consequential damage would have to occur by affecting the mitigation of the LOCA, or via a new initiating event that has not been previously evaluated in the PRAs. The safety functions required for LOCA mitigation include reactivity control, inventory control, and heat transfer. The control rods provide a portion of the first function. The ECCS provides all three functions. The only new initiating event of interest is LOCA with subsequent failure to shutdown the reactor. Therefore, it is important to consider the impact of the postulated consequential damage upon the ECCS function and the control rod trip function. Each of these is discussed in more detail below.

8.3 Effect of Consequential Damage on ECCS

ECCS effectiveness for this event is better than for the typical LOCA that is assumed in the safety analyses and the PRAs. That is because the postulated accident does not involve a break in the RCS piping between the ECCS injection location and the core. Since the break is located on top of the reactor vessel, it is on the hot side of the core and does not involve any borated ECCS fluid bypassing the core. Therefore, the full capacity of the ECCS is available for core heat removal and to compensate for the RCS inventory loss.

If a CRDM housing detaches, the CRDM missile will impact the missile shield that is directly above the reactor vessel head. There is no ECCS equipment in this vicinity that may be impacted. (ECCS systems are designed for protection against missiles via location behind missile shields and/or by physical separation.[6]) Some plants have high point vent lines above the vessel, which are unnecessary for this accident considering that the LOCA of interest is itself a high point vent. An inadvertent breaking of the high point vent line or breaching of the pressure boundary integrity of other CRDM housings (i.e., increasing the break size) would result in faster depressurization and more ECCS flow. Extensive secondary damage to the pressure boundary could increase the size of the LOCA to the equivalent of a large break, which in the PRAs of the various pressurized water reactors (PWRs) may have a slightly higher CCDP than a medium or small break LOCA. However this difference is insignificant relative to the likelihood of the damage that would be necessary to reclassify the LOCA size (i.e., multiple nozzle penetrations).

Some PWRs have instrumentation that is routed above the RV head that may be used to guide post-accident operator response. This includes the RV water level monitoring system, which may have cables (thermocouple design) or impulse lines (differential-pressure design) routed above the RV head. These instruments are used at some plants for verification and long-term surveillance of core cooling. At these plants, redundancy and physical separation minimize the likelihood that a missile or other consequential damage will affect both trains. This parameter is a supplement to core exit temperature and/or subcooling margin as an indicator of adequate core cooling. Subcooling margin is derived from RCS pressure and temperature (hot-leg temperature and/or core exit temperature, usually selected or auctioneered). Some plants have cabling for core exit thermocouples routed above the RV head as well. Since these originate from multiple thermocouples at different fuel locations, it is unlikely that a missile or other consequential damage will disable all of the core exit thermocouple indications. In addition, subcooling margin can be ascertained without core exit thermocouples via the other RCS temperature instrumentation (i.e., hot-leg temperature). However, for those plants that have both core exit thermocouple and RV level monitoring instrumentation routed above the head, an assessment may be warranted to ensure that operator reliability will not be significantly degraded for this particular LOCA.[7] Generally, operators do not rely exclusively upon the instrumentation that is

[6] In the unlikely event that there are deficiencies in ECCS missile protection, then plant-specific adjustments to the CCDP may be necessary. See Recommendations.

[7] If there is reliance upon instrumentation routed above the RV head, then plant-specific adjustments to the CCDP may be warranted based upon an assessment of the operator dependency on this instrumentation. See Recommendations.

routed above the RV head and they will have adequate indication of core cooling even if that instrumentation is lost.

If internal debris is generated as a result of the rod ejection, it may be blown out of the broken penetration. If the debris remains inside the vessel, only small pieces could travel to other parts of the RCS. In PWR reactor vessels, the area above the core contains RV internals structures that support and guide the control rods (control blades at two plants). These internals will restrict the movement of large debris between the upper plenum area and the RCS loops. Since the ECCS draws suction from the borated or refueling water storage tank (BWST/RWST), and then later in recirculation mode from the reactor building sump (RBS), small pieces of debris escaping to the RCS will not impact ECCS performance or event mitigation. Large pieces of debris cannot escape the upper head area. Since they would be trapped on the hot side of the core, they can have no effect on ECCS performance.

Debris may be generated external to the reactor vessel from damage caused by the detached CRDM or the associated water jet impingement. The area above the vessel contains cables and support equipment for the CRDMs and instrumentation, support structures, and some insulation. Some of these parts may find their way eventually to the RBS. The RBS designs have the usual protection (curbs, screens, cages, etc.) and their availability would be no different than for any other LOCA. (The LOCA analyses, upon which the ECCS mission success definitions are based, typically assume 50% blockage of the RBS flow area.)

However, sump blockage is a plant-specific issue, which has been researched in support of Generic Safety Issue 191, and more recently has been the subject of NRC Bulletin 2003-01 [8-5]. The NRC has recommended that plant-specific assessments be performed to determine if current RBS designs are able to handle the quantity of fibrous debris that may be transmitted to the sump during a LOCA. The control rod ejection accident is just one of the LOCAs that may challenge the RBS. Since the ability of the RBS to handle debris is applicable to all LOCAs, it should be accounted for in the plant-specific PRAs and included in the base CCDP for the equivalent sized LOCA.[8]

There are no other consequential damage effects identified with respect to affecting ECCS performance. Therefore, it is concluded that with respect to ECCS performance, the CCDP for a similar-sized break in an RCS loop, which most PRAs identify as a small or medium LOCA, is appropriate for the postulated LOCA involving a CRDM nozzle penetration.

8.4 Effect of Consequential Damage on Reactivity Control

For a LOCA initiated by a CRDM nozzle detachment, a reactor trip signal will be generated allowing the unaffected rods to fall into the core. Core shutdown will be augmented by soluble boron reactivity control via the boron in the ECCS injection fluid. Since the break location at the top of the vessel does not affect the operability of the ECCS, and none of the ECCS inventory

[8] If the character of fibrous debris above the RV head is different from the other RCS locations, or the PRA from which the CCDP was extracted (or the LOCA analysis upon which the PRA is based) does not include proper consideration of the debris effects, then plant-specific adjustments to the CCDP may be necessary. See Recommendations.

bypasses the core, the (borated) ECCS injection flow to the core is greater than is usually assumed in conventional LOCA analysis.

If there is a CRDM missile or an associated water jet impingement, there may be an impact on components above the reactor vessel and under the missile shield. This area contains other CRDMs and their related service and support equipment, such as power, control, and instrumentation cables. However, all of the power supplies and control signals are fail-safe with respect to control rod trip. There is no damage that could occur to any of the attached CRDM equipment that could prevent control rod trip.

If a severe impact occurs to nearby CRDM housings, it could be postulated that there is a remote possibility of adjacent CRDM housings being deflected enough to prevent control rod insertion, or being broken off and causing additional control rod ejections. It is also possible that internal debris could fall and be trapped in locations that could potentially block insertion of neighboring control rods.

With respect to core average reactivity, the shutdown margin is such that several control rods could fail to insert before the risk would increase over that of a single control rod failure. Even with conservative success criteria for reactor trip, several control rod failures could easily be tolerated from a reactivity standpoint. For example, per the NRC's publication of the ATWS Rule [8-6], insertion of only about 20% of the control rods uniformly spaced is needed to achieve hot, zero power. For long-term shutdown, LOCA analyses credit only a fraction (zero to 50%) of the available control rod worth.

The specific number of adjacent control rod failures that could be tolerated could be determined by core-specific analysis. For example, an analysis of a specific core at one PWR assumed that a cluster of five control rods failed to insert in addition to the control rod of maximum worth [8-7]. For immediate shutdown (no credit for additional boron), that analysis calculated the remaining available rod worth at 3.6% $\Delta k/k$. The rod worth needed to achieve 1% shutdown margin was 2.3% $\Delta k/k$. These results improved for long-term shutdown margin, with credit for additional boron from the ECCS. Thus the analysis showed that the shutdown margin was sufficient even with a cluster of five failed control rods. The negative reactivity in the inserted control rods and the boron concentration was sufficient to maintain the core subcritical. While this type of analysis is core-specific, it demonstrates that the shutdown margin is typically generous, and that it is forgiving of several adjacent control rod failures due to unlikely consequential damage. This conclusion is also supported by NRC analysis [8-4]. Therefore, inability to shutdown the reactor due to consequential damage from a CRDM nozzle failure is not a credible risk contributor, because of the number of simultaneous CRDM failures that would be required.

However, there may be a question of local reactivity effects from failure to trip of two or more adjacent control rods (i.e., tripped rods not uniformly spaced). If several adjacent control rods fail to drop, there will be an absence of negative reactivity insertion from control rods in a localized region of the core, which could result in a return to criticality and additional fission power that would heat up the rods and cause localized boiling. The boiling creates voids that provide negative reactivity that takes the region back to subcritical, thereby shutting down the additional fission power production. As subcooled liquid from the ECCS collapses the voids that

were generated, the negative reactivity is lost and the process may repeat itself in an oscillatory manner (with fluctuating power levels) in a localized region of the core, until sufficient boration from the ECCS injection is obtained to keep the entire reactor subcritical. Since the break is at the top of the RV and on the hot side of the core, the RV inventory should be sufficient to keep the core covered with a two-phase mixture level that will prevent excessive heat up of the fuel pins or cladding. With the ECCS pumping its full capacity into the RCS, highly borated water will be added to the original RCS inventory, increasing the total concentration of boron in the core region water. In the meantime, the RCS will continue to depressurize through the break in the system (i.e., the CRDM nozzle). Through (eventual) depressurization, the ECCS accumulator tanks will be emptied, and the low pressure injection (LPI) system will initiate. Accordingly, even with local power oscillations, the reactor can be safely shutdown, though the process may be more drawn out than usual.

On the other hand, if there was failure of a large number of control rods combined with a relatively small break area, then RCS depressurization could be limited. The high RCS pressure could limit the amount of borated water that ECCS injects into the vessel. The localized boiling could cause loss of inventory (via steam through the break) that could exceed the ability of the ECCS to make-up at the high pressure. This scenario would require failure of a larger number of control rods than suggested by the previous example, and would also require the CRDM nozzle pressure boundaries to remain mostly intact. (Multiple CRDM nozzle pressure boundary failures would increase RCS depressurization and possibly result in initial core shutdown by void generation.) This scenario is unlikely considering the number of control rod failures that would be required.

8.5 Generation of Loose Parts

One scenario for affecting multiple control rods, but without increasing the break size, is from the postulated generation of internal loose parts. Loose parts (such as pieces of the degraded nozzle underside or control rod fragments) could break off and drop down after the first rod ejection and before the reactor protection system (RPS) causes the other rods to trip. Consequential damage external to the vessel is less likely to affect rod trip or affect a sufficient number of rods, and any increase in break size (due to additional failed CRDM housings) defeats the scenario. The probability of internal debris affecting a large enough number of rods to cause the core to uncover is small, considering that the LOCA analysis credits only a fraction of the available rod worth. This unlikely scenario would require a sufficient number of loose parts from the initial rod ejection impact and dispersal of the parts among several adjacent untripped rods. The falling loose parts would have to be dispersed such that each piece entered a different control rod guide column and landed in just the right way in the control rod guides to block insertion. The likelihood of this scenario decreases dramatically as the crucial number of affected control rods is increased. Therefore, it is concluded that the probability of core damage due to multiple control rod insertion failures following a CRDM detachment is small relative to the CCDP for a medium or small LOCA.

As discussed in the FMEA of Section 2, the generation of loose parts due to RVCH nozzle cracking is a potential safety concern even in the absence of a nozzle ejection event. Loose parts may either be captured by a drive rod or released to the flow in the upper plenum of the reactor

vessel. Captured loose parts have the potential to prevent control rod motion, while non-captured loose parts have the potential to prevent control rod motion or to damage fuel pins, steam generator tubes, the steam generator tubesheet, or the bottom reactor vessel area. Therefore, generation of non-captured loose parts is more of a potential concern. Depending on whether the penetration contains a drive rod, release of a non-captured loose part would require either a 360° below-weld circumferential crack or multiple below-weld axial and circumferential cracks in a nozzle. However, because nozzle ejection is always assumed to produce a LOCA with a conditional core damage probability (CCDP) of roughly 1×10^{-3} to 1×10^{-2}, the potential effect of loose parts generation is judged to have an insignificant effect on nuclear safety in comparison to the process of nozzle ejection. Therefore, the nozzle ejection evaluations of Section 6 are the appropriate evaluations for setting nonvisual inspection intervals. However, the concern for loose parts generation is an important factor in determining the appropriate coverage zone for the nonvisual examinations.

8.6 Large Early Release Frequency (LERF)

The final additional potential concern related to the failure of a CRDM is the effect on LERF given nozzle ejection or head rupture due to boric acid wastage. The initiating events that contribute materially to LERF are ones that either involve containment bypass or which involve failure of systems important to containment heat removal. Because of this observation and because the LOCAs (small, medium, or large) do not produce any significant contributions to LERF, the increment in core damage frequency (CDF) and not LERF is expected to be the proper risk parameter for evaluation.

8.7 Conclusion

This evaluation considers whether consequential damage that may be caused by ejection of a single CRDM housing would cause the CCDP of the resulting LOCA to be worse than that of a representative LOCA in an RCS loop. It is concluded that the potential increase in CCDP over that of a representative LOCA as a consequence of consequential damage is not significant. This is because the consequences of consequential damage relative to ECCS performance and reactivity control are not significant. The location of the break at the top of the RV head is favorable, and the reactor shutdown margin is sufficiently generous that a limited number of adjacent control rod failures can be tolerated. The most likely outcome of the accident is, therefore, a LOCA that can be represented by an equivalent break in an RCS loop. Industry and NRC experts are in agreement that detailed mechanical analysis of the damage that might be caused by a detached CRDM is not useful. More rigorous analysis to precisely determine the probability of consequential damage would not change the conclusion that it is not risk significant for RV head penetrations. Therefore, it is concluded that the CCDP for a LOCA is representative of the risk from CRDM nozzle failure.

Finally, a study to determine the consequences of postulated breaks in the RV of PWRs was performed by the NRC in 2002 [8-8], and it was concluded that the consequences of failure to scram were minimal "because of the negative reactivity produced by core voiding and later by boric acid addition". Plants designed by B&W, Westinghouse and CE were analyzed in this

study. Therefore, the results of this study support the conclusions based on the assessment presented here.

8.8 Recommendations

Continuation of the RV head bare metal inspections and supplemental NDE are key to ensuring that the likelihood of CRDM nozzle detachment and boric acid wastage is small, and are credited in the safety evaluations and consequential damage assessments performed to date. For most plants, the CCDP for a small or medium LOCA that is extracted from the plant PRA is adequate to represent the CCDP for the postulated CRDM nozzle failure. However, it is recommended that users of this document review the applicability to their individual plants. Adjustments to the CCDP may be made on a plant-specific basis if the evaluation warrants. The following issues have been identified as potential bases for adjustment, and it is recommended that they be assessed on a plant-specific basis:

- Verify that the missile shields are positioned such that ECCS equipment is protected from CRDM missiles. If the ECCS is unprotected (unlikely), assess the impact upon the CCDP that may result if the probability of ECCS failure is affected.
- Verify that any instrumentation that may be routed above the RV head is not the only instrumentation relied upon for LOCA mitigation. If operators depend upon this instrumentation for LOCA mitigation, then assess the impact upon the CCDP that may result if operator error probabilities are affected.
- Verify that the character of any fibrous debris above the RV head is not different from the debris assumed for other LOCA locations, and ensure that the PRA from which the CCDP was extracted (or the LOCA analysis upon which the PRA is based) includes proper consideration of debris effects. If the debris is not properly considered, then assess the impact upon CCDP that may result if the ECCS failure probability is affected by differences in debris characterization.

8.9 References

8-1. *Materials Reliability Program: Probabilistic Fracture Mechanics Analysis of PWR Reactor Pressure Vessel Top Head Nozzle Cracking (MRP-105)*, EPRI, Palo Alto, CA: 2004. 1007834.

8-2. *Materials Reliability Program: RV Head Nozzle and Weld Safety Assessment for Westinghouse and Combustion Engineering Plants (MRP-104)*, EPRI, Palo Alto, CA: 2004. 1009403.

8-3. *Materials Reliability Program: RV Head Nozzle and Weld Safety Assessment for B&W Plants (MRP-103)*, EPRI, Palo Alto, CA: 2004. 1009402.

8-4. Letter from Richard A. Meserve (U.S. NRC) to The Honorable Edward J. Markey (U.S. House of Representatives), with enclosure "Response to Congressional Questions," June 28, 2002.

8-5. U.S. Nuclear Regulatory Commission, "Potential Impact of Debris Blockage on Emergency Sump Recirculation at Pressurized-Water Reactors," NRC Bulletin 2003-01, June 9, 2003.

8-6. U.S. Nuclear Regulatory Commission, Publication of Final Rule, "Reduction of Risk from Anticipated Transients Without Scram (ATWS) Events for Light-Water-Cooled Nuclear Power Plants," 49 FR 26044, June 1984 and 49 FR 27736, July 1984.

8-7. Letter from H. W. Bergendahl (FirstEnergy Nuclear Operating Company) to J. E. Dyer (U.S. NRC), "Safety Significance Assessment of Davis-Besse Nuclear Power Station, Unit 1 Reactor Pressure Vessel Head Degradation," U.S. NRC Docket Number 50-346, License Number NPF-3, Serial Number 1-1268, April 8, 2002.

8-8. Memorandum from W. Jensen (U.S. NRC) to G. Holahan (U.S. NRC), "Sensitivity Study of PWR Reactor Vessel Breaks," ADAMS Accession Number ML021340306, May 10, 2002.

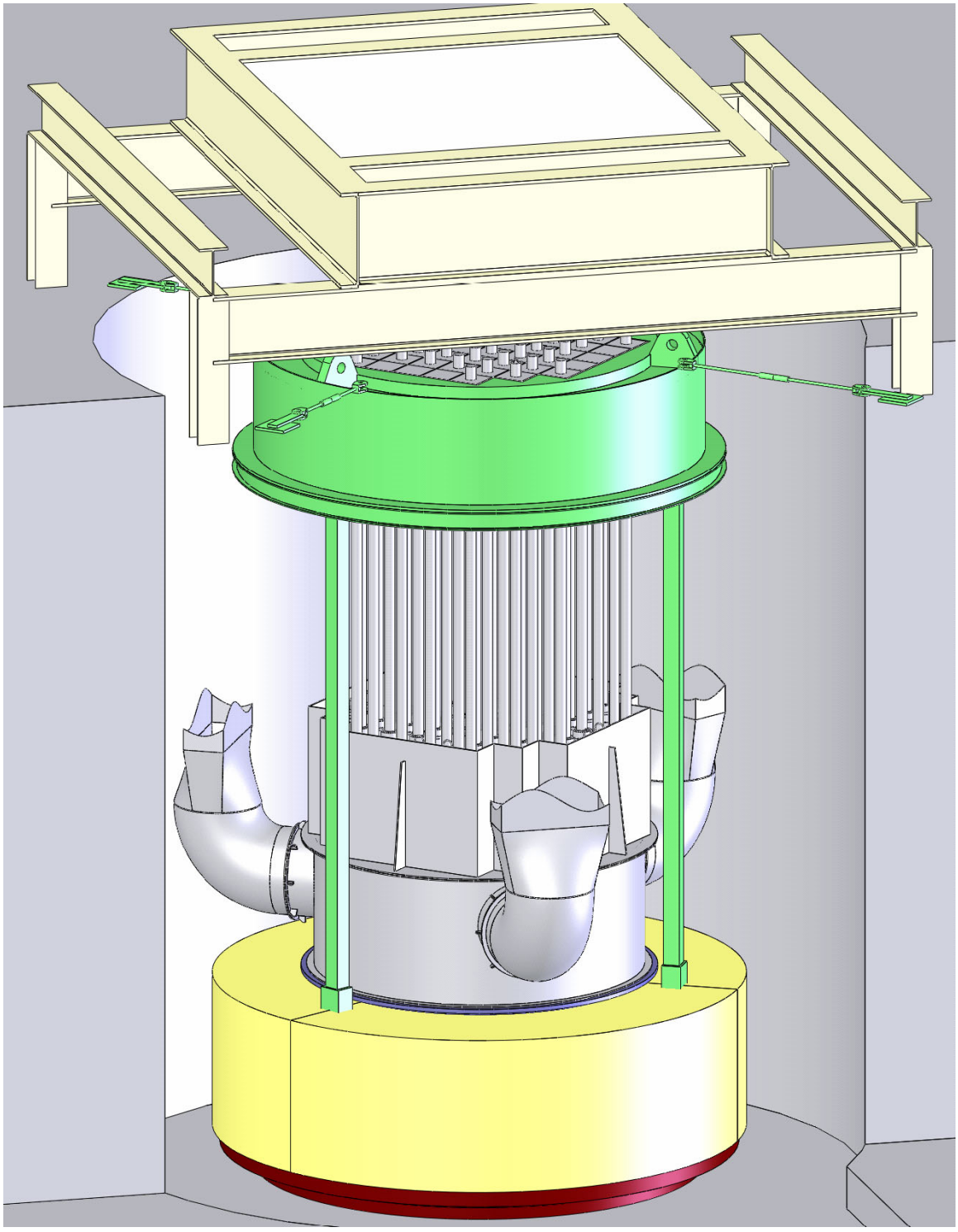

Figure 8-1
Typical Reactor Vessel Head—Assembled Isometric

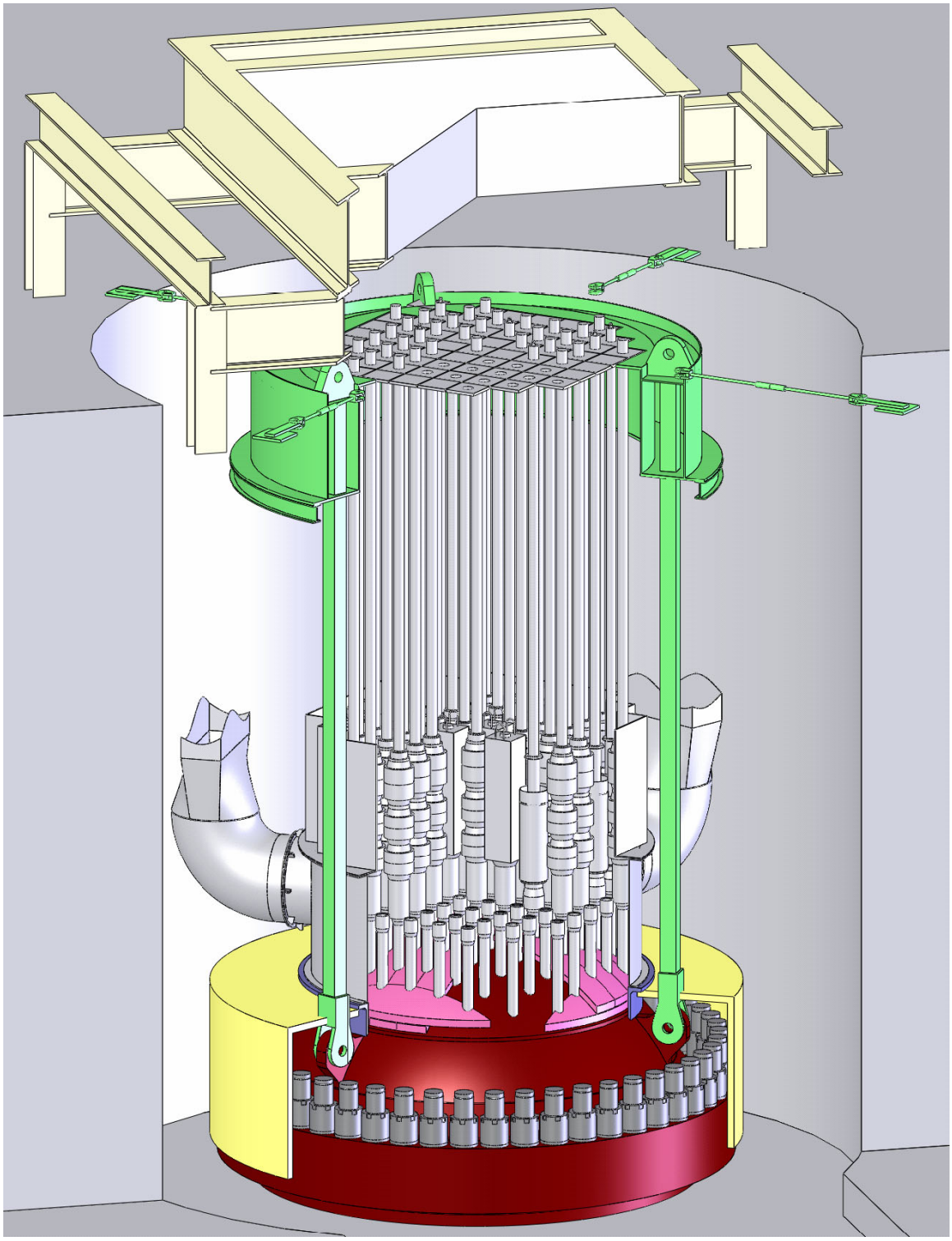

Figure 8-2
Typical Reactor Vessel Head—Cutaway Isometric

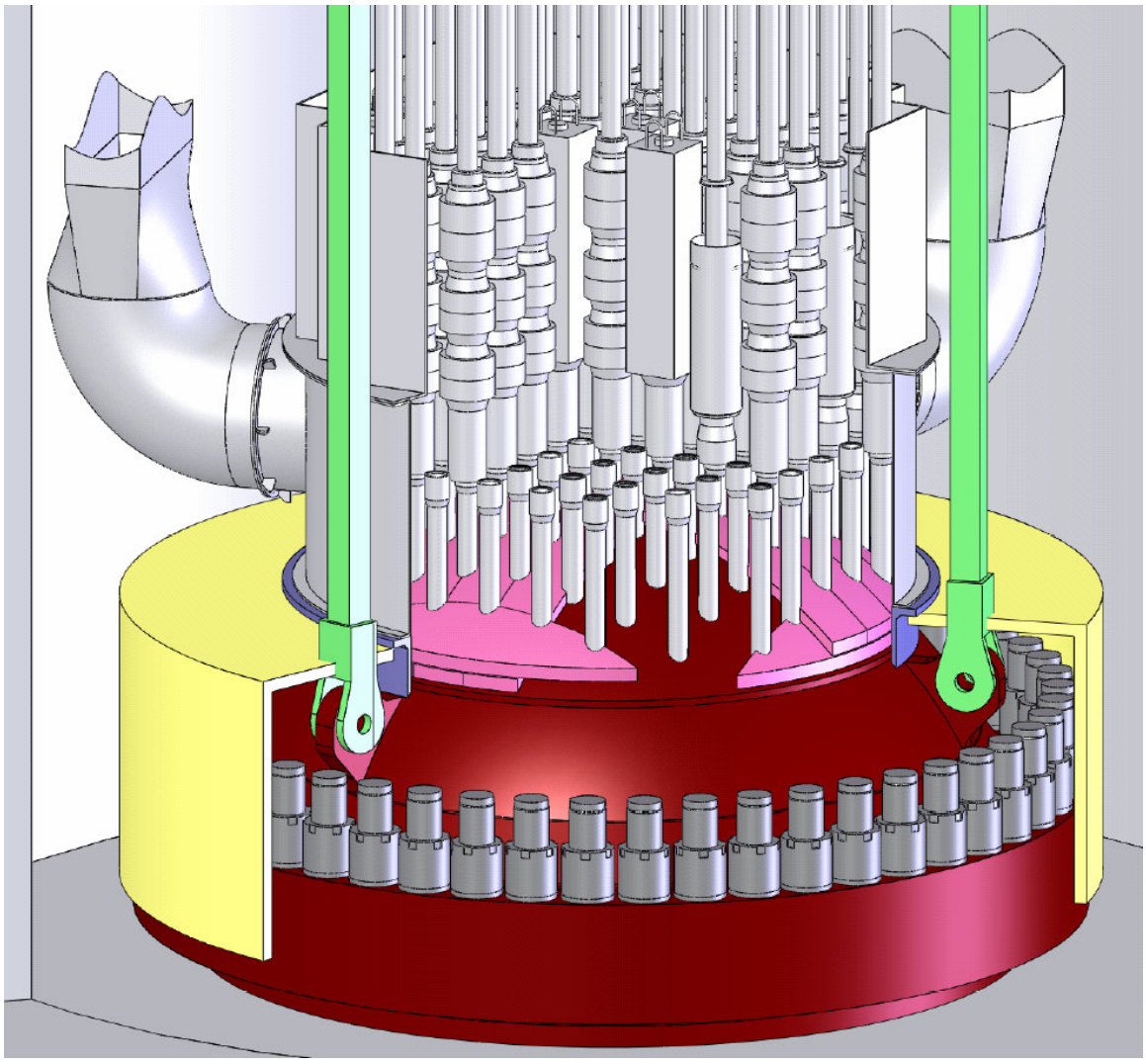

Figure 8-3
Typical Reactor Vessel Head—Close-up Cutaway Isometric

9
INSPECTION CAPABILITIES

There are a number of inspection techniques available to detect flaws or evidence of a leak due to a flaw in reactor vessel head penetrations. These inspections can be generalized into four categories: visual inspections for finding evidence of a leak, inspections using specialized leak detecting equipment, surface or volumetric examination of the penetration, and surface inspections of the base and weld metal around the penetration. An overview of the currently available inspection approaches is shown in Figure 9-1, which indicates the area covered by each inspection technique. Typically, two or more of these methods are combined. Not reflected in this figure is the capability to detect leaks from the primary pressure boundary during power operation provided through the periodic calculation of the unidentified leak rate and through other indirect indicators such as the clogging of containment air coolers.

9.1 Visual Examination for Detecting Leakage

One of the primary methods of checking the integrity of a reactor vessel penetration is to perform a bare metal visual inspection of the reactor vessel head. Such an inspection looks for the build-up of boric acid crystal residue around each penetration and across the top head surface. The current guidelines for bare metal visual inspections assembled by EPRI [9-1] specify that direct visual inspections may be used if the reactor vessel head can be seen without obstruction (i.e. by removing insulation). These formations will occur around the annulus of the reactor vessel penetration, so this region must be free of foreign objects. If detected, the boric acid crystal deposits may also be analyzed for iron or iron oxide content to indicate possible head wastage or for lithium to determine if the leak is indeed from the reactor coolant system. Supplemental visual tools such as borescopes, fiberscopes, pole-mounted cameras, or remote crawlers may be used, but must be qualified before use. Supplemental tools often have the benefit of providing a video record of the inspection [9-1].

Bare metal visual inspections must be able to differentiate boric acid crystal deposits from leaks due to vessel head penetrations from leaks due to other sources. This is done by examining the boric acid crystal deposit formation, evaluating the possible sources of the deposit based, and evaluating the physical characteristics of the deposits. The guidelines [9-1] contain practical guidance for visual examination procedures and include many example images from visual examinations to assist with evaluating examination results since boric acid deposits can take many different physical forms. Also, the guidelines alert examiners that the volume of boric acid deposits from a leak can be quite small, requiring close scrutiny of the examination areas. The guidelines are updated periodically to include recent visual examination experience.

Since boric acid deposits on the head may be a result of leakage from head penetrations or from other sources located above the head, these other sources have the potential for masking deposits caused by leaking penetrations. In those situations where the leak source cannot be positively identified, utilities may perform other examinations of the suspect penetrations, including volumetric NDE, to identify the leak source.

9.2 Specialized Leak Detection Sensors

Several online leak detection systems have been implemented in some plants to provide leak-detecting capabilities while the unit is operating [9-2]:

- The first of these is radiometric monitoring which measures abnormal levels of radioactive activity around the reactor vessel shroud.

- Another nonvisual leak detector is the measurement of acoustic emission, which records high-frequency structure-borne noise generate by fluid discharging through leaks in pipes, tank, vessels, and valves. The location of the leak and approximate leak rate can be determined from the amplitude of the noise signal, which decays with the distance from the leak.

- Hydrometric detection systems pull steam from a leak into a hose connected to a moisture sensor. The moisture sensor can determine the size and location of the leak based on the moisture level and transport time.

The MRP has performed a survey of potential technologies that could be applied for on-line leak detection and for enhanced capability to identify boron deposits in situ during outages [9-2].

9.3 Nondestructive Examination of Vessel Head Penetration Nozzles and Welds

The visual inspection methods described in Section 9.1 are useful for detecting evidence of leaks from defects that have already penetrated the pressure boundary. Several NDE methods are used to examine the penetration base metal and weld to detect part-through wall cracking and to characterize the condition of penetrations included in an expanded sample to determine the extent of condition for the entire RPV Head penetration population .

Several options are available for NDE of vessel head penetrations. The EPRI MRP has implemented a NDE performance demonstration program [9-3] that provides assurance that demonstrated NDE procedures are capable of detecting and characterizing defects that may be present in the penetration. Sections of nozzles containing service-induced PWSCC removed from service are used in the demonstration program to demonstrate the capability of NDE procedures to detect PWSCC. Realistic mockups containing intentional cracking in the nozzle base material and attachment weld are used in addition to the field-removed sections of nozzles in the demonstrations. These realistic mockups are used because the field-removed samples are limited in number and range of flaw sizes and locations. The additional mockups provide the capability

to more fully evaluate the capability of NDE procedures and delivery devices to address a wide range of flaw sizes, locations, and shapes and geometric features of penetrations. The intentional cracks in these mockups were produced by methods qualified to produce NDE responses that accurately represent NDE responses from real defects as observed during in-service inspections (ISI) [9-3]. The mockups include typical as-built features such as ovality, surface distortion, tight clearances, and a range of weld surface conditions. Inspection teams demonstrating procedure capability must follow a written protocol that requires a description of all procedure essential variables, including a description of the logic used to make decisions on flaw detection and flaw sizing. The demonstration addresses flaw detection, flaw location, flaw sizing, and false call performance. The essential variables are recorded in the demonstration record and are made available to utilities to follow during ISI to ensure that techniques are used as demonstrated. Reference 9-3 contains details of the demonstration process and the results of demonstrations conducted to date. The demonstration results are updated as needed to address new demonstrations that are conducted under the MRP program.

9.3.1 Nozzle Base Metal Non-Destructive Examinations

9.3.1.1 Surface Examinations Using Eddy Current Testing

Eddy current testing (ET) is used for crack detection on the inside surface of nozzles and the exposed (wetted) OD surface of nozzles [9-3]. ET is a very sensitive crack detection method and is also an accurate method to measure surface crack length. However, it has very limited crack depth measurement capability and, therefore, is not typically used for this purpose in vessel penetration examination. ET inspection is often followed with an ultrasonic examination to measure the depth of detected flaws and to confirm the existence and location of flaws. There are two types of probes commonly used, a rotating probe for open penetrations (those without a thermal sleeve) and a blade probe thin enough to scan the nozzle when a thermal sleeve is in place.

The EPRI MRP NDE demonstration program includes demonstration of the capability of ET to detect, locate, and length size surface cracking. The demonstration mockups include typical conditions encountered in ISI that can affect the capability of ET such as surface scratches, tightly clustered cracks, branched cracks, and off-axis cracks.

Low-frequency eddy current testing (LF-ET), another variant of ET testing, can penetrate the nozzle material and into the top head base metal between 0.050 and 0.100 inch to inspect for wastage. This method, however, has not been demonstrated in the EPRI MRP program.

9.3.1.2 Volumetric Examination Using Ultrasonic Testing

Ultrasonic testing (UT) is used for examining the nozzle volume and the tube-to-weld interface [9-3]. UT is accomplished by scanning UT probes along the inside surface of the nozzle using either blade-probes or open-tube probes. UT has proven effective for measuring the size of surface defects detected by ET as described above as well as detecting and sizing defects initiating from the inside or outside surface of the penetration. The EPRI MRP NDE

demonstration program includes evaluation of the capability of UT to detect, locate, and size defects and to discriminate defects from sources of false calls such as geometric features of the penetration assembly.

UT procedures are typically a combination of individual techniques, with each technique designed to examine a particular volume of material and to search for defects aligned in a particular direction (axial, circumferential, or off-axis). Therefore, UT procedure essential variables are rather complex. The demonstration results [9-3, 9-4] contain detailed descriptions of the procedures used by inspection vendors along with documentation of the performance of both the individual techniques and the performance of the combination of techniques used in the procedures and the delivery devices that carry the probes to the penetration. This information is important for utilities to consider when evaluating application of various combinations of procedures that are available.

UT is also capable of examining the tube-to-weld interface for both cracks and unfused areas between the weld and tube. Additionally the weld triple point can be inspected for flaws approaching the pressure boundary in this location. The mockups used in the MRP NDE demonstration program contain defects in this triple point region for the purpose of evaluating the capability of these techniques.

UT methods can also be used to examine for loss of material in the annulus just above the weld, which would indicate leakage into the annulus. This technique evaluates the signal reflected from the penetration outside surface that is in contact with the closure head to detect variations in the signal pattern indicative of wastage. This method, however, has not been demonstrated in the MRP program [9-3].

9.3.2 Penetration Weld Metal Non-Destructive Examinations

9.3.2.1 Surface Examinations Using Eddy Current Tests

ET is a common method used for surface examination of the J-groove weld attaching the penetration to the closure head. As described in Section 9.3.1.1, ET is a sensitive method for detecting surface defects. Assessment of ET capability for weld surface examination is included in the MRP NDE demonstration program. Mockups containing intentional defects in weld metal samples are used to evaluate the capability of ET to detect and length size defects and to discriminate defects from various sources of false calls. In particular, ET capability for examining the attachment weld is sensitive to the weld surface conditions. Rough or as-welded surfaces can introduce ET noise with the potential to mask flaw signals or cause false calls. The demonstration mockups were fabricated to address a broad range of surface conditions from as-welded to smoothly ground to simulate conditions expected to be encountered in ISI. Reference 9-3 contains detailed results of the capability demonstrations for these techniques.

While ET is a sensitive surface examination method, it can also produce false calls that must be evaluated. Since there are no preservice baseline ET results available (see Section 9.3.2.2), ET

findings can be difficult to disposition. In some situations, other methods are applied to confirm or evaluate the indications.

9.3.2.2 Surface Examinations Using Dye Penetrant Testing

Surface examinations may also be performed using dye penetrant testing (PT). This method is, in general, more manually intensive than ET tests, but is a reliable technique for detecting surface defects. PT is capable of detecting surface defects and enables measurement of defect length. However, as with ET, it has no depth measurement capability. ASME Section III requires PT of the weld surface before the component is placed into service. Therefore, baseline examination results are available to use for comparing subsequent in-service PT results. This baseline examination provides important information to accurately disposition inservice PT findings.

PT is commonly performed on the surface nozzle-to-head weld, but can also be performed on the nozzle outside and inside surface. Remotely operated PT equipment is available for these applications [9-3].

9.4 References

9-1. *Visual Examination for Leakage of PWR Reactor Head Penetrations: Revision 2 of 1006296, Includes 2002 Inspection Results and MRP Inspection Guidance*, EPRI, Palo Alto, CA: 2003. 1007842.

9-2. *Survey of On-Line PWR Primary Coolant Leak Detection Technologies (MRP-94)*, EPRI, Palo Alto, CA: 2003. 1009062.

9-3. *Materials Reliability Program: Demonstrations of Vendor Equipment and Procedures for the Inspection of Control Rod Drive Mechanism Head Penetrations (MRP-89)*, EPRI, Palo Alto, CA: 2003. 1007831.

9-4. Tom Alley, "Status of Reactor Vessel Head Penetration Inspection Activities," NRC-MRP Meeting," Rockville, MD, June 12, 2003.

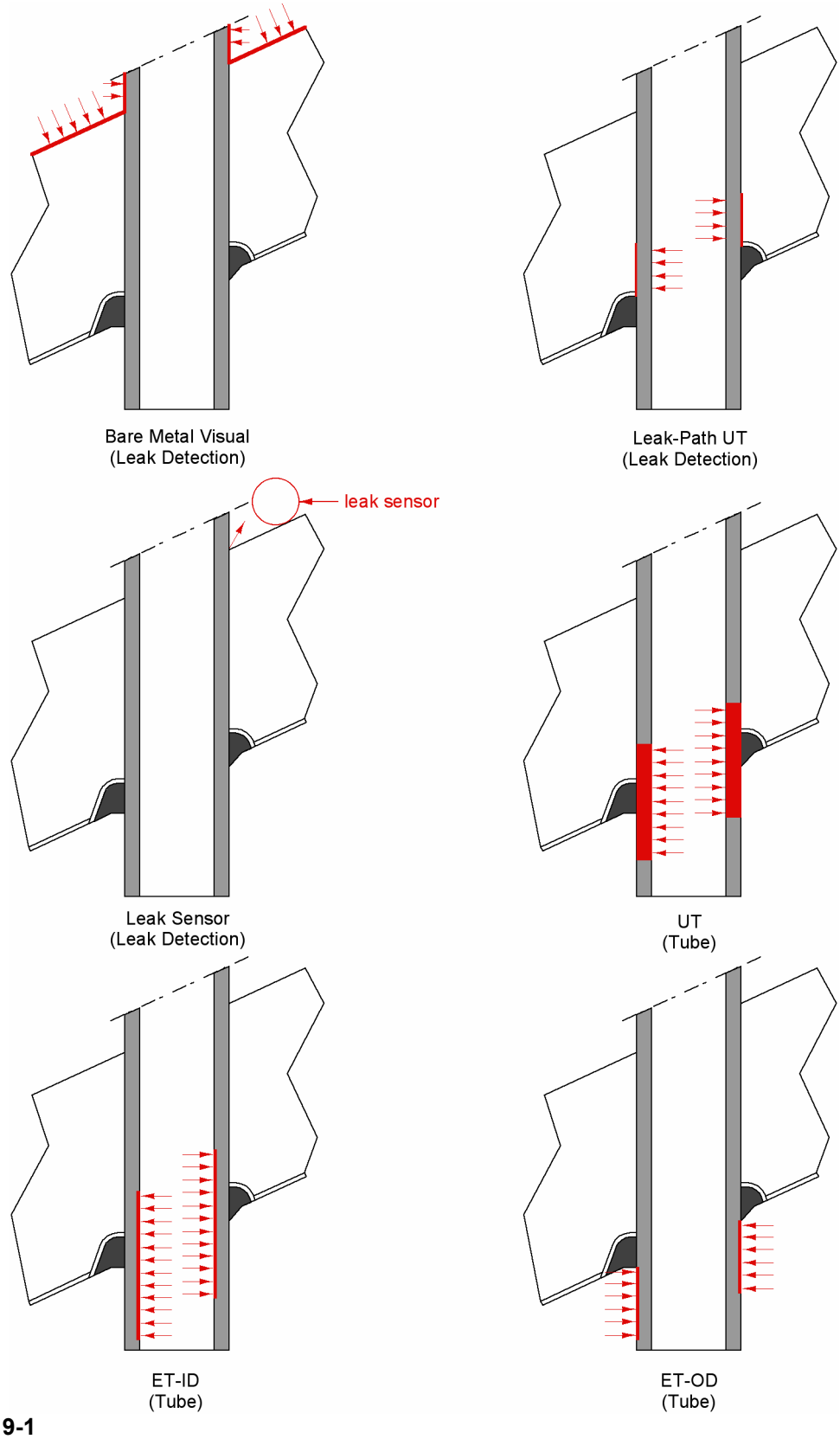

Figure 9-1
Available Inspection Options for RVCH Penetrations

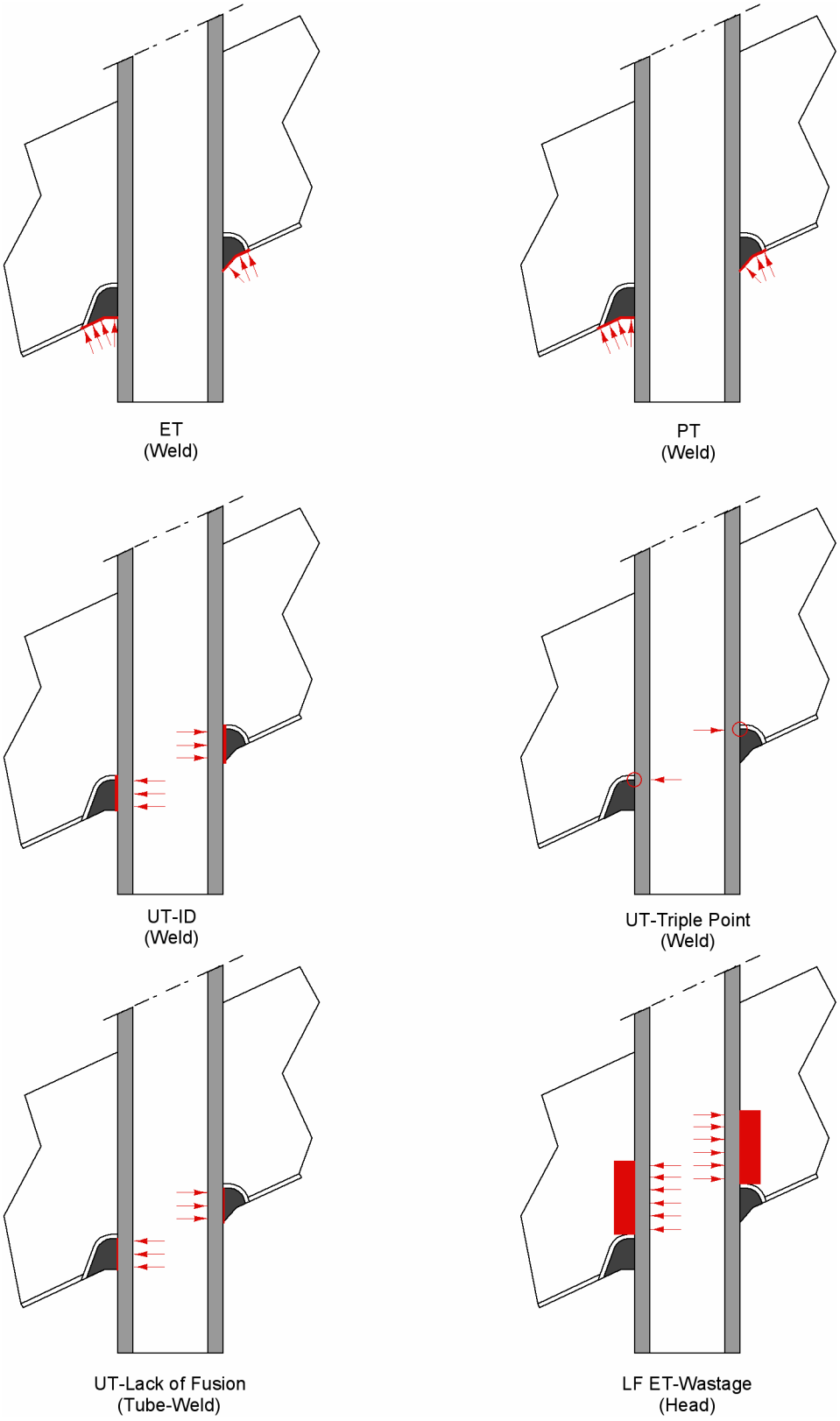

Figure 9-1
Available Inspection Options for RVCH Penetrations (continued)

10
REPLACEMENT HEAD MATERIALS

10.1 Introduction

Alloy 690 and its standard weld metals, Alloys 52 and 152, are generally used to fabricate the penetrations in replacement reactor vessel closure heads. The purpose of Section 10 is to provide a summary of the laboratory test data and PWR operating experience, which shows that the Alloy 690/52/152 family of materials has a much greater resistance to PWSCC than Alloy 600/82/182 nickel-based alloys. Report MRP-111 [10-2], a comprehensive literature survey of the relevant laboratory test data and plant experience for the replacement materials, is the primary source for these data.

The high resistance to PWSCC of the Alloy 690/52/152 nickel-based materials is mainly attributed to the higher chromium content compared to the Alloy 600/82/182 metals (approximately twice the weight fraction) [10-2]. The specified compositions of these alloys are shown in Table 10-1; the specified Alloy 690 chromium content range is 27 to 31% [10-1].

10.2 Summary of Laboratory Data

Section 10.2 is a brief summary of the comprehensive survey of laboratory test data investigating the PWSCC resistance of Alloy 690/52/152 materials in report MRP-111 [10-2]. This study also includes calculations of material improvement factors for the Alloy 690 type materials based on the laboratory test results documented in this report. EPRI report 1003589 [10-6], specifically written to address thermally-treated Alloy 600 and 690 steam generator tubes, is another document that includes calculations of material improvement factors for Alloy 690.

Most of the experimental work to investigate PWSCC in Alloy 690 has been performed using thin-wall Alloy 690 steam generator tube materials. However, there are no fundamental reasons why such results are not generally applicable to thick-wall Alloy 690 material. The PWSCC susceptibility of Alloy 600 tubing and thick-wall material has been observed to be similar, and to respond in the same manner to factors such as stress, microstructure, temperature, and cold work.

10.2.1 Test Conditions

Numerous investigations have been performed under a variety of environmental conditions relevant to the PWR primary circuit:

1. High temperature de-oxygenated (deaerated) and hydrogenated water
2. Simulated PWR primary water
3. Hydrogenated steam
4. Hydrogenated steam doped with chloride, fluoride, and sulfate anions
5. Additions of adventitious impurities or of potentially mitigating substances such as zinc

The various test conditions cited in MRP-111 [10-2] cover temperatures up to 689°F (365°C) in water, dissolved oxygen levels < 20 ppb, tests in doped and undoped 752°F (400°C) steam, lithium concentrations up to 3.5 ppm, boron concentrations up to 1800 ppm, hydrogen concentrations up to 100 cc/kg H_2O, and additions of chlorides and zinc.

10.2.2 PWSCC Test Data for Alloy 690 Base Metal

10.2.2.1 Thin-wall (Steam Generator Tube) Materials

Tables 10-2 and 10-3, which are reproduced from MRP-111, summarize tests performed using thin-wall material. Table 10-2 summarizes the tests performed in primary water environments, and Table 10-3 summarizes tests for hydrogenated and doped hydrogenated steam environments including one series of tests for Alloy 52M weld material. In addition to these tests, EPRI report 1003589 [10-6] considers a few additional tests for Alloy 690 thin-wall material in primary water environments [10-18 through 10-23].

10.2.2.2 Thick-wall Materials

The following tests investigating the PWSCC resistance of thick-wall Alloy 690 materials have been performed:

- Westinghouse performed a PWSCC initiation test that included six thick ring specimens fabricated from a single heat of thermally treated Alloy 690 (690TT) [10-27]. The rings were loaded to simulate residual stress levels typical for CRDM nozzles and then tested in a hydrogenated, doped steam environment at a temperature of 400°C (752°F). The six Alloy 690 specimens showed no SCC initiation after the total test time of 750 hours, whereas 10 of the 31 Alloy 600 specimens in the phase 2B test showed SCC initiation after less than 50 hours, implying an Alloy 690 improvement factor greater than 15.
- Summarized in paragraph 3.2.2.7.2 of MRP-111 [10-2], EDF performed PWSCC initiation testing for Alloy 690TT specimens fabricated from one experimental and one production heat of forged CRDM nozzle material [10-24]. Round gage slow strain rate tests (SSRTs), reverse U-bend (RUB) tests, and constant load tests were performed:
  - The specimens fabricated from the Alloy 690 CRDM materials were tested for 12,665 hours at 360°C (680°F) in PWR primary water with no SCC initiation noted.
  - The constant load specimens fabricated from the Alloy 690 CRDM materials were tested in PWR primary water at 360°C (680°F) with a nominal stress of 580 MPa (84.1 ksi) for a test time up to 18,500 hours. No SCC cracking was reported for these specimens.

  - The slow strain rate tests for the specimens fabricated from the Alloy 690 CRDM materials were performed in PWR primary water at 360°C (680°F) with a 5×10^{-8} s^{-1} strain rate. These SSRT specimens showed intergranular cracks that did not exceed one grain depth, in this case 70 μm (0.0028 inch) maximum, independent of the initial surface condition. The investigators judged that this indicated that no significant SCC had occurred.

- Summarized in paragraph 3.2.2.4 of MRP-111 [10-2], another EDF study was performed using constant extension rate test (CERT) specimens fabricated from Alloy 690 plate welded with Alloy 152 and also Alloy 82 [10-25,10-26]. No SCC was observed for the Alloy 690 material in the CERT specimens exposed to normal primary water at 343°C (650°F) for up to 4122 hours, or for the Alloy 690 material in the CERT specimens exposed to a faulted environment (150 ppb chloride; 343°C) for 140 hours. Note that the Alloy 690 plate material in the CERT specimens was from within the heat affected zone (HAZ) region of the plate.

10.2.3. PWSCC Test Data for Alloy 52 and 152 Weld Metal

The following tests investigating the PWSCC resistance of Alloy 52 or 152 weld metal materials have been performed:

- The EDF study cited above (paragraph 3.2.2.4 of MRP-111) also included Alloy 152 material in the CERT specimens [10-25,10-26]. No SCC was observed for the Alloy 152 material in the CERT specimens exposed to normal primary water at 343°C (650°F) for up to 4122 hours, or for the Alloy 152 material in the CERT specimens exposed to a faulted environment (150 ppb chloride; 343°C) for 140 hours. On the other hand, SCC was observed for the Alloy 82 material in the CERT specimens in some of the normal primary water testing.
- Summarized in paragraph 3.2.4.1 of MRP-111 [10-2], Jacko et al. performed accelerated tests of Alloy 52M weld mock-ups in a hydrogenated steam environment doped with fluoride, chloride, and sulfate anions at a temperature of 400°C (752°F) [10-29]. The specimens were prepared as flat plates and bolt loaded in four-point bend tests. The cumulative exposure time was 2051 hours, which was calculated to be equivalent to 45 EFPY in primary water at 323°C (613°F), based on an Arrhenius relationship. None of the two high-strain (1.0%) and two low-strain (0.35%) Alloy 52M specimens cracked in this time, whereas both of the high-strain Alloy 182 specimens cracked in less than 214 hours, and both of the low-strain Alloy 182 specimens cracked in less than 450 hours. The improvement factors implied by these data are included in Table 10-3.
- Summarized in paragraph 3.2.2.7.7 of MRP-111 [10-2], another EDF study included RUB specimens made with Alloy 52 and 152 weld metal which were tested in PWR primary water at 360°C (680°F) [10-28]. Longitudinal residual stresses in the RUB specimens were measured by x-ray analysis to be between 700 and 860 MPa (102 and 125 ksi). No SCC initiation was observed in the RUB tests, which had durations between 18,000 and 27,000 hours.

10.2.4. General Corrosion Rate and Metal Release Rate Tests

A number of tests have also been performed to determine the general corrosion rate and metal release rate for Alloy 690 material in primary water [10-2]. All studies agree that the general corrosion rate and metal release rate of nickel-base alloys decrease with an increasing chromium concentration in the alloy. The general corrosion rate and metal release rate of Alloy 690 material has been shown to be 2 to 4 times lower than Alloy 600 material.

10.2.5. Summary of Test Results

Accelerated stress corrosion testing has been performed on double U-bend (simulating crevice conditions), reverse U-bend (RUB), constant load test (CLT), four-point bend, and steam generator tubing mock-up specimens. The results of these accelerated stress corrosion tests have shown Alloy 690 and its weld metals to be extraordinarily resistant to cracking. In high temperature deaerated, hydrogenated water, no Alloy 690 material specimen at constant load or deformation has exhibited stress corrosion cracking[9] at testing times up to 100,000 hours at a temperature of 680°F (360°C). In this timeframe, most mill-annealed Alloy 600 (600MA) and thermally treated Alloy 600 (600TT) control specimens had developed cracking, often after relatively short periods. A test duration of 100,000 hours at 680°F is equivalent to approximately 230 years at 600°F, assuming the standard activation energy of 50 kcal/mole for PWSCC crack initiation in Alloy 600 applies to Alloy 690. This indicates that Alloy 690 material would not be expected to develop PWSCC during any feasible operating lifetime of PWRs.

No cracking of Alloy 690 has been observed under most other test conditions pertinent to primary water, or even under some non-primary water conditions, e.g. oxygenated conditions (up to 16 ppm) and crevice conditions. This experience includes material with carbon contents ranging from 0.001% to 0.065%, in the mill-annealed and thermally treated conditions, and with and without surface cold work. In addition, this Alloy 690 experience included material that exhibited surface microcracks (caused by specimen fabrication) before testing.

10.2.6. Calculated Material Improvement Factors

To quantify the improved PWSCC resistance for Alloy 690 type materials relative to Alloy 600 materials, a ratio called the improvement factor has been used. Nominally the factor is the ratio of times for PWSCC crack initiation, but two methods have been implemented in MRP-111 [10-2] to calculate this factor. The first method, illustrated in Figure 10-1, estimates the relative improvement factor, IF_R, based on a Weibull/Weibayes analysis. Using this method, MRP-111 reports an average IF_R of 26.5 for Alloy 690 relative to Alloy 600MA material and 13.3 relative to Alloy 600TT material.

Because not all the studies either obtained or reported sufficient test data to allow a Weibull type analysis, a second, simpler method was also used. Illustrated by Figure 10-2, this approach is

[9] There have been a few Alloy 690 specimens where shallow IGA has been observed but, as discussed later, these are attributed to mechanical cracking during fabrication and are judged to have not grown during SCC testing.

based on the ratio of the Alloy 690 material test time (without SCC being observed) to the time to the first observation of SCC for the Alloy 600 material. Using this approach, MRP-111 [10-2] reports an average IF_R of 27.1, i.e., about the same as the factor obtained for Alloy 600MA material by the first method. In addition, the IF_R is often found to be limited by the maximum test duration for the Alloy 690 specimens, rather than by observed PWSCC in this material.

Hence, the relative improvement factor for Alloy 690 can be conservatively estimated to be at least 26 relative to Alloy 600MA and 13 relative to Alloy 600TT material, based on the accelerated testing performed to date in high-temperature deaerated water. Furthermore, it is anticipated that these factors will increase in the future as data from longer Alloy 690 tests become available and are confirmed by further in-service inspection results.

Note that some tests have shown that cracking of Alloy 690 materials is possible, either under certain extreme testing conditions that are not found in PWRs or with experimental, pre-production materials (often with atypical heat treatments and chemical compositions). For example, in a deaerated and hydrogenated high temperature water environment, intergranular cracking has been observed during CERT experiments at a strain rate on the order of 10^{-7} s^{-1} or less. CERT is a very severe laboratory technique for evaluating susceptibility to stress corrosion cracking. The specimens are loaded well past the yield point to produce continuous, slow plastic deformation and eventually fail by ductile overload. Such mechanical loading is not directly relevant to component operating conditions in nuclear power plants.

10.3 Operating Experience for Alloy 690/52/152 Materials in PWRs

10.3.1 Steam Generator Tubing Experience

Many steam generators manufactured with Alloy 690 tubing material have been in service for significant times without any indications of corrosion-related degradation such as PWSCC. As of January 2004, there are approximately 71 PWR units worldwide, with 2–4 steam generators per unit, operating with Alloy 690 steam generator tubes.

Tables 10-4 and 10-5 show the U.S. and international PWRs that have steam generators with Alloy 690 tubes. U.S. plants have operated steam generators with Alloy 690 tubes with up to 15 calendar years of operation. The cumulative number of EFPYs of service for the U.S. population of Alloy 690 steam generator tubes is estimated to be about 2.1 million tube-EFPYs, corresponding to about 3.3 million tube-EDYs given a temperature normalization from the steam generator hot leg temperatures to 600°F. The international PWR steam generators with Alloy 690 tubes have operated up to nearly 15 calendar years as well. The overall number of tube-EDYs is estimated to be greater than 10 million, including the worldwide experience.

Throughout all of this experience, there has not been any reported corrosion-induced degradation of Alloy 690 tubes, from either the primary or secondary side. This assessment is reflective of considerable numbers of eddy current inspections of the Alloy 690 steam generator tubes, as indicated in the rightmost column of Tables 10-4 and 10-5.

10.3.2 Other PWR Experience Including Experience with Thick-wall Materials

A list of Alloy 690/52/152 replacement components installed in U.S. PWR plants (other than tubes in replacement steam generators) is shown in Table 10-6. This table shows that over 1000 such component items—including pressurizer heater sleeves, instrument nozzles, and CRDM nozzles—are currently in service, with some components in service for nearly 14 calendar years. The cumulative number of EFPYs of service for this population is estimated to be about 2800 part-EFPYs, corresponding to about 7300 part-EDYs given a temperature normalization to 600°F. Generally, visual inspections of these replacement components are performed regularly, and no corrosion related degradation has been reported for any Alloy 690/52/152 replacement components. This favorable experience includes the population of Alloy 690/52/152 components in international PWRs; Table 10-7 lists most of the international applications of Alloy 690/52/152 replacement components (other than steam generator tubes).

In addition to the replacements listed in Table 10-6, the 16 small-diameter thermocouple penetrations in two B&W design plants (Oconee 1 and TMI 1) were plugged using Alloy 690 material and Alloy 52/152 welds. The heads containing these repaired penetrations have been replaced, so these thermocouple nozzle repairs are no longer in service. It has been reported that at the time the original Oconee 1 head was replaced in fall 2003, evidence of leakage from one of the eight repaired thermocouple nozzles was detected during a visual check of the top surface of this head. However, as this head was removed from service at that time, no inspections were performed to determine the cause of the leakage. It is considered highly unlikely that this leakage was the result of stress corrosion cracking originating in the new Alloy 690 base metal or Alloy 52/152 weld metal after the three years of service for the repair. The reported leakage may have been caused by any number of factors not indicative of the SCC resistance of the Alloy 690/52/152 materials in the repair.

10.4 Conclusions

The MRP-111 evaluation of laboratory and plant experience indicates a material improvement factor of at least 26 for Alloy 690 versus Alloy 600MA, with larger improvement factors expected with more years of experience accumulated in the laboratory and field. (CRDM nozzles and other primary system penetration nozzles were fabricated from mill-annealed Alloy 600 materials.) Alloy 690 and its weld metals have been utilized in PWR replacement component items such as steam generator tubes, pressurizer heater sleeves, and CRDM nozzles since 1989. No SCC degradation of the Alloy 690/52/152 family of materials has been reported for any replacement application to date.

Given the laboratory data and plant experience, there is a strong basis for concluding that the Alloy 690/52/152 replacement head materials are greatly more resistant to PWSCC than the corresponding Alloy 600/82/182 materials. The basic source of the difference is the much higher chromium content of the Alloy 690/52/152 family of materials.

10.5 References

10-1. *Materials Handbook for Nuclear Plant Pressure Boundary Applications*, EPRI, Palo Alto, CA: 2002. 1002792.

10-2. *Materials Reliability Program (MRP): Resistance to Primary Water Stress Corrosion Cracking and Current Operating Experience with Alloys 690, 52, and 152 in Pressurized Water Reactors (MRP-111)*, EPRI, Palo Alto, CA: 2004. 1009801.

10-3. Specification for Nickel-Chromium-Iron Alloys (UNS N06600, N06601, N06603, N06690, N06025, and N06045) and Nickel-Chromium-Cobalt-Molybdenum Alloy (UNS N06617) Rod, Bar and Wire, ASME/ASTM SB/B 166.

10-4. Specification for Nickel and Nickel-Alloy Welding Electrodes for Shielded Metal Arc Welding, ASME SFA-5.11 and AWS A5.11/5.11M-97.

10-5. Specification for Nickel and Nickel Alloy Bare Welding Electrodes and Rods, ASME SFA-5.14 and AWS A5.14/A5.14M-97.

10-6. *Pressurized Water Reactor Generic Tube Degradation Predictions: U.S. Recirculating Steam Generators with Alloy 600TT and Alloy 690TT Tubing*, EPRI, Palo Alto, CA: 2003. 1003589.

10-7. A. J. Sedricks, J. W. Schultz, and M. A. Cordovi, "Inconel Alloy 690 – A New Corrosion Resistant Material," *Corrosion Engineering* (Boshoku Gijutsu), vol. 28, pp. 82–95, 1979, Japan Society of Corrosion Engineering.

10-8. K. Smith, A. Klein, P. Saint-Paul, and J. Blanchet, "Inconel 690, A Material with Improved Corrosion Resistance for PWR Steam Generator Tubes," *Proceedings of 2nd International Symposium on Environmental Degradation of Materials in Nuclear Power Systems – Water Reactors*, Monterey, CA, 1985, pp. 319–328.

10-9. T. Yonezawa, K. Onimura, N. Sasaguri, T. Kusakabe, H. Nagano, K. Yamanaka, T. Minami, and M. Inoue, "Effect of Heat Treatment on Corrosion Resistance of Alloy 690," *Proceedings of 2nd International Symposium on Environmental Degradation of Materials in Nuclear Power Systems – Water Reactors*, Monterey, CA, 1985, pp. 593–600.

10-10. A. Smith and R. Stratton, "Relationship between Composition, Microstructure and Corrosion Behavior of Alloy 690 Steam Generator Tubing for PWR Systems," *Proceedings of 4th International Symposium on Environmental Degradation of Materials in Nuclear Power Systems – Water Reactors*, Jekyll Island, GA, 1989, pp.5-33 to 5-46.

10-11. A. Smith and R. Stratton, "Thermal Treatment, Grain Boundary Composition and Intergranular Attack Resistance of Alloy 690," *Proceedings of 5th International Symposium on Environmental Degradation of Materials in Nuclear Power Systems – Water Reactors*, Monterey, CA, 1991, pp. 855–860.

10-12. K. Norring, J. Engstrom, and P. Norberg, "Intergranular Stress Corrosion Cracking in Steam Generator Tubing, Testing of Alloy 690 and Alloy 600 Tubes," *Proceedings of 3rd International Symposium on Environmental Degradation of Materials in Nuclear Power Systems – Water Reactors*, Traverse City, MI, 1987, pp. 587–593.

10-13. K. Norring, J. Engstrom, and H. Tornblom, "Intergranular Stress Corrosion Cracking Steam Generator Tubing: 25,000 hours Testing of Alloy 690 and Alloy 600," *Proceedings of 4th International Symposium on Environmental Degradation of Materials in Nuclear Power Systems – Water Reactors*, Jekyll Island, GA, 1989, pp.12-1 to 12-10.

10-14. K. Norring, K. Stiller, and J. Nilsson, "Grain Boundary Microstructure, Chemistry, and IGSCC in Alloy 600 and Alloy 690," *Proceedings of 5th International Symposium on Environmental Degradation of Materials in Nuclear Power Systems – Water Reactors*, Monterey, CA, 1991, pp. 482–487.

10-15. N. Ogawa, T. Nakashiba, R. Umehara, S. Okamoto, and T. Tsuruta, "PWSCC Susceptibility Tests for Improving Primary Water Chemistry Control," *Proceedings of 8th International Symposium on Environmental Degradation of Materials in Nuclear Power Systems – Water Reactors*, Amelia Island, FL, 1997, pp. 395–401.

10-16. M. G. Angell, S. J. Allan, and G. P. Airey, "The Effect of Primary Coolant Zinc Addition on the SCC Behavior of Alloy 600 and 690," *Proceedings of 9th International Symposium on Environmental Degradation of Materials in Nuclear Power Systems – Water Reactors*, Newport Beach, CA, 1999, pp. 97–102.

10-17. F. Vaillant, J. D. Mithieux, O. de Bouvier, D. Vancon, G. Zacharie, Y. Brechet, and F. Louchet, "Influence of Chromium Content and Microstructure on Creep and PWSCC Resistance of Nickel Base Alloys," *Proceedings of 9th International Symposium on Environmental Degradation of Materials in Nuclear Power Systems – Water Reactors*, Newport Beach, CA, 1999, pp. 251–260.

10-18. G. P. Airey, et al., "A Stress Corrosion Cracking Evaluation of Inconel 690 for Steam Generator Tubing Applications," *Nuclear Technology*, volume 55, Nov. 1981, pp. 436–448.

10-19. G. P. Airey, et al., "Inconel 690 Steam Generator Tubing: Material Specification and Corrosion Resistance," *Proceedings of the International Symposium Fontevraud II, Contribution of Materials Investigation to the Resolution of Problems Encountered in PWR Plants*, SFEN, Sept. 10–14, 1990, pp. 408–417.

10-20. Y. Rouillon, *Essais de corrosion sous contrainte en eau pure et en mileau primaire de réacteurs à eau pressurisée sur tubes de générateurs de vapeur en alliages 600 et 690*, EDF report HT/PV D 588 MAT/T 42, May 10, 1985.

10-21. C. Gimond, "The Corrosion Performance of Alloy 690," *Proceedings: Workshop on Thermally Treated Alloy 690 Tubes for Nuclear Steam Generators*, Paper 14, EPRI NP-4665S-SP, July 1986.

10-22. B. P. Miglin and C. E. Shoemaker, "A Comparison of the Stress Corrosion Cracking Behavior of Alloys 600 and 690 in AVT Water," *NACE Corrosion 86*, Paper 255, March 17–21, 1986.

10-23. T. Nakayama, et al., "IGC/IGSCC and General Corrosion Behavior of Alloy 800 as a PWR S/G tube Material," *Corrosion 87*, Paper No. 82, NACE, March 1987.

10-24. F. Vaillant, EDF Report HT-44/95/013/A, *Résistance a la corrosion sous contrainte en milieu primaire des alliages 690 et 800 – Point des résultats en Décembre 1995* (*Resistance of Alloys 690 and 800 to Stress Corrosion Cracking in PWR Primary Water – Status of Results Available to December 1995*), 1996.

10-25. M. J. Psaila-Dombrowski, J. M. Sarver, P. E. Doherty, W. G. Schneider, "Evaluation of Weld Metal 82 and Weld Metal 152 Stress Corrosion Cracking Susceptibility," *Proceedings of 7th International Symposium on Environmental Degradation of Materials in Nuclear Power Systems – Water Reactors*, Breckenridge, Colorado, 1995, pp. 81–91.

10-26. M. J. Psaila-Dombrowski, C. S. Wade, J. M. Sarver, W. A. Van Der Sluys, and P. E. Doherty, "Evaluation of Weld Metals 82, 152, 52, and Alloy 690 Stress Corrosion Cracking and Corrosion Fatigue Susceptibility," *Proceedings of 8th International Symposium on Environmental Degradation of Materials in Nuclear Power Systems – Water Reactors*, Amelia Island, FL, 1997, pp. 412–421.

10-27. *Evaluation of Crack Initiation of Alloy 600 Reactor Vessel Head Penetration Materials*, EPRI, Palo Alto, CA: 1998. TR-108970.

10-28. F. Vaillant, EDF Report HT-44/98/016/A, *Métaux déposés base nickel contenant 15 to 30% de chrome: bilan des essais de corrosion en milieu primaire* (*Nickel Base Weld Deposits Containing 15 To 30% Chromium: Status of Corrosion Tests In Primary Water*), 1998.

10-29. R. J. Jacko, R. E. Gold, and A. Kroes, "Accelerated Corrosion Testing of Alloy 52M and Alloy 182 Weldments," *Proceedings of the 11th International Symposium on Environmental Degradation of Materials in Nuclear Power Systems – Water Reactors*, American Nuclear Society, 2003.

10-30. G. Sui, G. B. Heys, and J. Congleton, "Stress Corrosion Cracking of Alloy 600 and Alloy 690 in Hydrogen/Steam and Primary Water Side Water," *Proceedings of 8th International Symposium on Environmental Degradation of Materials in Nuclear Power Systems – Water Reactors*, Amelia Island, FL, 1997, pp. 274–281.

Table 10-1
Specified Compositions of Alloy 600 and Alloy 690 and Associated Weld Materials (wt %)

	Material	Ni	Cr	Fe	Mn	C	Cu	Si	S	P	Ti	Cb + Ta	Note
Alloy 600 Type Materials	Alloy 600 wrought [10-3]	72.0 min	14.0 – 17.0	6.0 - 10.0	1.0 max	0.15 max	0.5 max	0.5 max	0.015 max	--	--	--	
	Alloy 182 weld [10-4]	59.0 min	13.0 – 17.0	10.0 max	5.0 - 9.5	0.10 max	0.50 max	1.0 max	0.015 max	0.03 max	1.0 max	1.0 - 2.5 (1)	(2) (3)
	Alloy 82 weld [10-5]	67.0 min	18.0 - 22.0	3.0 max	2.5 - 3.5	0.10 max	0.50 max	0.50 max	0.015 max	0.03 max	0.75 max	2.0 - 3.0 (1)	(2) (3)
Alloy 690 Type Materials	Alloy 690 wrought [10-3]	58.0 min	27.0 - 31.0	7.0 - 11.0	0.5 max	0.05 max	0.5 max	0.5 max	0.015 max	--	--	--	
	Alloy 152 weld [10-4]	Rem.	28.0 – 31.5	7.0 – 12.0	5.0 max	0.05 max	0.50 max	0.75 max	0.015 max	0.03 max	0.50 max	1.0 - 2.5	(2) (4)
	Alloy 52 weld [10-5]	Rem.	28.0 – 31.5	7.0 – 11.0	1.0 max	1.0 max	0.30 max	0.50 max	0.015 max	0.02 max	1.0 max	0.10 max	(2) (5)

1) Tantalum 0.30% maximum when specified
2) Sum of all other elements 0.50% maximum
3) Cobalt 0.12% maximum, when specified
4) Al 0.50% maximum, Mo 0.50% maximum
5) Al 1.10% maximum, Mo 0.50% maximum

Table 10-2
Summary of Alloy 690 Primary Water Stress Corrosion Test Data [10-2]

Reference	Test	Test Environ.	Test Temp (°F)	Alloy 690 Heat Number	Alloy 690 Heat Cond.	Total Spec. No.[1]	Test Time at Test Temp. (hour)	Eq. Test Time at 600°F[2] (year)	Time to First Alloy 600 failure (hour)	Improv. Factor (IF_R)
Sedricks [10-7]	Double U-Bend	Deaerated water	600	Y24A7L	MA, TT, MA+CW, MA+Weld	52	8,064	0.9	3024	2.7
	Double U-Bend	Deaerated water	680	NX4458H NX4460H	MA, TT	8	8,064	23.2	No 600 control	N/A
K. Smith [10-8]	RUB	Deaerated water + B + Li	680	Three pre-series, Heats 1-3	MA, TT	20	13,000	29.9	1500	6.5
						20	16,000	36.8	2000	6.4
Yonezawa [10-9]	RUB	Deaerated water + B + Li	680	One Alloy 690 heat	MA	3	6,600	15.2	340	19.4
					TT	2	12,000	27.6		35.3
	CLT				TT	5	7,000	16.1	1144	6.1
A. Smith [10-10, 10-11]	C-Ring	Deaerated water	644	Two industrial heats A, E	TT	2	1,500	0.9	No 600 control	N/A
Norring [10-12, 10-13, 10-14]	RUB	Deaerated water	689	F	MA	6	33,000	103.6	800	41.3
				H, G, A, B, D, C, I	MA, TT	47	25,000	78.5		31.3
				PP	TT	6	23,000	72.2		28.8
				Y, Z	MA	8	20,500	64.3		25.6
Ogawa [10-15]	RUB	Deaerated water + B + Li	680	One Alloy 690 heat	TT	40	10,000	23.0	3000	3.3
	CLT					20	10,000	23.0	1142[3]	8.8
Angell [10-16]	RUB	Deaerated water + B + Li with or without Zn	662	752246	TT	20	7,500	9.1	5500	1.4
Vaillant [10-17]	RUB	Deaerated water + B + Li	680	9.092Exp 9.592Exp 9.799Ind 9G4	TT, MA	4	54,000	124.1	500	108
AREVA, France [App. B of 10-6]	SG Mockup	Deaerated water	680	WE094, Pre-series	TT	16	100,000	229.8	800	125

1) Total number of specimens of similar heat treatment and test condition and duration.
2) The equivalent test time at 600°F for Alloy 690 is calculated based a PWSCC crack initiation time of 50 kcal/mole.
3) 1,142 hours is the equivalent of the 4,179 hours failure time at 644°F for the Alloy 600 control CLT specimens based on Note 2. Only two of four Alloy 600 MA series results were reported. Hence, the time to the first Alloy 600 failure could be less than 4,179 hours.

Table 10-3
Summary of Alloy 690/52/152 Hydrogenated and Doped Hydrogenated Steam Stress Corrosion Test Data [10-2]

Reference	Test	Test Environ.	Test Temp (°F)	Alloy 690 Heat Number	Alloy 690 Heat Cond.	Total Spec. No.[1]	Test Time at test temp. (hour)	Eq. Test Time at 600°F[2] (year)	Time to First Alloy 600 failure (hour)	Improve. Factor (IF_R)
Sui [10-30]	RUB	H_2 Steam	716	690 (A)	TT,	1	13824	107.4	552	25.0
				690 (B)	TT	1	12600[3]	97.9		22.8
					TT+aged	1	12600[3]	97.9		22.8
Jacko [10-29]	4-point Bend 1% strain	H_2 Steam + 30ppm for each Cl^-, F^- ,SO_4^{-2}	752	Alloy 52M Weld, Y9570	Weld	2	2051	50.1	214[4]	9.6
	4-point Bend 0.3% strain					2	2051	50.1	450[4]	4.6
Framatome, Germany [App. A of 10-2]	RUB	H_2 Steam	752	754380	TT	3	9720	237.4	336	28.9
	RUB surface scored					3	9720	237.4	336	28.9

1) Total number of specimens of similar heat treatment and test condition and duration.
2) The equivalent test time at 600°F for Alloy 690 is calculated based a PWSCC crack initiation time of 50 kcal/mole.
3) Two of the three Alloy 690 specimens in Sui's investigation cracked after 13824 hours of testing. To be conservative, it is assumed here that these two Alloy 690 specimens developed crack soon after the previous examination made after accumulating 12600 hours. None of the other Alloy 690 specimens in this table failed during the test duration.
4) The Alloy 52M is compared with Alloy 182.

Table 10-4
U.S. PWR Steam Generators with Alloy 690[1] Tubes (as of March 2004)

Country	Plant	Original or Repl. SGs	Date of Commer-cial Operation or Repl.	SG Design	SG Model	No. SG	Number Tubes per SG	Calendar Years at 3/2004	Current HL Temp. (°F)	Approx. EFPY at 3/2004	Approx. EDY[2,3] at 3/2004	Tube-EFPYs	Tube-EDYs	Inspection Scope at Most Recent ISI[4]
U.S.	ANO 2	Repl.	09/2000	West	Δ109	2	10637	3.5	608	2.9	3.9	61,000	84,000	0.47% FL BC + 0.47% RECP of R1 & R2 U-bends
U.S.	Braidwood 1	Repl.	01/1999	BWI	7720	4	6633	5.1	617	5.0	9.9	133,000	262,000	No Inspection; Previous RFO – 100% FL BC
U.S.	Byron 1	Repl.	02/1998	BWI	7720	4	6633	6.1	618	5.6	11.5	150,000	306,000	No Inspection; Previous RFO – 50% FL BC + 25% RECP HL TTS
U.S.	Calvert Cliffs 1	Repl.	02/2002	BWI	Unknown	2	8471	2.0	595	1.8	1.5	31,000	25,000	Baseline – 100% FL BC
U.S.	Calvert Cliffs 2	Repl.	04/2003	BWI	Unknown	2	8471	0.9	595	0.9	0.7	15,000	12,000	50% FL BC
U.S.	Catawba 1	Repl.	10/1996	BWI	Unknown	4	6633	7.4	613	7.0	11.7	185,000	311,000	40% FL BC[5]
U.S.	Cook 1	Repl.	12/2000	BWI	51R	4	3496	3.2	599	3.0	2.9	42,000	40,000	For 1 SG – 20% FL BC + 0.3% RECP FS + 0.2% RECP U-bends + 0.1% RECP CL TTS
U.S.	Cook 2	Repl.	03/1989	West	54F	4	3592	15.0	606	9.1	11.6	131,000	167,000	12.5% FL BC + 5% RECP of HL TTS + 1.3% RECP of R1 & R2 U-bends
U.S.	Farley 1	Repl.	05/2000	West	54F	3	3592	3.8	607	3.5	4.6	37,000	49,000	100% FL BC + 20% RECP of HL TTS + 100% RECP of R1 & R2 U-bends[5]
U.S.	Farley 2	Repl.	05/2001	West	54F	3	3592	2.8	607	2.6	3.4	27,000	36,000	Baseline[5]
U.S.	Ginna	Repl.	06/1996	BWI	44R	2	4765	7.7	589	8.2	5.2	78,000	50,000	50% FL BC + 20% RECP of HL TTS + 20% RECP of R1 & R2 U-bends[5]
U.S.	Indian Point 3	Repl.	06/1989	West	44F	4	3214	14.7	593	9.7	7.3	125,000	94,000	25% FL BC + 25% RECP of HL TTS + 8.2% RECP of R1 & R2 U-bends
U.S.	Kewaunee	Repl.	12/2001	West	54F	2	3592	2.2	592	2.0	1.5	15,000	11,000	1.4% FL BC + 0.3% RECP HL TTS + 0.3% RECP U-bends; Previous RFO – 1.4% FL BC
U.S.	McGuire 1	Repl.	05/1997	BWI	Unknown	4	6633	6.8	614	6.3	11.0	167,000	292,000	0.4% FL BC; Previous RFO – 0.1% FL BC
U.S.	McGuire 2	Repl.	12/1997	BWI	Unknown	4	6633	6.2	614	5.5	9.6	146,000	256,000	0.4% FL BC; Previous RFO – 0.1% FL BC
U.S.	Millstone 2	Repl.	01/1993	BWI	Unknown	2	8523	11.2	601	6.0	6.3	103,000	107,000	50% FL BC + 0.3% RECP of Various Regions
U.S.	North Anna 1	Repl.	04/1993	West	54F	3	3592	10.9	613	10.0	16.8	108,000	181,000	20% FL BC + 6.7% RECP of HL TTS + 33% RECP of R1 U-bends
U.S.	North Anna 2	Repl.	06/1995	West	54F	3	3592	8.7	613	8.0	13.4	86,000	144,000	20% FL BC + 6.7% RECP of HL TTS + 33% RECP of R1 U-bends
U.S.	Palo Verde 2	Repl.	11/2003	CE	80	2	12580	0.3	611	0.3	0.5	7,000	12,000	100% FL BC + 100% RECP of HL TTS + 2.3% RECP U-bends

Table 10-4
U.S. PWR Steam Generators with Alloy 690[1] Tubes (as of March 2004) (continued)

Country	Plant	Original or Repl. SGs	Date of Commer-cial Operation or Repl.	SG Design	SG Model	No. SG	Number Tubes per SG	Calendar Years at 3/2004	Current HL Temp. (°F)	Approx. EFPY at 3/2004	Approx. EDY[2,3] at 3/2004	Tube-EFPYs	Tube-EDYs	Inspection Scope at Most Recent ISI[4]
U.S.	Point Beach 2	Repl.	12/1996	West	Δ47F	2	3499	7.2	597	5.2	4.6	36,000	32,000	100% FL BC + 40% RECP of HL TTS + 0.6% RECP of R1 U-bends
U.S.	Sequoyah 1	Repl.	03/2003	West	57AG	4	4983	1.0	612	0.9	1.5	18,000	29,000	100% FL BC + 100% RECP of HL TTS + 3.7% RECP U-bends
U.S.	Shearon Harris	Repl.	10/2001	West	Δ75	3	6307	2.4	619	1.9	4.1	36,000	77,000	Baseline
U.S.	South Texas 1	Repl.	05/2000	West	Δ94	4	7585	3.8	620	3.6	7.9	108,000	239,000	100% FL BC[5]
U.S.	South Texas 2	Repl.	10/2002	West	Δ94	4	7585	1.4	620	1.2	2.7	37,000	83,000	100% FL BC + 100% RECP of HL TTS + 100% RECP of R1 U-bends + 20% RECP of R2 U-bends[5]
U.S.	St. Lucie 1	Repl.	01/1998	BWI	Unknown	2	8523	6.2	599	5.7	5.5	98,000	94,000	55% FL BC + 30% RECP of R1 & R2 U-bends
U.S.	Summer	Repl.	12/1994	West	Δ75	3	6307	9.2	619	8.1	17.3	154,000	327,000	No inspection; Previous RFO – 0.5% FL BC + 0.03% RECP of HL TTS + 0.1% RECP of R1 U-bends
											Total	2,135,000	3,320,000	

Notes:
1) All Alloy 690 tubes in U.S. replacement SGs are thermally treated (Alloy 690TT).
2) Effective Degradation Year (EDY) defined as equivalent time at temperature using a reference temperature of 600°F and an activation energy of 50 kcal/mole.
3) Based on current hot leg temperature; no corrections are made for changes in hot leg temperature over life.
4) Definitions of abbreviations for inspections:
FL = Full Length
BC = Bobbin Coil
FS = Free Span
RECP = Rotating Eddy Current Probe (Plus Point or Pancake)
CL TTS = Cold Leg Top of Tubesheet
HL TTS = Hot Leg Top of Tubesheet
R1 = Row 1, R2 = Row 2
5) The inspection scope reflects the most recent ISI as of 4/2002.

Table 10-5
International PWR Steam Generators with Alloy 690[1] Tubes (as of March 2004)

Country	Plant	Original or Repl. SGs	Date of Commer-cial Operation or Repl.	SG Design	SG Model	No. SG	Number Tubes per SG	Calendar Years at 3/2004	Current HL Temp. (°F)	Approx. EFPY at 3/2004	Approx. EDY[2,3] at 3/2004	Tube-EFPYs	Tube-EDYs	Inspection Scope at Most Recent ISI[4]
Belgium	Doel 4	Repl.	07/1996	Fram	79/19	3	6019	7.7	621	6.9	15.8	124,000	285,000	20% FL BC of 2 SGs every 3 years
Belgium	Tihange 1	Repl.	06/1995	MHI	51F	3	5330	8.7	609	7.7	11.1	124,000	177,000	3.3% FL BC
Belgium	Tihange 2	Repl.	06/2001	MHI	Unknown	3	5372	2.7	617	2.4	4.7	38,000	75,000	13% FL BC
Belgium	Tihange 3	Repl.	08/1998	Fram	79/19	3	6019	5.6	623	5.0	12.5	91,000	225,000	13% FL BC
China	Daya Bay 1[o]	Orig.	02/1994	Fram	55/19	3	4474	10.1	621	9.1	20.8	122,000	280,000	Unknown
China	Daya Bay 2[o]	Orig.	05/1994	Fram	55/19	3	4474	9.8	621	8.9	20.3	119,000	273,000	Unknown
France	Chooz B1	Orig.	01/1990	Fram	73/19	4	5559	14.2	625	5.0	13.3	111,000	296,000	15% FL BC
France	Chooz B2	Orig.	01/1994	Fram	73/19	4	5559	10.2	625	4.7	12.5	104,000	279,000	15% FL BC
France	Civaux 1	Orig.	01/1995	Fram	73/19	4	5559	9.2	625	4.3	11.5	96,000	256,000	10% FL BC
France	Civaux 2	Orig.	01/1997	Fram	73/19	4	5598	7.2	625	3.6	9.6	81,000	216,000	9% FL BC
France	Dampierre 1	Repl.	02/1990	Fram	51B	3	3330	14.0	613	11.5	19.3	115,000	193,000	100% FL BC + 3% RECP of HL TTS
France	Dampierre 3	Repl.	11/1995	Fram	47/22	3	3330	8.3	613	6.8	11.4	68,000	114,000	26% FL BC
France	Fessenheim 1	Repl.	05/2002	Fram	47/22	3	3330	1.8	613	1.1	1.9	11,000	19,000	Unknown
France	Golfech 2	Orig.	01/1992	Fram	68/19	4	5342	12.2	616	9.2	17.4	197,000	372,000	28% FL BC
France	Gravelines 1	Repl.	02/1994	Fram	47/22	3	3330	10.1	613	8.8	14.7	87,000	147,000	100% FL BC and Helium
France	Gravelines 2	Repl.	08/1996	Fram	47/22	3	3330	7.5	613	6.4	10.7	64,000	107,000	8% FL BC
France	Gravelines 4	Repl.	07/2000	Fram	47/22	3	3330	3.6	613	3.1	5.2	31,000	52,000	26% FL BC
France	Penly 2	Orig.	01/1990	Fram	68/19	4	5342	14.2	616	10.4	19.7	223,000	421,000	25% FL BC
France	St-Laurent B1	Repl.	08/1995	Fram	47/22	3	3330	8.5	613	6.9	11.5	68,000	115,000	25% FL BC
France	Tricastin 1	Repl.	11/1998	Fram	47/22	3	3330	5.3	613	4.3	7.2	43,000	72,000	26% FL BC
France	Tricastin 2	Repl.	05/1997	Fram	47/22	3	3330	6.8	613	5.6	9.4	56,000	94,000	100% FL BC
France	Tricastin 3	Repl.	10/2001	Fram	47/22	3	3330	2.4	613	2.2	3.6	22,000	36,000	Baseline
Japan	Genkai 1	Repl.	11/1994	MHI	52F	2	3382	9.3	613	7.7	13.0	52,000	88,000	50% FL BC[5]
Japan	Genkai 2	Repl.	03/2001	MHI	54F	2	3386	3.0	613	2.1	3.5	14,000	24,000	Baseline[5]
Japan	Genkai 3	Orig.	03/1994	MHI	52FA	4	3382	10.0	617	8.9	17.5	121,000	237,000	50% FL BC[5]
Japan	Genkai 4	Orig.	11/1997	MHI	52FA	4	3382	6.3	617	5.9	11.6	80,000	157,000	50% FL BC[5]
Japan	Ikata 1	Repl.	05/1998	MHI	54F	2	3386	5.8	613	5.4	9.0	36,000	61,000	50% FL BC[5]
Japan	Ikata 2	Repl.	09/2001	MHI	54F	2	3386	2.5	613	2.2	3.8	15,000	26,000	Baseline[5]
Japan	Ikata 3	Orig.	12/1994	MHI	52F	3	3382	9.2	613	8.4	14.1	85,000	143,000	50% FL BC[5]
Japan	Mihama 1	Repl.	04/1996	West	35F	2	2918	7.9	603	7.0	7.9	41,000	46,000	50% FL BC[5]
Japan	Mihama 2	Repl.	08/1994	MHI	46F	2	3382	9.6	607	7.9	10.5	54,000	71,000	50% FL BC[5]
Japan	Mihama 3	Repl.	04/1997	MHI	54F	3	3592	6.9	608	6.5	9.0	70,000	97,000	50% FL BC[5]

Table 10-5
International PWR Steam Generators with Alloy 690[1] Tubes (as of March 2004) (continued)

Country	Plant	Original or Repl. SGs	Date of Commer-cial Operation or Repl.	SG Design	SG Model	No. SG	Number Tubes per SG	Calendar Years at 3/2004	Current HL Temp. (°F)	Approx. EFPY at 3/2004	Approx. EDY[2,3] at 3/2004	Tube-EFPYs	Tube-EDYs	Inspection Scope at Most Recent ISI[4]
Japan	Ohi 1	Repl.	05/1995	MHI	52FA	4	3382	8.8	617	6.8	13.4	92,000	181,000	50% FL BC[5]
Japan	Ohi 2	Repl.	09/1997	MHI	54FA	4	3592	6.5	613	5.5	9.3	79,000	133,000	50% FL BC[5]
Japan	Ohi 3	Orig.	12/1991	MHI	52FA	4	3382	12.2	617	11.1	21.7	150,000	294,000	50% FL BC[5]
Japan	Ohi 4	Orig.	02/1993	MHI	52FA	4	3382	11.1	617	9.9	19.5	134,000	264,000	50% FL BC[5]
Japan	Takahama 1	Repl.	08/1996	MHI	54F	3	3592	7.6	613	6.6	11.1	71,000	120,000	50% FL BC[5]
Japan	Takahama 2	Repl.	08/1994	MHI	52F	3	3382	9.6	613	8.0	13.5	81,000	137,000	100% FL BC[5]
Slovenia	Krško	Repl.	06/2000	KWU	72W-D4/2	2	5428	3.7	620	3.5	7.8	38,000	84,000	100% FL BC[5]
South Korea	Kori 1	Repl.	07/1998	West	D60	2	4934	5.7	607	4.7	6.3	47,000	62,000	Unknown
Sweden	Ringhals 2	Repl.	08/1989	KWU	51W	3	5130	14.6	610	11.3	16.8	173,000	258,000	No NDE inspection; Previous RFO – 50% FL BC + 5% RECP of HL TTS
Sweden	Ringhals 3	Repl.	08/1995	KWU	72W/DR/R	3	5130	8.6	606	7.3	9.3	113,000	143,000	50% FL BC + 10% RECP of HL TTS + 3.3% RECP U-bend
Switzerland	Beznau 1	Repl.	07/1993	Fram	33/19	2	3238	10.7	594	9.6	7.5	62,000	49,000	No inspection; Previous RFO – 100% FL BC + 10% RECP of HL and CL TTS + 100% RECP of R1 & R2 U-bends
Switzerland	Beznau 2	Repl.	06/1999	Fram	33/19	2	3238	4.7	594	4.1	3.2	27,000	21,000	100% FL BC + 10% RECP of HL and CL TTS + 100% RECP of R1 & R2 U-bends
U.K.	Sizewell B	Orig.	02/1995	West	F	4	5626	9.1	620	7.8	17.2	176,000	388,000	0.1% FL BC + 0.1% RECP of HL TTS
											Total[6]	3,806,000	7,189,000	

Notes:
1) All tubes in international SGs that have Alloy 690 tubes are thermally treated (Alloy 690TT).
2) Effective Degradation Year (EDY) defined as equivalent time at temperature using a reference temperature of 600°F and an activation energy of 50 kcal/mole.
3) Based on current hot leg temperature; no corrections are made for changes in hot leg temperature over life.
4) Definitions of abbreviations for inspections:
FL = Full Length
BC = Bobbin Coil
FS = Free Span
RECP = Rotating Eddy Current Probe (Plus Point or Pancake)
CL TTS = Cold Leg Top of Tubesheet
HL TTS = Hot Leg Top of Tubesheet
R1 = Row 1, R2 = Row 2
5) The inspection scope reflects the most recent ISI as of 4/2002.
6) Because of a lack of available information, Daya Bay 1 & 2 are assumed to have 4474 tubes per SG.

Table 10-6
Alloy 690/152/52 RCS (Excluding Steam Generators) Replacement Component Items and Welds for U.S. PWRs[1,2]

Location	Component Item	Wrought Material	Weld Materials	Plant	Date Replaced	Calendar Years at 3/2004	# Parts	Temp.[3] (°F)	Approx. EFPY at 3/2004	Approx. EDY at 3/2004[4]	Part-EFPYs	Part-EDYs
RV Closure Head	CRDM Nozzle	None	Alloy 52/152	ANO 1	10/2002	1.4	6	602	1.3	1.4	7.9	8.5
		Alloy 690	Alloy 52/152	Crystal River 3	11/2003	0.3	69	601	0.3	0.3	20.5	21.3
		Alloy 690	Alloy 52/152	Ginna	10/2003	0.4	37	580	0.3	0.2	12.9	5.7
		Alloy 690	Alloy 52/152	Millstone 2	03/2002	2.0	3	594	1.9	1.4	5.6	4.3
		Alloy 690	Alloy 52/152	North Anna 1	04/2003	0.9	65	600	0.8	0.8	52.4	52.4
		Alloy 690	Alloy 52/152	North Anna 2	02/2003	1.1	65	600	1.0	1.0	64.9	64.9
		Alloy 690	Alloy 52/152	Oconee 1	12/2003	0.2	69	602	0.2	0.2	13.5	14.6
		None	Alloy 52/152	Oconee 2	05/2001	2.8	4	602	2.6	2.8	10.5	11.4
		None	Alloy 52/152	Oconee 2	10/2002	1.4	15	602	1.3	1.4	19.7	21.3
		Alloy 690	Alloy 52/152	Oconee 3	06/2003	0.7	69	602	0.7	0.7	45.5	49.3
		None	Alloy 52/152	St. Lucie 2	06/2003	0.8	2	596	0.7	0.6	1.4	1.2
		Alloy 690	Alloy 52/152	Surry 1	06/2003	0.7	65	598	0.7	0.6	43.2	39.8
		Alloy 690	Alloy 52/152	Surry 2	11/2003	0.3	65	598	0.3	0.3	17.8	16.4
		Alloy 690	Alloy 52/152	TMI 1	12/2003	0.2	69	601	0.2	0.2	15.6	16.2
Hot Leg	Instrument Nozzle	Alloy 690	Alloy 52	ANO 1	02/2000	4.1	6	602	3.8	4.1	22.7	24.6
		Alloy 690	Alloy 52/152	ANO 2	07/2000	3.7	1	608	3.4	4.7	3.4	4.7
		Alloy 690	Alloy 52	Davis Besse	01/2003	1.2	4	605	0.0	0.0	0.0	0.0
		Alloy 690	Alloy 52	Palo Verde 1	10/1999	4.4	2	614	4.1	7.1	8.2	14.3
		Alloy 690	Alloy 52	Palo Verde 1	05/2001	2.8	15	614	2.6	4.6	39.3	68.7
		Alloy 690	Alloy 52	Palo Verde 1	11/2002	1.3	10	614	1.2	2.2	12.3	21.5
		Alloy 690	Alloy 52	Palo Verde 2	12/1991	12.3	8	614	10.0	17.4	79.7	139.3
		Alloy 690	Alloy 52	Palo Verde 2	11/2000	3.3	9	614	3.1	5.4	27.7	48.4
		Alloy 690	Alloy 52	Palo Verde 3	05/2000	3.8	4	614	3.5	6.2	14.2	24.8
		Alloy 690	Alloy 52	Palo Verde 3	11/2001	2.3	13	614	2.2	3.8	28.0	49.0
		Alloy 690	Alloy 52	Palo Verde 3	05/2003	0.8	10	614	0.8	1.4	7.7	13.5
		Alloy 690	Alloy 152	San Onofre 2	06/1993	10.8	1	595	9.2	7.5	9.2	7.5
		Alloy 690	Alloy 152	San Onofre 2	02/1998	6.1	11	595	5.6	4.6	61.6	50.3
		Alloy 690	Alloy 152	San Onofre 2	02/1999	5.1	20	595	4.7	3.8	93.9	76.7
		Alloy 690	Alloy 152	San Onofre 3	07/1995	8.7	2	595	7.4	6.0	14.8	12.0
		Alloy 690	Alloy 152	San Onofre 3	04/1997	6.9	8	595	5.9	4.8	47.0	38.4
		Alloy 690	Alloy 152	San Onofre 3	03/1998	6.0	7	595	5.6	4.5	38.9	31.7
		Alloy 690	Alloy 152	San Onofre 3	04/1999	4.9	15	595	4.6	3.7	68.3	55.7
		Alloy 690	Alloy 52	St. Lucie 1	04/2001	2.9	1	604	2.7	3.2	2.7	3.2
		Alloy 690	Alloy 52	St. Lucie 2	12/1995	8.3	9	604	7.1	8.3	63.6	74.7
		Alloy 690	Alloy 52	St. Lucie 2	06/2003	0.7	10	604	0.7	0.8	6.9	8.2
		Alloy 690	Alloy 52	Waterford 3	10/2000	3.4	3	605	3.2	3.9	9.5	11.6
	RV HL Safe End	None	Alloy 52	V.C. Summer	10/2000	3.4	1	619	3.2	6.7	3.2	6.7
	Surge Nozzle Weld	None	A52 Weld Overlay (O.D. of Pipe)	TMI 1	12/2003	0.2	1	603	0.2	0.3	0.2	0.3

Table 10-6
Alloy 690/152/52 RCS (Excluding Steam Generators) Replacement Component Items and Welds for U.S. PWRs[1,2] (continued)

Location	Component Item	Wrought Material	Weld Materials	Plant	Date Replaced	Calendar Years at 3/2004	# Parts	Temp.[3] (°F)	Approx. EFPY at 3/2004	Approx. EDY at 3/2004[4]	Part-EFPYs	Part-EDYs
Cold Leg	Instrument Nozzle	Alloy 690	Alloy 52	Davis Besse	01/2003	1.2	4	555	0.0	0.0	0.0	0.0
		Alloy 690	Alloy 152	San Onofre 2	02/1998	6.1	12	540	5.6	0.4	67.2	5.2
		Alloy 690	Alloy 152	San Onofre 3	04/1997	6.9	1	540	5.9	0.5	5.9	0.5
		Alloy 690	Alloy 152	San Onofre 3	03/1998	6.0	11	540	5.6	0.4	61.1	4.7
RV Lower Head	BMI Nozzle	Alloy 690	Alloy 52/152	South Texas 1	08/2003	0.6	2	561	0.5	0.1	1.0	0.2
Pressurizer	Heater Sleeve	Alloy 690	Alloy 52/152	ANO 2	07/2000	3.7	12	633	3.4	12.4	40.7	148.2
		Alloy 690	Alloy 52/152	Calvert Cliffs 1	02/1994	10.1	2	633	9.3	34.0	18.7	67.9
		Alloy 690	Alloy 52/152	Calvert Cliffs 1	03/1998	6.0	1	633	5.6	20.2	5.6	20.2
		Alloy 690	Alloy 182/82	Calvert Cliffs 2	07/1990	13.7	119	633	10.2	37.2	1,216.6	4,428.3
		Alloy 690	Alloy 52	Palo Verde 2	10/2000	3.4	2	633	3.2	11.5	6.3	23.0
		Alloy 690	Alloy 52	Palo Verde 2	12/2003	0.2	34	633	0.2	0.8	7.8	28.5
		Alloy 690	Alloy 52	San Onofre 3	04/1999	4.9	1	633	4.3	15.6	4.3	15.6
		Alloy 690	Alloy 52/152	Waterford 3	10/2000	3.4	1	633	3.2	11.5	3.2	11.5
	Instrument Nozzle Liquid Space	Alloy 690	Alloy 82	Palo Verde 1	04/1992	11.9	3	633	10.4	37.9	31.2	113.7
		Alloy 690	Alloy 52	Palo Verde 2	03/1993	11.0	3	633	9.2	33.3	27.5	99.9
		Alloy 690	Alloy 52	Palo Verde 3	11/1994	9.3	3	633	8.5	31.1	25.6	93.3
		Alloy 690	Alloy 52/152	San Onofre 2	03/1997	7.0	1	633	6.4	23.2	6.4	23.2
		Alloy 690	Alloy 52	St. Lucie 2	12/1995	8.3	3	633	7.6	27.7	22.8	83.0
	Instrument Nozzle Steam Space	Alloy 690	Alloy 182/82	Calvert Cliffs 2	07/1990	13.7	4	633	10.2	37.0	40.7	148.2
		Alloy 690	Alloy 82	Palo Verde 1	04/1992	11.9	4	633	10.4	37.9	41.6	151.6
		Alloy 690	Alloy 52	Palo Verde 2	01/1994	10.2	4	633	8.9	32.2	35.4	128.9
		Alloy 690	Alloy 52	Palo Verde 3	11/1994	9.3	4	633	8.5	31.1	34.2	124.4
		Alloy 690	Alloy 52/152	San Onofre 2	06/1993	10.8	4	633	9.9	36.2	39.8	144.9
		Alloy 690	Alloy 52/152	San Onofre 3	07/1995	8.7	4	633	8.0	29.2	32.1	116.8
		Alloy 690	Alloy 52	St. Lucie 1	10/1999	4.4	4	633	4.2	15.3	16.8	61.2
		Alloy 690	Alloy 182	St. Lucie 2	04/1994	10.0	4	633	8.8	32.0	35.2	128.1
		Alloy 690	Alloy 52/152	Waterford 3	02/1999	5.1	2	633	4.7	17.1	9.4	34.2
		Alloy 690	Alloy 52/152	Waterford 3	10/2000	3.4	2	633	2.7	9.7	5.3	19.4
	Manway Diaphragm Plate	Alloy 600	Alloy 52/152	Catawba 1	05/2002	1.8	1	650	1.7	11.7	1.7	11.7
						Total	1026			*Total*	2,838	7,349

Notes:
1) Table entries are based on the information currently available. Additional replacements may exist, which are not included in this table.
2) This table reflects replacements that are currently in service (as of 3/04). Overlay weld repairs of CRDM penetrations are not included.
3) For pressurizer component temperatures of 633°F, the temperature value is estimated for the location of the new pressure boundary weld at the pressurizer OD.
4) Effective Degradation Year (EDY) defined as equivalent time at temperature using a reference of 600°F and an activation energy of 50 kcal/mole.
Also, the EDY calculation is based on the current operating temperature at that location; no corrections are made for past changes in temperature.

Table 10-7
Alloy 690/152/52 Reactor Coolant System (Excluding Steam Generators) Original Equipment or Replacement Component Items and Welds for International PWRs[1]

Component Item	In-Service Date	PWR	Material
RV Head CRDM Nozzles/Welds[2]	1994	Bugey-2, Bugey-3, Bugey-5, Blayais-1, Gravelines-4	Alloy 690 Tubing and Alloy 152/52 Weld
	1995	Blayais-2, St. Alban-1, Flamanville-1, Gravelines-3, Blayais-3, Tricastin-1	
	1996	Tricastin-4, Paluel-4, St. Laurent-B2, Blayais-4, Dampierre-1, Fessenheim-1, St. Alban-2, Ringhals 2	
	1997	Bugey-4, Dampierre-2, Dampierre-4, Belleville-2, Cruas-4, Gravelines-5	
	1998	Flamanville-2, Dampierre-3, Paluel-3, Cattenom-2, Fessenheim-2, Cruas-2	
	1999	Chooz-B1, Chooz-B2, Cattenom-1, Cattenom-3, Gravelines-1, Tricastin-2, Tihange 1	
	2000	Civaux-1, Civaux-2, Belleville-1, Chinon-B2, Gravelines-2, Nogent-1	
	2001	Gravelines-6, Nogent-2, Paluel-2	
RV Lower Head BMI Nozzles	2000	Civaux-1, Civaux-2	Alloy 690 Tubing and Alloy 152/52 Weld

1) Table entries are based on the information currently available. Additional replacements may exist, which are not included in this table.
2) This list represents complete RV closure head replacements. Numerous CRDM nozzle repairs on various existing RV closure heads are also in service at this time.

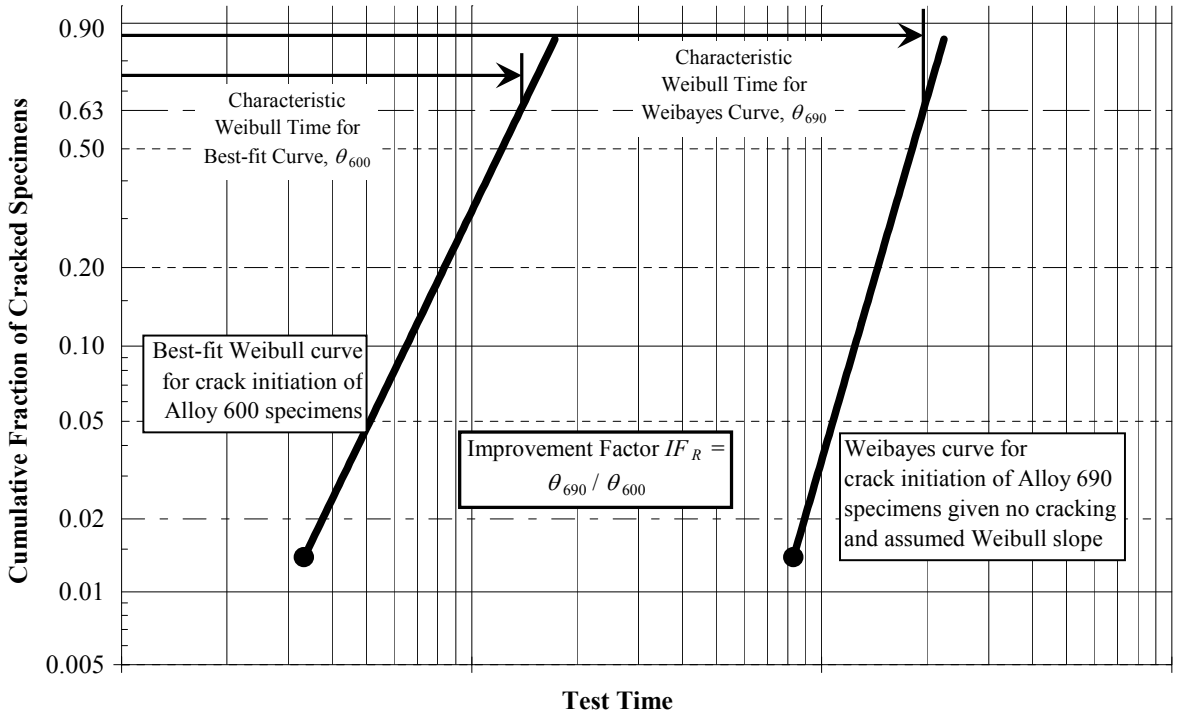

Figure 10-1
Weibull Plot Illustrating First Method for Determining Material Improvement Factor

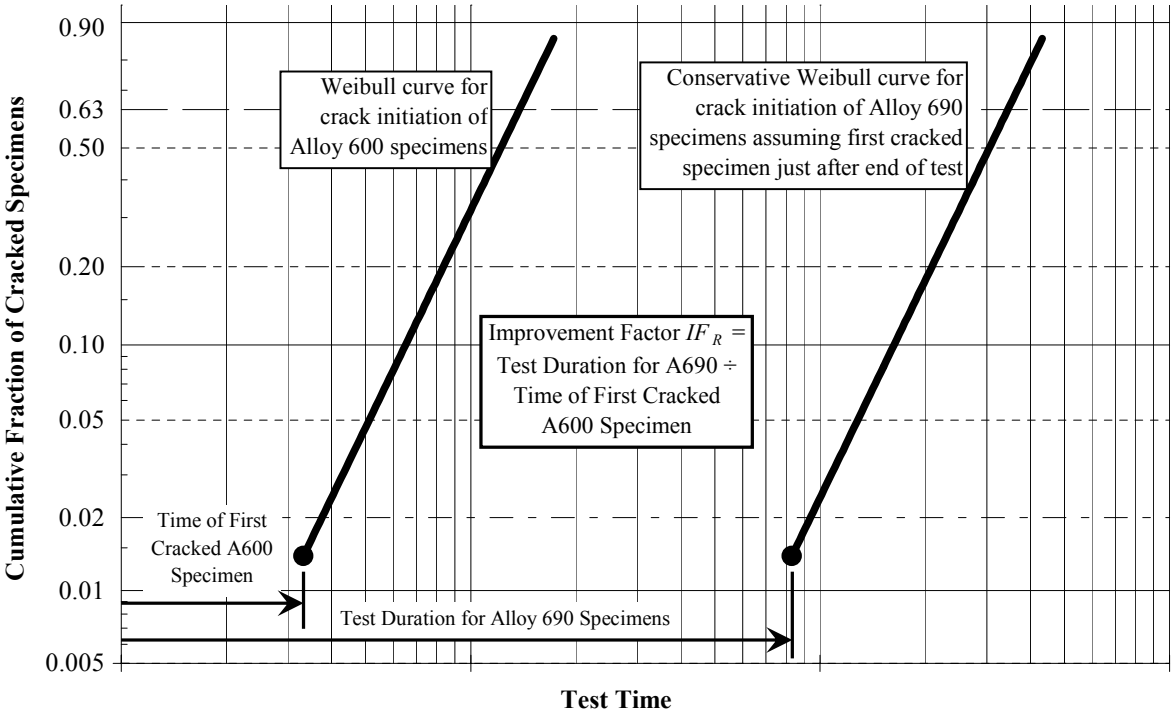

Figure 10-2
Weibull Plot Illustrating Second Method for Determining Material Improvement Factor

A
HEAD MAPS AND PENETRATION DESIGNS

This appendix identifies the locations and types of Alloy 600 reactor vessel head penetrations and the associated Alloy 182 J-groove weld configurations.

A.1 Penetration Locations on Reactor Vessel Heads

Figures A-1 through A-8 show the locations of Alloy 600 penetrations on PWR reactor vessel heads in the U.S. The types of penetrations used and locations on the head vary by plant design and plant size.

A.2 Penetration Designs

Figures A-9 through A-16 show the different types of penetration designs. Most are attached to the underside of the vessel head by Alloy 182 J-groove welds. However, some nozzles are welded to stub tubes or weld built-up pads on the top surface of the vessel heads.

The CRDM, CEDM, ICI, J-groove type auxiliary head adapter and de-gas line nozzles are installed into the vessel head with a shrink (interference) fit prior to welding the nozzle to the underside of the head. The head vent nozzles are installed with a clearance fit.

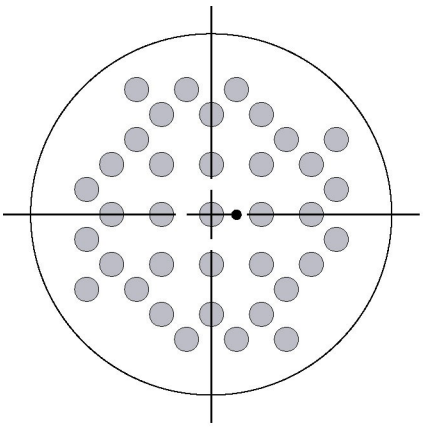

37 CRDM Nozzles
1 Head Vent Nozzle

Figure a

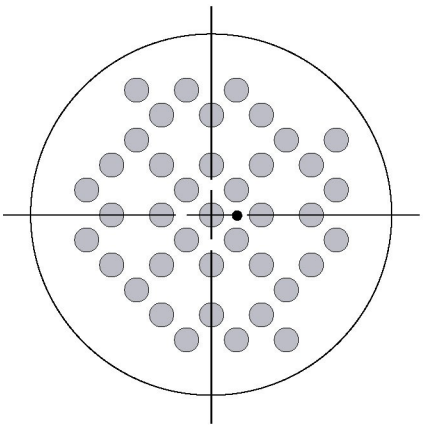

40 CRDM Nozzles
1Head Vent Nozzle

Figure b

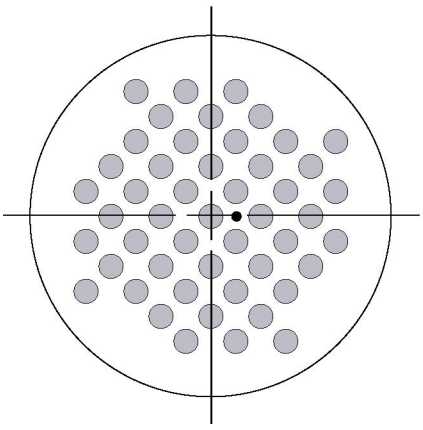

49 CRDM Nozzles
1Head Vent Nozzle

Figure c

Figure A-1
Penetration Locations—Westinghouse 2-Loop Plants

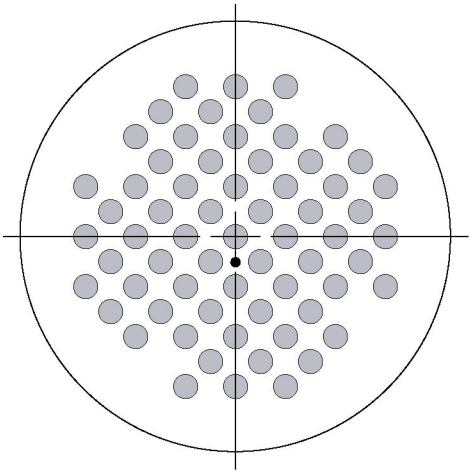

65 CRDM Nozzles
1Head Vent Nozzle

Figure a

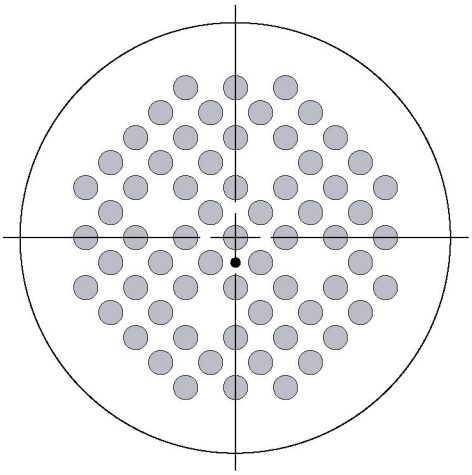

65 CRDM Nozzles
1Head Vent Nozzle

Figure b

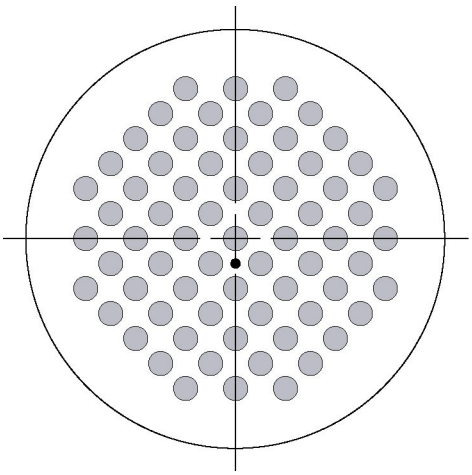

69 CRDM Nozzles
1Head Vent Nozzle

Figure c

Figure A-2
Penetration Locations—Westinghouse 3-Loop Plants

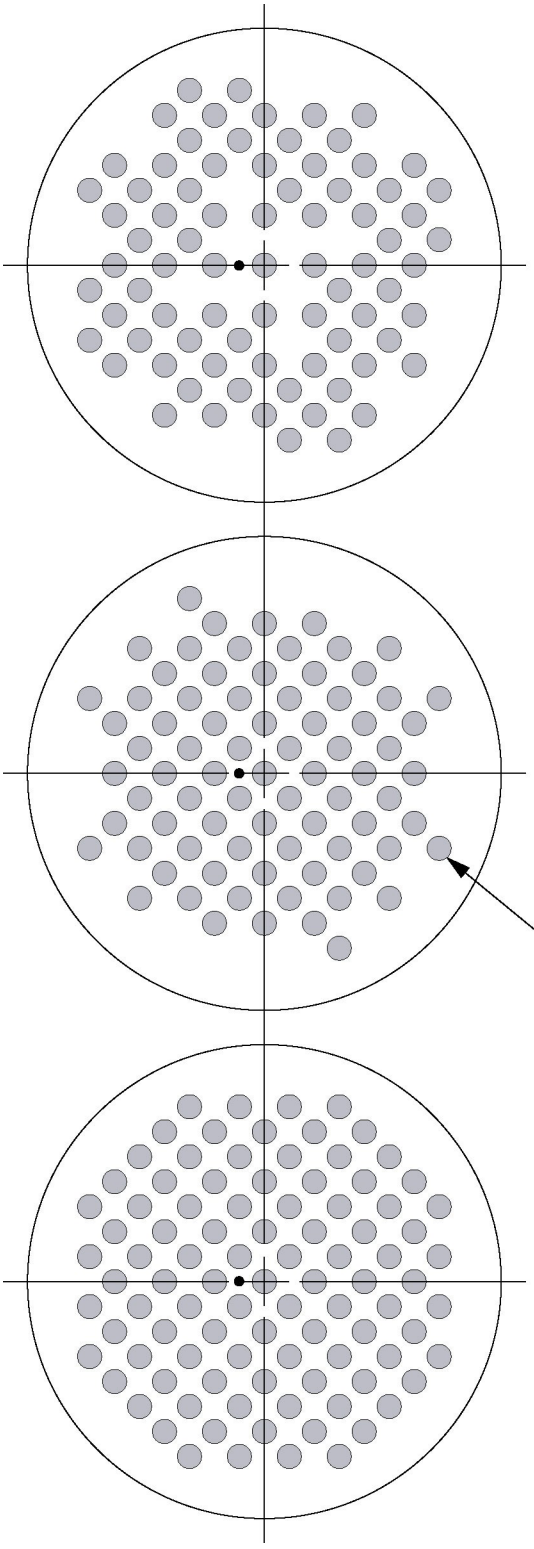

78 CRDM Nozzles
1Head Vent Nozzle

Figure a

78/79 CRDM Nozzles
1 Head Vent Nozzle

Figure b

Some plants are missing this nozzle

97 CRDM Nozzles
1Head Vent Nozzle

Figure c

Figure A-3
Penetration Locations—Westinghouse 4-Loop Plants Without Adapters

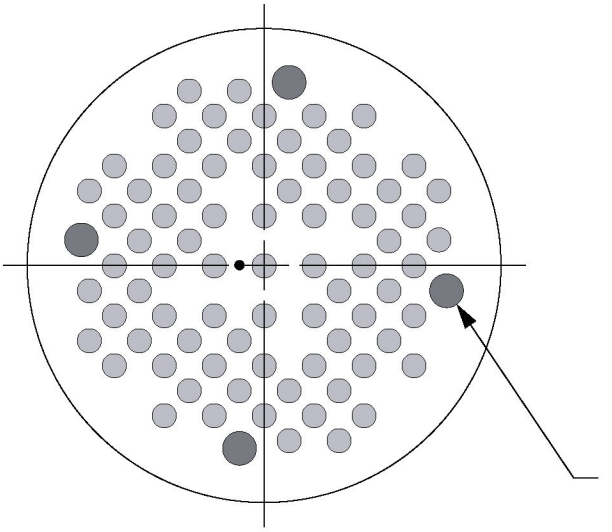

78 CRDM Nozzles
4 Auxiliary Head Adapters
1Head Vent Nozzle

Figure a

Auxiliary Head Adapters (4)

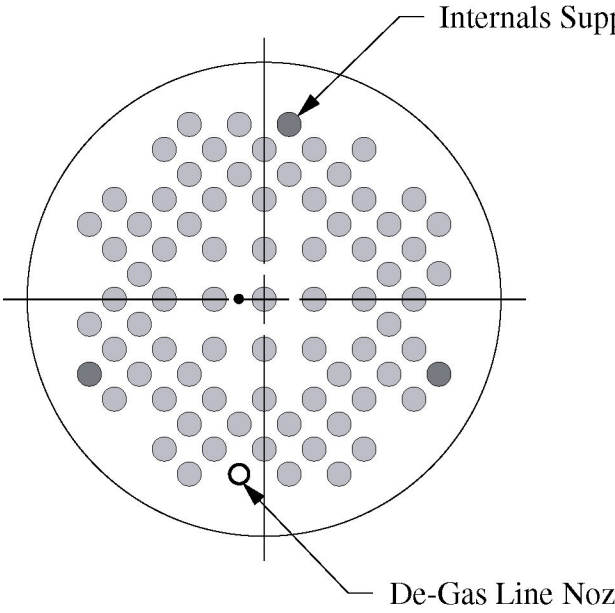

Internals Support Housings (3)

74 CRDM Nozzles
3 Internals Support Housings
1 De-Gas Nozzle
1 Head Vent Nozzle

Figure b

De-Gas Line Nozzle (1)

Figure A-4
Penetration Locations—Westinghouse 4-Loop Plants With Adapters

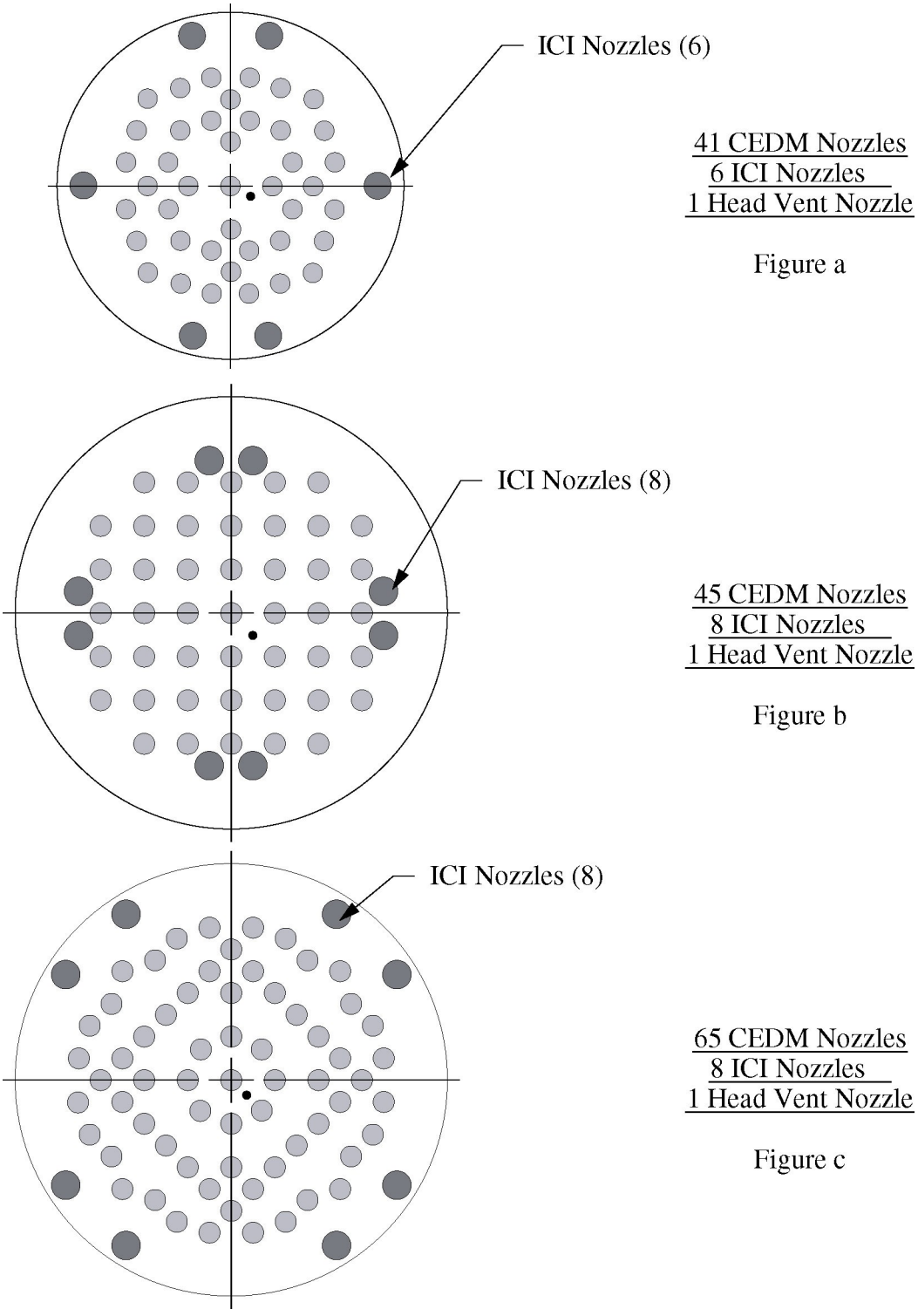

Figure A-5
Penetration Locations—Combustion Engineering Plants

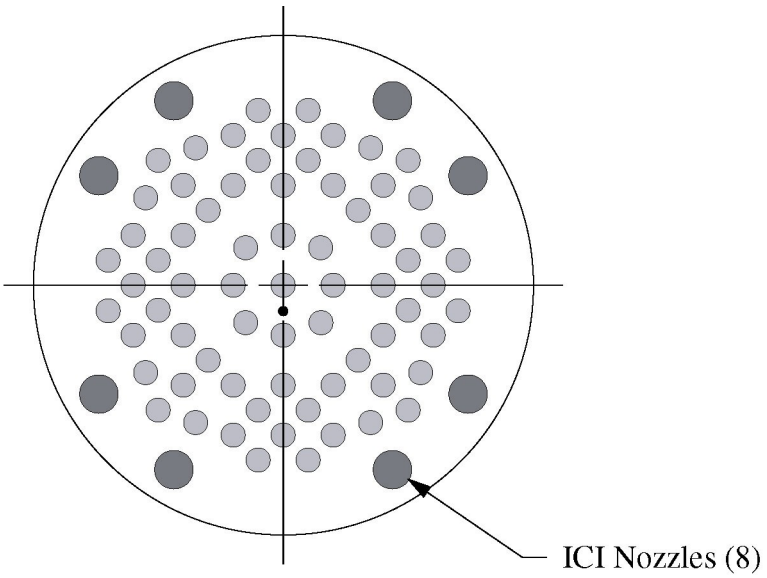

69 CEDM Nozzles
8 ICI Nozzles
1 Head Vent Nozzle

Figure a

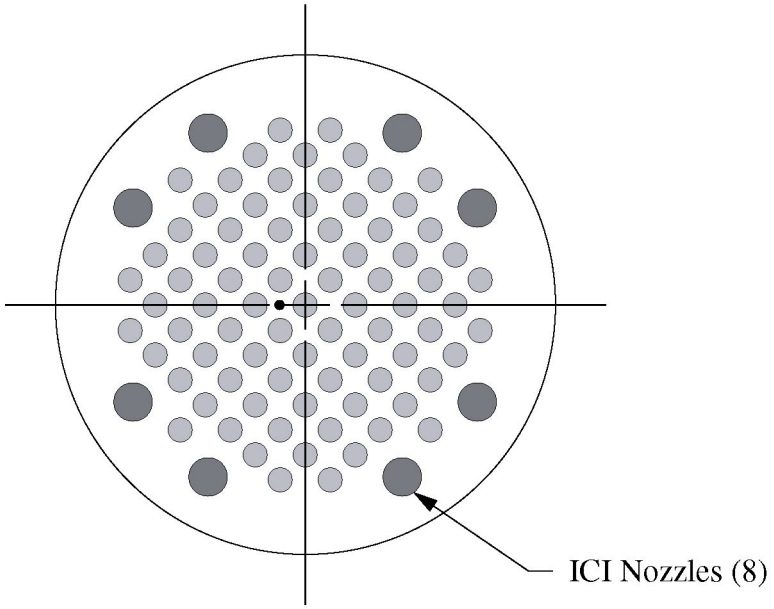

81 CEDM Nozzles
8 ICI Nozzles
1 Head Vent Nozzle

Figure b

Figure A-6
Penetration Locations—Combustion Engineering Plants

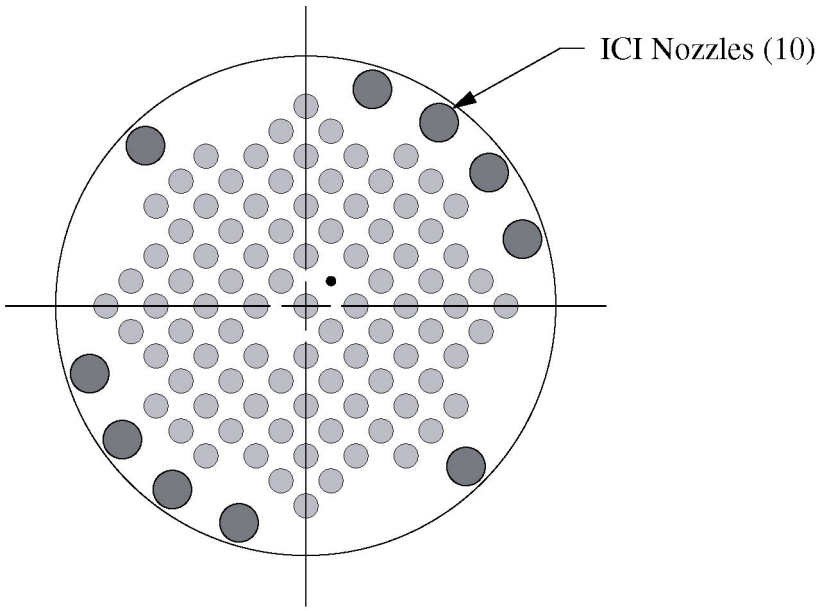

91 CEDM Nozzles
10 ICI Nozzles
1 Head Vent Nozzle

Figure a

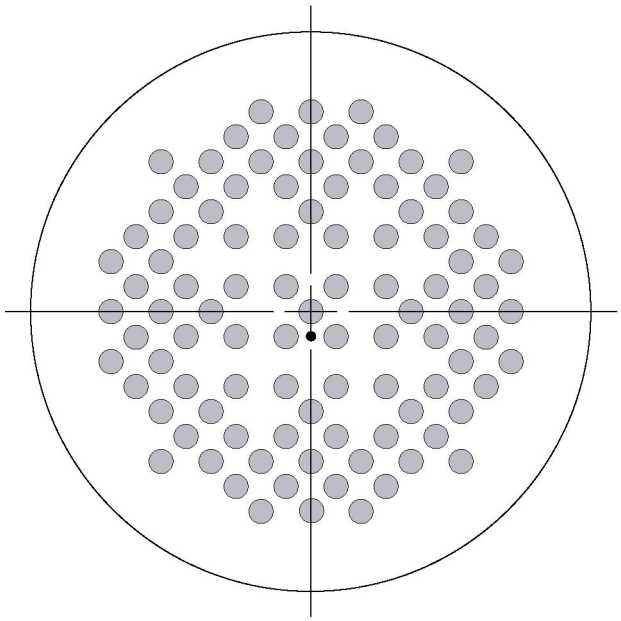

97 CEDM Nozzles
1 Head Vent Nozzle

Figure b

Figure A-7
Penetration Locations—Combustion Engineering Plants

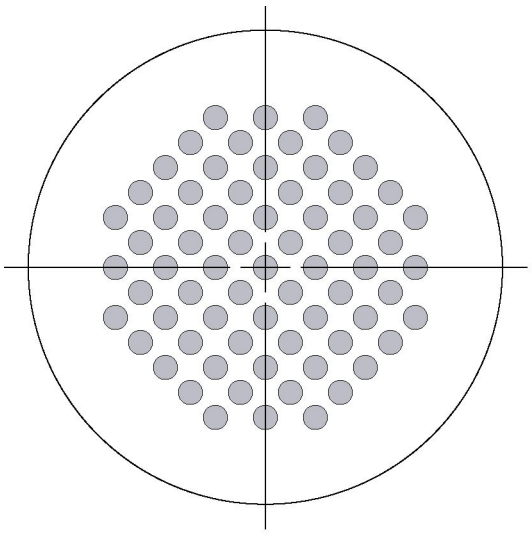

69 CRDM Nozzles

Figure a

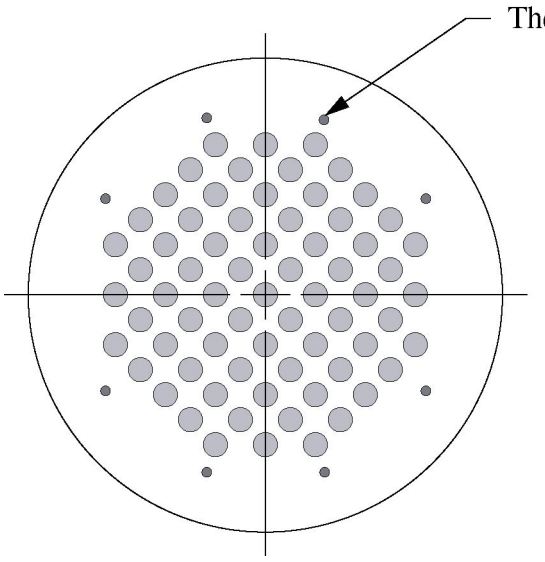

69 CRDM Nozzles
8 Thermocouple Nozzles

Figure b

Figure A-8
Penetration Locations—B&W Plants

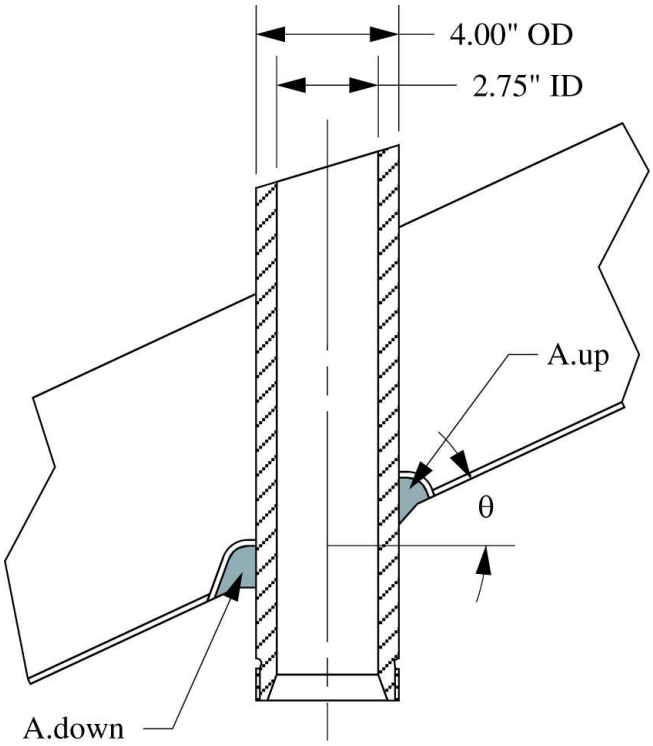

Figure A-9
Penetration Designs—Control Rod Drive Mechanism (CRDM) Nozzles

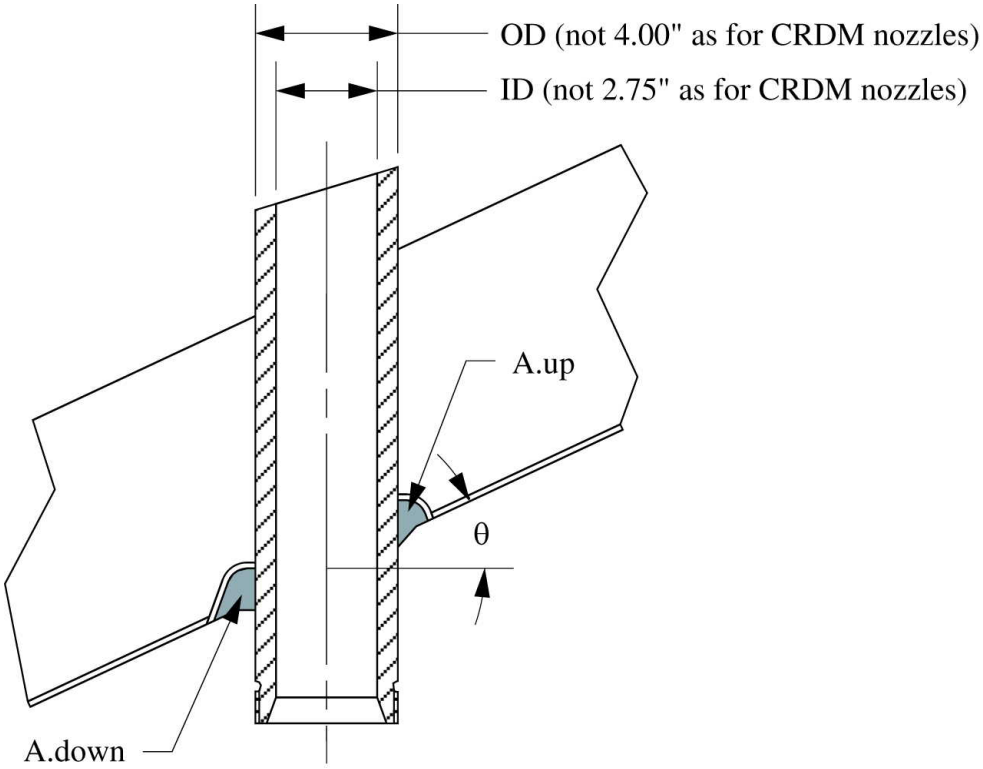

Figure A-10
Penetration Designs—Control Element Drive Mechanism (CEDM) Nozzles

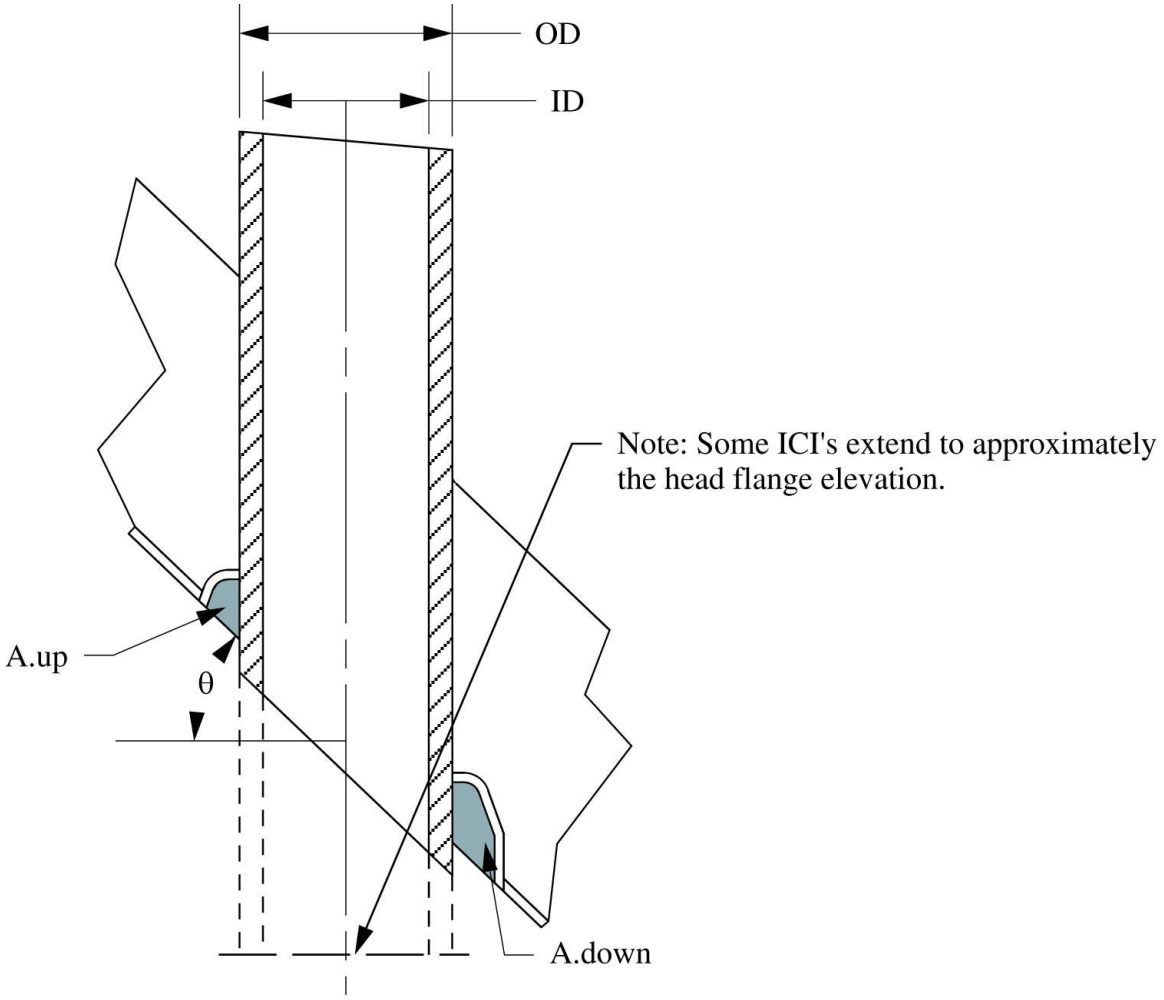

Figure A-11
Penetration Designs—Incore Instrument (ICI) Nozzles

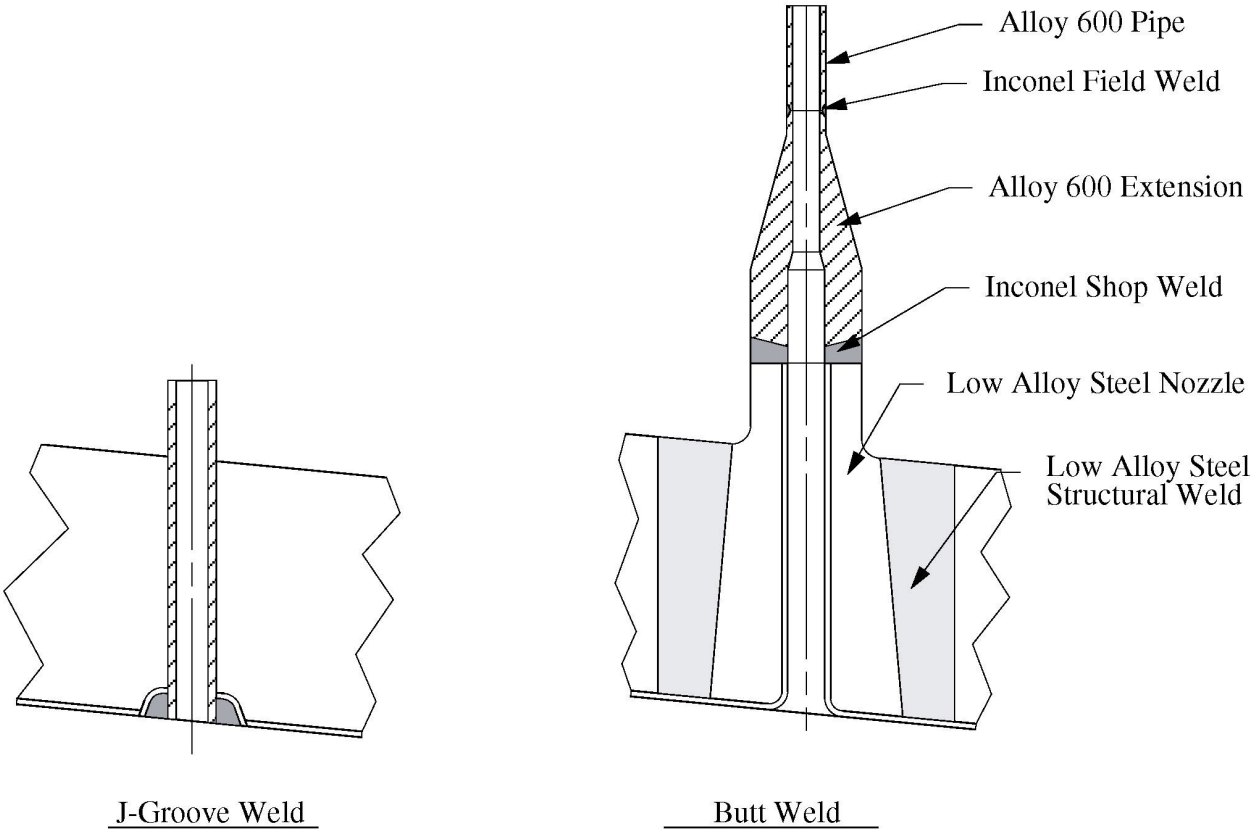

Figure A-12
Penetration Designs—Head Vent Nozzles

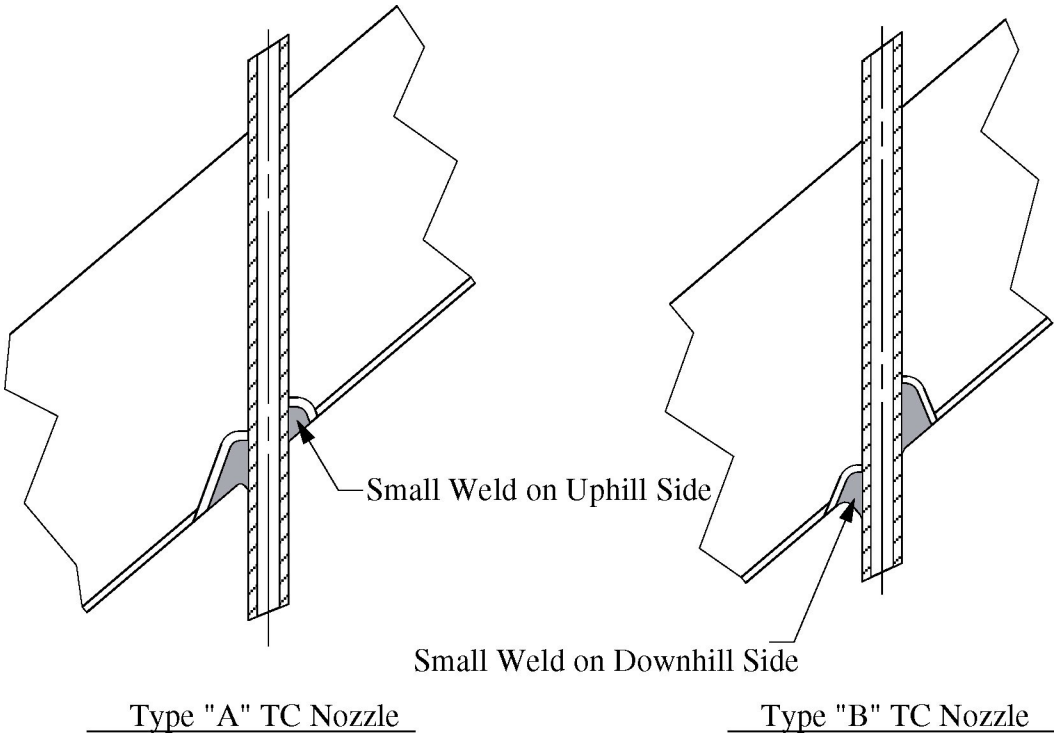

Figure A-13
Penetration Designs—Thermocouple Nozzles (Small Diameter ~1 inch)

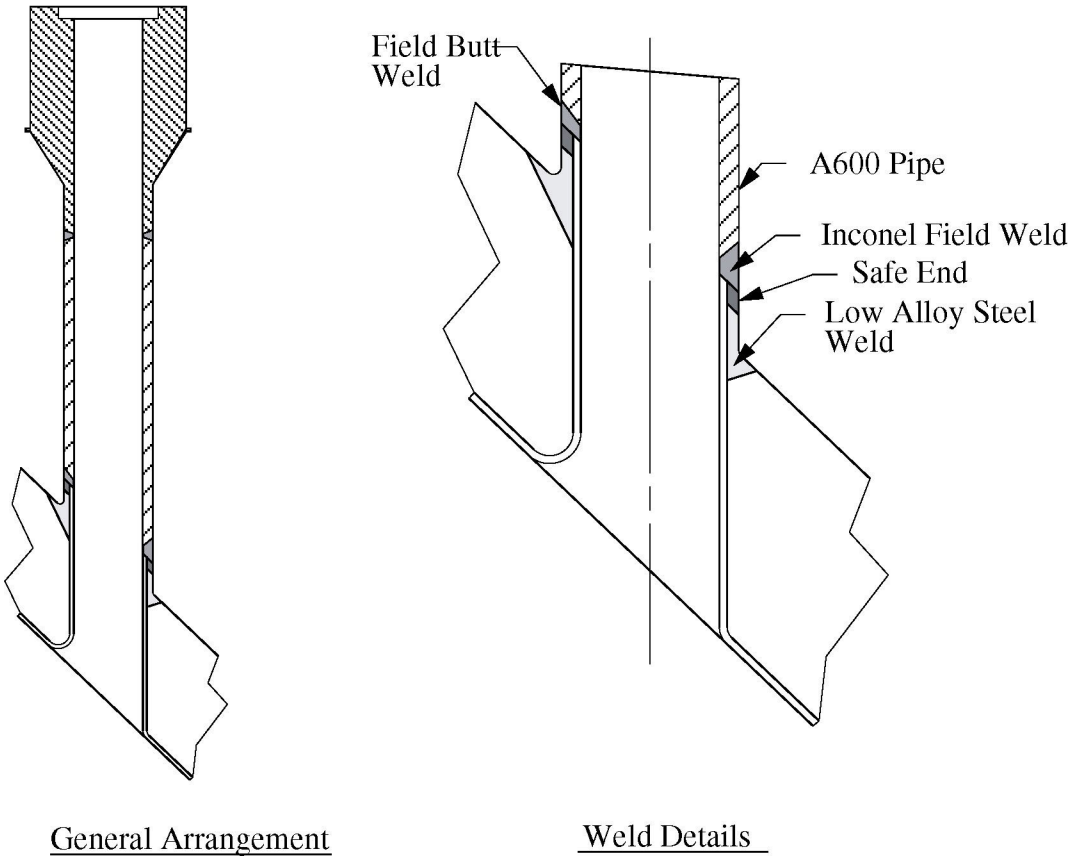

Figure A-14
Penetration Designs—Internals Support Housing Nozzles

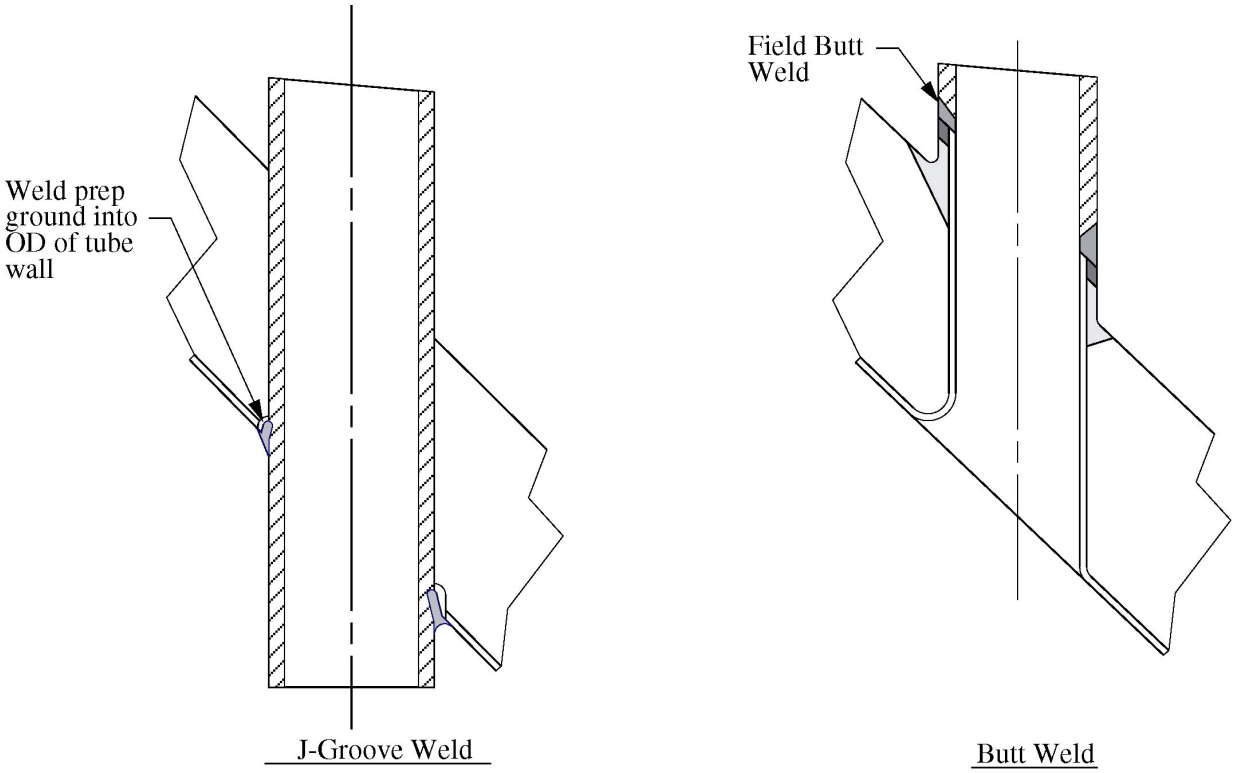

Figure A-15
Penetration Designs—Auxiliary Head Adapter Nozzles

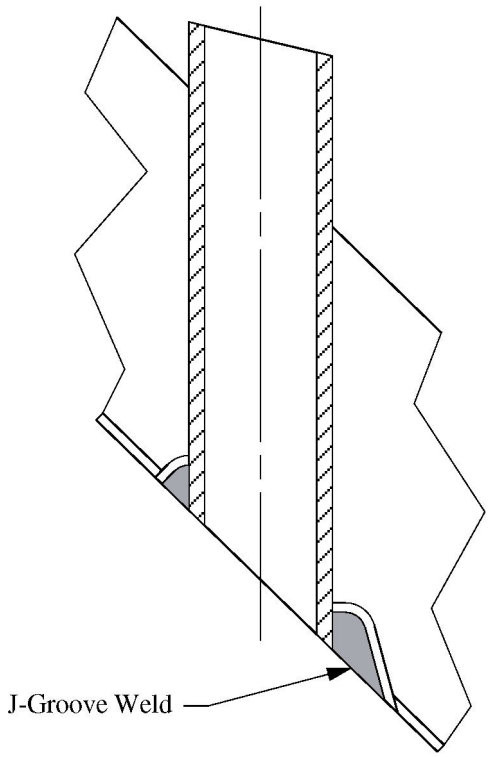

Figure A-16
Penetration Designs—De-Gas Line Nozzles

B
FMEA FAILURE-PATH DISPOSITION TABLE

Content Deleted – MRP/EPRI Proprietary Material

Table B-1
Failure Path Disposition Table for RVCH Penetration FMEA

Level	Upstream Condition	Downstream Condition	Disposition	Evaluation				Expected Effect on SA	Status
				Type	Summary	References	SA Location		

Table B-1
Failure Path Disposition Table for RVCH Penetration FMEA

Level	Upstream Condition	Downstream Condition	Disposition	Evaluation				Expected Effect on SA	Status
				Type	Summary	References	SA Location		

Table B-1
Failure Path Disposition Table for RVCH Penetration FMEA

Level	Upstream Condition	Downstream Condition	Disposition	Evaluation				Expected Effect on SA	Status
				Type	Summary	References	SA Location		

Table B-1
Failure Path Disposition Table for RVCH Penetration FMEA

Level	Upstream Condition	Downstream Condition	Disposition	Evaluation				Expected Effect on SA	Status
				Type	Summary	References	SA Location		

Table B-1
Failure Path Disposition Table for RVCH Penetration FMEA

Level	Upstream Condition	Downstream Condition	Disposition	Evaluation				Expected Effect on SA	Status
				Type	Summary	References	SA Location		

Table B-1
Failure Path Disposition Table for RVCH Penetration FMEA

Level	Upstream Condition	Downstream Condition	Disposition	Evaluation				Expected Effect on SA	Status
				Type	Summary	References	SA Location		

Table B-1
Failure Path Disposition Table for RVCH Penetration FMEA

Level	Upstream Condition	Downstream Condition	Disposition	Evaluation				Expected Effect on SA	Status
				Type	Summary	References	SA Location		

Table B-1
Failure Path Disposition Table for RVCH Penetration FMEA

Level	Upstream Condition	Downstream Condition	Disposition	Evaluation				Expected Effect on SA	Status
				Type	Summary	References	SA Location		

Table B-1
Failure Path Disposition Table for RVCH Penetration FMEA

Level	Upstream Condition	Downstream Condition	Disposition	Evaluation				Expected Effect on SA	Status
				Type	Summary	References	SA Location		

Table B-1
Failure Path Disposition Table for RVCH Penetration FMEA

Level	Upstream Condition	Downstream Condition	Disposition	Evaluation				Expected Effect on SA	Status
				Type	Summary	References	SA Location		

Table B-1
Failure Path Disposition Table for RVCH Penetration FMEA

Level	Upstream Condition	Downstream Condition	Disposition	Evaluation				Expected Effect on SA	Status
				Type	Summary	References	SA Location		

Table B-1
Failure Path Disposition Table for RVCH Penetration FMEA

Level	Upstream Condition	Downstream Condition	Disposition	Evaluation				Expected Effect on SA	Status
				Type	Summary	References	SA Location		

Table B-1
Failure Path Disposition Table for RVCH Penetration FMEA

Level	Upstream Condition	Downstream Condition	Disposition	Evaluation				Expected Effect on SA	Status
				Type	Summary	References	SA Location		

Table B-1
Failure Path Disposition Table for RVCH Penetration FMEA

Level	Upstream Condition	Downstream Condition	Disposition	Evaluation				Expected Effect on SA	Status
				Type	Summary	References	SA Location		

Table B-1
Failure Path Disposition Table for RVCH Penetration FMEA

Level	Upstream Condition	Downstream Condition	Disposition	Evaluation				Expected Effect on SA	Status
				Type	Summary	References	SA Location		

Table B-1
Failure Path Disposition Table for RVCH Penetration FMEA

Level	Upstream Condition	Downstream Condition	Disposition	Evaluation				Expected Effect on SA	Status
				Type	Summary	References	SA Location		

Table B-1
Failure Path Disposition Table for RVCH Penetration FMEA

Level	Upstream Condition	Downstream Condition	Disposition	Evaluation				Expected Effect on SA	Status
				Type	Summary	References	SA Location		

Table B-1
Failure Path Disposition Table for RVCH Penetration FMEA

Level	Upstream Condition	Downstream Condition	Disposition	Evaluation				Expected Effect on SA	Status
				Type	Summary	References	SA Location		

Table B-1
Failure Path Disposition Table for RVCH Penetration FMEA

Level	Upstream Condition	Downstream Condition	Disposition	Evaluation				Expected Effect on SA	Status
				Type	Summary	References	SA Location		

Table B-1
Failure Path Disposition Table for RVCH Penetration FMEA

Level	Upstream Condition	Downstream Condition	Disposition	Evaluation				Expected Effect on SA	Status
				Type	Summary	References	SA Location		

Table B-1
Failure Path Disposition Table for RVCH Penetration FMEA

Level	Upstream Condition	Downstream Condition	Disposition	Evaluation				Expected Effect on SA	Status
				Type	Summary	References	SA Location		

Table B-1
Failure Path Disposition Table for RVCH Penetration FMEA

Level	Upstream Condition	Downstream Condition	Disposition	Evaluation				Expected Effect on SA	Status
				Type	Summary	References	SA Location		

Table B-1
Failure Path Disposition Table for RVCH Penetration FMEA

Level	Upstream Condition	Downstream Condition	Disposition	Evaluation				Expected Effect on SA	Status
				Type	Summary	References	SA Location		

Table B-1
Failure Path Disposition Table for RVCH Penetration FMEA

Level	Upstream Condition	Downstream Condition	Disposition	Evaluation				Expected Effect on SA	Status
				Type	Summary	References	SA Location		

Table B-1
Failure Path Disposition Table for RVCH Penetration FMEA

Level	Upstream Condition	Downstream Condition	Disposition	Evaluation				Expected Effect on SA	Status
				Type	Summary	References	SA Location		

Table B-1
Failure Path Disposition Table for RVCH Penetration FMEA

Level	Upstream Condition	Downstream Condition	Disposition	Evaluation				Expected Effect on SA	Status
				Type	Summary	References	SA Location		

Table B-1
Failure Path Disposition Table for RVCH Penetration FMEA

Level	Upstream Condition	Downstream Condition	Disposition	Evaluation				Expected Effect on SA	Status
				Type	Summary	References	SA Location		

Table B-1
Failure Path Disposition Table for RVCH Penetration FMEA

Level	Upstream Condition	Downstream Condition	Disposition	Evaluation				Expected Effect on SA	Status
				Type	Summary	References	SA Location		

Table B-1
Failure Path Disposition Table for RVCH Penetration FMEA

Level	Upstream Condition	Downstream Condition	Disposition	Evaluation				Expected Effect on SA	Status
				Type	Summary	References	SA Location		

Table B-1
Failure Path Disposition Table for RVCH Penetration FMEA

Level	Upstream Condition	Downstream Condition	Disposition	Evaluation				Expected Effect on SA	Status
				Type	Summary	References	SA Location		

C
FMEA TECHNICAL DISCUSSIONS

C.1 Materials and Effects on Cracking

C.1.1 Material Properties due to Thermal Processing

Content Deleted – MRP/EPRI Proprietary Material

Content Deleted – MRP/EPRI Proprietary Material

C.1.2 Defects due to Initial Material Processing

Content Deleted – MRP/EPRI Proprietary Material

C.1.3 Nozzle Roll Straightening During Material Processing

Content Deleted – MRP/EPRI Proprietary Material

Content Deleted – MRP/EPRI Proprietary Material

C.2 Fabrication and Effects on Cracking

Content Deleted – MRP/EPRI Proprietary Material

C.2.1 Stress Impact of Machining, Reaming, or Grinding of Nozzle ID or OD Surfaces

Content Deleted – MRP/EPRI Proprietary Material

Content Deleted – MRP/EPRI Proprietary Material

C.2.2 Defects Introduced by Nozzle ID Processing

Content Deleted – MRP/EPRI Proprietary Material

C.2.3 Weld Fabrication Flaws

Content Deleted – MRP/EPRI Proprietary Material

Content Deleted – MRP/EPRI Proprietary Material

C.2.4 Nozzle Straightening After Installation

Content Deleted – MRP/EPRI Proprietary Material

Content Deleted – MRP/EPRI Proprietary Material

C.2.5 Grinding of Weld During Head Fabrication

Content Deleted – MRP/EPRI Proprietary Material

C.2.6 Welding Residual Stresses

Content Deleted – MRP/EPRI Proprietary Material

Content Deleted – MRP/EPRI Proprietary Material

C.2.7 Fabrication Residual Stresses

Content Deleted – MRP/EPRI Proprietary Material

C.2.8 Lack-of-Fusion Flaws

Content Deleted – MRP/EPRI Proprietary Material

Content Deleted – MRP/EPRI Proprietary Material

Content Deleted – MRP/EPRI Proprietary Material

Table C-1
North Anna 2 CRDM Nozzle Lack-of-Fusion Indications, Fall 2002 UT Inspection

Penetration No.	*Circ. Extent (orient., deg.)*	*Circ. Extent (size, deg.)*	*Circ. Extent (size, in.)*	*Axial Extent (loc., in.)*	*Axial Extent (size, in.)*	*Approx. LOF Surf. Area (in^2)*	*LOF Surf. Area (% of Total)*
Content Deleted – MRP/EPRI Proprietary Material							

Content Deleted – MRP/EPRI Proprietary Material

Content Deleted – MRP/EPRI Proprietary Material

C.2.9 Surface Contaminants

Content Deleted – MRP/EPRI Proprietary Material

Content Deleted – MRP/EPRI Proprietary Material

Content Deleted – MRP/EPRI Proprietary Material

C.3 Water Chemistry and Effects on Cracking

Content Deleted – MRP/EPRI Proprietary Material

C.3.1 Typical Primary-Side Chemistry During Power Operation

Content Deleted – MRP/EPRI Proprietary Material

C.3.2 Impact of Hydrogen at Low Temperature

Content Deleted – MRP/EPRI Proprietary Material

C.3.3 Water Chemistry During Hot Functional Testing

Content Deleted – MRP/EPRI Proprietary Material

C.3.4 Impact of Reduced Sulfur Species on Sensitized Alloy 600

Content Deleted – MRP/EPRI Proprietary Material

Content Deleted – MRP/EPRI Proprietary Material

Content Deleted – MRP/EPRI Proprietary Material

Content Deleted – MRP/EPRI Proprietary Material

C.3.5 Lead Involvement in Causing PWSCC

Content Deleted – MRP/EPRI Proprietary Material

C.3.6 Conclusions on Water Chemistry

Content Deleted – MRP/EPRI Proprietary Material

Content Deleted – MRP/EPRI Proprietary Material

C.4 PWSCC

Content Deleted – MRP/EPRI Proprietary Material

C.4.1 Weibull Distributions for PWSCC Initiation

Content Deleted – MRP/EPRI Proprietary Material

Table C-2
Typical Values of Weibull Slopes for Steam Generator Tube PWSCC Based on Plant Data [C-40]

Type of PWSCC	*Number of Plants*	Weibull Slope		
		Median	*Average*	*Standard Deviation*
Content Deleted – MRP/EPRI Proprietary Material				

C.4.2 PWSCC Crack Growth

Content Deleted – MRP/EPRI Proprietary Material

Content Deleted – MRP/EPRI Proprietary Material

Content Deleted – MRP/EPRI Proprietary Material

C.4.3 PWSCC Location and Orientation

Content Deleted – MRP/EPRI Proprietary Material

Content Deleted – MRP/EPRI Proprietary Material

Table C-3
Summary of Industry Experience Regarding Circumferential Nozzle Cracking and Leakage

No.	Unit	NSSS Supplier	Number of Nozzles on Head				A. Leak OR Circ. Crack above or near Top of J-Groove Weld		B. Circ. Crack above or near Top of J-Groove Weld		Ratio B/A
			CRDM	CEDM	ICI	Total	No. Nozzles	Percentage	No. Nozzles	Percentage	
Content Deleted – MRP/EPRI Proprietary Material											

C.5 Fatigue

Content Deleted – MRP/EPRI Proprietary Material

Content Deleted – MRP/EPRI Proprietary Material

C.5.1 Plant Temperature and Pressure Changes

Content Deleted – MRP/EPRI Proprietary Material

C.5.2 Temperature Cycling Inside the CRDM Nozzle

Content Deleted – MRP/EPRI Proprietary Material

C.5.3 Mechanical Vibrations

Content Deleted – MRP/EPRI Proprietary Material

Content Deleted – MRP/EPRI Proprietary Material

C.5.4 Summary on Fatigue

Content Deleted – MRP/EPRI Proprietary Material

C.6 Low-Temperature Crack Propagation

Content Deleted – MRP/EPRI Proprietary Material

C.7 Nozzle Repair Reliability

Content Deleted – MRP/EPRI Proprietary Material

C.7.1 Embedded Flaw Repairs

Content Deleted – MRP/EPRI Proprietary Material

C.7.2 Application of a New Structural Weld in the Existing Nozzle

Content Deleted – MRP/EPRI Proprietary Material

Content Deleted – MRP/EPRI Proprietary Material

C.8 References

Content Deleted – MRP/EPRI Proprietary Material

Content Deleted – MRP/EPRI Proprietary Material

Content Deleted – MRP/EPRI Proprietary Material

Content Deleted – MRP/EPRI Proprietary Material

Content Deleted – MRP/EPRI Proprietary Material

Content Deleted – MRP/EPRI Proprietary Material

D
FLAW AND WASTAGE TOLERANCE CALCULATIONS

This appendix provides details regarding the flaw and wastage cavity tolerance calculations summarized in Section 3. Axial and circumferential nozzle flaws, circumferential "lack of fusion" type flaws at the interface between the nozzle and the J groove weld, and head wastage cavities are evaluated. The results presented below are indicative of the structural margin inherent in the general design of the reactor vessel closure head and its penetrations.

D.1 Limiting Crack Sizes in Nozzles and Welds

Presented below are calculations of the critical flaw size corresponding to the three types of RVCH penetration crack geometries of potential concern for producing a pressure boundary break:

1. an axial through-wall flaw in the nozzle above the J-groove weld,
2. a through-wall partial arc circumferential flaw above the J-groove weld, and
3. a circumferential flaw at the fusion line between the nozzle and the J-groove weld.

These types of flaws are illustrated in Figure D-1. In each case, the analysis will show the limiting flaw size with and without applying a safety factor of 2.7 on the standard design pressure loading of 2500 psi.[10] In safety assessments, such a safety factor may be applied to the critical crack size to add conservatism to deterministic evaluations of the time for hypothetical cracks to grow until a break of the primary pressure boundary is produced.

As discussed in Section 6, the limiting case is case 2, a through-wall circumferential flaw above the J-groove weld that potentially could grow to a sufficient size to cause net section collapse of the remaining nozzle ligament and nozzle ejection. Therefore, the calculation for case 2 has been performed to cover the specific nozzle geometry parameters applicable to the CRDM, CEDM, and ICI nozzles in the full set of 69 original reactor vessel closure heads. Calculations

[10] The safety factor of 2.7 for the calculations presented in Appendix D.1 is chosen based on the approach specified in Paragraph IWB-3644 of Section XI of the 2002 version of the ASME Boiler and Pressure Vessel Code [D-1] for evaluation of flaws in Service Level A austenitic or ferritic piping for continued service. Note that the calculations presented here are not applicable for acceptance of actual flaws for continued service because the current acceptance criteria for RVCH penetration flaws [D-2] are designed primarily to prevent pressure boundary leakage and the generation of loose parts. For example, the current acceptance criteria for RVCH penetration flaws [D-2] do not permit acceptance of circumferential flaws located in the nozzle wall at or above the J-groove weld, regardless of size. In addition, surface flaws of any size in the J-groove weld are not acceptable for continued service. Finally, note that the operating plants generally are required to use versions of Section XI of the ASME Code that are earlier than the 2002 edition. Therefore, the safety factor of 2.7 does not generally apply for plants that apply Section XI for evaluation of actual piping flaws for continued service on the basis of stress level.

for cases 1 and 3 have been performed for a typical CRDM nozzle geometry having an OD of 4 inches and an ID of 2.75 inches.

D.1.1 Axial Flaw in Nozzle Above J-Groove Weld

The limit pressure for a through-wall axial crack in a tube subjected to internal pressure loading is given by the EPRI *Ductile Fracture Handbook* [D-3] as follows:

$$P_{lim} = \sigma_f (t/R) / M$$

where,

P_{lim} = limit pressure = 2.7 × design pressure = 2.7 (2500 psi) = 6750 psi
σ_f = tensile flow stress = 0.5 ($\sigma_y + \sigma_u$)
σ_y = Alloy 600 yield strength at the design temperature of 650°F (ksi) [D-4]
σ_u = Alloy 600 tensile strength at the design temperature of 650°F (ksi) [D-4]
D_o = minimum nozzle outside diameter
D_i = maximum nozzle inside diameter
t = minimum nozzle wall thickness = $(D_o - D_i)/2$
R = nozzle mean radius = $(D_o + D_i)/4$
λ = $c/(Rt)^{0.5}$
c = half crack length
M = $[1 + 1.2987\,\lambda^2 - 2.6905\times10^{-2}\,\lambda^4 + 5.3549\times10^{-4}\,\lambda^6]^{0.5}$

Solving iteratively, an axial crack length of 5.1 inches results in a limit pressure of 6750 psi for the standard CRDM nozzle geometry (safety factor of 2.7). The corresponding length for a limit pressure of 2500 psi is considerably longer, 14.1 inches. It should be noted that this calculation is conservative since the amount of crack opening displacement will be limited by the fit of the nozzle in the hole in the vessel head.

D.1.2 Circumferential Flaw in Nozzle Above J-Groove Weld

The relatively tight fit of the nozzle in the vessel head will ensure that moment loads on the nozzle are low and that the limit load will be equal to the material flow stress acting on the remaining ligament. The calculation of the critical flaw size may be based on the design pressure, or a factor of safety of 2.7 on the pressure loading may be applied as discussed above. In the calculation below, it is assumed that the pressure load is applied to the crack face as well as the nozzle bore diameter:

$$P_{\lim} = \sigma_f \left[\frac{A_{wall}\left(1 - \frac{\theta}{360}\right)}{A_{bore} + A_{wall}\left(\frac{\theta}{360}\right)} \right]$$

where,

P_{lim} = limit pressure = safety factor × design pressure
σ_f = tensile flow stress = 0.5 ($\sigma_y + \sigma_u$)
σ_y = yield strength at the design temperature (ksi)
σ_u = tensile strength at the design temperature (ksi)

Solving for the crack angle θ that produces the limit pressure,

$$\theta = \frac{360\left[\sigma_f - P_{\lim}\left(\frac{A_{bore}}{A_{wall}}\right)\right]}{P_{\lim} + \sigma_f}$$

where,

θ = circumferential crack length (degrees)
A_{bore} = nozzle bore area = $\pi D_i^2/4$
A_{wall} = nozzle wall area = $\pi (D_o^2 - D_i^2)/4$

The minimum required ligament for structural integrity was calculated for the full range of CRDM, CEDM, and ICI nozzle dimensions and minimum material strengths. As noted above, because of the tight fitting annulus and of the high ductility of the nozzle materials, bending loads on the nozzle at the top of the vessel head, including seismic moments, will not affect the required minimum ligament.

Therefore, the required ligament is that which will withstand 1.0 or 2.7 times the design pressure acting on the nozzle bore and the crack face at flow stress levels in the ligament. For large crack sizes, the stress level may be calculated as the pressure force over the combined bore and crack face areas divided by the cross-sectional area of the ligament. For smaller size cracks, the maximum permissible pressure is limited by the burst pressure in cracked tubes rather than axial stress in the remaining ligament. The evaluation presented here is restricted to the methodology for large circumferential cracks because it is the axial stress in the ligament that controls the limiting crack size at 2.7 times design pressure.

The required inputs are the inside and outside nozzle diameters for the region immediately above the J-groove weld, the nozzle material minimum flow strength, and the design pressure for the various types of CRDM, CEDM, and ICI nozzles. The values of σ_y and σ_u for Alloy 600 nozzle material procured to ASME specifications SB-166 and SB-167 at the standard design temperature of 650°F are given in Section II of the ASME Boiler & Pressure Vessel Code [D-4]. As noted in the equations above and according to standard practice, the minimum nozzle flow strength is taken as the average of the minimum yield and ultimate tensile strengths. Note that these minimum strength values depend slightly on the material condition (e.g., hot-worked and annealed or cold-worked and annealed) and product size.

Figure 3-1 in Section 3 shows the results of the calculations for the limiting CRDM, CEDM, and ICI nozzles. The critical crack size for a limit load at 2.7 times the design pressure of 2500 psi varies from 195° for the limiting ICI nozzle, to 254° for the limiting CEDM nozzle, to 281° for

the limiting CRDM nozzle. The largest circumferential flaw above the J-groove weld detected in a plant of 165° (see Table 4-6) is significantly less than the calculated limit of 281° for a pressure of 2.7 times design pressure. Evaluated from a different perspective, the remaining ligament of 195° was 2.5 times the required ligament of 79°. Table D-1 shows the results of the calculation of the limiting flaw angle for the various types of CRDM, CEDM, and ICI nozzles, including identification of the limiting nozzle geometry for each basic type.

D.1.3 Lack of Fusion or Circumferential Weld Crack at J-Groove Weld Interface

The limiting area of lack of fusion between the nozzle and J-groove weld is calculated using the axial pressure load acting on the outside diameter of the nozzle and the allowable shear stress on the weld. Per standard practice [D-5], the weld flow shear stress is taken as 50% of the nozzle base material flow stress:

$$0.5\sigma_f = \frac{P_{\lim}\pi D_o^2 / 4}{\pi D_o H_{weld}\left[\frac{(360-\phi)}{360}\right]}$$

$$\phi = 360 - 180\left(\frac{P_{\lim} D_o}{\sigma_f H_{weld}}\right)$$

where,

H_{weld} = minimum height of J-groove weld at nozzle wall

ϕ = circumferential lack of fusion length (degrees)

A typical CRDM penetration geometry (OD of 4 inches and H_{weld} = 1 inch) will support the standard design pressure of 2500 psi given a circumferential area of lack of fusion between the weld and nozzle wall extending roughly 325° around the nozzle. Applying a factor of safety of 2.7 on the pressure loading, the typical CRDM penetration geometry will support a pressure of 6750 psi given a circumferential area of lack of fusion between the weld and nozzle wall extending roughly 265° around the nozzle.

D.2 Allowable Wastage Volume at Reactor Vessel Head CRDM Nozzles

The purpose of this calculation is to determine the volume of low-alloy steel that can be lost from the top surface of a reactor vessel head by boric acid corrosion without the stresses in the remaining material exceeding the ASME Code allowable values [D-4].

Safety analyses prepared by the NSSS vendors in the early 1990s showed that the head could loose about 6 in^3 of material and still meet ASME Code stress requirements [D-6,D-7,D-8]. These calculations were not directed towards determining the allowable material loss, but rather to confirm that about 6 in^3 of material loss is acceptable. The 6 in^3 volume was based on six

years of leakage with a material loss rate of about 1.07 in^3 per year determined from tests performed by Combustion Engineering [D-9].

D.2.1 Allowable Corrosion Volume Based on Finite Element Analysis

In support of this safety assessment document, finite element analyses of a typical PWR vessel head were performed to determine the amount of wastage that can be accommodated such that the head meets the ASME Code allowable primary membrane and primary membrane plus bending stress limits (which include the required safety factor). No credit was taken for the elastic-plastic characteristics of the low-alloy steel head base material or for the membrane pressure capability of unsupported cladding. These factors provide additional margin above that determined using normal elastic stress analysis methods.

The analyses were performed using the ANSYS finite element code; the model geometry for the vessel head as shown in Figure D-2. The model consists of a 1/8 symmetry sector of the vessel head including the head shell, all of the CRDM nozzles, and the vessel flange. Welding residual stresses were simulated by use of constraint equations between the nozzle OD surface and the shell in the region of the J-groove weld. Typical specified bolt preload was applied to the flange. Operating pressure was applied out to the inner o-ring sealing diameter, and operating temperature was applied to all elements.

Two conditions were evaluated. The first was a case similar to that which occurred at Davis-Besse nozzle #3, where a pool of borated water apparently developed on the top surface of the head between two nozzles and then corroded the low-alloy steel material from the top. The second was a hypothetical case where the corrosion occurs uniformly around a single nozzle.

D.2.1.1 Allowable Wastage Volume—Wastage Located Between Nozzles

Figure D-3 shows the elements on the top surface of the vessel head that were assumed to be lost due to wastage that occurs between two nozzles as was discovered at Davis-Besse nozzle #3. The elements selected for modeling the wastage were selected based on the actual shape of the Davis-Besse wastage.

Analyses were performed after removing each layer of material (3 layers of elements) except for the last layer. After each new volume of material was removed, ANSYS computed the primary membrane and primary membrane plus bending stress at a path through the center of the corroded ligament as shown in Figure D-3.

Figure D-4 shows the primary membrane (P_m) and primary membrane plus bending ($P_m + P_b$) stress through the center of the remaining ligament for increasing volumes of wastage. Also shown on this figure are the allowable membrane (S_m) and membrane plus bending ($1.5S_m$) stresses at a design temperature of 650°F.

These calculations show that the low-alloy steel head can lose approximately 150 in^3 of material and still meet the ASME Code allowables for primary membrane and membrane plus bending stresses.

D.2.1.2 Allowable Wastage Volume—Wastage Distributed Around Nozzle

A check calculation was made to confirm that wastage distributed between two adjacent nozzles in D.2.2.1 is more limiting than the case of wastage uniformly distributed around a nozzle.

Figure D-5 shows the location of the assumed wastage. Calculations were performed for the cases in which of one and two rows of elements adjacent to the nozzle are corroded respectively.

After each volume of material was removed, the primary membrane and primary membrane plus bending stresses at a path midway between two adjacent nozzles as shown in Figure D-5 were computed with ANSYS. Figure D-6 shows these stresses for the two volumes of wastage. Like Figure D-4, Figure D-6 includes curves for the allowable membrane (S_m) and membrane plus bending ($1.5S_m$) stresses at the 650°F design temperature.

These calculations confirm that the previous case of wastage located between two adjacent nozzles is conservative relative to wastage of the same volume of material uniformly distributed around a single nozzle.

D.2.2 Allowable Corrosion Volume for Other Head Designs

The finite element analyses described in this section are for the case of a typical PWR vessel head similar to the Davis-Besse head. These results are considered representative for other vessels as well since the design analyzed had a relatively high diameter to thickness (D/T) ratio and therefore relatively low margin of excess thickness over that required to meet the Code minimum wall thickness.

In summary, the above calculations show that all vessels should be able to accommodate wastage of up to about 150 in^3 and still meet ASME Code primary membrane and membrane plus bending stress requirements.

D.3 References

D-1. ASME Boiler and Pressure Vessel Code, Section XI, Paragraph IWB-3640 and Paragraph IWB-3644, July 1, 2002 Edition.

D-2. Letter from R. Barrett (NRC) to A. Marion (NEI) dated April 11, 2003, "Flaw Evaluation Guidelines." This document includes two enclosures: Enclosure 1: *Flaw Evaluation Guidelines and Acceptance Criteria for PWR Reactor Vessel Upper Head Penetration Nozzles*, and Enclosure 2: *Appendix A: Evaluation of Flaws in PWR Reactor Vessel Upper Head Penetration Nozzles*.

D-3. *Ductile Fracture Handbook*, EPRI, Palo Alto, CA: 1989. NP-6301-D.

D-4. ASME Boiler and Pressure Vessel Code, Section II – Material Properties and Section III – Division 1 – Subsection NB – Class 1 Components, July 1, 2002 Edition.

D-5. J. Lagerström, B. Wilson, B. Persson, W. H. Bamford, and B. Bevilacqua, "Experiences with Detection and Disposition of Indications in Head Penetrations of Swedish Plants," PVP-Vol. 288, *Service Experience and Reliability Improvement: Nuclear, Fossil, and Petrochemical Plants*, ASME, 1994.

D-6. *Safety Evaluation for B&W-Design Reactor Vessel Head Control Rod Drive Mechanism Nozzle Cracking*, BAW-10190P (Proprietary), BAW-10190 (Non-Proprietary), B&W Nuclear Technologies, May and June 1993.

D-7. *Safety Evaluation of the Potential for and Consequence of Reactor Vessel Head Penetration Alloy 600 ID Initiated Nozzle Cracking*, CEN-607, ABB Combustion Engineering Nuclear Operations, May 1993.

D-8. *Alloy 600 Reactor Vessel Head Adaptor Tube Cracking Safety Evaluation*, WCAP-13565, Rev. 1 (Proprietary and Non-Proprietary), Westinghouse Electric Corporation, February 1993.

D-9. *Boric Acid Corrosion Guidebook, Revision 1: Managing Boric Acid Corrosion Issues at PWR Power Stations*, EPRI, Palo Alto, CA: 2001. 1000975. pp. 4-54 to 4-56 (Test Reference M).

Table D-1
Critical Flaw Angles for Through-Wall Circumferential Nozzle Flaws

Nozzle Type	Nozzle Geometry	*OD* (in)	Flaw Angle θ for P_{flow} = 2500 psi (deg)	Flaw Angle θ for P_{flow} = 6750 psi (deg)	Limiting Nozzle of Type
CRDM	Westinghouse	4.000	330	285	
	CRDM		329	281	
	B&W CRDM	4.002	328	281	✓
CEDM	CE CEDM Type 1a	4.050	331	288	
	CE CEDM Type 1b	4.050	331	288	
	CE CEDM Type 2	3.850	323	268	
	CE CEDM Type 3/4	3.495	318	254	✓
	CE CEDM Type 5	4.275	334	293	
ICI	CE ICI Type 1	5.563	293	195	✓
	CE ICI Type 2	4.500	309	232	
	CE ICI Type 3	6.625	313	244	

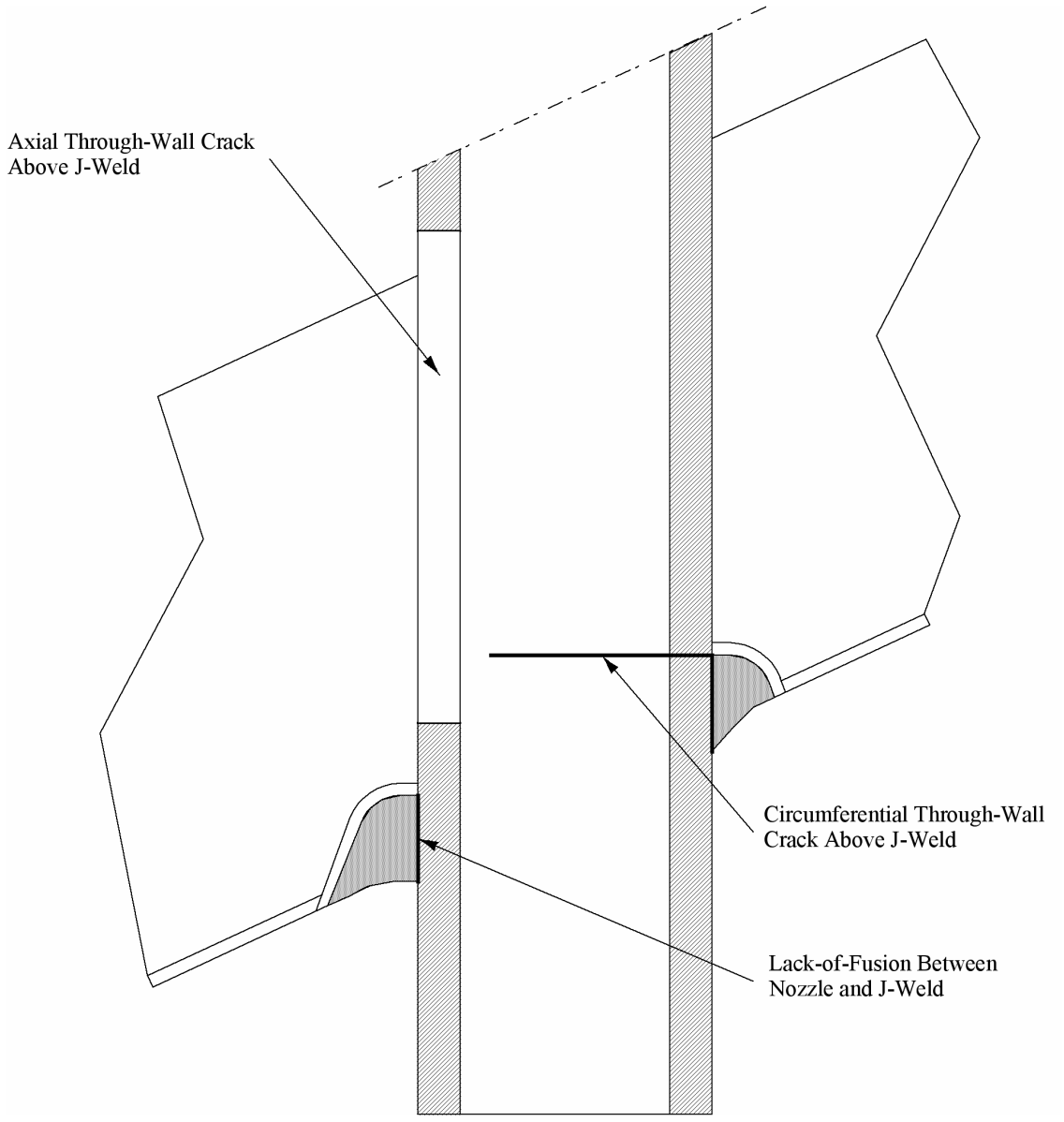

Figure D-1
Basic Flaw Orientations on a Typical CRDM Nozzle

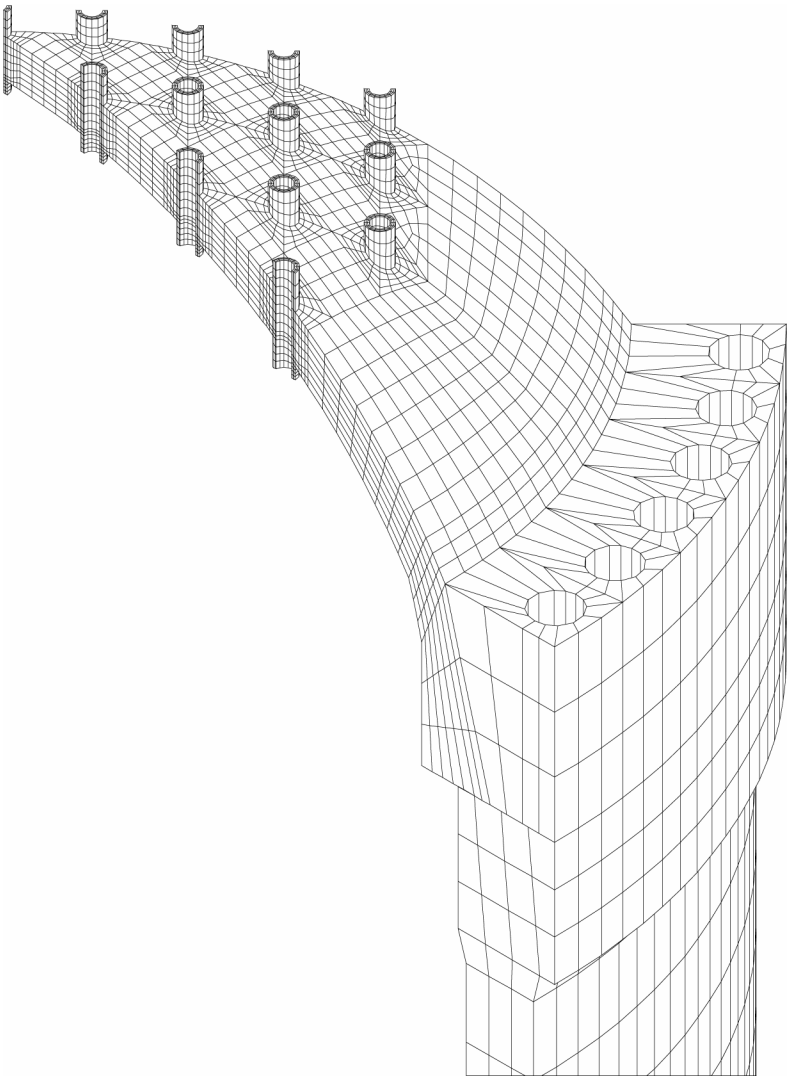

Figure D-2
Finite Element Model of Typical PWR Head Used for Allowable Wastage Volume Calculation

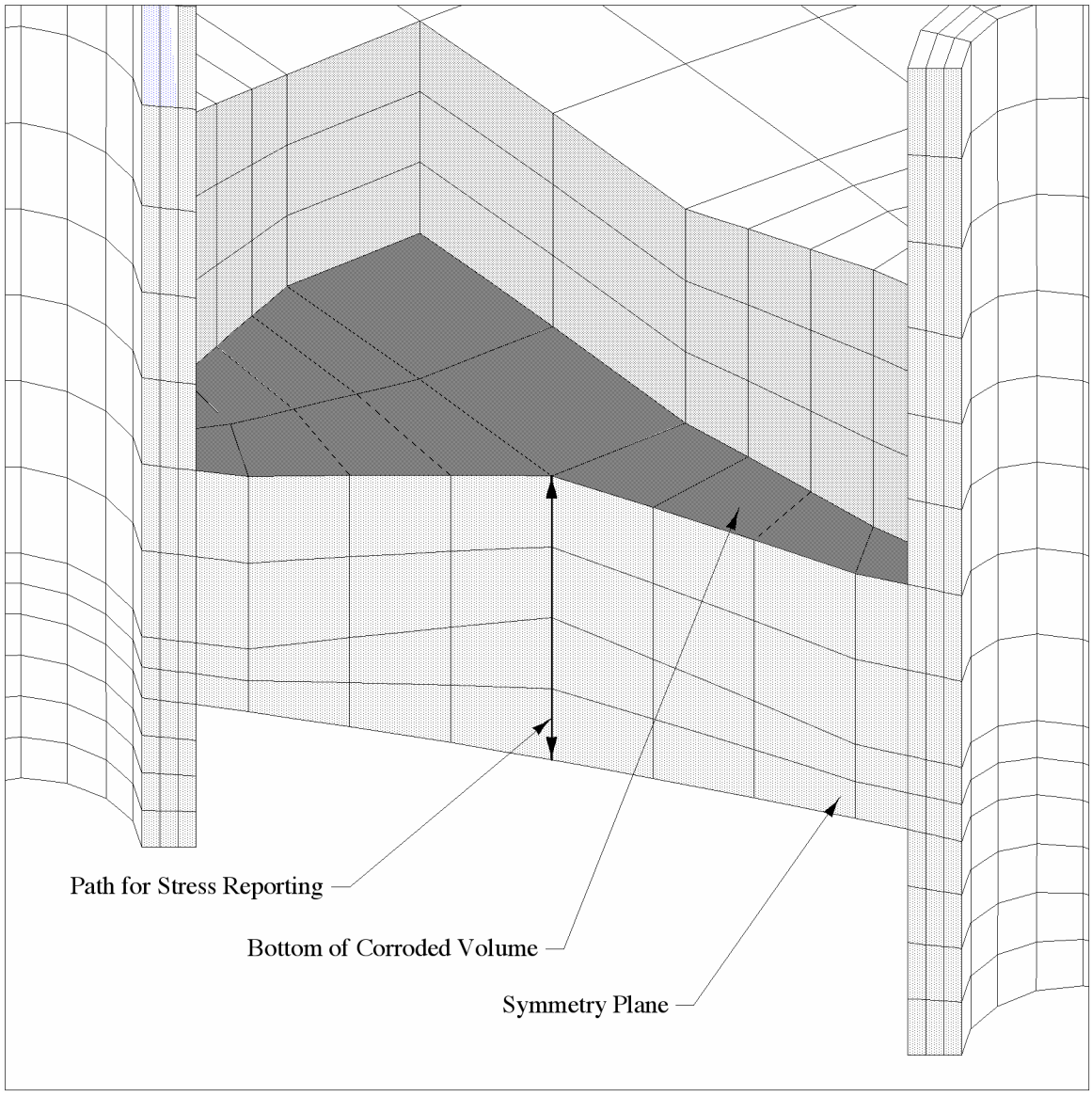

Figure D-3
Finite Element Model—Wastage Between Adjacent Nozzles

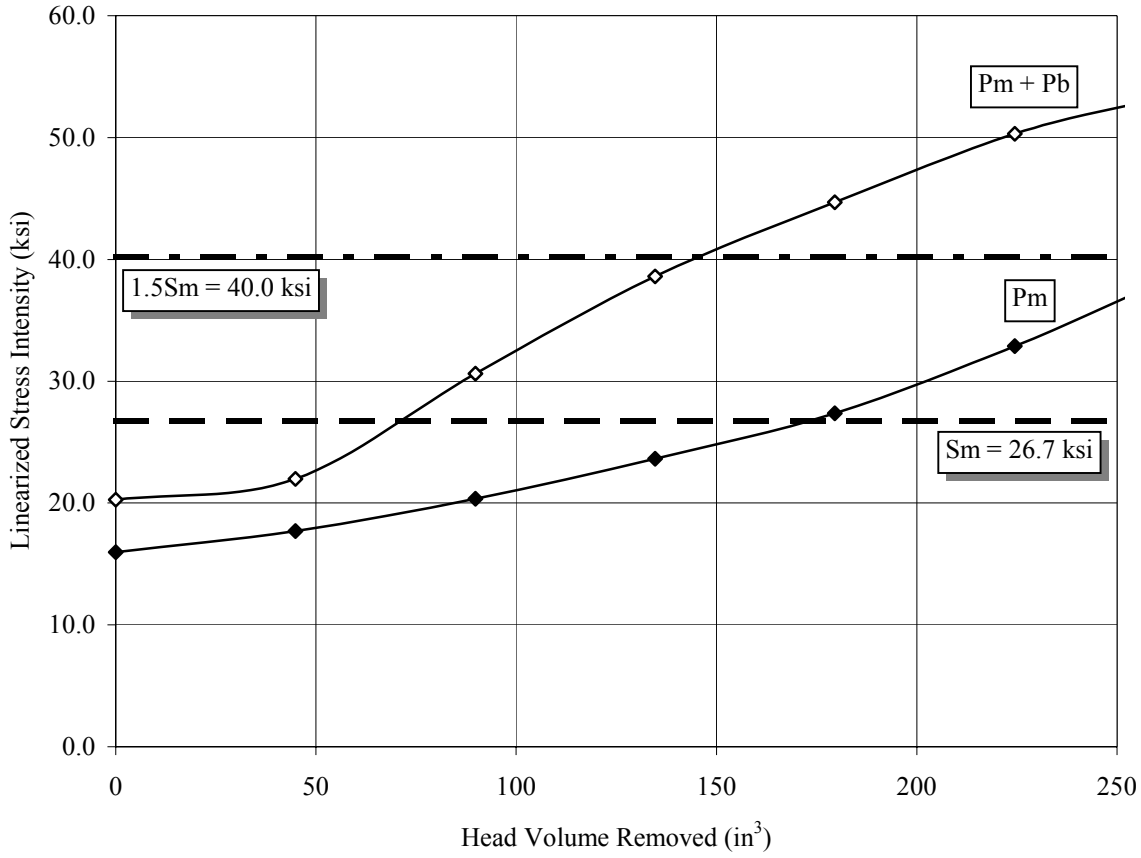

Figure D-4
Finite Element Analysis Results—Wastage Between Adjacent Nozzles

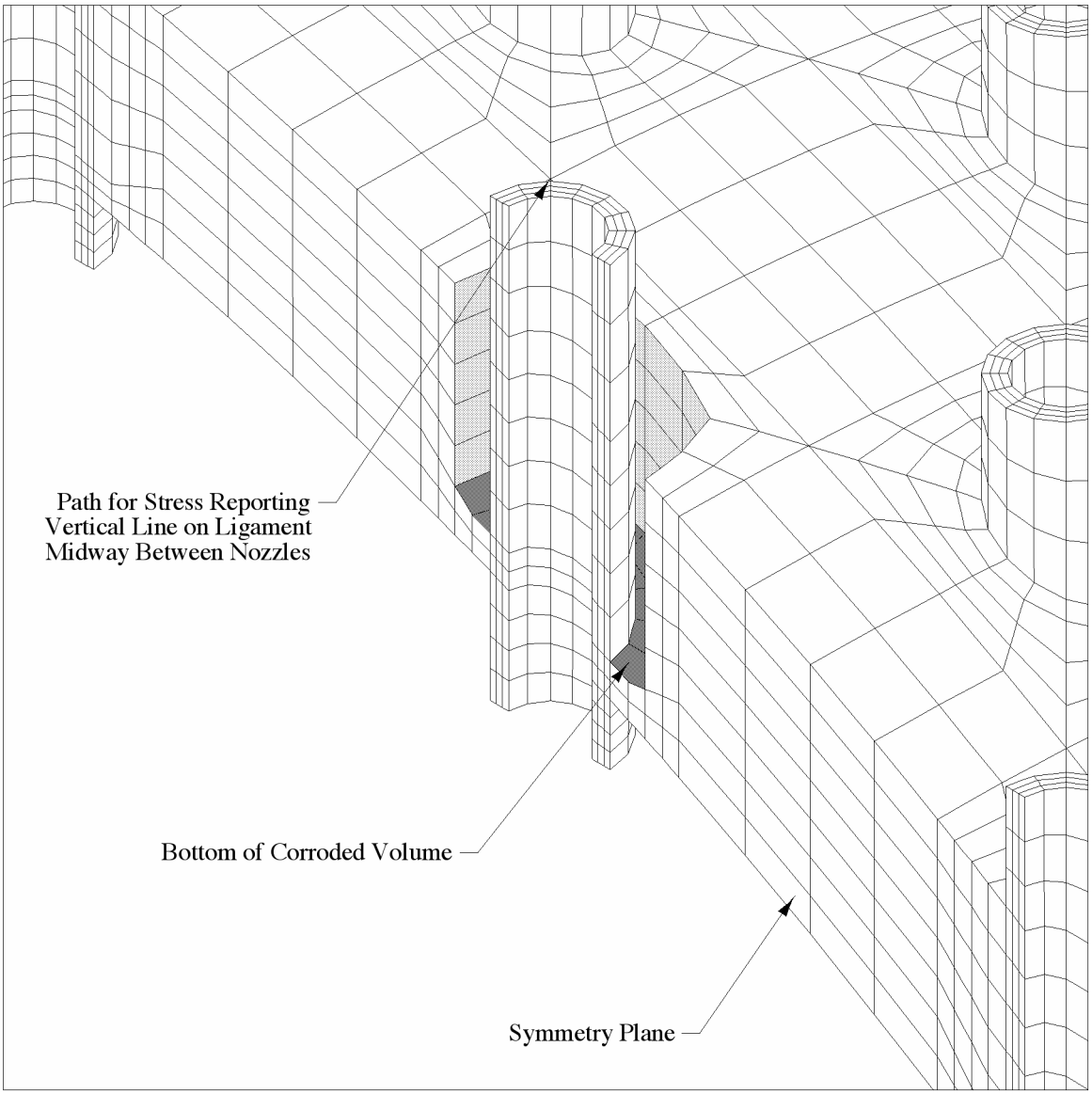

Figure D-5
Finite Element Model—Wastage Distributed Around Single Nozzle

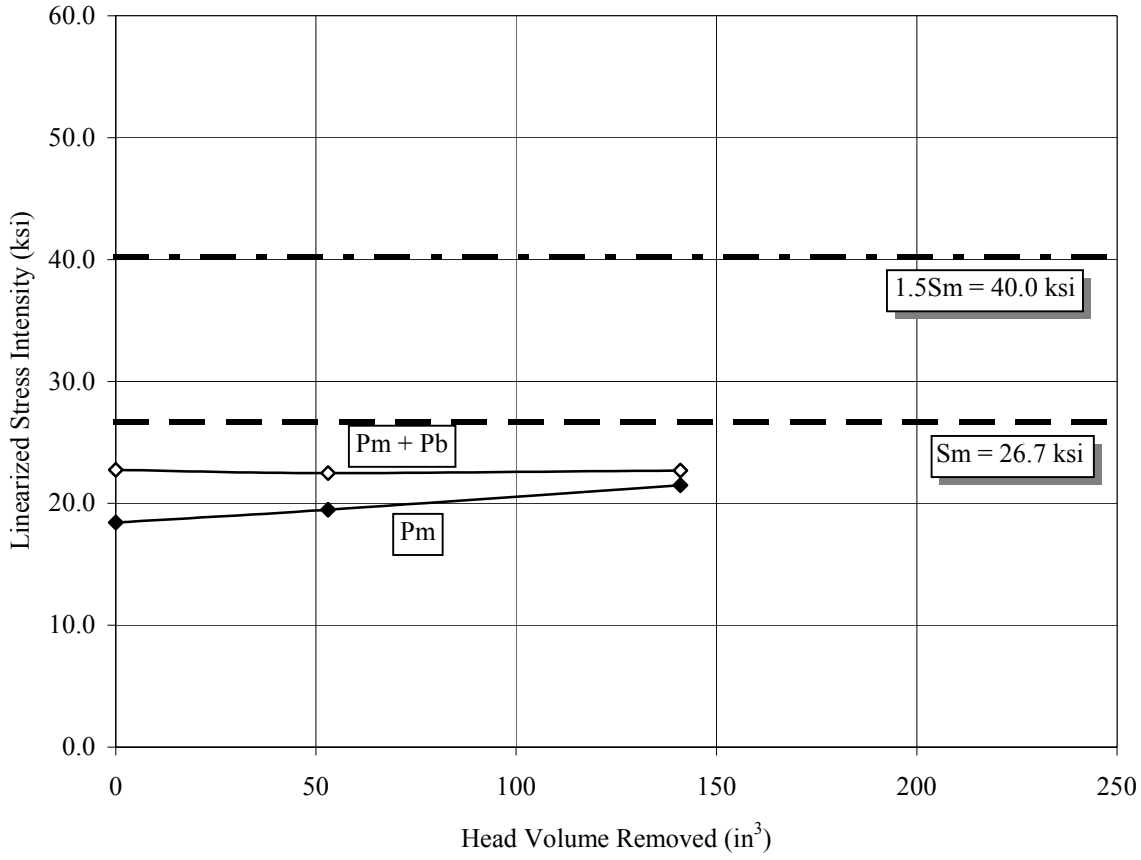

Figure D-6
Finite Element Analysis Results—Wastage Distributed Around Single Nozzle

E
MODELING OF HEAD WASTAGE PROCESS

This appendix describes deterministic and probabilistic models of the head wastage process, such as that observed at the Davis-Besse plant. These models support the conclusion that bare metal visual examinations performed at appropriate intervals provide adequate protection against wastage. Credit for the performance of periodic nonvisual examinations is not taken in the modeling. Rather, the modeling is conservatively predicated on the existence of a leaking CRDM nozzle.

E.1 Volume of Boric Acid Deposits Detectable by BMV Inspection

For this technical evaluation, it is assumed that the BMV inspections of the entire circumference of the RVCH penetration at the top surface of the head performed at a particular plant are only capable of detecting a volume of approximately 10 in^3 of boric acid deposits produced by a leaking CRDM nozzle. As documented in Section 4 and in EPRI report 1007842 [E-1], plant experience indicates that BMV inspections are capable of readily detecting boric acid deposit accumulations on the order of 0.5 in^3. The assumption that the BMV sensitivity is 20 times poorer allows for the possibility that a sizable fraction of the released boric acid deposits do not remain local to the intersection between the nozzle OD and the top head surface.

Given the density of solid boric acid crystals is 1.44 g/cm^3, the mass of boric acid deposits corresponding to a volume of 10 in^3 is 0.5 lbs, in comparison to the 900 lbs of deposits reported to be located on top of the head at Davis-Besse in 2002 [E-2]. For illustrative purposes, the 10 in^3 volume roughly corresponds to a 1/2-inch thick layer covering a ring approximately 6.4 inches across surrounding a 4-inch diameter nozzle. If concentrated at one point, the 10 in^3 volume would result in a sphere of boric acid crystals about 2.7 inches in diameter. For the probabilistic calculations, the detection limit is assumed to follow a triangular distribution with a lower bound of 5 in^3 and an upper bound of 20 in^3.

E.2 Volume of Boric Acid Deposits versus Leak Rate

Based on a simple mass balance, Figure E-1 shows the volume of boric acid deposits produced as a function of leak rate over the typical 1.5 years for one operating cycle. In this figure, an effective average boron concentration in the primary coolant of 750 ppm is assumed. In the context of the sensitivity of visual examinations for leakage, this concentration is a conservatively low value for the actual average over an operating cycle because the actual volume of boric acid deposits produced would be somewhat larger. Note also that Figure E-1 conservatively assumes no porosity for the accumulated boric acid deposits.

Also shown on this figure is the volume of boric acid deposits produced through leakage that is assumed to be detectable by a BMV inspection of the vessel head during a refueling outage. The boron mass balance calculation shows that a BMV inspection capable of detecting 10 in^3 of released deposits will detect a leak rate of about 2×10^{-5} gpm over a period of 1.5 years. For plants with a two year cycle, a greater amount of deposits would be produced for this leak rate, so the leakage would be more likely to be detected through visual examination. Note that the probabilistic evaluation presented below specifically considers the change in boron concentration over the fuel cycle.

E.3 Leak Rate to Produce Rapid Corrosion

The main conclusion of an analytical assessment of the Davis-Besse degradation performed by the MRP [E-3] is that local cooling to temperatures approaching the boiling point of water at atmospheric pressure (212°F) is a necessary condition for the rapid corrosion rates and large wastage volume observed at Davis-Besse to occur. Large local cooling creates the conditions for rapid corrosion by allowing aerated, concentrated boric acid solution to pool on the top head surface. Calculations have also shown that an aggressive chemical environment (e.g., low pH) is more likely to occur for solution temperatures approaching 212°F [E-3]. As discussed in Section E.6.2 below, the extent of local cooling is primarily a function of the leak rate. The leak rate is also the main driver for any erosion or flow accelerated corrosion mechanisms—to the extent that they may accelerate the boric acid chemical wastage—because the leak rate is the main factor that determines the magnitude of the flow velocities along the leak path. The crack width and length affect the local velocities near the exit of the crack, but the leak rate is still the key parameter since it can vary over several orders of magnitude.

There are three potential sources of information that are available for determining the minimum, or critical, leak rate that may lead to rapid corrosion. These are (1) the results of two sets of boric acid corrosion tests for leakage into an annulus, (2) the plant experience including Davis-Besse and leaking CRDM nozzles at other plants that produced little or no wastage, and (3) the results of a thermal analysis performed by the MRP and described in Section E.6.2 below. Unfortunately, several limitations in the two experiments (Test Series M and EPRI-6 in the EPRI *Boric Acid Corrosion Guidebook* [E-4], briefly described in Section 7.4) make application of the experimental data very difficult. Such limitations for one or both of the tests include a limited range of tested leak rates, lack of control and measurement of the thermal-hydraulic and chemical environments along the leak path, limited test length, lack of data on time dependence of corrosion rate, size of the initial annulus gap, and the nozzle orientation (down versus up for CRDM nozzles). After evaluation of all the available information for these two tests, it was decided to base the determination of the critical leak rate that leads to rapid corrosion on the MRP thermal analysis, with the plant experience as a consistency check.

As described above, the thermal analysis is based on an enthalpy balance for the leakage flow in combination with a three-dimensional finite element model of an reactor vessel head. This calculation shows that a leak rate of roughly 0.1 gpm is required to permit pooling of concentrated boric acid solution on the top head surface. This value is consistent with the Davis-Besse root cause report [E-2], which indicates that the leak rate through nozzle #3 at the time of the adjacent rapid corrosion was likely in the range of 0.04 to 0.2 gpm. On the other hand, little

(i.e., less than 1 in^3) or no wastage has been reported for the 48 detected leaking CRDM nozzles at U.S. plants other than Davis-Besse, despite the direct inspection of the lower section of the annulus made possible by the repair process used for the large majority of these nozzles (see paragraph 7.4 and Table 7-1). This experience is also consistent with the 0.1 gpm value for the critical leak rate since the volume of boric acid deposits associated with all the leaking CRDM nozzles other than those at Davis-Besse indicates leak rates much lower than 0.1 gpm, typically on the order of 1 gallon per year or 2×10^{-6} gpm.

Therefore, a leak rate of 0.1 gpm is used in the deterministic calculation as the critical leak rate that produces rapid corrosion. The deterministic evaluation presented below is based on the time for the leak rate to increase from that which is detectable by a BMV inspection to the critical value of 0.1 gpm. The probabilistic calculation uses 0.1 gpm for the nominal critical leak rate, but also uses a corresponding lower bound of 0.02 gpm to account for uncertainties in the thermal analysis as well as those related to the role of molten boric acid, which may retain some moisture even at atmospheric pressure and temperatures significantly higher than 212°F (e.g., 450°F) [E-3].

E.4 Deterministic Evaluation Based on Crack Growth Rate

The deterministic evaluation is based on the time for the leak rate to increase from the level that is detectable over a single cycle (2×10^{-5} gpm) to the estimated leak rate that is necessary for rapid corrosion (0.1 gpm). Based on plant experience and leakage modeling work, the primary driver for the increase in leak rate is the length of the nozzle crack above the top of the J-groove weld.

The left side of Figure E-2 illustrates the fundamental industry experience with leakage through CRDM nozzles. Inspections of nozzles with reported small amounts of leakage (order of 1 gallon per year or 2×10^{-6} gpm) have shown that the lengths of deep axial cracks in these nozzles tend to be in the range of 0.25 to 0.6 inch above the top of the J-groove weld. There is no report of any of these leaks resulting in significant corrosion (e.g., greater than 1 in^3) (see paragraph 3.9). On the other hand, the crack at Davis-Besse opposite the large wastage cavity extended 1.3 inches above the top of the weld and was through-wall over most of the crack extension above the top of the weld. This crack produced a best-estimate leak rate of 0.15 gpm based on the Davis-Besse root cause report [E-2].

The results of leakage modeling work for Davis-Besse are presented in Figure E-3, which shows the predicted leak rate as a function of the crack length above the top of the weld. This figure was originally published in the Davis-Besse root cause report [E-2], and this work was extended to show that the effect of the flow resistance of the annulus is small after the initially tight annulus opens slightly (e.g., by a few thousandths of an inch). This work was presented to the NRC staff on May 22, 2002, and repeated at the 2002 MRP Boric Acid Corrosion Workshop [E-3]. Pages 17 and 18 of the root cause report [E-2] describe the methodologies used, including (1) either an analytical model for a through-wall axial crack in a pipe (Zahoor) or a custom finite element analysis for calculation of the crack opening displacement (COD) in a CRDM nozzle with welding residual stresses, and (2) the methodology for predicting leak rate as a function of COD and crack opening area (COA) developed by Laborelec for leaks through PWSCC cracks

in steam generator tubes.[11] However, these models do not predict the low leak rates observed for cracks extending on the order of 0.5 inch above the top of the weld. This may at least partially be due to the actual through-wall crack profile, for which data are not readily available except for Davis-Besse [E-5]. A highly uneven through-wall profile would tend to decrease the flow area through the crack compared to the case of an even through-wall profile having the same extent above the weld by reducing both the COD and the crack length on the nozzle ID. Another factor not well captured by the leakage models is the initially tight, three-dimensional intergranular crack structure and its potential clogging by particulates in the primary coolant or boric acid deposits.

Given the above difficulties in directly applying the leakage models, the empirical leak rate curve shown in Figure E-4 was developed to predict the leak rate as a function of axial crack extent above the top of the weld. The power-law shape of the curve was chosen based on the shape of the curves in Figure E-3. Figure E-4 predicts that about 0.65 inch of axial crack growth would be required for the leak rate to increase from the rate that produces detectable leakage over one 18-month operating cycle (2×10^{-5} gpm) to the rate that may produce rapid top-down corrosion, the critical leak rate (0.1 gpm). Note that the unavailable profiles for the cracks that extended about 0.5 inch above the top of the weld, but produced low leakage, are a potential source of conservatism for the evaluation because the average distance traveled by the crack front is greater than 0.65 inch for the case of an initially uneven crack front.

The final step in the deterministic evaluation is to calculate the time for the crack to grow the 0.65 inch in the axial direction cited above. For this purpose, the standard methodology that assumes that the crack growth rate follows a power-law dependence to the crack tip stress intensity factor is assumed [E-6]. In addition, a uniform through-wall crack profile is assumed as shown on the right side of Figure E-2. Calculations for the Davis-Besse penetrations have shown that the stress intensity factor for such cracks growing axially above the top of the J-groove weld is in the range of 40–70 ksi√in (44–77 MPa√m) for crack lengths of 0.5 to 1.3 inches above the top of the weld. For the analyses performed here, a conservative value of 80 MPa√m (73 ksi√in) was used to account for the possibility of plant-to-plant variability for this parameter. Figure E-5 shows that, for this stress intensity factor of 80 MPa√m and the deterministic MRP crack growth rate curve developed in report MRP-55 [E-6],[12] it would take about 2.0 EFPYs at a head temperature of 602°F for a crack to grow the 0.65 inch cited above, and 1.9 EFPYs at a head temperature of 605°F. Therefore, the deterministic evaluation shows that performing BMV inspections during each refueling outage (i.e., conservatively every 1.5–2.0 EFPYs) is sufficient to prevent the rapid top-down corrosion mode from occurring (assuming a leaking nozzle), except in the case of plants having a head temperature greater than 602°F. However, in the case of a head temperature at the maximum U.S. value of 605°F and a refueling outage interval of 2.0 EFPYs, only about 0.1 EFPYs of rapid corrosion is predicted to occur, which would not be

[11] For reference, the Laborelec methodology [E-11] predicts a leak rate of about 0.054 gpm for an axial crack having a length of 1.0 inch and an average crack opening displacement (crack width) of 0.001 inches.

[12] No multiplicative factor was applied to increase the crack growth rate to account for uncertainties in the exact composition of the local chemical environment at the crack tip. The potential accelerating effect of the chemical environment at the crack tip being more aggressive than normal specification primary water tends to be balanced by not taking any credit for the reduced temperature at the crack tip caused by the two-phase expansion cooling for relatively high leak rates.

expected to produce a wastage volume approaching the 150 in^3 allowable limit calculated in Appendix D.

It should be noted that the preceding evaluation considers the leak rate that results from leak-path cracks in the Alloy 600 base metal material. Leaks can also result from cracks in the Alloy 182 weld metal material. Such cracks can potentially have either a radial-axial or a circumferential orientation. Radial-axial weld cracks in the absence of accompanying nozzle cracking are expected to result in relatively small leak rates based on the small flow area at the intersection between the weld material and the bottom of the annulus. Such small leak rates are expected to be insufficient to cause the local cooling that is required to produce rapid corrosion.[13] Circumferential weld cracks cannot be ruled out, and such flaws have been observed in CRDM penetration welds. However, these cracks and resultant leaks resulted in no reported significant low-alloy steel wastage.[14] The probabilistic evaluation presented below—through its large tolerance bands for many of the input parameters such as the crack growth rate power-law constant *A*—is considered to address the possibility of leaks from circumferential weld cracks.

E.5 Probabilistic Evaluation Based on Monte Carlo Wastage Model

The probabilistic wastage model takes the same basic form as the deterministic model—the leak rate increase is driven by axial crack growth in the nozzle until cooling is sufficient to cause rapid corrosion—but allows the key inputs to take on distributions of values. The flow chart in Figure E-6 shows the basic approach of the probabilistic model, which is described in detail in Section E.6 below. The probabilistic wastage model explicitly calculates the volume of wastage as the leak rate increases from zero to values greater than the critical leak rate and also the volume of boric acid deposits produced over time.

The wastage cavity progression assumed in the model is based on the Davis-Besse experience [E-2,E-7] in combination with the analytical results that show the potential for aerated, concentrated boric acid solutions to pool on the top head surface at relatively high leak rates. Figure E-7 shows the assumed progression through three stages of growth:

- Stage 1: Radial growth of the annulus
- Stage 2: Top-down growth on top head surface
- Stage 3: Outward growth after the cladding is exposed

The tapered shape of the cavity at the top head surface is strong evidence that the top-down mode dominated most of the material loss at Davis-Besse. As the top-down corrosion mode initiated, the wastage cavity became large enough to hold the boiling effluent, and subsequently the edges of the liquid pool receded back toward the leaking nozzle as the cavity grew down, the

[13] The Davis-Besse destructive examination work [E-7] revealed a radial-axial crack through most of the weld cross section at the circumferential position of the long axial nozzle crack that was centered on the large wastage cavity adjacent to Nozzle #3. This crack may have acted to increase the leak rate.

[14] The MRP has initiated a program to investigate the crack morphology and extent of wastage for several of the cracked North Anna 2 penetrations through destructive examinations of the replaced North Anna 2 head. Most of the North Anna 2 penetrations were reported to have weld flaws, including circumferential weld flaws, based on the results of nondestructive inspections at the plant.

result being the tapered appearance at the edges of the top of the cavity. The horizontal striations for the large Davis-Besse wastage cavity shown in Figure E-8 are further evidence of a top-down corrosion progression. Moreover, the closure head wastage experience at Turkey Point in 1986 [E-4] and Beznau in 1970 [E-8] demonstrates that the top-down corrosion mode can occur when concentrated boric acid solution pools on the top head surface (see paragraph 7.4). Unlike at these two plants, the Davis-Besse corrosion, which resulted from nozzle leakage rather than leakage from mechanical joints located above the head, was allowed to continue until the cladding was uncovered.[15]

The corrosion rate at which the cavity grows—on the active portion of the annulus area for Stage 1 growth or on an assumed area of the top head surface for Stage 2 growth—was developed using the model shown in Figure E-9. This figure shows the nominal dependence of the wastage rate in inches per year as a function of leak rate. Note the assumed upper shelf behavior for leak rates greater than the critical value. The exponential behavior in wastage rate shown in the figure was assumed based on the premise that the corrosion rate accelerates nonlinearly as the degree of local cooling increases. However, the results of the model are not very sensitive to the form of the assumed curve linking the values for WR_{low} and WR_{crit}. At each time step, the probabilistic model calculates the incremental volume of material corroded using the current wastage rate and the assumed geometry of the growing cavity. Figure E-10 illustrates the assumed cavity geometry and also compares the model geometry progression with that believed to have characterized the large Davis-Besse cavity.

The results of the probabilistic wastage calculation are shown in Figure E-11. This figure shows the cumulative distribution function of the cavity size at the time of detection, either through observation of boric acid accumulation during a BMV inspection or by the leak rate exceeding the typical technical specification limit of 1.0 gpm for unidentified primary leakage. For example, there is a 95% probability that the wastage cavity adjacent to a leaking CRDM nozzle will have a volume less than 23 in^3 for a head operating at 605°F given a program of BMV inspections performed every refueling outage at 1.5 EFPY intervals. This compares to the allowable wastage volume to maintain ASME Code margins of about 150 in^3 as shown in Appendix D. The model shows that the probability of the wastage cavity size exceeding the allowable wastage volume of about 150 in^3 is less than 1×10^{-4} for both 1.5 and 2.0 EFPY cycles given a head temperature of 605°F. Therefore, a BMV inspection at each outage will ensure that Code margins are maintained with high confidence, even given the assumption of a leaking nozzle and not taking credit for nonvisual examinations. Note that the probabilistic wastage model predicts that there is about a 90–95% probability that the wastage cavity would be detected during a BMV inspection, as opposed to through the unidentified leak rate exceeding the typical technical specification limit for leakage of 1.0 gpm.

The probabilistic analysis does not specifically address the issue of corrosion volumes associated with two adjacent nozzles merging. However, because the probabilities involved are so low, the probability of a combination of such events is negligible. For example, the probability of wastage exceeding 75 in^3 in 2.0 EFPYs is approximately 0.01. Therefore, the probability of two

[15] Previous leakage from CRDM flanges located above the Davis-Besse head cannot be ruled out as an aggravating factor in the wastage process, and the pre-existing deposits certainly complicated interpretation of the visual inspection results at this plant.

volumes exceeding 75 in^3 each, such that the combined volume exceeded 150 in^3 would be $(0.01)^2$ or 1×10^{-4}. This simple analysis is conservative in that it neglects the low probability that two adjacent nozzles would both leak and that both wastage volumes would grow toward each other (rather than in the same direction or away from each other).

Finally, it should be noted that there are several factors that may tend to make the probabilistic evaluation described above conservative, i.e., predict a greater wastage volume than would actually be expected:

- The probabilistic evaluation is based on a simulation of a single leaking CRDM nozzle. At the inception of the simulation, the modeled axial crack has just reached the annulus on the nozzle OD, meaning the nozzle has just begun to leak. The current programs of baseline and repeat nonvisual nondestructive examinations that are being implemented for all heads are expected to significantly reduce the future frequency of reactor vessel head nozzle leakage.
- The wastage model does not take credit for any nonvisual nondestructive examinations that are performed. The model assumes that the only methods for detecting wastage are through BMV inspection or the unidentified leakage rate exceeding 1.0 gpm.
- The simulation uses the typical technical specification limit of 1.0 gpm for triggering of plant shutdown based on on-line leak detection. In practice, it is expected in the future that unidentified leak rates significantly less than 1.0 gpm would trigger corrective action and that other plant indications such as clogging of the containment air coolers would also trigger corrective action soon after the leak rate reaches 0.1 gpm [E-2].

E.6 Description of the Probabilistic Wastage Model

One approach for evaluating the potential for wastage due to a leaking reactor vessel head nozzle is a deterministic calculation. However, a probabilistic approach allows the uncertainties associated with the inputs to be fully considered. The end product of the probabilistic wastage model presented here is the statistical distribution of wastage cavity size at the time that the cavity is detected. Detection of the cavity is assumed to be either by observation of boric acid crystal accumulation during a bare metal visual (BMV) inspection or by the unidentified leak rate exceeding the typical technical specification limit of 1.0 gpm, triggering a search for the source of the leakage. This section describes the Monte Carlo probabilistic wastage model for a single leaking CRDM nozzle. The section is organized as follows:

- E.6.1 WASTAGE MODEL BASICS. Describes the steps used to connect the growth of a postulated axial crack extending above the top of the CRDM nozzle J-groove weld to the resultant wastage rate and wastage cavity volume.
- E.6.2 LEAK RATE TO PRODUCE RAPID CORROSION BASED ON THERMAL ANALYSIS. Briefly describes the thermal analysis used to determine the extent of local cooling due to vaporization of the effluent. The extent of local cooling is the key parameter determining the potential for rapid corrosion.
- E.6.3 STATISTICAL DISTRIBUTIONS USED FOR INPUTS. Defines the parameters of each statistical distribution used to model the inputs necessary for calculating the wastage rate and inspection sensitivity.

- E.6.4 MONTE CARLO CALCULATIONS. Summarizes the steps used to calculate the wastage volume associated with a range of confidence levels (e.g., volume of wastage for which 95% of the trials yielded a smaller result).

E.6.1 Wastage Model Basics

This section describes the basic calculation sequence used to estimate the extent of wastage at any particular point in time. In particular, the following steps are used:

- Predict the crack growth for an axial crack extending above the top of the CRDM J-groove weld. Crack growth rates are calculated using the standard power-law expression $\dot{a} = A(K - K_{th})^n$ where A, K_{th}, and n are constants and K is the crack tip stress intensity factor. The constant A is modified using a standard thermal activation energy having a nominal value of 31.0 kcal/mole to account for the effect of head temperature. Because of uncertainties associated with the chemical environment on the nozzle OD for relatively high leak rates, it is conservatively assumed that the local cooling due to the leakage does not reduce the rate of crack growth. No multiplicative factor is applied to increase the crack growth rate to account for uncertainties in the exact composition of the local chemical environment at the crack tip.
- Predict the associated leak rate as a function of the crack length above the weld. Past predictions based on crack opening area and displacement (finite element analysis or EPRI algorithm for an axial crack in a pipe) have tended to overpredict leakage for small cracks based on industry experience. Hence, an empirical curve based on available plant data for CRDM nozzles was developed for this model (Figure E-4).
- Predict the wastage rate as a function of the leak rate. This model is based on two key inputs:
  - The estimated critical leak rate, LR_{crit}, which results in sufficient head cooling to permit concentrated liquid over a significant region of the top head surface, where the presence of the aerated, concentrated boric acid solution may lead to relatively high corrosion rates. The nominal value for LR_{crit}, 0.1 gpm, is correlated with a nominal wastage rate of 2.5 in/yr based on the Davis-Besse experience and laboratory testing.
  - A baseline low rate, LR_{low}, of 0.001 gpm, which produces relatively little local cooling, is correlated with a wastage rate of 0.072 in/yr, a conservative value based on the testing reported in the EPRI *Boric Acid Corrosion Guidebook* [E-4] for deaerated and low-oxygen, concentrated boric acid solutions.
- For leak rates below LR_{low}, a linear relationship starting at zero leak rate and zero wastage rate is assumed. For rates between LR_{low} and LR_{crit}, the profile is assumed to follow an exponential relationship reflecting the role of increased cooling on corrosion rates. This is illustrated in Figure E-9. For leak rates above LR_{crit}, the constant upper shelf wastage rate, nominally 2.5 in/yr, is assumed. This behavior may be conservative since higher leak rates could tend to "wash" the corrosion sites of the most concentrated boric acid.
- Compute the associated wastage volume (loss of material). This is modeled in the following fashion, as shown in Figure E-10:

- Stage 1: The initial wastage "front" (exposed area being wasted) is assumed to be a region of the CRDM nozzle penetration hole extending up from the top of the weld a distance equal to one fourth of the total distance to the top head surface and over an arc extending a total of 30°. The active corrosion area is assumed to increase in height at four times the wastage rate and circumferential extent at twice the wastage rate on each side. The maximum circumferential extent of the wastage front is assumed to be 180°. The assumed size of the penetration hole inside diameter is the standard value of 4.0 inches, and the assumed annulus height from the top of the weld to the top head surface is 5.8 inches.
- Stage 2: Once the leak rate reaches LR_{crit}, there is assumed to be sufficient cooling to permit concentrated boric acid solution to cause wastage at the top surface of the head. Based on the Davis-Besse experience [E-2,E-7], an area measuring 7 inches by 3.5 inches, with the leaking nozzle located at one end, is assumed to be subject to wastage at the upper shelf wastage rate WR_{crit} once LR_{crit} is reached. The model assumes that this top-down mode causes additional volume loss independent of the amount of material corroded during Stage 1.

  Note that the results of the probabilistic wastage model are relatively insensitive to the assumption of a top-down progression in Stage 2 versus continued radial growth of the cavity at the upper shelf wastage rate. Under this alternative progression, rapid corrosion would begin once the annulus opens up to the point that oxygen can penetrate deep into the cavity. However, the rate of material volume loss would be similar because half the surface area of the low-alloy steel bore is comparable to the assumed 25 in^2 (7 by 3.5 inches) area for the top-down corrosion front.
- Stage 3: Once the top-down corrosion mode removes material all the way down to the inside surface cladding, additional material loss is assumed to occur at the WR_{crit} wastage rate on the sides of the cavity. The assumed head thickness in the model is 6.4 inches.

- The wastage volume at the time of detection is recorded. As mentioned, detection may be by observation of boric acid accumulation during a BMV inspection or by the leak rate exceeding the typical technical specification limit for the unidentified leak rate, 1.0 gpm. The volume of boric acid (H_3BO_3) deposits produced by the leaking primary water is calculated using a boron mass balance assuming that the boron concentration in the primary water decreases linearly from 1500 ppm at the start of the cycle down to 0 ppm at the end of the cycle. This assumed dependence of boron concentration versus time produces a conservatively low estimate of the volume of deposits produced because the actual volume of deposits would be greater and thus more easily detected.

Later sections of this appendix describe how this calculation methodology is incorporated in a Monte Carlo probabilistic analysis.

E.6.2 Leak Rate to Produce Rapid Corrosion Based on Thermal Analysis

Large local cooling creates the conditions for rapid corrosion by allowing an aerated, concentrated boric acid solution to pool on the top head surface. Calculations have also shown

that an aggressive chemical environment (e.g., low pH) is more likely to occur for solution temperatures approaching 212°F [E-3]. The extent of cooling along the leak path is primarily a function of the leak rate since the rate of heat transfer required to completely vaporize the effluent is directly proportional to the leak rate. Therefore, an analysis was performed to determine the extent of cooling as a function of leak rate [E-3].

Using a simple enthalpy balance, Figure E-12 shows the size of the effluent heat sink produced as a function of the leak rate and the steam quality or superheat of the escaping steam. The assumption in this figure of atmospheric pressure for the exiting flow is based on two-phase pressure drop calculations that have shown that early in the cavity growth progression the pressure in the cavity becomes nearly atmospheric pressure [E-3]. For leaking primary water at 600°F, 45% of the effluent mass will flash to steam without any heat input. Heat input from the head material to the effluent will act to increase the quality to saturated conditions and then superheat the steam back to a temperature of 600°F.

The second step in the thermal analysis was to construct a finite element model of an example head and apply thermal boundary conditions including a uniform heat sink on a 45° or 90° arc surface on the OD of a CRDM nozzle along a postulated leak path. Figure E-13 shows an example temperature field resulting from this analysis for the case of a total 45° arc surface heat sink with a magnitude of 1860 Btu/h. This size heat sink corresponds to complete vaporization of a 0.007 gpm leak. Figure E-14 summarizes the results of several such finite element cases by showing the average metal surface temperature in the annulus along the leak path as a function of heat sink magnitude.

The results of the thermal analysis were applied as follows. For a leak rate of 0.001 gpm, Figure E-12 shows that a heat sink of roughly 300 Btu/h would be expected for complete effluent vaporization. Then Figure E-14 shows that the extent of cooling would be expected to be relatively minor, on the order of 10°F. For a leak rate of 0.01 gpm and the corresponding heat sink of 3000 Btu/h, the extent of cooling is calculated to approach 100°F, still not enough cooling to support a liquid pool developing on the top head surface. On the other hand, a leak rate of 0.1 gpm is calculated to be sufficient to cool the local metal surface to temperatures below the boiling point of water at atmospheric pressure (212°F). Since cooling below this temperature cannot be supported, the actual heat sink magnitude in the annulus region must be less than that corresponding to complete effluent vaporization. In this case, the steam quality exiting the annulus would be less than 100%, indicating possible development of a liquid pool on the top head surface.

E.6.3 Statistical Distributions Used for Inputs

Due to inherent uncertainties, many of the variables on which the potential wastage depends are better represented by statistical distributions rather than by single values. The use of appropriately chosen statistical distributions allows the possibility for unlikely, extreme values to be accounted for in a quantitative fashion. All variables used to compute wastage are assigned one of three types of statistical distribution, listed below along with the corresponding probability density function $f(x)$:

UNIFORM:
$$f(x)=\begin{cases}\dfrac{1}{b-a}, & a\le x\le b\\ 0, & x<a, x>b\end{cases}$$

TRIANGULAR:
$$f(x)=\begin{cases}\dfrac{2(x-a)}{(b-a)(c-a)}, & a\le x\le c\\ \dfrac{2(b-x)}{(b-a)(b-c)}, & c\le x\le b\end{cases}$$; min. a, max. b, mode c

LOG-TRIANGULAR:
$$f(x)=\begin{cases}\dfrac{2(\ln x-\ln a)}{(\ln b-\ln a)(\ln c-\ln a)}, & a\le x\le c\\ \dfrac{2(\ln b-\ln x)}{(\ln b-\ln a)(\ln b-\ln c)}, & c\le x\le b\end{cases}$$; min. a, max. b, mode c

The cumulative distribution function $F(x)$ is the integral of the probability density function $f(x)$ (PDF) and thus represents the probability that the variable of interest is equal to or less than the value x. Further characteristics of these distributions—such as formulas for the mean, mode, and median—can be found in standard statistics references (e.g., see Chapter 6 of Law and Kelton [E-9]).

The values for the statistical input distributions for the probabilistic wastage model are listed in Table E-1. This table is constructed in the following fashion:

- The two leftmost columns describe the variable of interest and the variable nomenclature.
- The next two columns list the nominal value and the applicable units.
- The next four columns define the statistical distribution used to model each variable and the associated parameter values (e.g., a, b, and c for a triangularly distributed variable). Triangular and log-triangular distributions are commonly used for variables with limited available data and are hence used for the majority of the inputs.

The following list summarizes the basis for each input parameter in Table E-1.

- HEAD TEMPERATURE. The nominal value for the head temperature is the highest reported value for a U.S. plant of 605°F (Table 4-2). A tolerance band of ±5°F is assumed based on engineering judgment.
- FRACTION OF CYCLE WHEN LEAK BEGINS. The use of a uniform distribution reflects the assumption that a leak is equally likely to initiate at any point during a cycle.
- STRESS INTENSITY FACTOR. Used in projecting crack growth rates, the values for this input distribution are based on Davis-Besse-specific finite element calculations that consider all operating stresses including welding residual stresses and assume a through-wall axial crack extending 0.5 to 1.5 inches above the top of the J-groove weld. The actual values (60 to 100

MPa√m) used are higher than those calculated for Davis-Besse (40 to 70 ksi√in, or 44 to 77 MPa√m) to account for possible variability between plants.

- CRACK GROWTH RATE POWER LAW COEFFICIENT. The statistical distribution for this coefficient is based on the evaluation of laboratory Alloy 600 crack growth rate data presented in report MRP-55 [E-6]. This distribution accounts for the heat-to-heat variability in the crack growth rate of Alloy 600. The same log-triangular distribution used for the probabilistic wastage model was also used for the MRP-105 probabilistic evaluation of nozzle ejection [E-10]. The upper bound of the distribution accounts for the physical upper limit to the rate of SCC crack growth. Per MRP-55 [E-6] the apparent stress intensity factor threshold K_{th} and power-law exponent n are taken to be the recommended values of 9 MPa√m and 1.16, respectively.
- CRACK GROWTH RATE THERMAL ACTIVATION ENERGY. The nominal value of 31 kcal/mole is an industry consensus value [E-6], and the tolerance band of ±4 kcal/mole is conservative given the good consistency for this parameter in the crack growth testing literature for Alloy 600 material [E-6]. In the wastage model, the activation energy is used to apply the MRP-55 [E-6] crack growth rate data, which are normalized to a reference temperature of 617°F (325°C), to the assumed head temperature.
- WITHIN-HEAT CRACK GROWTH RATE VARIABILITY MULTIPLIER. This distribution accounts for variability arising from within-heat variations in the crack growth rate of Alloy 600. The statistical distribution for this multiplier is based on the evaluation of Alloy 600 crack growth rate data presented in report MRP-55 [E-6] and is the same as that used for the MRP-105 probabilistic evaluation of nozzle ejection [E-10].
- LEAK RATE FOR CRACK 0.5-INCH ABOVE WELD. The distribution used for this leak rate (2×10^{-6} gpm nominal with 10^{-6} and 10^{-4} triangular bounds) is based on industry experience with such cracks. The leak rate is estimated based on the small volumes of boric acid deposit accumulations typically observed adjacent to leaking CRDM nozzles. Details regarding the small volumes of boric acid deposit accumulations typically observed are available in EPRI 1007842 [E-1].
- LEAK RATE FOR CRACK 1.3-INCH ABOVE WELD. This distribution is based on the Davis-Besse experience as evaluated in the Davis-Besse root cause report [E-2] with statistical bounds chosen in light of the variability of crack geometry.
- LEAK RATE YIELDING WASTAGE RATE WR_{low}. The values for this input distribution were chosen because they result in a relatively low level of local cooling and relatively small flow velocities. As discussed above in the section describing the thermal analysis, the nominal value of 0.001 gpm for LR_{low} is expected to produce only about 10°F of local cooling. The bounds to this parameter cover a total range of two orders of magnitude in order to account for the uncertainties in the thermal analysis.
- CRITICAL LEAK RATE YIELDING UPPER SHELF WASTAGE RATE WR_{crit}. The nominal value of 0.1 gpm was chosen based on the results of the thermal analysis, and also on the Davis-Besse experience [E-2] that indicated rapid corrosion beginning for a leak rate in the range of 0.04 to 0.20 gpm. For this leak rate, the thermal analysis shows that the extent of local cooling is sufficient for a pool of concentrated boric acid solution to form on the top head surface. The lower bound of 0.02 gpm for this parameter accounts for uncertainties in the thermal

analysis. This lower bound also addresses the concern that relatively high corrosion rates could possibly occur in a highly concentrated molten boric acid solution at temperatures significantly higher than 212°F (e.g., 450°F). Molten boric acid is known to be slow to lose moisture at temperatures up to roughly 450°F [E-3].

- WASTAGE RATE AT LEAKAGE RATE LR_{low}. The nominal value of 0.072 in/yr is based on laboratory test data summarized in the EPRI *Boric Acid Corrosion Guidebook* [E-4]. This value is considered to be conservative because it is somewhat greater than the maximum value reported for corrosion of low-alloy steel in low-oxygen, concentrated boric acid solutions.
- UPPER-SHELF WASTAGE RATE. This parameter describes the wastage rate applied in the model after the leak rate reaches LR_{crit}. It describes wastage from the top head surface down toward the cladding (Stage 2 in Figures E-7 and E-10). The nominal value of 2.5 in/yr is based on the Davis-Besse experience (the size of the nozzle #3 cavity and the probable time interval of rapid corrosion) and laboratory test data reported in the EPRI *Boric Acid Corrosion Guidebook* [E-4] for aerated, concentrated boric acid solutions. The upper bound value of 7 in/yr accounts for the high rates reported for some tests.
- DETECTION SENSITIVITY FOR BORIC ACID CRYSTAL RELEASE. The nominal value of 10 in^3 was developed in Chapter 3 of this document; see the heading "3.3 Volume of Boric Acid Deposits Detectable by BMV Inspection." The upper- and lower-bound parameters for the triangular distribution account for the uncertainty in the estimation of this parameter.

E.6.4 Monte Carlo Calculations

The sequence of steps listed in "E.6.1 Wastage Model Basics" was implemented in a Monte Carlo simulation to predict the probability associated with different levels of wastage. The Monte Carlo analysis is carried out as follows:

- For each trial, each statistical distribution in Table E-1 is sampled using a random number generator, yielding a value from the permissible range for each input according to the cumulative distribution function for the distribution used. For example, the stress intensity factor K is assigned a value according to the applicable triangular distribution. The value is most likely close to the mode (80 MPa√m) but could be anywhere between the minimum of 60 MPa√m and the maximum of 100 MPa√m.
- Using all of the inputs sampled in this fashion from the respective statistical distributions, the total wastage volume is calculated using the approach outlined under "E.6.1 Wastage Model Basics" above. For each trial, the wastage volume at 0.1-EFPY intervals is computed up through 50 total EFPY.
- A total of 1 million trials are executed in this fashion, and the wastage volumes for each stored.
- The full array of 1,000,000 wastage volumes are sorted from lowest to highest, permitting the values associated with specific statistical significance levels to be identified. For example, the median wastage volume (significance level of 0.5) is that representing the 500,000th value in the sorted list, while the 90% one-sided upper-bound volume is the 900,000th value in the

sorted list (i.e., only 100,000 of the trials produced larger volumes). The resulting curve of wastage volume versus significance level is the cumulative distribution function for the wastage volume. This distribution can then be compared to the wastage volume required to maintain code stress margins. Note that the number of Monte Carlo trials used is sufficiently large so that the results are insensitive to further increases in the number of trials.

E.7 Refinement of Modeling Assumptions and Inputs

Work is ongoing to further refine understanding of the wastage process. The statistical inputs to the probabilistic evaluation presented here were designed to capture the process uncertainties to the extent possible at the current time. The new MRP boric acid corrosion test program being managed by EPRI is being designed to address the uncertainties in the current understanding of the wastage process.

E.8 References

E-1. *Visual Examination for Leakage of PWR Reactor Head Penetrations: Revision 2 of 1006296, Includes 2002 Inspection Results and MRP Inspection Guidance*, EPRI, Palo Alto, CA: 2003. 1007842.

E-2. *Root Cause Analysis Report: Significant Degradation of the Reactor Pressure Vessel Head*, Davis-Besse Nuclear Power Station report CR 2002-0891, April 2002.

E-3. G. White, C. Marks, and S. Hunt. "Technical Assessment of Davis-Besse Degradation," *Materials Reliability Program: EPRI Boric Acid Corrosion Workshop, July 25-26, 2002 (MRP-77)*, EPRI, Palo Alto, CA: 2002. 1007336. Also presented at the MRP-NRC technical meeting on May 22, 2002, in Rockville, MD (NRC ADAMS Accession No. ML021420150).

E-4. *Boric Acid Corrosion Guidebook, Revision 1: Managing Boric Acid Corrosion Issues at PWR Power Stations*, EPRI, Palo Alto, CA: 2001. 1000975.

E-5. "Supplemental Information in Response to NRC Question Number 24 on the Preliminary Probable Cause Summary Report Dated March 22, 2002," Letter from H. W. Bergendahl (FENOC) to J. E. Deyer (NRC), May 15, 2002.

E-6. *Materials Reliability Program (MRP) Crack Growth Rates for Evaluating Primary Water Stress Corrosion Cracking (PWSCC) of Thick-Wall Alloy 600 Materials (MRP-55) Revision 1*, EPRI, Palo Alto, CA: 2002. 1006695.

E-7. *Examination of the Reactor Vessel (RV) Head Degradation at Davis-Besse*, Final Report, BWXT Services, Inc., Lynchburg, VA: 2003. 1140-025-02-24.

E-8. R. Kilian, P. Scott, A. Roth, and U. Wesseling, "Boric Acid Corrosion - European Experience," *Materials Reliability Program: EPRI Boric Acid Corrosion Workshop, July 25-26, 2002 (MRP-77)*, EPRI, Palo Alto, CA: 2002. 1007336.

E-9. M. Law and W. D. Kelton. *Simulation Modeling and Analysis*, Second Edition. New York: McGraw-Hill, Inc., 1991.

E-10. *Materials Reliability Program: Probabilistic Fracture Mechanics Analysis of PWR Reactor Pressure Vessel Top Head Nozzle Cracking (MRP-105)*, EPRI, Palo Alto, CA: 2004. 1007834.

E-11. *PWR Steam Generator Tube Repair Limits: Technical Support Document for Expansion Zone PWSCC in Roll Transitions – Rev. 2*, EPRI, Palo Alto, CA: 1993. NP-6864-L, Rev. 2.

Table E-1
Input Statistical Distributions Used in Monte Carlo Calculations of Wastage

Quantity / Description	*Symbol*	*Nominal Value*	*Units*	*Statistical Distribution*	*Parameter 1* Triangular = *c* Log-triang = *c*	*Parameter 2 (lower bound)* Triangular = *a* Log-triang = *a* Uniform = *a*	*Parameter 3 (upper bound)* Triangular = *b* Log-triang = *b* Uniform = *b*
Head Temperature	T_{head}	605	°F	Triangular	605	600	610
Fraction of Fuel Cycle Completed When Leak Begins	f_{t0}	0.5		Uniform		0.0	1.0
Stress Intensity Factor Driving Axial Crack Growth Above Top of Weld	K	80	MPa√m	Triangular	80	60	100
Crack Growth Rate Power Law Coefficient × 10^{13}	A_{ref}	13.4	$(m/s) \times (MPa\sqrt{m})^{-1.16}$	Log-triang	13.4	1.58	114.2
Crack Growth Rate Activation Energy	Q_g	31	kcal/mol	Triangular	31	27	35
Within Heat Crack Growth Rate Variability Multiplier	f_{wh}	1.00	–	Log-triang	1.00	0.238	4.20
Leak Rate for Crack Extending 0.5" Above Top of Weld	LR_0	2.0E-06	gpm	Log-triang	2.0E-06	1.0E-06	1.0E-04
Leak Rate for Crack Extending 1.3" Above Top of Weld	LR_1	0.15	gpm	Log-triang	0.15	0.001	1.0
Leak Rate Yielding Wastage Rate WR_{low}	LR_{low}	0.001	gpm	Log-triang	0.001	0.0001	0.01
Critical Leak Rate Yielding Upper Shelf Rapid Corrosion Rate WR_{crit}	LR_{crit}	0.10	gpm	Log-triang	0.10	0.02	0.20
Wastage Rate at Leakage Rate LR_{low}	WR_{low}	0.072	in/yr	Triangular	0.072	0.010	0.250
Upper-Shelf Wastage Rate for Leak Rates Greater than LR_{crit}	WR_{crit}	2.5	in/yr	Triangular	2.5	1.0	7.0
BMV Detection Sensitivity for Boric Acid Crystal Release	BAC_{det}	10	in^3	Triangular	10	5	20

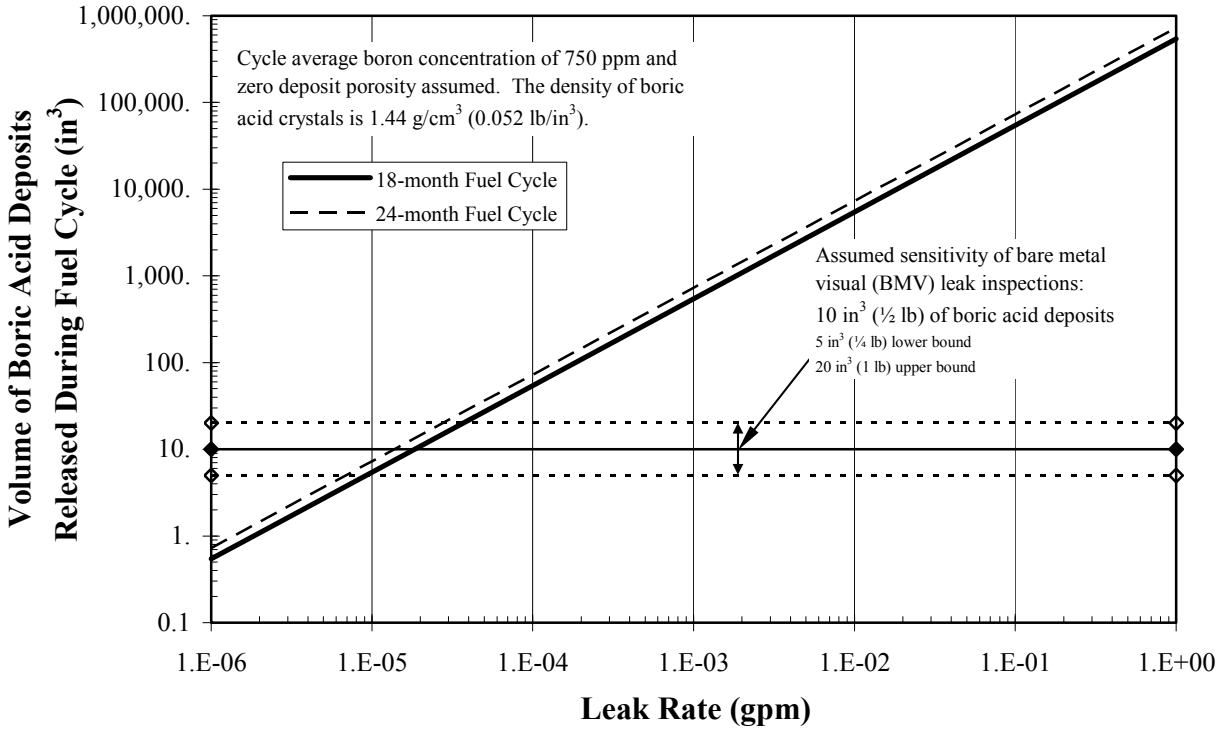

Figure E-1
Leakage Detectability

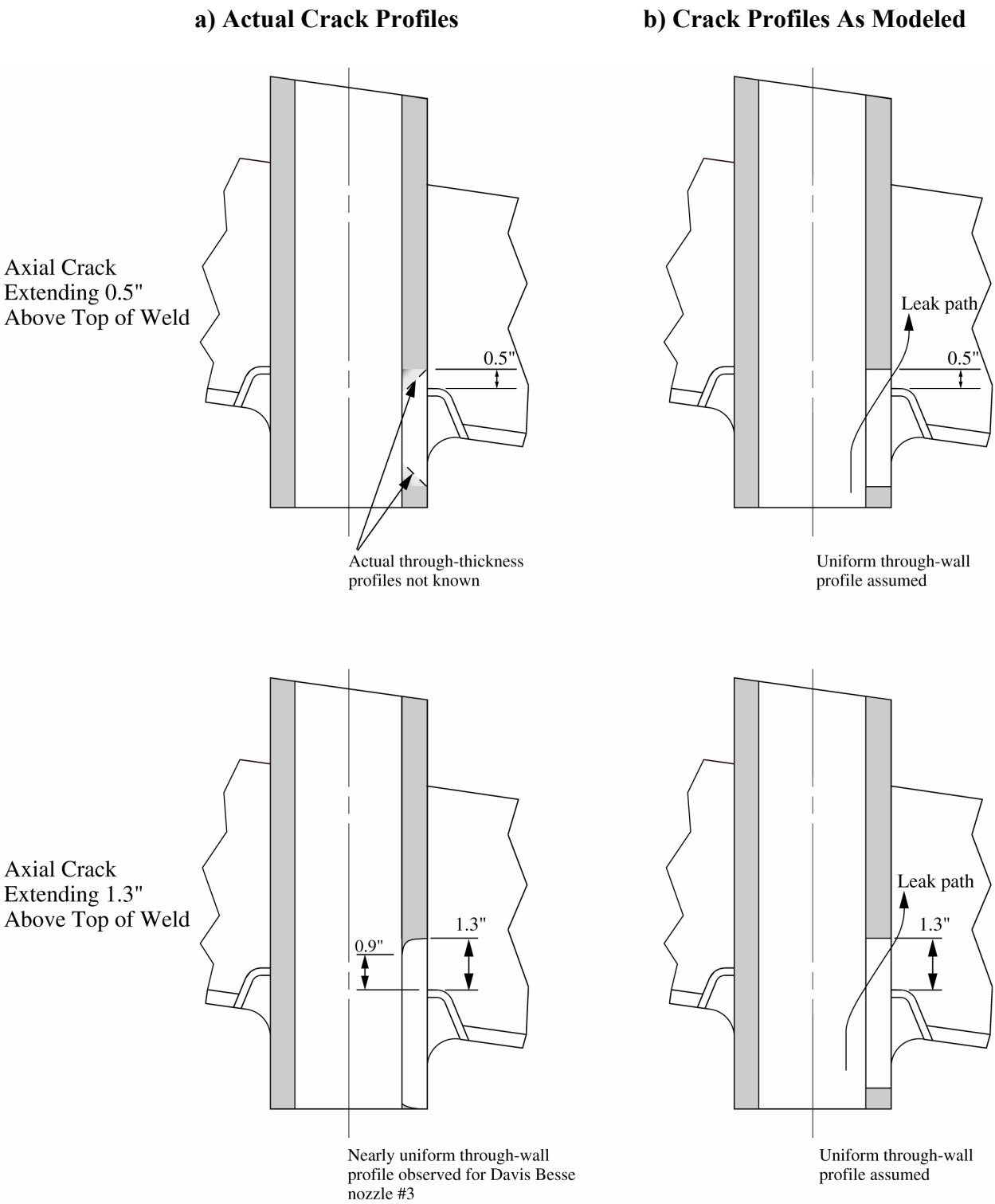

Figure E-2
Through-Wall Axial Crack Profiles: a) Crack geometry based on available plant data; b) Uniform crack profile assumed in leak rate and crack growth modeling

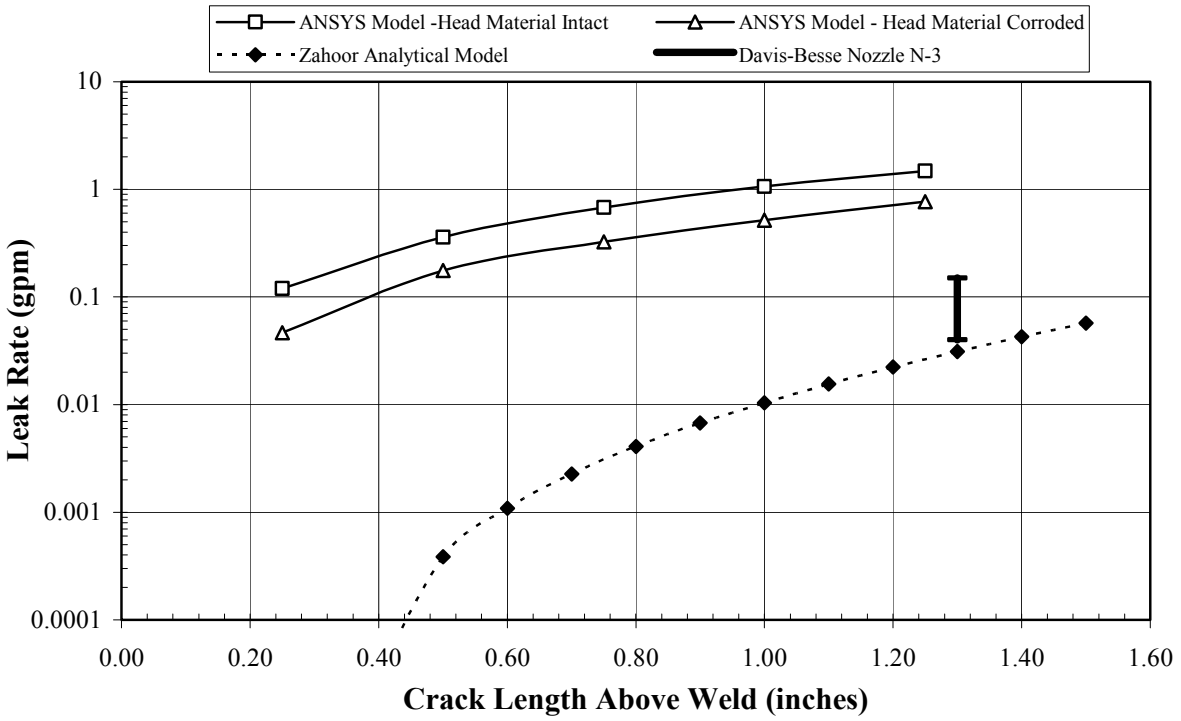

Figure E-3
Leak Rate versus Crack Length According to Analytical Models

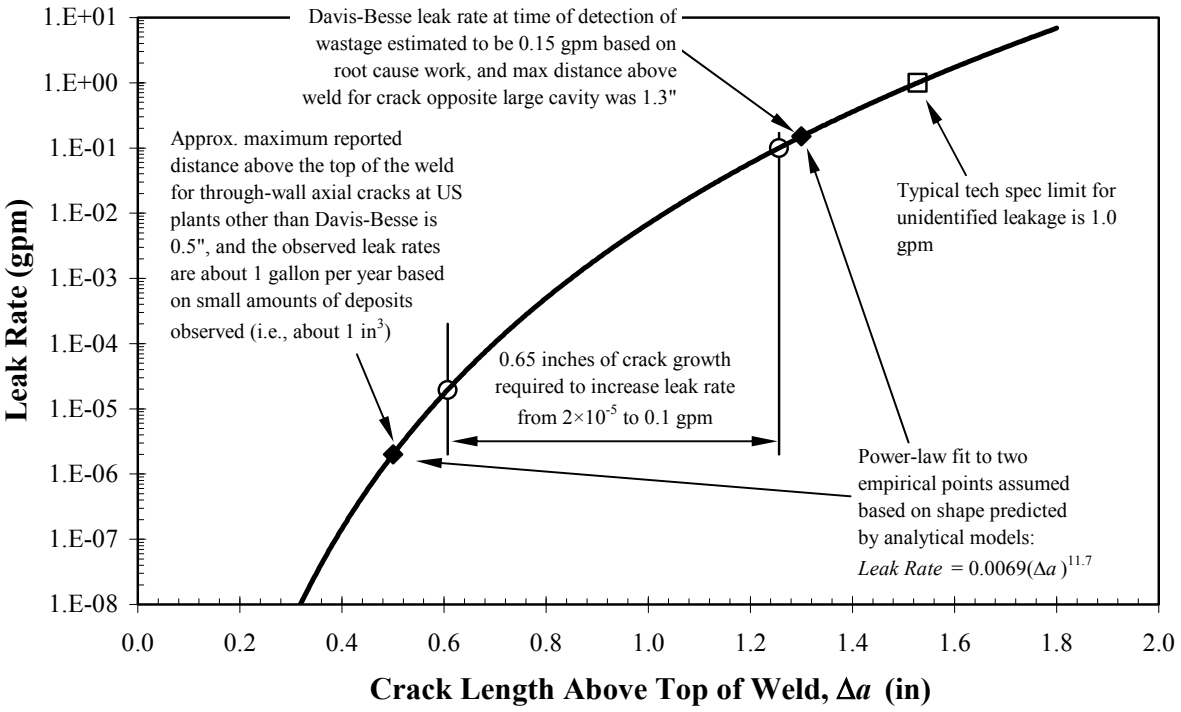

Figure E-4
Assumed Nominal Leak Rate versus Crack Length Relationship Based on Available Plant Data

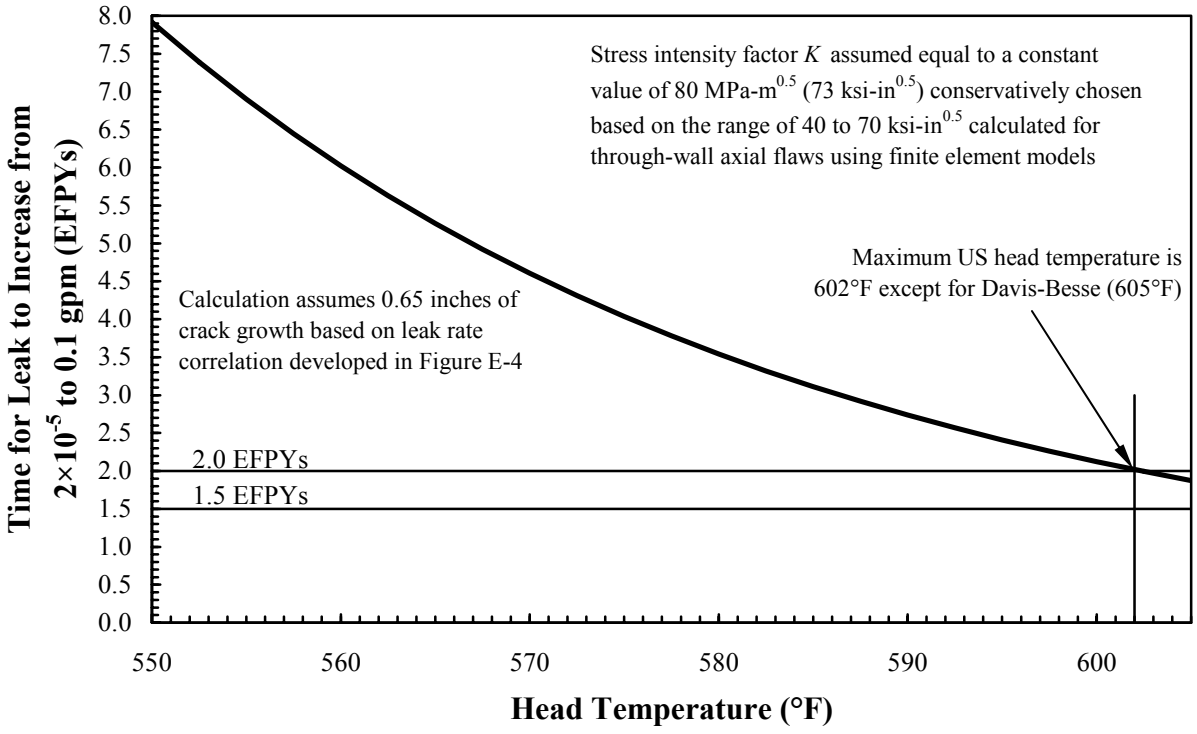

Figure E-5
Time for Leak Rate to Increase from Level Detectable by Bare Metal Visual (BMV) Inspections (2×10^{-5} gpm) to the Critical Leak Rate that May Lead to Rapid Corrosion (0.1 gpm) Using the Deterministic Crack Growth Rate Curve Recommended by Report MRP-55 [E-6] for Alloy 600

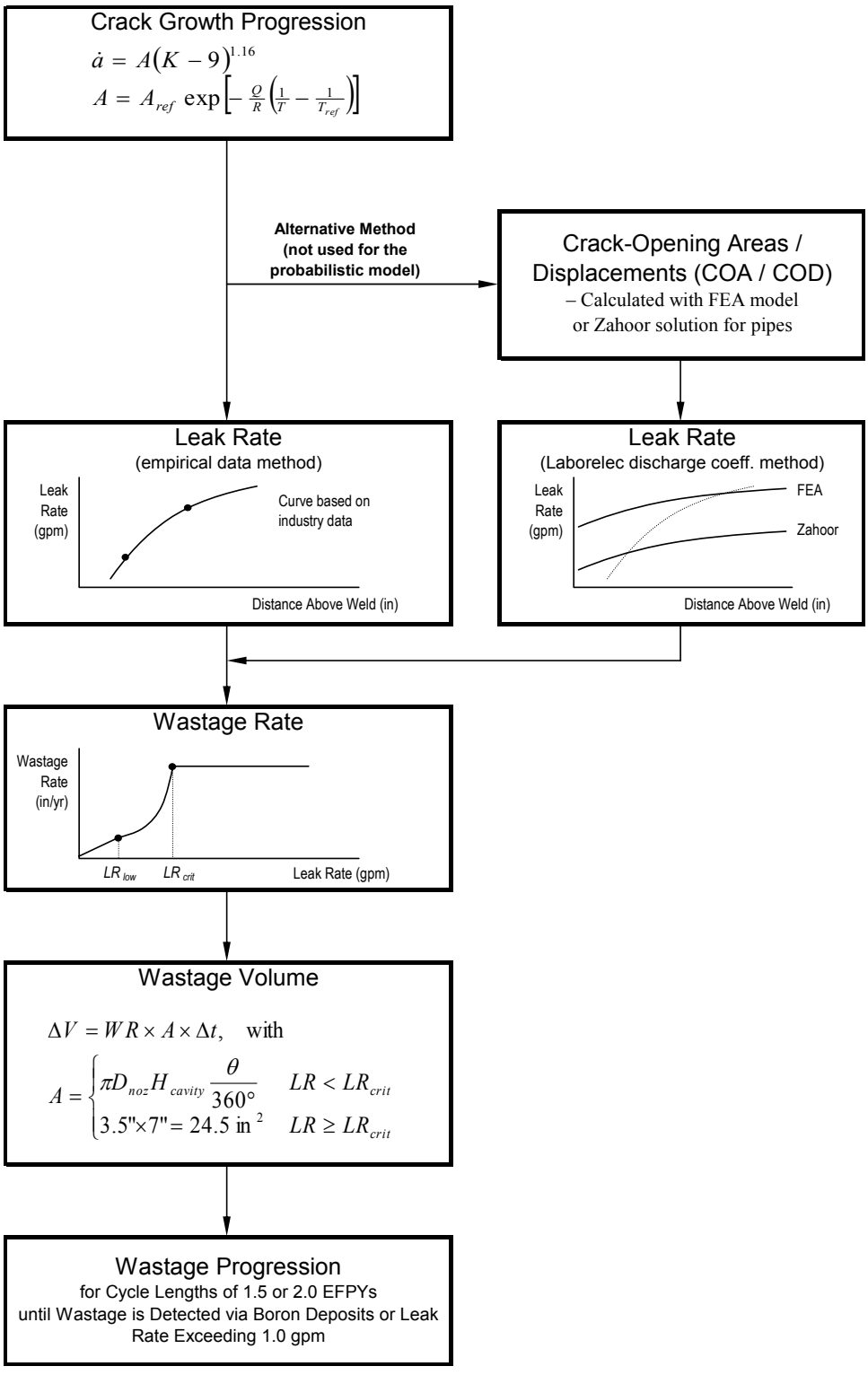

Figure E-6
Simplified Flow Chart for the Probabilistic Wastage Model

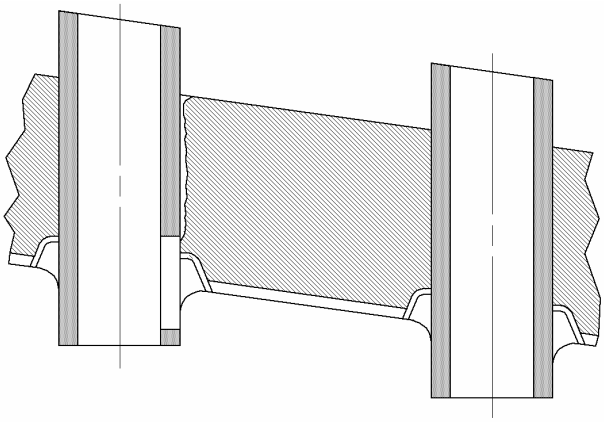

Stage 1: For relatively small initial leak rates, cooling is insufficient to support liquid on the top head surface and the rate of corrosion in the annulus is limited by the lack of oxygen. Steam cutting may act to open up the initially tight annulus.

Note: The presence of a growing pile of boric acid deposits in the area of the growing wastage cavity is not reflected in these sketches.

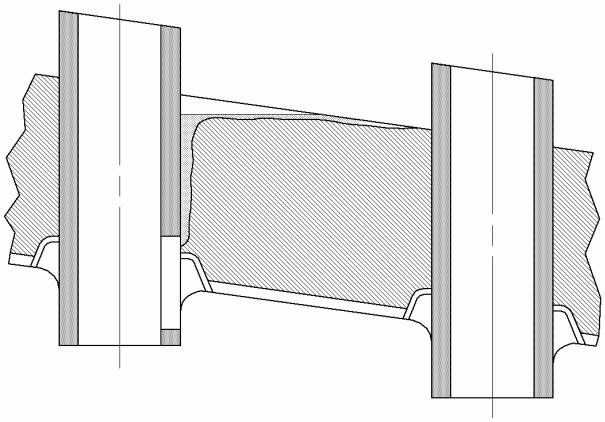

Early Stage 2: The leak rate increases with increasing crack length. Oxygen begins to penetrate into the increasing gap between the nozzle and vessel head and liquid begins to flow out onto the head surface, concentrating boric acid as the water evaporates. The oblong shape of the cavity viewed from above is the result of gravity displacing the liquid in the downhill direction. Corrosion behavior on the top head surface is somewhat analogous to borated water dripping onto a hot metal surface.

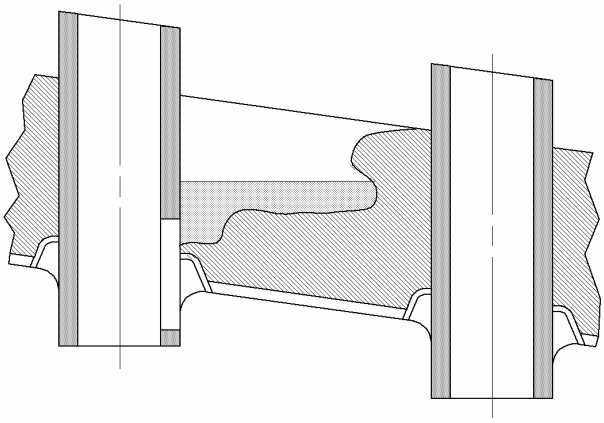

Later Stage 2: As a cavity forms and deepens on the top head surface, the edges of the pool recede back towards the leaking nozzle. A constant leak rate (about 0.1 gpm) results in an equilibrium volume of liquid on the head surface that corrodes predominantly downward through the low-alloy steel head.

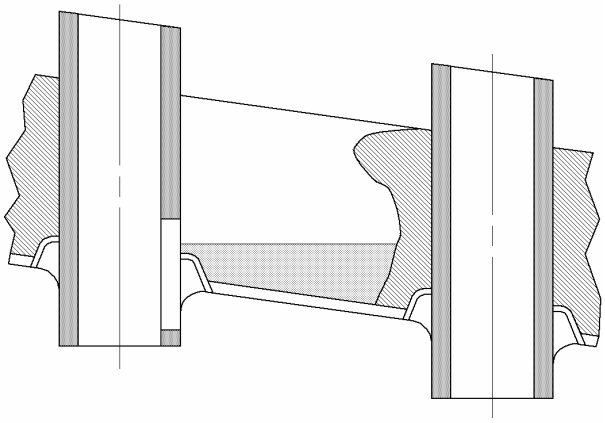

Stage 3: Downward corrosion is arrested by the stainless steel clad. Corrosion continues on the exposed low-alloy steel surfaces due to the equilibrium volume of liquid on the clad surface.

Figure E-7
Cavity Progression for a Top-Down Corrosion Mode

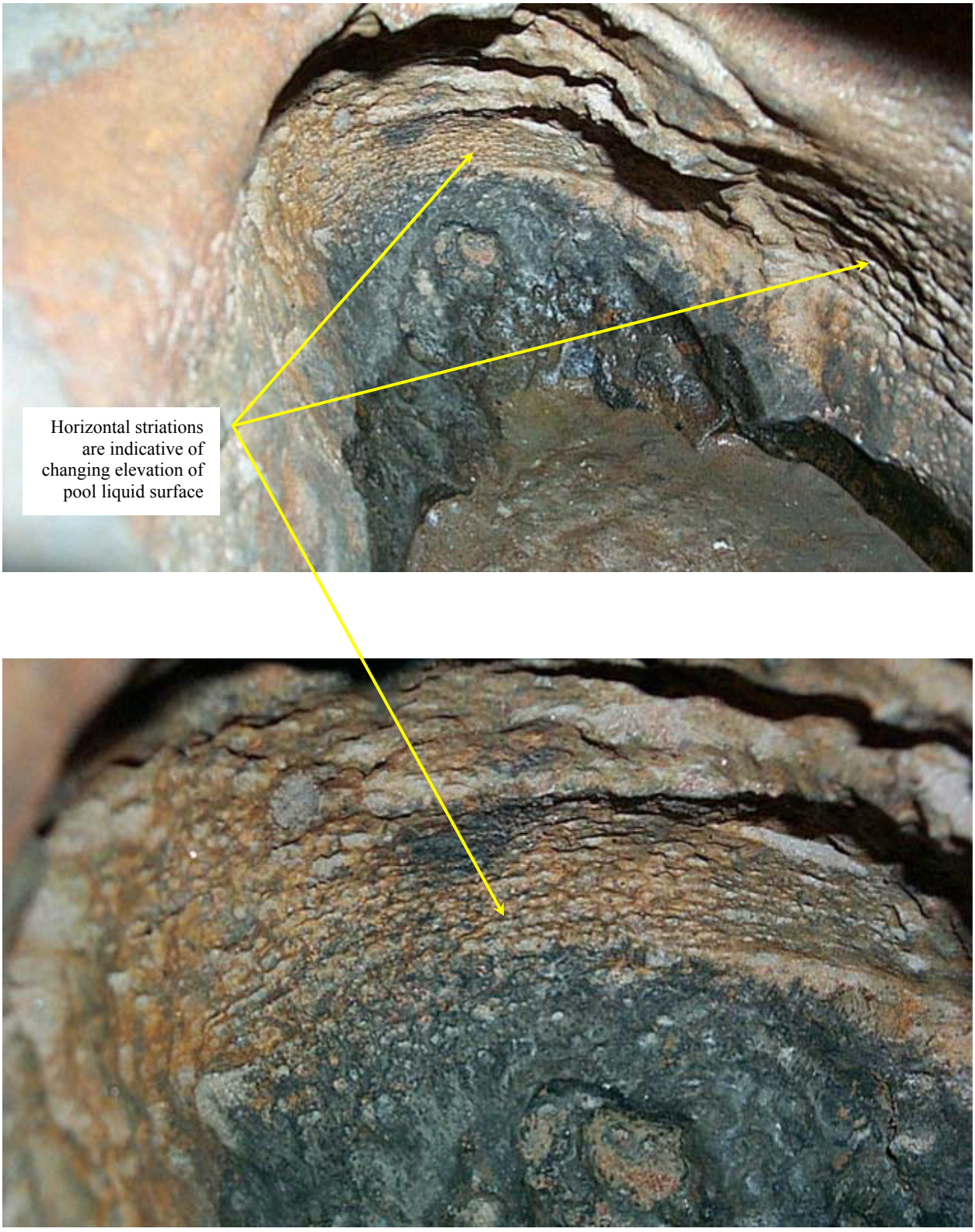

Figure E-8
Photographs of Davis-Besse Wastage Cavity Adjacent to Nozzle #3 [E-7]

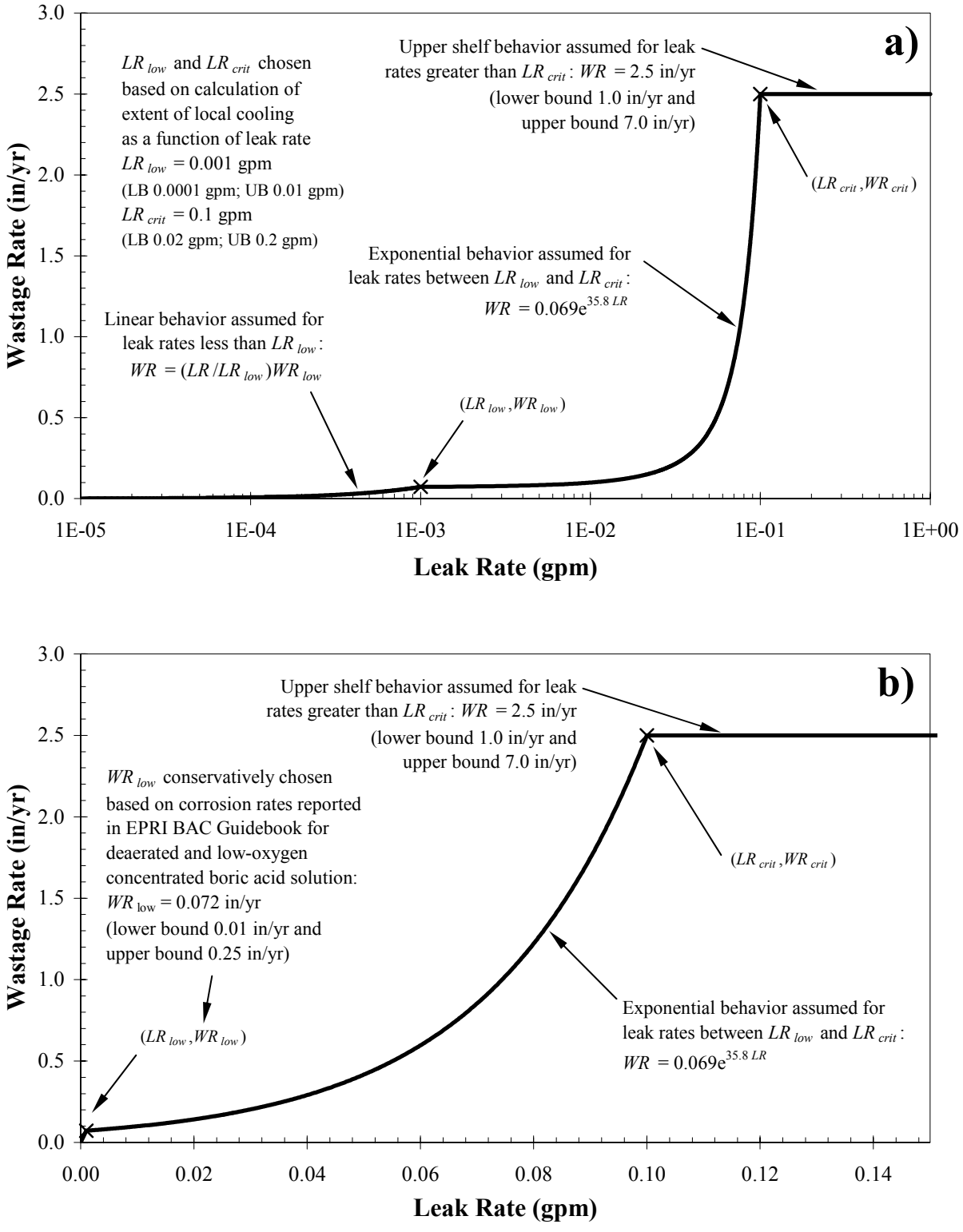

Figure E-9
Assumed Dependence of Linear Wastage Rate on Leak Rate Based on Available Data: a) Log scale for leak rate; b) Linear scale for leak rate

a) Apparent Actual Cavity Growth **b) Cavity Growth Model**

Stage 1

(e.g., Davis-Besse Nozzle #2)

Stage 2

(e.g., Midterm Davis-Besse Nozzle #3)

Stage 3

(e.g., Late Davis-Besse Nozzle #3)

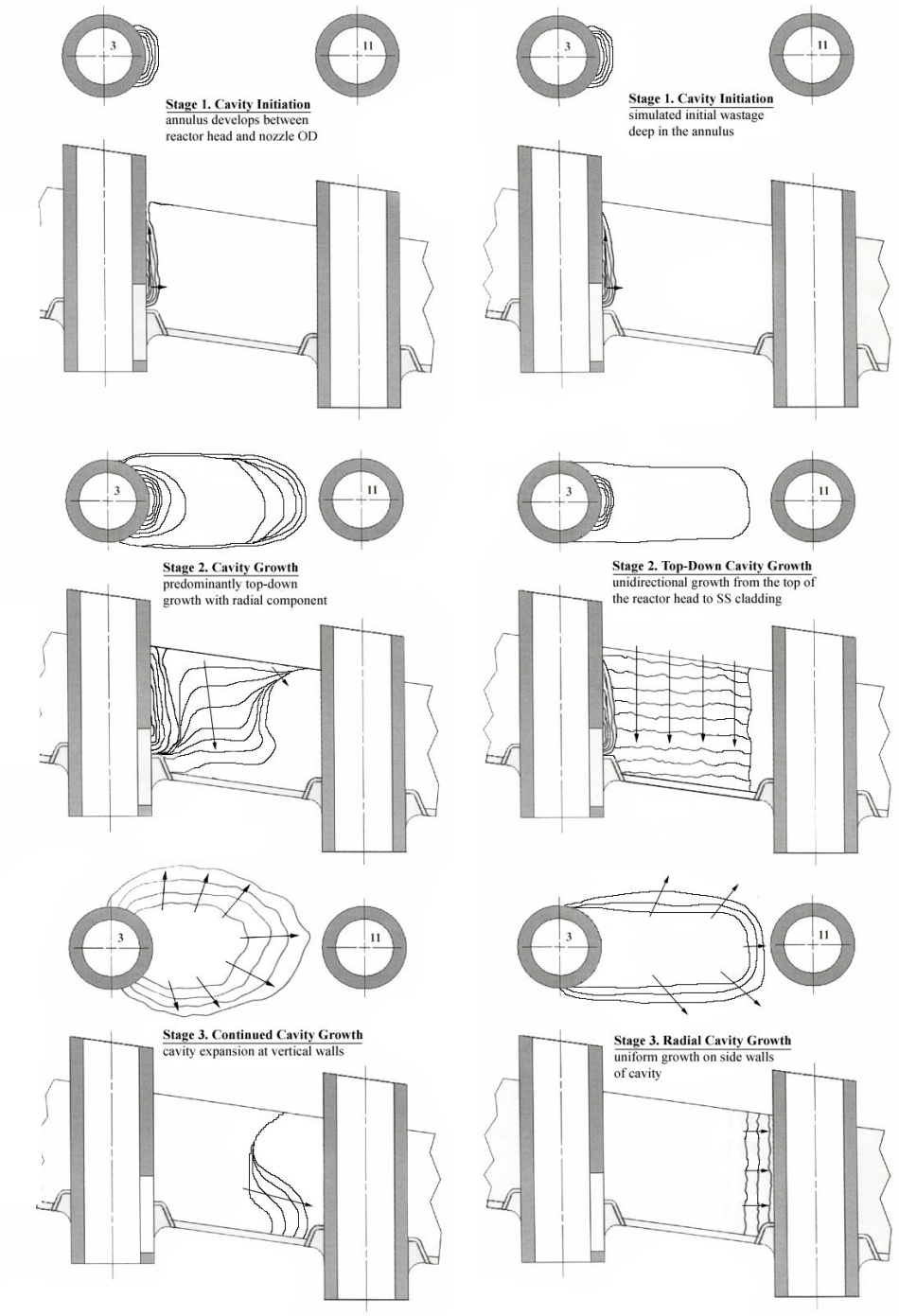

Figure E-10
Development of Wastage Cavity: a) Apparent actual cavity development adjacent to Davis-Besse nozzle #3; b) Cavity growth geometry assumed for the probabilistic wastage model

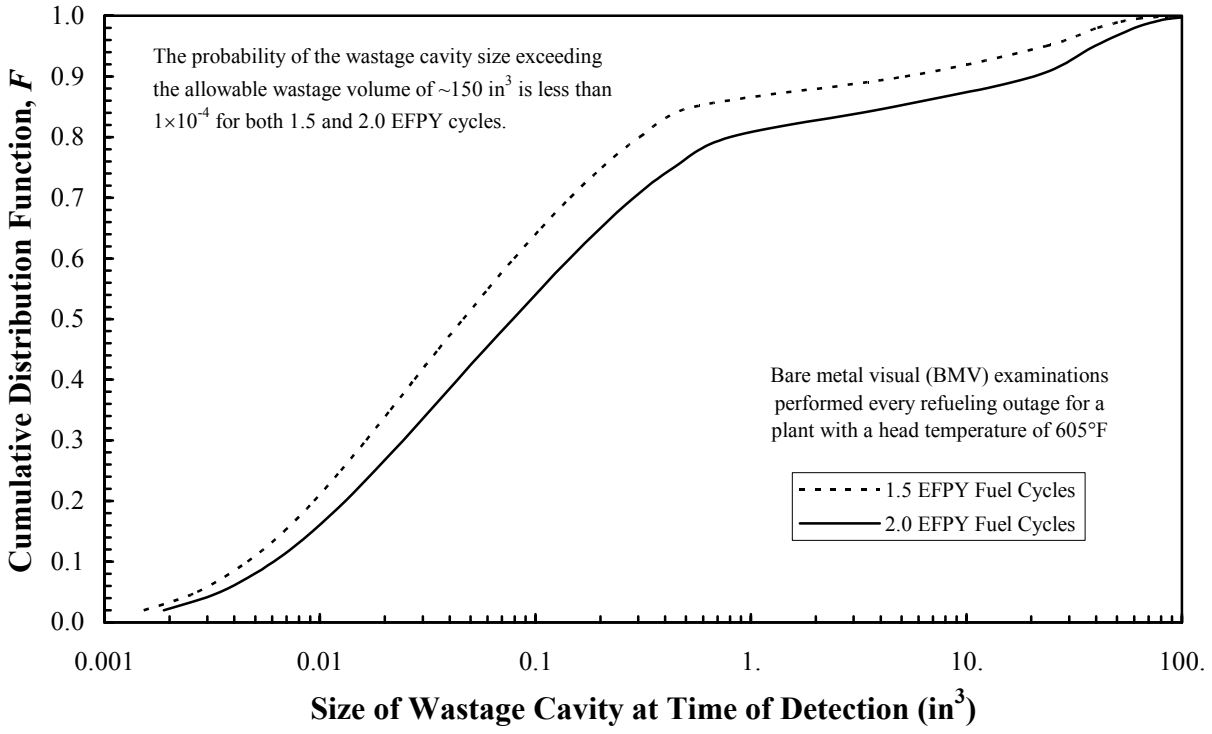

Figure E-11
Results of the Probabilistic Wastage Calculations

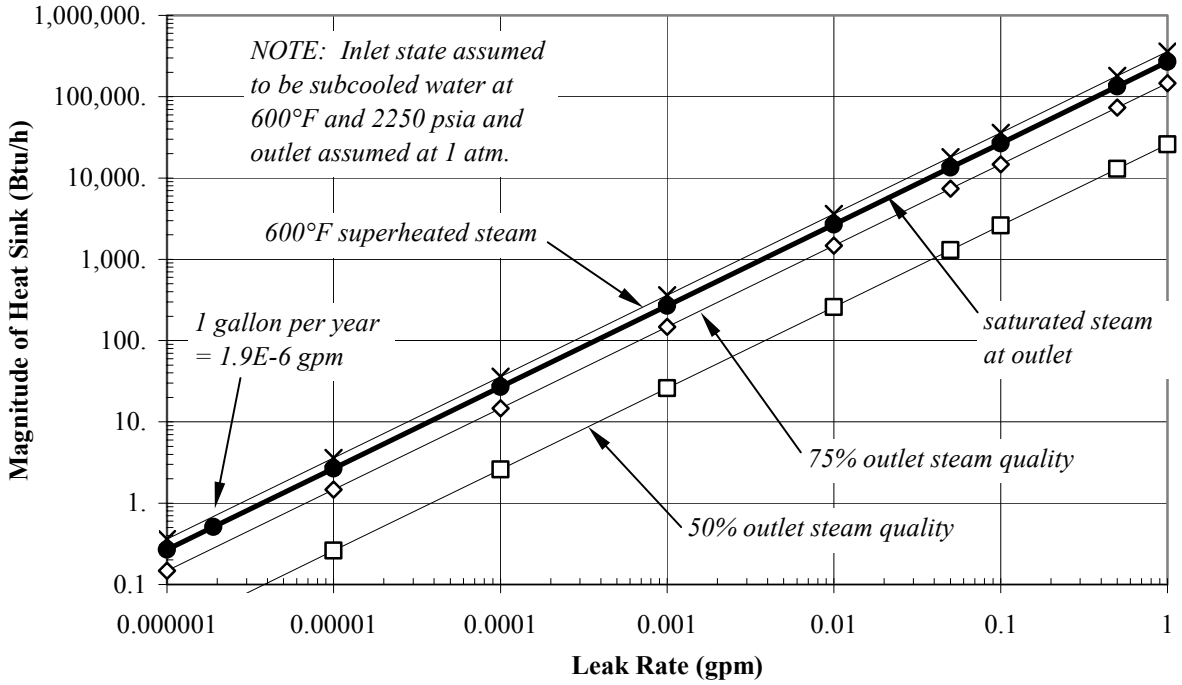

Figure E-12
Expansion Cooling Heat Sink Rate Versus Leak Rate

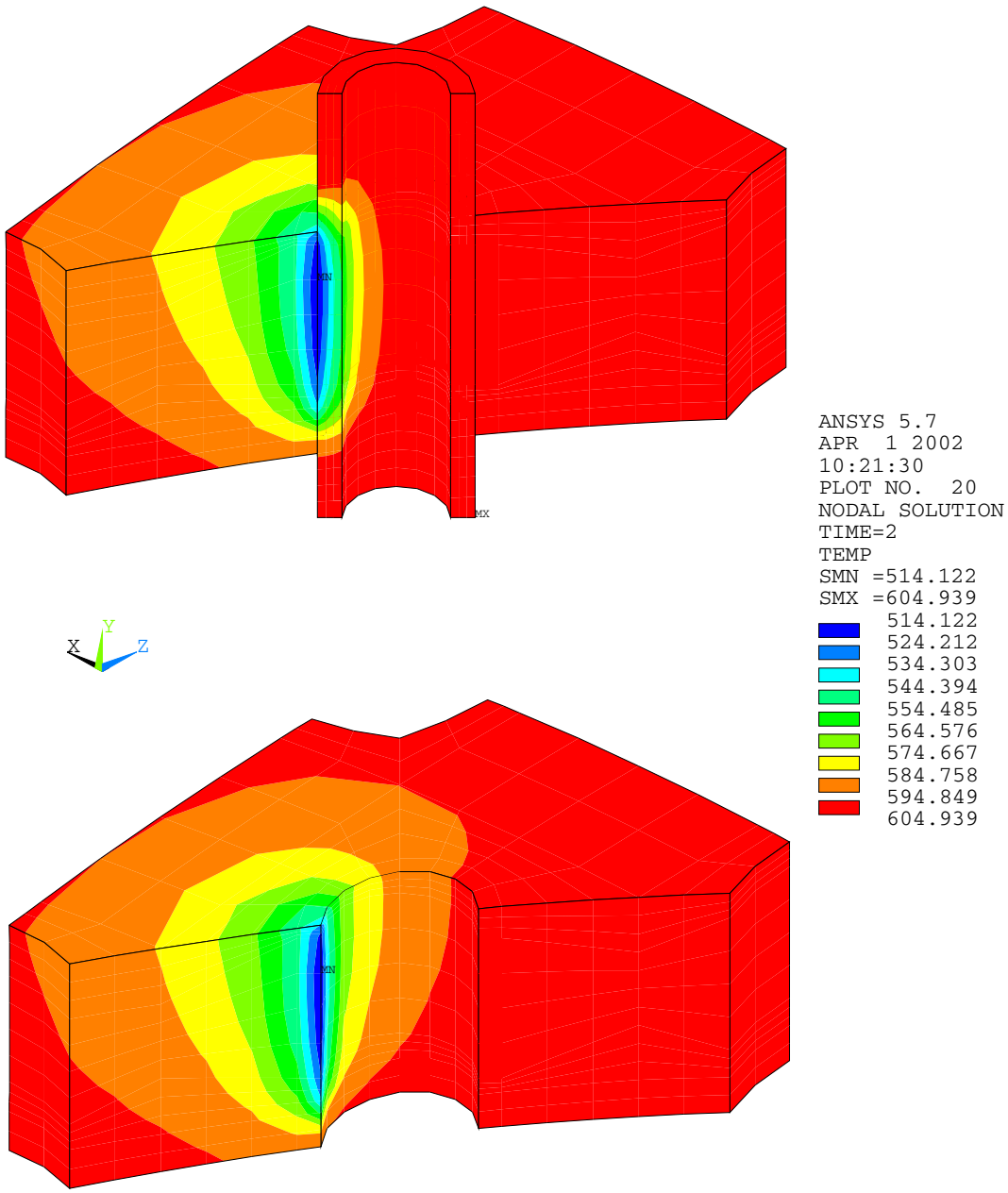

Figure E-13
Example Thermal Analysis Results: Temperature Contours (°F) for a Uniform 1860 Btu/h Heat Sink on 45° Total Arc Surface Corresponding to Complete Vaporization of a 0.007 gpm Leak (Heat Transfer Coefficient on Inside Head Surface of 110 Btu/h-ft^2-°F)

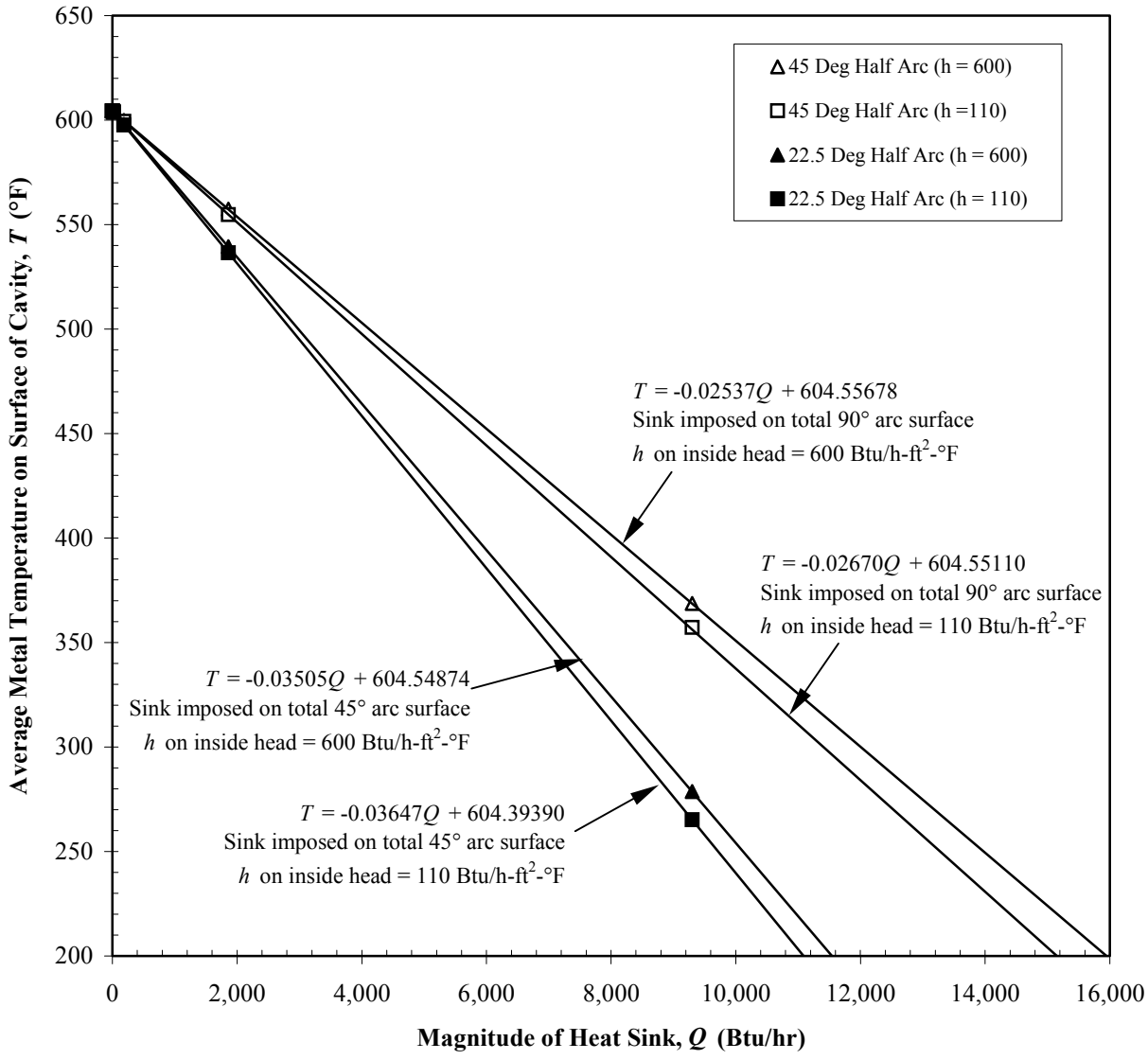

Figure E-14
Average Metal Temperature Along Small Cavity Leak Path Versus Heat Sink Magnitude